CONJUGATED POLYELECTROLYTES: SYNTHESIS, PHOTOPHYSICS, AGGREGATION STUDIES AND SENSOR APPLICATIONS

By

XUZHI ZHU

A DISSERTATION PRESENTED TO THE GRADUATE SCHOOL
OF THE UNIVERSITY OF FLORIDA IN PARTIAL FULFILLMENT
OF THE REQUIREMENTS FOR THE DEGREE OF
DOCTOR OF PHILOSOPHY

UNIVERSITY OF FLORIDA

2013

To my family and my friends

ACKNOWLEDGMENTS

First of all, I would like to express my deep and sincere gratitude to my advisor, Professor Dr. Kirk S. Schanze for his support, advice and encouragement. My Ph. D. study and research could not have been finished without his guidance. He led me into the amazing area of conjugated polyelectrolytes and helped me to learn independent research and scientific writing. He is such a great supervisor with enthusiasm for science and patience to his students.

Besides my advisor, I would like to thank the rest of my committees: Dr. McElwee-White, Dr. Castellano, Dr. Brennan, and Dr. Smith, for their time, encouragement, insightful comments and suggestions. I warmly thank Dr. Parkinson from University of Wyoming for his nice advice on one of my projects.

My deep gratitude also goes to all the former and current members from Dr. Schanze's group for all the help, support, advice and happy memories. Especially I want to thank Dr. Fude Feng and Dr. Chen Liao for all the discussion and advices on synthesis. They shared their broad knowledge and extensive experiences about Polymer Chemistry and Organic Synthesis with me. I really want to thank Dr. Galyna Dubinina for the help on the dissertation. She looked carefully and made a lot of valuable suggestions. Dr. Abby Shelton, Dr. Anand Parthasarathy and Dr. Randi Price taught me how to use almost all the instruments in my lab and helped me whenever I had a problem. I would like to thank Dr. Dongping Xie and Dr. Zhuo Chen for their help and support not only on research but also on life. They are my best friends here. I also want to thank Dr. Jie Yang for her help and advice on FCS experiments. Of course, I would like to thank Dr. Jan-Moritz Koenen, Dr. Gyu Leem, Dr. Danlu Wu, Russell Winkel, Zhenxing Pan, Hsien-Yi Hsu, Subhadip Goswami, Ali Gundogan for their valuable

advice and friendship. In one of my projects, I collaborated with Dr. Alexander Nepomnyashchii in Dr. Parkinson's group. I would like to show my gratitude to him for his wonderful work in AFM images and photoelectrochemical experiments.

This dissertation would not have been possible without the love and support of my family. I want to express my deepest gratitude to my parents. They always encourage and support me to continue my study abroad.

Finally, I want to give my biggest thanks to my girlfriend Duo, without whose love and understanding my work could not have been completed.

TABLE OF CONTENTS

page

LIST OF TABLES

LIST OF FIGURES

LIST OF ABBREVIATIONS

3D	Three dimensions
10CPC	Phospholipid
ADP	Adenosine diphosphate
AFM	Atomic force microscopy
ALP	Alkaline phosphate
AMP	Adenosine monophosphate
AQS	9.10-Anthraquinone- 2,6-disulfonic acid disodium salt
ATP	Adenosine triphosphate
BOC	tert-Butyloxycarbonyl
$BpPPESO_3$	Sulfonated poly(phenylene ethynylene-*co*-pyridine ethynylene)
CO_2^-	Carboxylate
CPE	Conjugated polyelectrolyte
D	Diffusion coefficient
DABCY	4-(4-Dimethylamino)phenyl-azo)-benzoid acid
DLS	Dynamic light scattering
DNA	Deoxyribonucleic acid
DSSC	Dye sensitized solar cell
FCS	Fluorescence correlation spectroscopy
FET	Field-effect transistor
FRET	Förster resonance energy transfer
FTIR	Fourier transform infrared spectroscopy
$G(\tau)$	Autocorrelation function
GPC	Gel permeation chromatography
GU-P1	Poly(phenylene ethynylene) with guanidinium side chains

GU-P2	Homopolymer of poly(phenylene ethynylene) with guanidinium side chains
HEX	Hexachlorofluorescein
HOMO	Highest occupied molecular orbital
I	Fluorescence intensity
K_{sv}	Stern-Volmer constant
LED	Light emitting device
LUMO	Lowest unoccupied molecular orbital
MES	2-(N-morpholino) ethanesulfonic acid
MPS-PPV	Sulfonated poly(phenylene vinylene)
MV^{2+}	Methyl viologen
MW	Molecular weight
M_n	Number average molecular weight
M_w	Weight average molecular weight
NR_3^+	Quaternary ammonium
O-p	Homopolymer of poly(phenylene ethynylene) with carboxylate side chains
OPE	Oligo(phenylene ethynylene)
OPEC1	Cationic oligo(phenylene ethynylene) with trimethylsilyl acetylene
P1	Poly(phenylene ethynylene) with methylene carboxylate side chains
P2	Poly(phenylene ethynylene-*co*-thiophene ethynylene) with methylene carboxylate side chains
P2-H	Poly(phenylene ethynylene-*co*-thiophene ethynylene) with methylene carboxylic acid side chains
P3	Poly(phenylene ethynylene-*co*-ethylenedioxythiophene ethynylene) with methylene carboxylate side chains
P4	Poly(phenylene ethynylene-*co*-tetrafluorophenylene ethynylene) with methylene carboxylate side chains

P1-N	Poly(phenylene ethynylene) with methylene ammonium side chains
P2-N	Poly(phenylene ethynylene-*co*-thiophene ethynylene) with methylene ammonium side chains
PAE	Poly(arylene ethynylene)
PDI	Polydispersity
PF	Polyfluorene
Pi	Phosphate
PLC	Phosphatase C
PNA	Peptide nucleic acid
PO_3^{2-}	Phosphate
PPi	Pyrophosphate
PPE	Poly(phenylene ethynylene)
PPE-CO_2	Carboxylated poly(phenylene ethynylene)
PPE-$^{d}CO_2$	Anionic poly(phenylene ethynylene) with dendric carboxylate side chains
PPE-NH_3	Cationic poly(phenylene ethynylene) with dendric ammonium side chains
PPE-OEG	Poly(phenylene ethynylene) with oligo(ethylene glycol) side chains
PPE-Th-NMe_3	Cationic poly(phenylene ethynylene-*co*-thiophene ethynylene) with trimethyl ammonium side chains
PPE-SO_3	Sulfonated poly(phenylene ethynylene)
PPP	Poly(phenylene phenylene)
PPV	Poly(phenylene vinylene)
PT	Polythiophene
R_H	Hydrodynamic radius
RNA	Ribonucleic acid
SEM	Scanning electron microscopy

SiO_2-OH	Blank silica particles
SiO_2-N_3	Azide modified silica particles
SiO_2-OPEC1	OPEC1 modified silica particles
SS-DNA	Single strand DNA
SV	Stern-Volmer
S-Rho	Rhodamine B thiolactone
TCSPC	Time-correlated single photon counting
TEM	Transmission electron microscopy
TGA	Thermogravimetric analysis
THF	Tetrahydrofuran
TMS	Trimethylsilyl
TNT	Trinitrotoluene
V_{eff}	Effective detection volume
Φ_F	Fluorescence quantum yield
λ_{max}	Wavelength of maximum emission peak
η	Viscosity of the solvent
τ	Diffusion time or lifetime
k	Boltzmann's constant
ω	Structure parameter
ω_r	Transversal or waist radius of confocal volume
ω_z	Longitudinal radius of confocal volume

Abstract of Dissertation Presented to the Graduate School
of the University of Florida in Partial Fulfillment of the
Requirements for the Degree of Doctor of Philosophy

CONJUGATED POLYELECTROLYTES: SYNTHESIS, PHOTOPHYSICS, AGGREGATION STUDIES AND SENSOR APPLICATIONS

By

Xuzhi Zhu

August 2013

Chair: Kirk S. Schanze
Major: Chemistry

Over the past several years, significant efforts have been devoted to synthesize new sets of conjugated polyelectrolytes (CPEs) and explore their application as chemical and biosensors for the detection and analysis of a variety of molecules of environmental and biological interests, including small molecules, ions and biological targets. In this dissertation, we focus on the design and synthesis of functional poly(phenylene ethynylene)s (PPEs) and the development of fluorescent sensors. In addition, we investigate the photophysical properties and the aggregation behaviors of PPEs to get deeper understanding and provide some guidelines for future PPE-based sensors.

First, a OPE derivative, cationic alkylammonium-substituted oligo(phenylene-ethynylene) was designed and synthesized. A new graft-strategy for surface modifications of silica particles was designed based on click reaction. The grafting process was successful that the functional material (**SiO_2-OPEC1**) was able to show fluorescence under luminescence and singlet oxygen production in oxygen-saturated deuterated methanol.

Then, a new series of water-soluble PPEs with guanidinium side chains were synthesized and characterized. The photophysical properties indicated that this family of PPEs was aggregated in aqueous solution. A fluorescent “turn-off” sensor for PPi was developed based on **GU-P1**/surfactant complex, by taking advantage of the specified interaction between guanidinium and PPi, and the amplified quenching effects of PPEs.

In order to relieve the aggregation of PPEs in aqueous solution, a novel family of PPEs was designed and synthesized. The introduction of methylene carboxylate side groups significantly suppressed the aggregation of PPEs in H_2O, resulting in outstanding photophysical properties. In an application of dye-sensitized solar cell, the non-aggregated PPEs in solution led to non-aggregated PPEs chains on surface, confirmed by AFM images. A fluorescent sensor for mercury ions was developed based on **P4**/rhodamine system.

Last, a new family of cationic methylene ammonium substituted PPEs was designed and synthesized. The excellent photophysical properties supported our promise that the methylene ammonium side groups can suppress the aggregation of PPEs, similar to methylene carboxylate groups. By taking advantage of their remarkable photophysical properties, a fluorescent sensor for ATP was developed and could be applied as a potential fluorescence assay for phosphatase (ALP) in the future.

CHAPTER 1
INTRODUCTION

Conjugated Polyelectrolytes

In the past decades, conjugated polymers including poly(phenylene ethynylene) (PPE), poly(phenylene vinylene) (PPV), polythiophene (PT), polyfluorene (PF) and poly(*para*-phenylene) (PPP) (Figure 1-1) have been extensively studied. Many applications have been developed owing to their unique properties such as high conductivity, charge transport and π-electron polarization.[1-5]

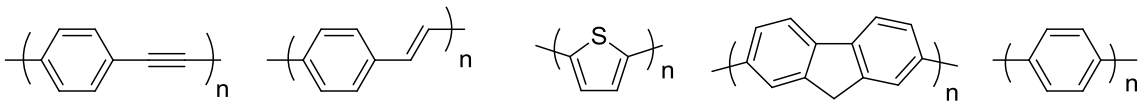

Figure 1-1. Structures of different conjugated polymers (PPE, PPV, PT, PF, PPP).

Conjugated polyelectrolytes (CPEs) are conjugated polymers with ionic functional groups such as sulfonate (SO_3^-), carboxylate (CO_2^-), phosphate (PO_3^{2-}) and ammonium (NR_3^+). Some examples are shown in Figure 1-2. The π-conjugated backbone defines the optical and electronic characteristics of the polymers. The pendant ionic solubilizing groups provide the polymers with solubility in polar solvents, including methanol and water.[6,7] Since the first anionic PPV-type CPE developed by Whitten, Wudl, and co-workers in 1999,[8,9] extensive studies have been performed by many scientists over the world to develop a variety of applications such as organic light emitting diodes (OLEDs),[10-12] field effect transistors (FETs),[13] dye-sensitized solar cells (DSSCs),[14-16] antibacterial materials[17-23] and chemo- and biosensors.[24,25]

Poly(phenylene ethynylene)s (PPEs) comprise one of the most important types of CPEs, and receive considerable attentions due to their remarkable fluorescence properties and facile synthesis based on palladium catalyzed Sonogashira cross

coupling reaction.[7,26-28] PPEs possess the unique electronic and optical properties which arise from the conjugated polymer backbone and good solubility in water. For example, the interplay between the hydrophilic ionic side groups and the hydrophobic conjugated polymer backbone affords PPEs with amphiphilic character and ability to form supra-structures. As a result, many studies have explored the self-assembly of PPEs in solution to form nanoscale colloidal aggregates as well as solid-liquid interfaces to form self-assembled layer-by-layer (LbL) films.[7,29,30] In addition, the ionic side groups enable PPEs to bind strongly to ionic species by electrostatic interactions. Many fluorescent sensors have been developed based on PPEs, such as trinitrotoluene sensors,[31-34] mercury sensors,[35,36] DNA sensors,[37-39] and enzyme assays.[18,40,41]

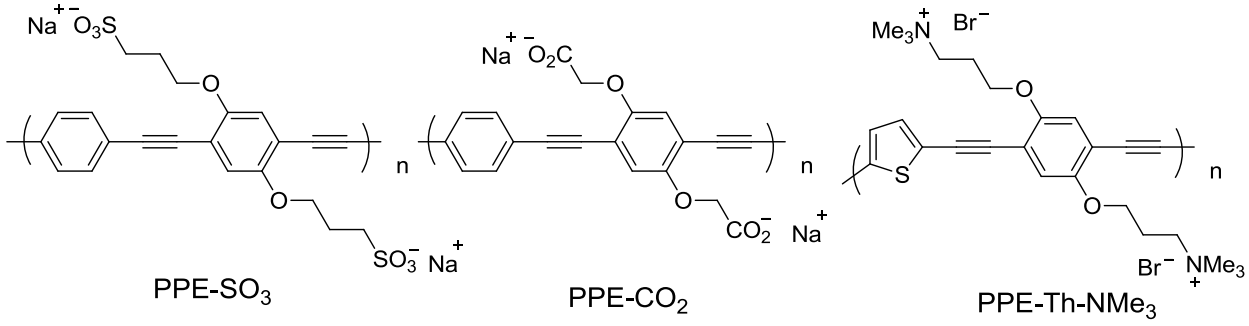

Figure 1-2. Structures of ionic conjugated polyelectrolytes.

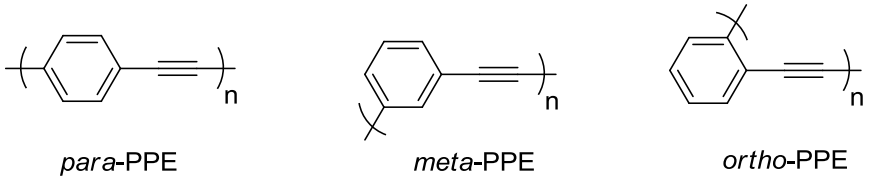

Figure 1-3. Structures of *para*-, *meta*- and *ortho*-PPE.

Based on the man chain conformation, PPEs can be divided into three categories: *para*-, *meta*- and *ortho*-poly(phenylene ethynylene)s (Figure 1-3). While *meta*- and *ortho*-PPEs exist as helical conformations,[42,43] *para*-PPEs adopt a linear rigid-rod structure.[44,45] The PPEs discussed in this dissertation are mainly *para*-PPEs.

Synthesis of Poly(phenylene ethynylene)s

Pd-Catalyzed Sonogashira Reaction

As well-known in literatures, the most common synthetic method to prepare poly(phenylene ethynylene)s is Pd-catalyzed Sonogashira cross coupling reaction between terminal alkynes and terminal iodides or bromides. The use of CuI as a co-catalyst enables the reaction to occur at a lower temperature or even at room temperature. In addition, the Sonogashira reaction can be carried out in both organic solvents and aqueous solutions, which provides a way to prepare the desired compounds with a variety of functional groups in mild and compatible conditions.

The mechanism of Sonogashira reaction has not been clearly understood yet, and the general accepted mechanism pathway includes a palladium cycle and a copper cycle as shown in Figure 1-4.[46] In the palladium cycle, the active catalyst, 14-electron Pd^0L_2 is either commercially available as $Pd(PPh_3)_4$ or generated from a palladium (II) source such as $Pd(PPh_3)_2Cl_2$ by reduction. Then the oxidative addition happens between the aryl iodide or bromide with Pd(0) center. The next step in the Pd-cycle would connect with the cycle of copper co-catalyst. Then a usually rate-determining transmetallation from copper acetylide to Pd center generates the $R^1Pd(-C\equiv C-R^2)L_2$ specie. The final coupled alkyne is produced by reductive elimination after trans/cis isomerization and the catalyst is regenerated. The second copper cycle is still poorly understood. It is suggested that the presence of base (usually amine) results in the formation of a Cu-alkyne complex, which makes the terminal proton on the alkyne more acidic. The abstraction of the proton by the amine leads to the formation of copper acetylide.

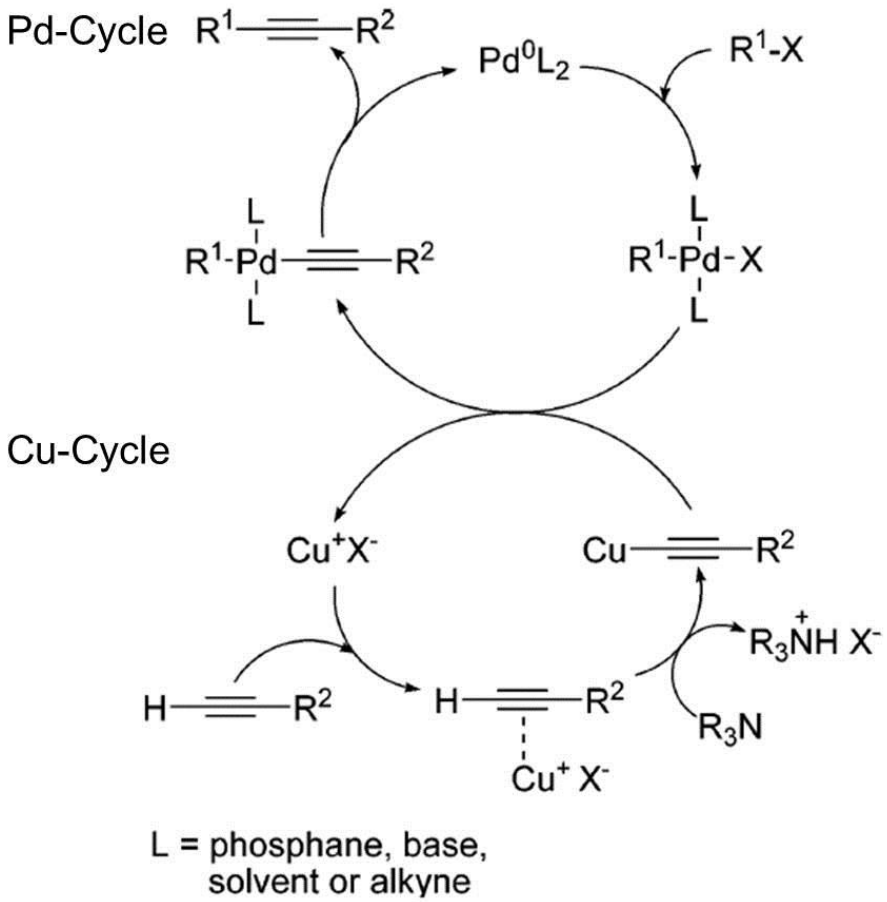

Figure 1-4. Mechanism of Sonogashira reaction.

Direct Synthetic Approach for PPEs

PPE-type conjugated polyelectrolytes are generally prepared by the same methods used to synthesize the non-ionic PPEs. The most important distinction is the timing and method for incorporation of the ionic units. In general, two different well-known approaches have been used in the literatures. The first, which we refer to as the "direct approach" involves the direct polymerization of ionic monomers to afford the PPE-type conjugated polyelectrolytes (Figure 1-5A). This method has some advantages, and the polyelectrolyte is prepared directly from the ionic monomers. However, a big disadvantage of the approach is that it is much more difficult to apply gel permeation

chromatography (GPC) to determine the relative molecular weight of the resulting CPE sample. Molecular weight determination of water soluble, amphiphilic polymers by GPC is difficult because it requires special columns and instrumentation compatible with the aqueous mobile phase. In addition, the tendency of CPEs to aggregate in aqueous solution can further complicate the molecular weight and polydispersity analysis.

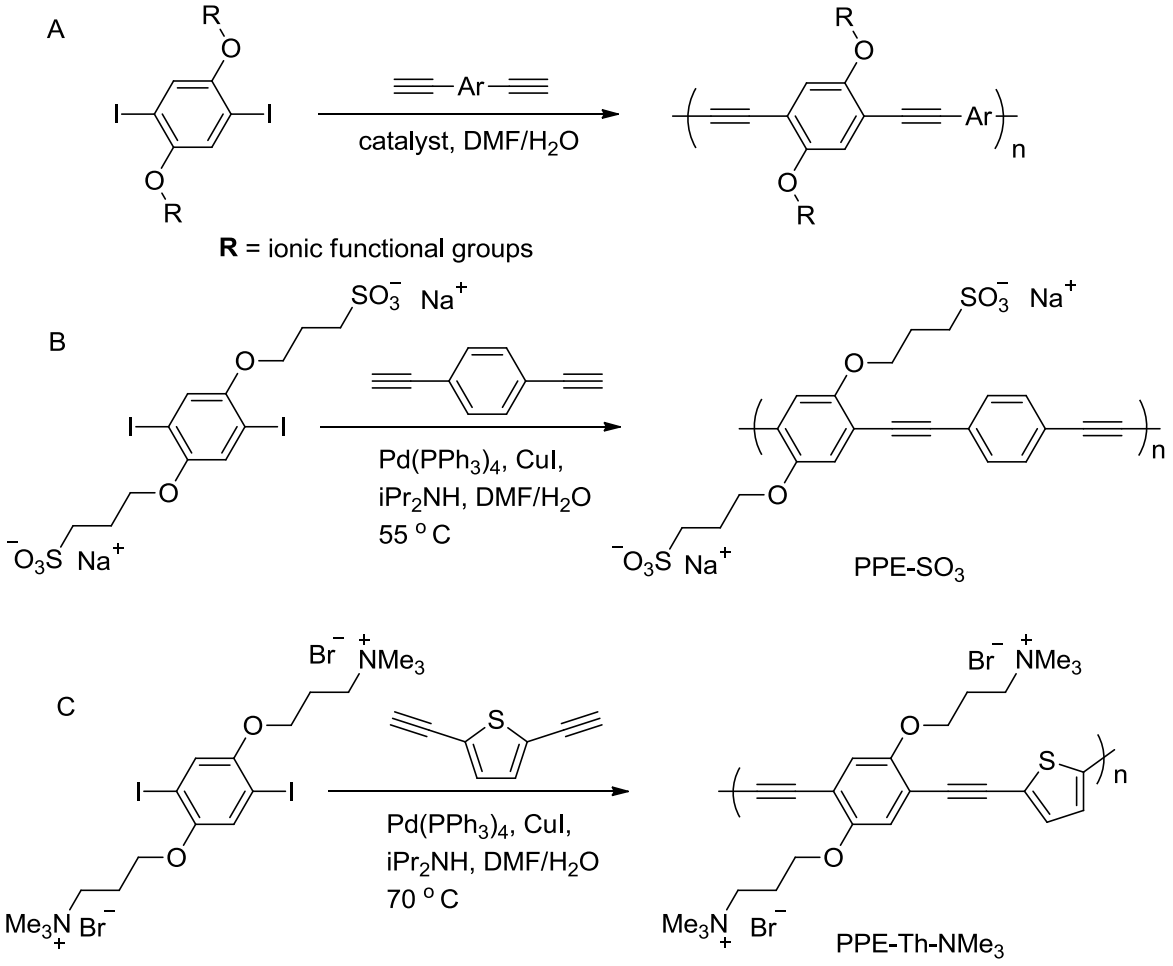

Figure 1-5. Direct synthetic approach for PPE-type CPEs. (A) General direct approach; (B) Synthesis of PPE-SO_3; (C) Synthesis of PPE-Th-NMe_3.

Most early studies of conjugated polyelectrolytes and their synthesis relied on preparations that followed the direct approach (Figure 1-5). Here we provide some examples of PPEs that were prepared by the direct route. Pinto, Tan and Schanze were

the first who reported the synthesis of an anionic CPE featuring a PPE backbone (PPE-SO_3, Figure 1-5B).[6] By using a direct approach, the anionic alternating polymer PPE-SO_3 was prepared in a Sonogashira coupling reaction between a bis-sulfonate 1,4-diiodobenzene monomer and 1,4-diethynylbenzene. The reaction was carried out in aqueous/DMF solution, with a Pd/Cu catalyst system in the presence of diisopropylamine as a base. The relative molecular weight of PPE-SO_3 was determined by intrinsic viscometer and it was found that the behavior of the polymer was corresponding to ~ 200 repeat units.[47] In a further study, Schanze and co-workers reported a direct approach to prepare the cationic poly(arylene ethynylene) (PPE-Th-NMe_3) which featured a backbone that alternated thiophene ethynylene and phenylene ethynylene repeat units.[18] The polymerization of the cationic trimethylammonium substituted 1,4-diiodobenzene with 2,5-diethynylthiophene was carried out in aqueous/DMF solution via Sonogashira reaction. The resulting polymer PPE-Th-NMe_3 was purified by dialysis using an 8 kD molecular weight cut-off membrane. The molecular weight of the cationic polymer was not determined.

Precursor Approach for PPEs

The second approach which has been widely used was referred to as the "precursor approach" (Figure 1-6).[24,48-50] In this approach, the monomers used in the polymerization are uncharged because the ionic units are protected or masked; thus polymerization leads to a conjugated polymer precursor which is soluble in organic solvents. In the next step, the ionic groups are de-protected by base-assisted hydrolysis for the esters or acid-assisted hydrolysis of the BOC groups. Despite the extra synthetic step, the precursor approach has several distinct advantages. First, the precursor polymer is uncharged and soluble in organic solvents, which allows determinations of

the molecular weight and polydispersity by standard GPC. Second, high resolution ^{1}H and ^{13}C NMR spectroscopy can be applied for structural and end-group analysis because of the better solubility of the precursor in organic solvents. The previous experience showed that ^{1}H NMR signals of PPEs in aqueous solvents typically appeared as broad lines, due to the slow rotational and translational diffusion of the chains and the possible aggregation.

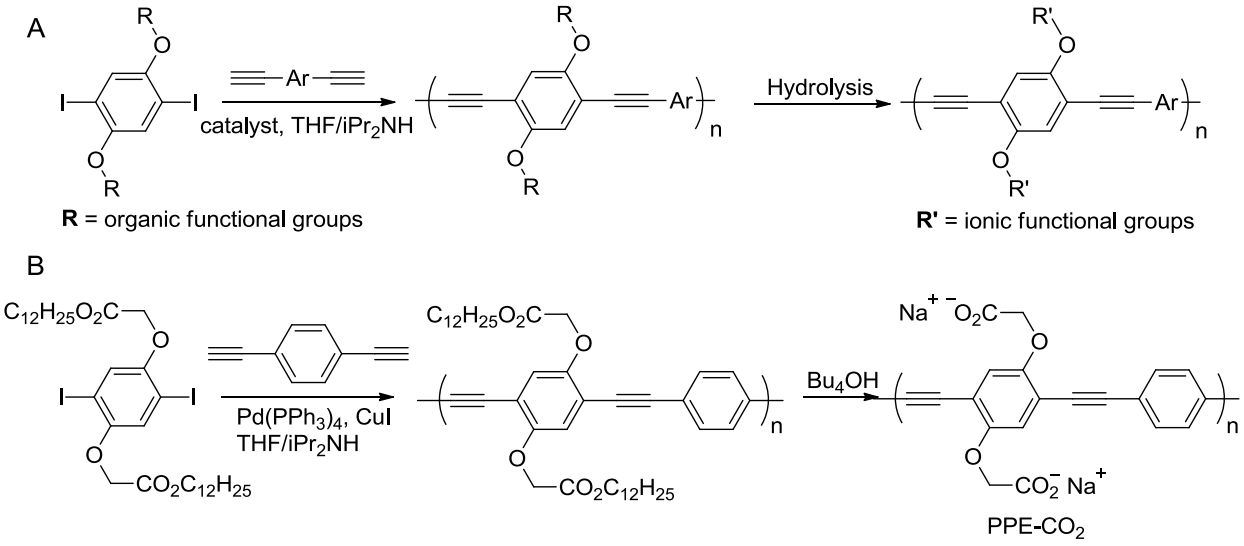

Figure 1-6. Precursor approach for synthesis of PPE-type CPEs. (A) General precursor approach; (B) Synthesis of PPE-CO_2.

A variety of PPEs have been prepared by the precursor route. In most cases, the precursors feature ester (for anionic) or alkyl bromide (for cationic) functionality that can be easily converted to the ionic form in high yield by the follow up reaction. A prototypical example of the use of the precursor approach to synthesize PPE-type CPE is shown in Figure 1-6B. The polymer PPE-CO_2 is prepared by Sonogashira polymerization of a dodecyl ester protected 2,5-dicarboxy-1,4-diiodobenzene monomer with 1,4-diethynylbenzene. The precursor polymer is very soluble in organic solvents, due to the presence of the long dodecyl chains. The molecular weight and

polydispersity are characterized by GPC. The subsequent base-assisted hydrolysis of the ester groups using tetrabutylammonium hydroxide (Bu_4OH) gives rise to the water-soluble PPE-CO_2. In a detailed study, Zhao and Schanze reported the synthesis of a series of PPE-CO_2 with different molecular weight using an end-cap strategy.[50] The series of end-capped ester polymers were analyzed by GPC. The molecular weights obtained from the GPC analysis were compared to those obtained by ^{1}H NMR spectra analysis. It was found that the GPC method systematically overestimates the degree of polymerization by a factor of ~ 1.5 compared to NMR method.[50]

Amplified Quenching Effects

Most of interest related properties and applications of PPEs are associated with the observation of efficient fluorescence quenching at low quencher concentration, which is also referred to as super quenching or amplified quenching.[51,52] The increased sensitivity arises from the ability of a conjugated polymer to serve as a highly efficient transport medium. Conjugated polymers transport excited states, which are referred to as quasiparticles called excitons. Excitons in the conjugated polymer are highly mobile and can diffuse throughout the polymer chains. Before discussing the amplified quenching effects in more details, it is necessary to briefly review the mechanisms for the fluorescence quenching.[53]

Stern-Volmer Fluorescence Quenching

$$\mathrm{F}^* + \mathrm{Q} \xrightarrow{K_q} \mathrm{F} + \mathrm{Q} \tag{1-1}$$

$$\mathrm{F} + \mathrm{Q} \underset{\rightleftharpoons}{K_a} [\mathrm{F},\mathrm{Q}] \xrightarrow{hv} [\mathrm{F}^*,\mathrm{Q}] \rightarrow \mathrm{F} + \mathrm{Q} \tag{1-2}$$

$$I_0/I = 1 + K_{sv}[Q] \tag{1-3}$$

In Equations 1-1 and 1-2, F* is an excited-state chromophore, Q is a quencher molecule, k_q is the bimolecular quenching rate constant, and K_a is the association constant for the ground-state complex formation [F, Q]. Treatment of the fluorescence quenching data with the Stern-Volmer method yields to the Equation 1-3, where I_0 is the fluorescence intensity without a quencher, I is the fluorescence intensity in the presence of a quencher, and K_{sv} is the Stern-Volmer quenching constant. Fluorescence quenching can occur by two different mechanisms, namely dynamic quenching and static quenching. The dynamic quenching (Equation 1-1) is a diffusive process in which the excited-state chromophore encounters the quencher molecule and the fluorescence is quenched. In the static quenching mechanism, the quencher is bound to the chromophore. Once generated, the excited state is immediately and quantitatively quenched (Equation 1-2). In the case of dynamic quenching, K_{sv} is equal to $k_q\tau_0$, where τ_0 is the fluorescence lifetime of F*. On the other hand, $K_{sv} = K_a$, if quenching is dominated by the static mechanism. The fluorescence lifetime is independent on the quencher concentration. In static quenching or dynamic quenching, the Stern-Volmer plots of I_0/I versus [Q] should be linear according to Equation 1-3. However, in most cases, the Stern-Volmer plots are curved upward. This can be explained by a lot of complex processes, such as variation in the association constant with quencher concentration, mixed dynamic and static quenching mechanism, and chromophore aggregation.

Molecular Wire Effects

The concept of “amplified quenching” in conjugated polymers was first described by Swager and co-workers in 1995.[51] To study the amplified quenching effects, fluorescence quenching of a cyclophane-containing poly(phenylene ethynylene) and an

oligo(phenylene ethynylene) by methyl viologen (MV^{2+}) was compared. Methyl viologen (MV^{2+}) is a well-known electron transfer quencher and can bind to the cyclophane unit, thus the fluorescence of the polymer was efficiently quenched. This study also showed that the fluorescence of the polymer was quenched about 60 times more efficiently compared to the oligomer (Figure 1-7).

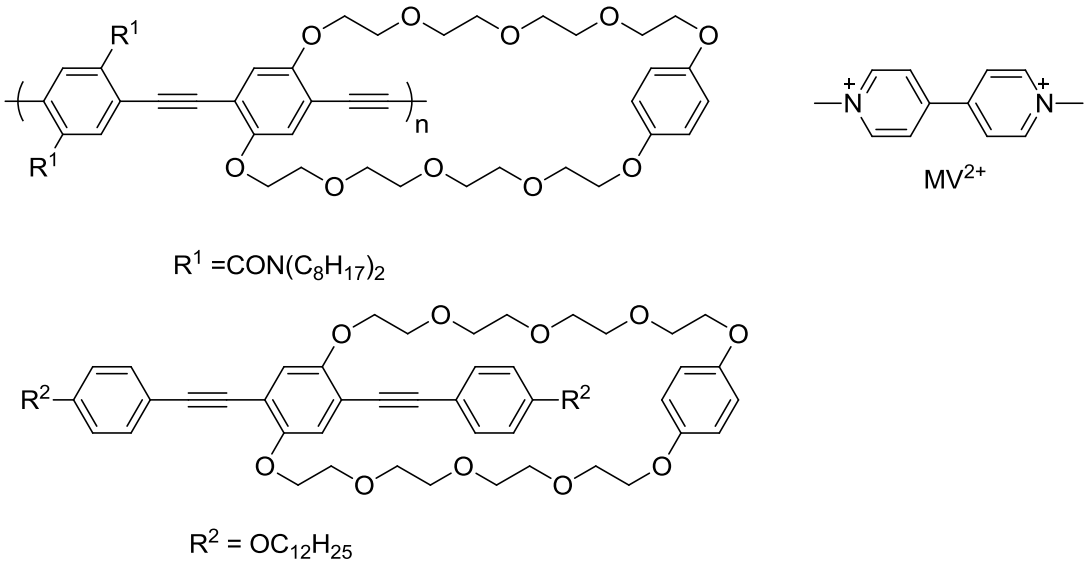

Figure 1-7. Structure of polymer, oligomer and quencher (MV^{2+}) studied by Swager's group.[51]

In the mono-receptor system (oligomer), the fluorescence is quenched only for the receptor forming complex with methyl viologen. In contrast, the fluorescence of the entire polymer chain will be quenched once one or several units are occupied by the quencher. The amplified quenching effect in the conjugated polymers is attributed to the molecular wire effect via exciton delocalization and transport by the polymer chain (Figure 1-8). Upon excitation, an exciton (a bound electron-hole pair) is generated on the polymer backbone. The conjugated polymer acts as a conduit wire for the exciton, allowing it to migrate rapidly along the chain. When the exciton reaches a repeat unit that is occupied by a quencher, it is quenched. Because of the extremely efficient

exciton migration, a single quencher bound to one receptor unit can quench many repeat units in the polymer chain, leading to the amplified response to the target analyte.

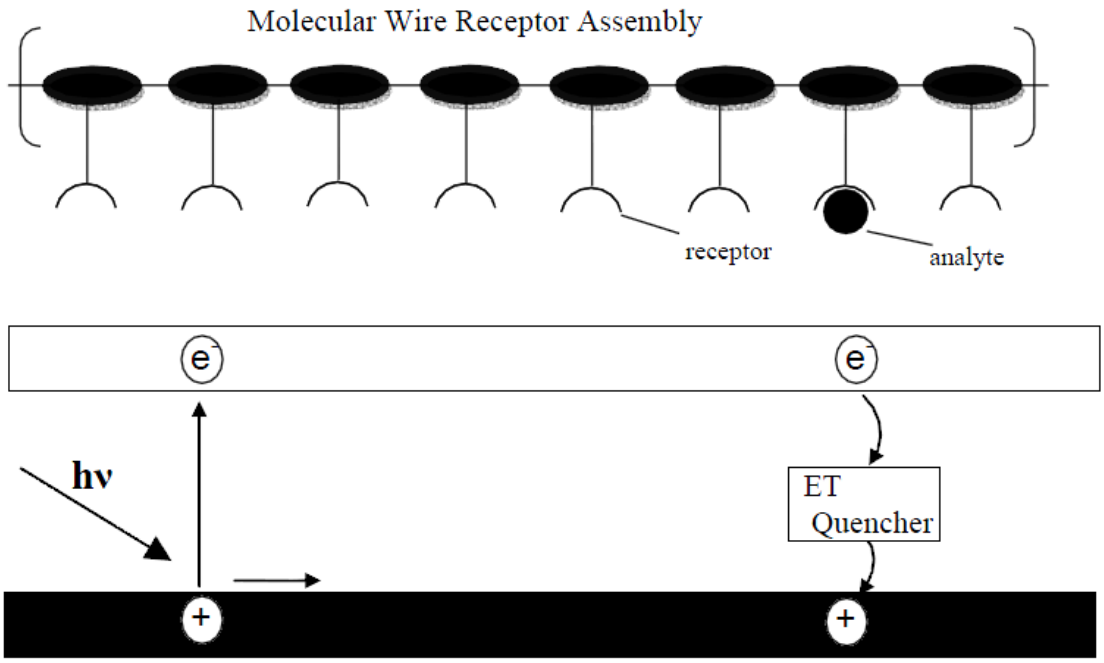

Figure 1-8. Quenching mechanism of molecular wire effect in conjugated polymers. Reprinted with permission from Zhou *et al*.[51]

Amplified Fluorescence Quenching in Conjugated Polyelectrolytes

The amplified quenching effect in CPEs was first reported by Whitten and co-workers in the investigation of the fluorescence quenching of MPS-PPV by MV^{2+} (Figure 1-9A).[9] The fluorescence of MPS-PPV solution (10 μM) was quenched by MV^{2+} (100 nM) very efficiently, with an extremely large K_{sv} value ~ 1.7 x 10^7 M^{-1}(Figure 1-9B). The negatively charged polymer formed complex with MV^{2+}, driven by the electrostatic interaction. The quenching effects were amplified by the ability of this CPE to allow excitons diffuse rapidly and efficiently within the polymer chains. In addition, the distinct

red shift in absorption spectrum indicated that other mechanism may also be present such as quencher induced aggregation of the polymer chains.[9]

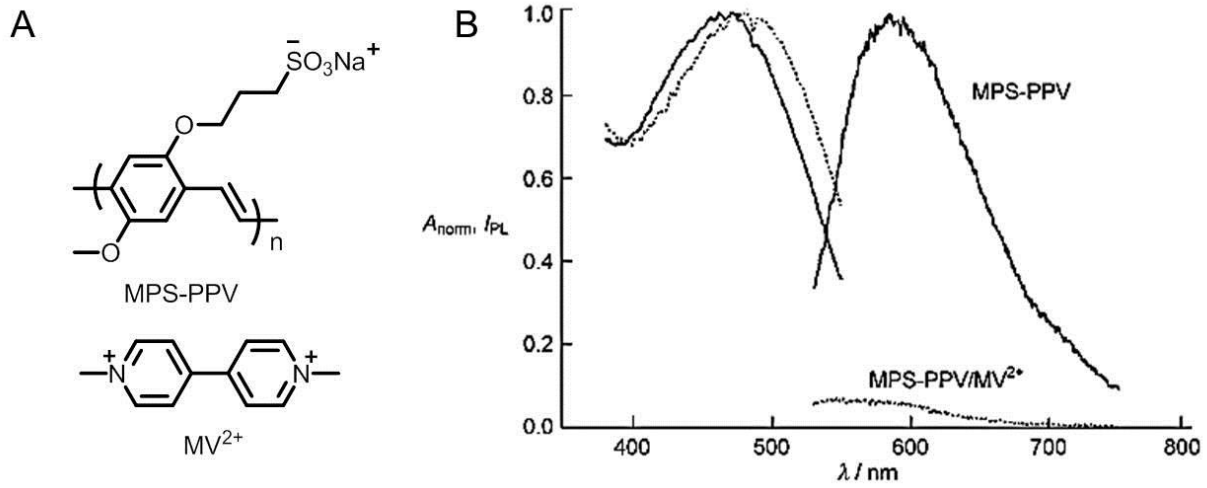

Figure 1-9. (A) Structures of MPS-PPV and quencher (MV^{2+}). (B) Absorption and fluorescence spectra of MPS-PPV in water in the presence (dotted line) or absence (solid line) of 100 nM MV^{2+}. Reprinted with permission from Chen *et al*.[9]

Side Group Effects on Aggregation of PPEs

The photophysical properties of PPEs have been extensively studied in different solvents. In general, their optical properties are determined by the chemical and electronic structure of the conjugated backbone. Similar absorption and fluorescence spectra are usually obtained for PPEs, because they have the same phenylene ethynylene backbone. However, their photophysical properties can be strongly dependent on the solvent, because of the hydrophobic backbone and hydrophilic side groups. PPEs with ionic side groups such as sulfonate (SO_3^-), carboxylate (CO_2^-) or alkyl ammonium (NR_3^+) are molecularly dissolved in methanol. However, PPEs exist as aggregates in water solution, due to the hydrophobic interaction and π-π stacking effect.[6,54] Although the aggregation sometimes brings positive effects including

enhanced response for analytes sensing, it also results in poor solubility, low fluorescence quantum yield, broad and weak emission. Therefore, significant efforts have been put forward to reduce the aggregation of PPEs by changing different side groups.

Linear Side Group

Tan and Schanze reported the first water-soluble PPE with anionic side groups (PPE-SO_3, Figure 1-5B) in 2002.[6] In order to obtain the conformational information, the absorption and fluorescence properties of PPE-SO_3 were investigated in water, methanol and water/methanol (1:1) mixture.

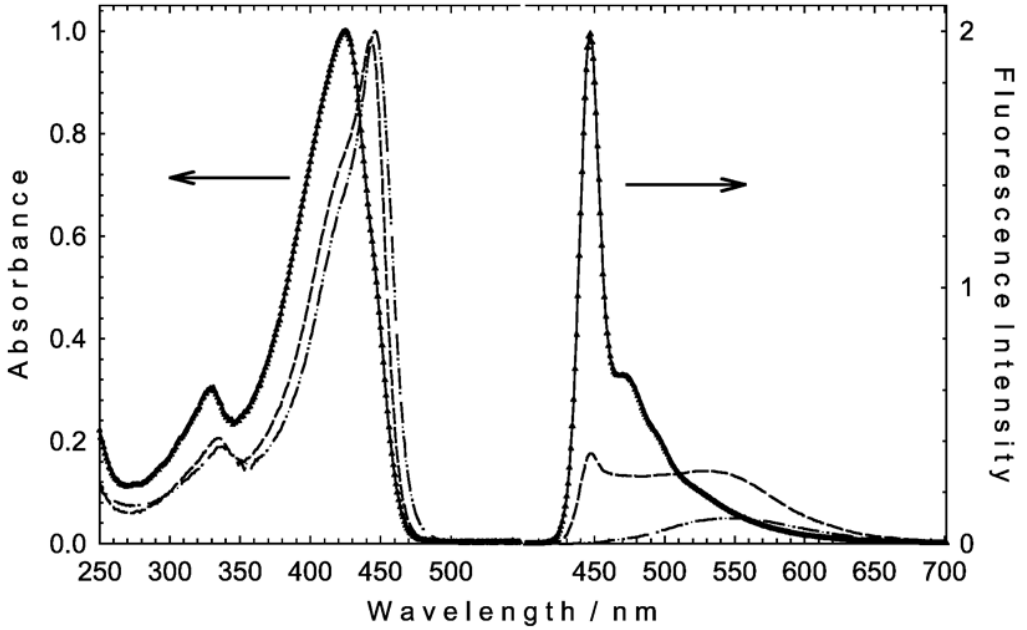

Figure 1-10. Absorption (left) and fluorescence (right) spectra of PPE-SO_3 in MeOH (solid line), H_2O (dashed line), and H_2O/MeOH (1:1) (dash dot line). Fluorescence spectra are area normalized to reflect relative quantum yields. Reprinted with permission from Tan *et al*.[6]

As shown in Figure 1-10, the absorption spectrum gradually shifted to the longer wavelength as the ratio of water increased. The solvents effect was more pronounced in the fluorescence spectra. In pure MeOH, the fluorescence of PPE-SO_3 was sharp,

structured with a maximum ~ 450 nm. Upon the introduction of water, the fluorescence intensity decreased significantly and a broad “excimer-like” band showed up at a longer wavelength ~ 550 nm. In MeOH, PPE-SO_3 existed as “molecularly dissovled” polymer chains with photophysical properties similar to non-ionic PPEs in organic solvents like THF or $CHCl_3$.[55] However, PPE-SO_3 was believed to aggregate in aqueous solution, driven by the hydrophobic interaction and π-π stacking interaction between adjacent polymer chains.[56-58] The decreased fluorescence intensity and the red-shift to longer emission wavelength were attributed to the formation of aggregates, which had lower energies and longer radiative lifetimes. In addition, the fluorescence quantum yield was very low ~ 0.04 in aqueous solutions. Similar aggregation behaviors are observed for PPEs with linear cationic or anionic side groups.[47]

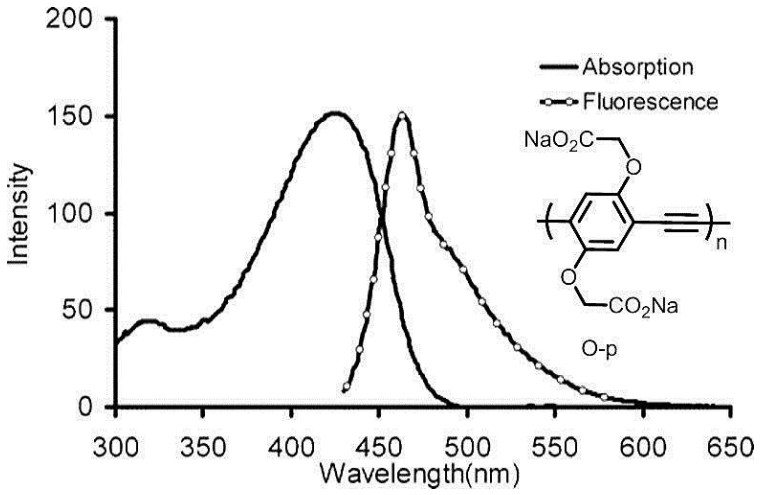

Figure 1-11. Normalized absorption and emission spectra of polymer O-p in water. Reprinted with permission from Kim *et al*.[59]

In order to reduce the aggregation, Schanze and co-workers reported a homopolymer O-p with two linear carboxylate side groups per benzene.[60,61] By increasing the functional group density, the aggregation tendency in aqueous solution seemed to be reduced, resulting in a emission similar to that in MeOH. In addition,the

fluorescence quantum yield was improved to ~ 0.08. This work was repeated by Bunz and co-workers in 2005 and a similar result was observed (Figure 1-11).[59]

Branched Side Group

Aggregation of PPEs in aqueous solution can be avoided by incorporating branched side groups. Hecht and co-workers reported a poly(phenylene ethynylene) featuring branched oligo(ethylene glycol) side chains (PPE-OEG, Figure 1-12) with a surprisingly high quantum yield in aqueous solution ~ 0.43.[62]

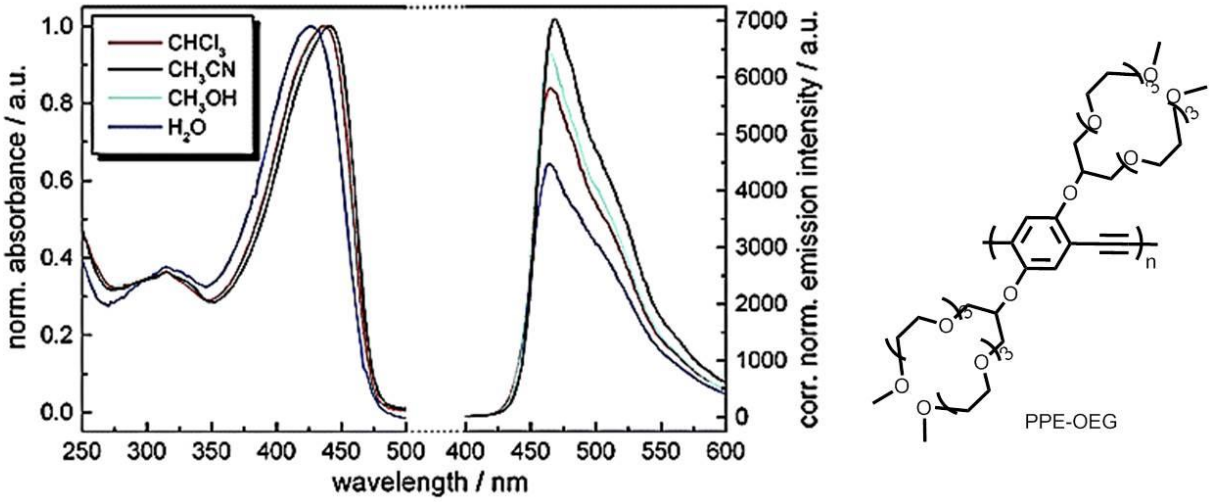

Figure 1-12. Absorption and fluorescence spectra of PPE-OEG in various solvents. Absorption spectra are scaled to the same optical density, while emission spectra are corrected according to quantum yield. Reprinted with permission from Khan *et al*.[62]

This non-ionic PPE was soluble in both organic solvents, including $CHCl_3$, CH_3CN, and polar solvents like MeOH and H_2O. The fluorescence of PPE-OEG in aqueous solution was similar to those in organic solvents with a slightly lower fluorescence quantum yield. By introduction of the branched oligo(ethylene glycol) side chains, aggregation of PPE-OEG was efficiently suppressed. Based on this discovery,

PPEs with branched oligo(ethylene glycol) side chains have been synthesized and used in the area of DNA detection.[39,63,64]

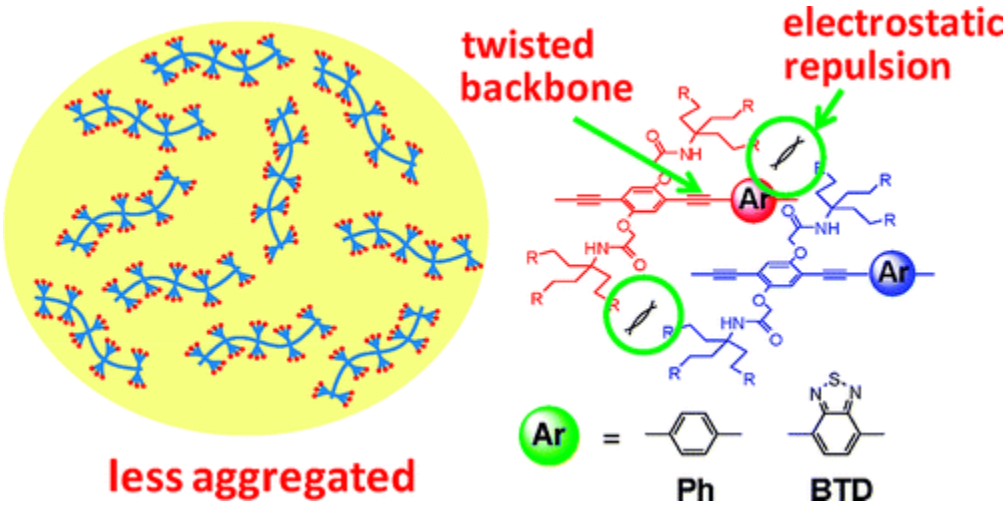

Figure 1-13. Structures of CPEs with polyionic side groups. R = CO_2^- or NH_3^+. Reprinted with permission from Lee *et al*.[48]

Recently, Schanze and co-workers reported a set of poly(arylene ethynylene)s featuring branched polyionic side groups.[24,48] The new series of CPEs consisted of different arylene-ethynylene backbone including phenyl and 2,1,3-benzothiadiazole (Figure 1-13). These bulky and highly charged functional groups increased the electrostatic repulsion between adjacent polymer chains and twisted the backbone, effectively decreasing the hydrophobic interaction and π-π stacking interaction. The presence of these large ionic groups also significantly enhanced the solubility of CPEs in aqueous solution. Figure 1-14B shows the absorption and fluorescence spectra of PPE-NH_3 in methanol and water. PPE-NH_3 showed a negligible change in absorption spectrum with a maximum at 405 nm in water, the same as that in methanol. The fluorescence quantum yield was lower ~ 0.13 in aqueous solution.

In summary, significant efforts have been made to reduce the aggregation of PPE in aqueous solution by introducing bulky and highly charged side groups. Most

PPEs with branched side groups maintain the structured emission with an improved emission quantum yield in aqueous solution. However, the synthesis efforts needed for the branched side groups are usually tough and time-consuming, which limit the application.

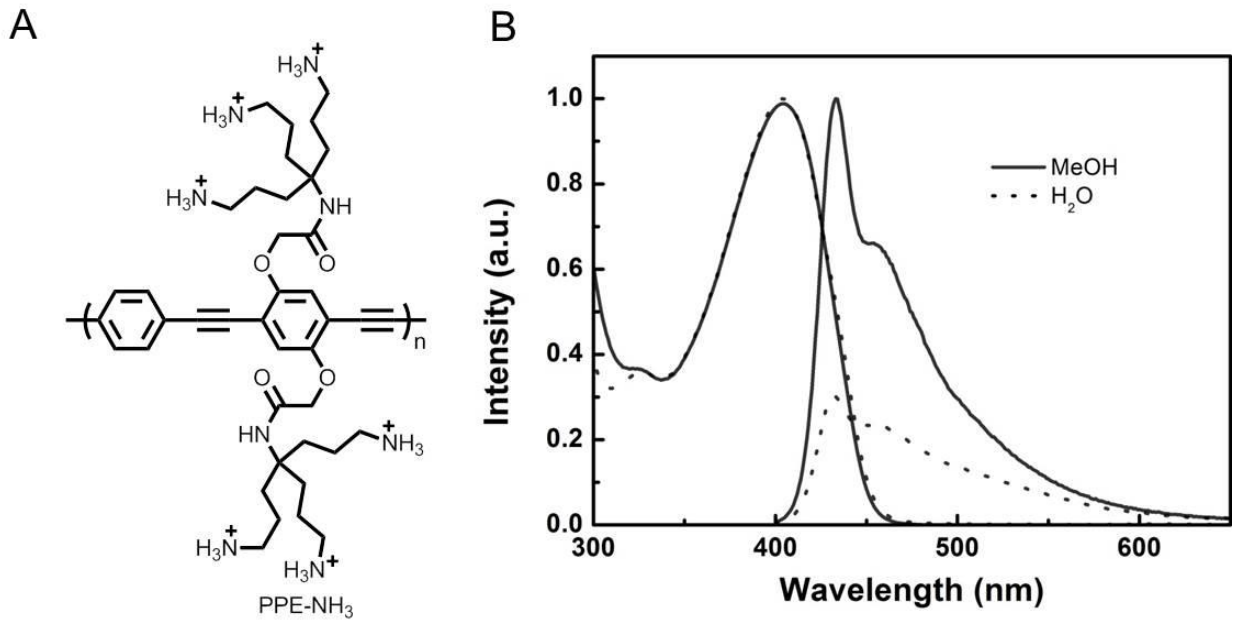

Figure 1-14. (A) Structure of PPE-NH_3. (B) Absorption and fluorescence spectra of PPE-NH_3 in methanol and water. [PPE-NH_3] = 4 μM. Reprinted with permission from Zhao *et al*.[24]

Fluorescence Correlation Spectroscopy

In order to obtain the direct information of polymer size, dynamic light scattering (DLS) was initially applied. However, under the experiment conditions like millimolar concentration, PPEs tend to form aggregates in aqueous solution, which makes the results complicated and not trustable. In 1972, fluorescence correlation spectroscopy (FCS) was first reported by Webb and co-workers in a study of DNA-drug intercalation.[65] Similar to the dynamic light scattering (DLS) technique, FCS is based on the statistical analysis of spontaneous fluorescence fluctuations. This method is very

sensitive to polymers or materials with fluorescence at very low concentrations such as micromolar even nanomolar concentrations.[66] FCS can provide useful information such as diffusion constants, hydrodynamic radius, and conformational changes. In addition, it is an ideal approach to investigate the thermodynamics and kinetics of molecular interactions.[67-69]

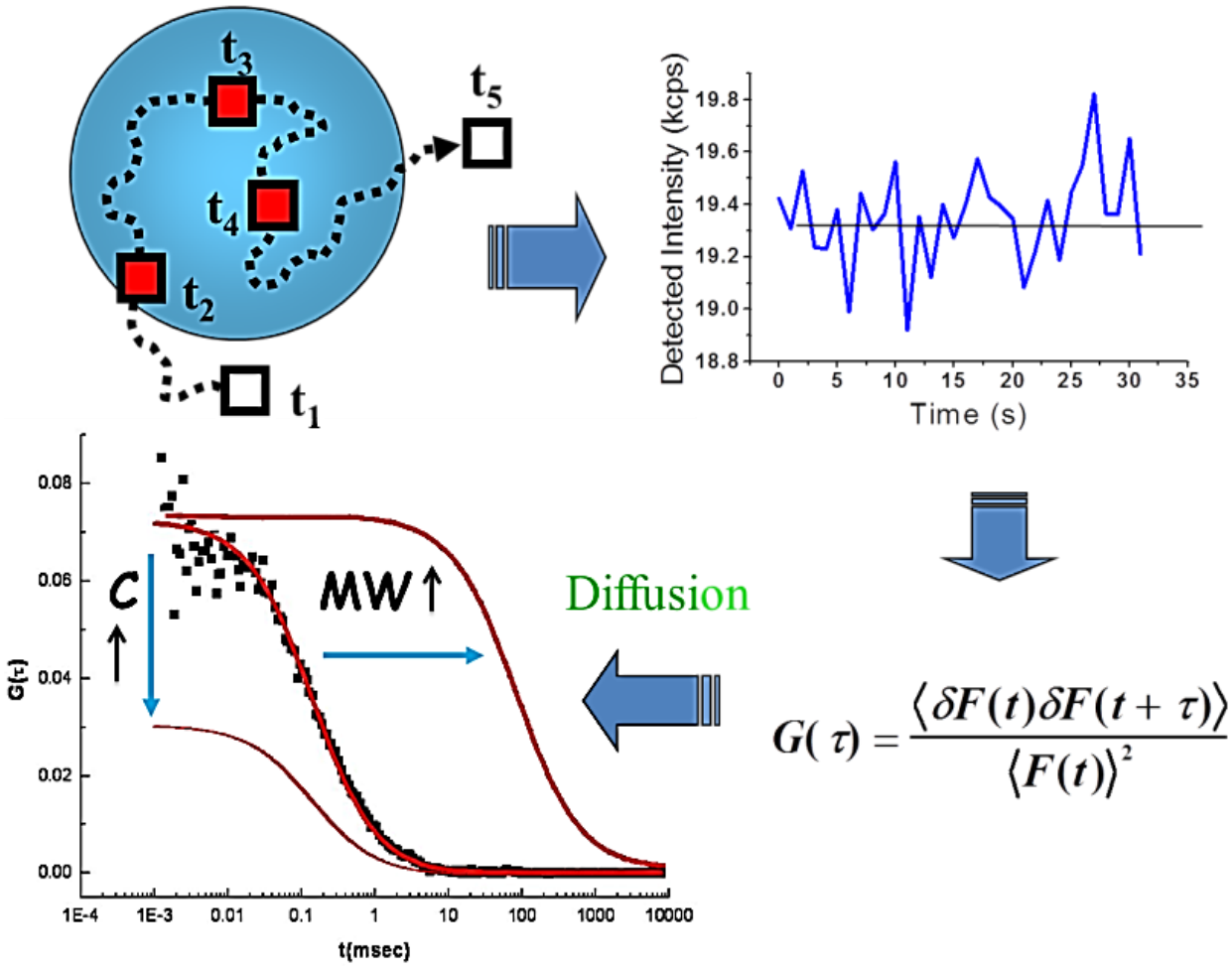

Figure 1-15. Working principles of fluorescence correlation spectroscopy.

FCS analysis calculates a correlation function from the time dependent intensity fluctuations of fluorescent particles observed by confocal microscopy. As shown in

Figure 1-15, the detector records the emission fluctuations from fluorescent particles moving in and out of a femtoliter confocal volume formed by a focused laser beam.

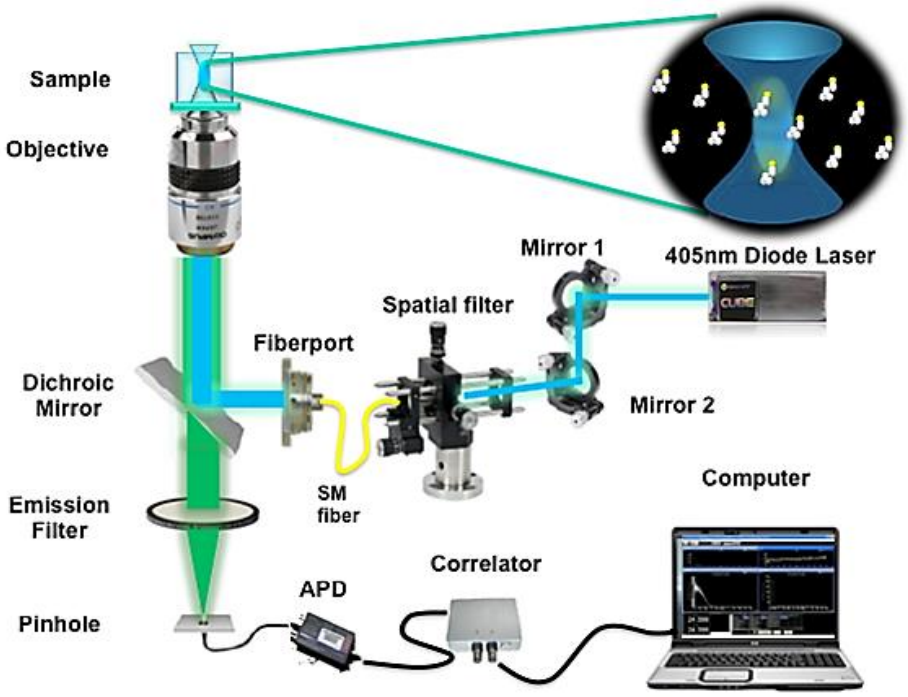

Figure 1-16. Setup of FCS system in our lab.

The fluorescence intensity fluctuates, due to Brownian motion, which can provide the useful information including conformational change and molecular weight change.[70,71] After an auto correlation function $G(\tau)$ is applied, the data are transformed into a correlation curve. Two major results can be obtained from this correlation curve: the diffusion time which is defined by the temporal autocorrelation; and the average number of fluorescent particles in the detection volume which is calculated from the variance of the intensity. Larger molecules usually diffuse slowly thus feature longer diffusion time, resulting in a correlation curve at longer time. In addition, the values of $G(\tau)$ decrease as the number of particles in the volume increase. Therefore, FCS has been used extensively to determine sample concentrations, diffusion coefficients and

rate constants related to rotation and translation, and some other important parameters in biophysics and chemistry.[72]

Sensor Applications

Over the past several years, the use of PPEs as chemo- or biosensor has been the subject of considerable research interest. Numerous sensor systems based on PPEs have been developed for various analytes, including metal ions, biomolecules,[24,25] proteins,[60] enzymes[18,41,73] and nucleic acids.[38,39,74] Compared to the conventional sensory methods, the fluorescence sensors based on PPEs have several advantages. First, PPEs are water-soluble and bio-compatible. Second, the amplified quenching effects of PPEs provide the sensors with high sensitivity. Third, the measurement of fluorescence is easy and convenient.

In general, PPE-based fluorescent sensors can operate either in “turn-off” or “turn-on” modes. In the turn-off mode, the polymer is fluorescent without quencher, and upon addition of the analyte, the polymer fluorescence is quenched. By contrast, in the turn-on mode, the addition of the analyte recovers the fluorescence of the polymer. Most PPE-based fluorescence sensors utilize one of the following mechanisms: photo-induced electron transfer, Förster energy transfer (FRET) and conformational change (including analyte-induced aggregation quenching mechanism). Since these three mechanisms are not independent, some sensors systems utilize more than one mechanism.

Small Ion Sensing

Many fluorescence sensors based on PPEs have been developed for small ions including Hg^{2+} and pyrophosphate (PPi). In a study reported by Schanze and co-workers in 2008, it was found that the fluorescence of the polymer PPE-CO_2 (Figure 1-2)

was selectively quenched by Cu^{2+} in aqueous solution with a K_{sv} ~ 2.5 x 10^6 M^{-1}.[25] Several other divalent metal ions including Ca^{2+}, Mn^{2+}, Co^{2+}, Ni^{2+}, Zn^{2+} and Hg^{2+} were tested and none of them was able to induce significant fluorescence quenching as shown in Figure 1-17A.

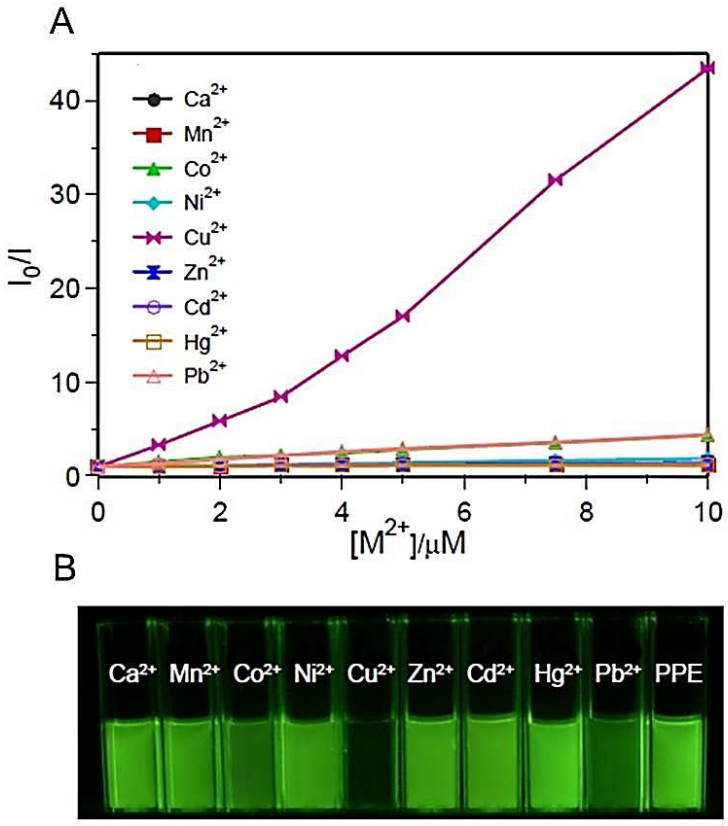

Figure 1-17. (A) Stern-Volmer plots of PPE-CO_2 (5 μM) with different metal ions (M^{2+}) in HEPES buffer solution (0.01 M, pH 7.5). (B) Photography of solutions of PPE-CO_2/M^{2+} (5 μM/10 μM) illuminated with a UV-lamp. Reprinted with permission from Zhao *et al*.[25]

A photography of PPE-CO_2 (5 μM) with different metal ions (10 μM) under the illumination of a UV lamp is shown in Figure 1-17B. Clearly, the polymer solution containing Cu^{2+} was dark, which indicated that the fluorescence of PPE-CO_2 was quenched. It was also found that the quenched fluorescence of PPE-CO_2 can be recovered upon addition of small ion pyrophosphate (PPi).[25] Figure 1-18 shows the

proposed sensing mechanism for PPi based on PPE/Cu^{2+} complex. The fluorescence was first quenched by the introduction of Cu^{2+} via the photo-induced electron transfer mechanism. Upon addition of PPi, which can chelate Cu^{2+} from polymer chains, the fluorescence of the polymer was recovered. Therefore, a turn-on fluorescence sensor for PPi was successfully developed.

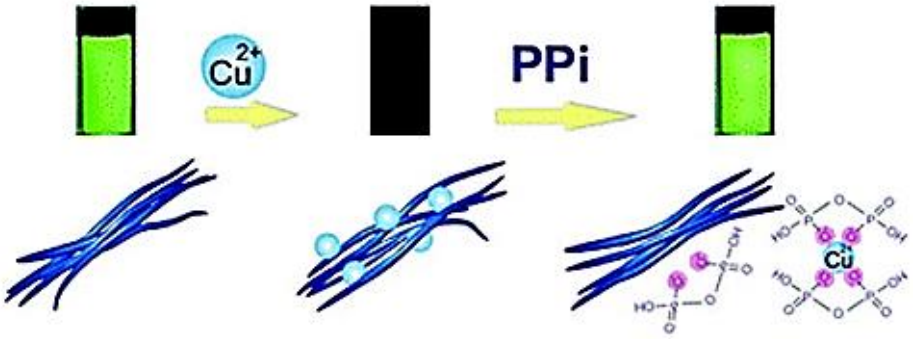

Figure 1-18. Proposed mechanism for PPi sensor based on PPE-CO_2/Cu^{2+} complex. Reprinted with permission from Zhao *et al*.[25]

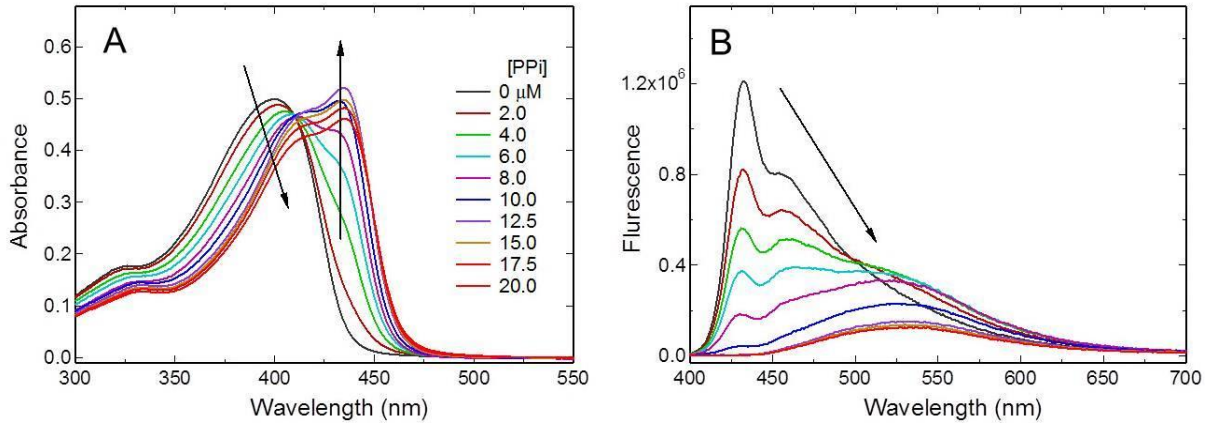

Figure 1-19. Absorption (A) and fluorescence (B) spectra of PPE-NH_3 in buffered solutions (pH = 6.5) with increasing PPi concentration. [PPE-NH_3] = 10 μM. Reprinted with permission from Zhao *et al*.[24]

A direct detection of PPi in aqueous solution using PPE-NH_3 (Figure 1-14) was reported by Schanze and co-workers in 2010.[24] PPE-NH_3 was molecularly dissolved in aqueous solution with blue fluorescence by incorporation of branched ammonium side groups. It was found that pyrophosphate can induce the aggregation of PPE-NH_3 and quench the fluorescence. As shown in Figure 1-19, upon addition of PPi, the absorption spectra gradually red shifted and a shoulder at longer wavelength showed up, indicating the formation of aggregation. The fluorescence intensity of PPE-NH_3 at ~ 430 nm decreased and an excimer-like band at 540 nm appeared as the PPi concentration increased.

Protein Sensing

Proteins are one of the most important biological molecules, which have a variety of physiological and biological functions such as molecular recognition, gene expression, and reaction catalysis as enzymes.[52] Therefore, thousands of protein sensors have been developed for detection and analysis in medical and biological research. In a study reported by Schanze and co-workers in 2008, a fluorescence turn-off assay for phospholipase C (PLC) was developed based on the reversible interaction between the natural substrate, phosphatidylcholine and a water-soluble BpPPESO_3.[73] As shown in Figure 1-20B, the fluorescence intensity of BpPPESO_3 solution in water was dramatically increased upon addition of the phospholipid (10CPC) due to the formation of a PPE-lipid complex. Incubation of the PPE-lipid solution with the enzyme PLC caused the fluorescence intensity to decrease. This decrease in fluorescence intensity was attributed to the disruption of PPE-lipid complex, due to the hydrolysis of the phosphatidylcholine. The optimized assay provides an easy, rapid and real-time sensor for PLC with a detection limit as low as 1 nM.

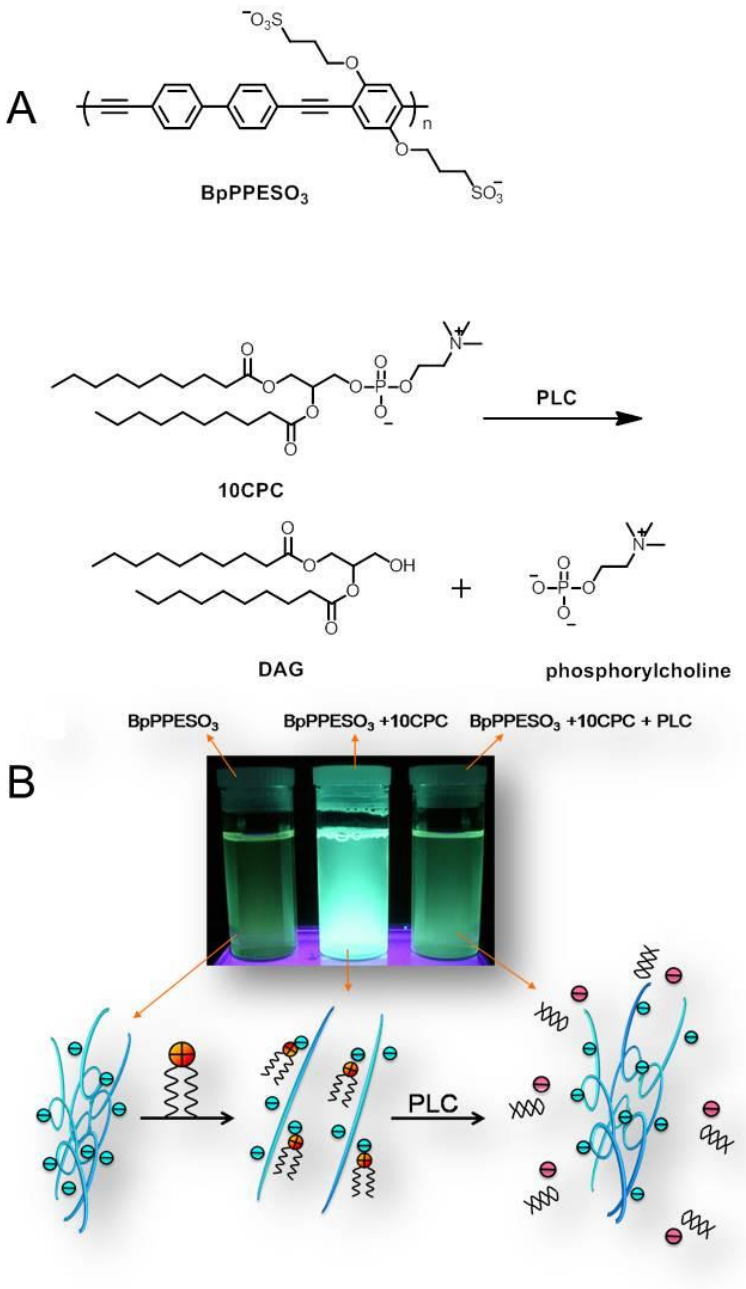

Figure 1-20. (A) Structures of polymer $BpPPESO_3$, 10CPC and reaction scheme for hydrolysis of 10CPC by PLC. (B) Proposed mechanism of PLC turn-off assay. Reprinted with permission from Liu *et al*.[73]

DNA Sensing

Along with RNA and proteins, DNA is one of the three major macromolecules that are essential for life. Most DNA molecules are double-stranded helices, consisting

of two long polymers of the complimentary nucleotides. Many research groups have reported DNA sensors using various types of CPEs. Bazan *et al*. used the FRET mechanism to detect a target DNA through triplex formation of DNA/PNA or DNA/DNA with cationic poly(fluorine-co-phenylene)s.[74] This methodology was based on electrostatic interaction between cationically charged CPE and negatively charged oligonucleotide.

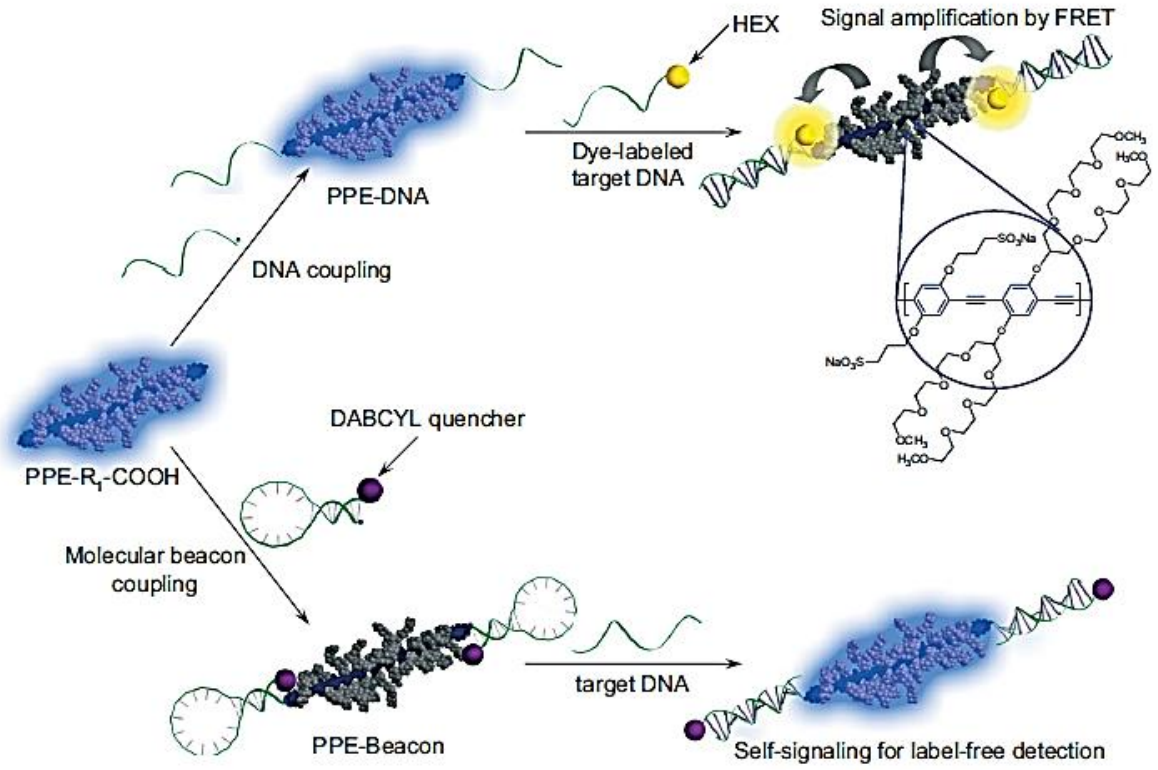

Figure 1-21. DNA sensing strategy based on PPE-DNA (top) and PPE-DNA beacon (bottom). Reprinted with permission from Lee *et al*.[38]

In a work reported by Kim and co-workers, DNA probe sequences were successfully conjugated to PPE polymers using carbodiimide chemistry.[38] The resulted single stranded DNA (ssDNA), coupled at the end of PPEs, selectively hybridized with HEX (hexachlorofluorescein)-labeled target complementary DNA. As shown in Figure 1-21, the fluorescence energy for PPE was efficiently transferred to the target HEX-DNA

upon DNA/DNA hybridization. In addition, a special oligonucleotide probe with a quencher at the end was conjugated to the PPE polymers. The oligonucleotide can form a hairpin-shape in buffer solution, leading to the fluorescence quenching of the PPE. Upon the addition of the complementary target DNA, a DNA double helix was formed and the quencher DABCYL (4-(4-dimethylamino)phenyl-azo)-benzoid acid) was far away from the polymer chain, resulting in the fluorescence recovery of PPE.

Overview of This Dissertation

The primary goal of the present study is to design and synthesize functional poly(phenylene ethynylene)s (PPEs) and study the structure-property relationship. Their photophysical properties are studied by the spectroscopic analysis such as UV-Vis absorption, fluorescence spectroscopy, and fluorescence lifetime measurements. In addition, fluorescence correlation spectroscopy (FCS) and atomic force microscope (AFM) are used to study the aggregation behaviors. The PPEs in this dissertation have been successfully applied to develop the new fluorescence sensors, DSSCs and antibacterial materials.

In chapter 2, a fluorescent oligo(phenylene ethynylene) was designed and synthesized through multiple-step Sonogashira reaction. This oligomer features an alkyl ammonium side group at one end and a trimethylsilyl-protected acetylene group at the other end, which is ready to act as a reaction site for the next “Click Reaction”. Absorption and fluorescence of the oligomer were investigated, and the results indicated that this oligomer was slightly aggregated in water. The oligomer modified silica particles were able to show fluorescence in water under luminescence and produce singlet oxygen in the oxygen purged deuterated methanol solution.

In chapter 3, a new family of cationic poly(phenylene ethynylene) polymers featuring guanidinium side groups was synthesized. The photophysical properties of the series of PPEs were investigated in methanol and aqueous solution by absorption, steady-state fluorescence spectroscopy. Both polymers showed slight aggregation in water. Fluorescence quenching experiments with different quenchers such as AQS, $K_4Fe(CN)_6$, PPi and Pi were conducted in methanol in order to test the molecular recognition capabilities. A fluorescent sensor for PPi in aqueous solution based on **GU-P1**/Triton complex was developed, which showed a great selectivity over Pi.

In chapter 4, a new series of poly(arylene ethynylene) (PAE) conjugated polyelectrolytes featuring methylene carboxylate side chains have been prepared. The absorption and fluorescence properties of the PAEs were investigated in methanol and water. The photophysical data suggested that this family of PAEs did not aggregate in aqueous solution. Stern-Volmer fluorescence quenching studies were carried out using methyl viologen (MV^{2+}) as an electron acceptor in water. The linear shape of Stern-Volmer plots and the low K_{sv} values suggested that this set of PAEs did not aggregate in water, which was also confirmed by FCS data. The tendency of aggregation in water was strongly suppressed, resulted in enhanced fluorescence quantum yields (~0.16). Through careful structure-property relationship study, we conclude that the introduction of methylene carboxylate side groups is the key to reduce aggregation in water. Some applications based on this set of PAEs were developed, such as DSSC and mercury ion sensor.

In chapter 5, a new family of poly(phenylene ethynylene)s (PPEs) with methylene ammonium side groups was synthesized. The photophysical properties of the series of

PPEs were investigated in methanol and aqueous solution by absorption, and steady-state fluorescence spectroscopy. Both polymer **P1-N** and **P2-N** showed very high fluorescence quantum yields in water with characteristic molecularly dissolved emission. A fluorescent sensor for ATP was developed based on **P1-N**. In the future, this sensor can be applied as a potential fluorescence assay for phosphatase enzyme (ALP), which catalyzes the dephosphorylation of ATP in cells.

CHAPTER 2
SURFACE MODIFICATION OF SILICA PARTICLES USING A NOVEL WATER-SOLUBLE OLIGO(PHENYLENE ETHYNYLENE)

Background

Bacterial infection has become a global issue, and resistance to antibiotics makes the problem even worse. Antimicrobial agents capable of killing pathogenic microorganisms have gained interest in various areas, such as medical devices, healthcare products, water purification systems, hospital, etc.[75,76] Cationic conjugated polymers and oligomers containing pendant quaternary ammonium groups have been among the most promising candidates as effective antimicrobials and biocides, because of the light switch properties, low cost and high killing efficiency.[17-19,21] The interaction of cationic polymers or oligomers with bacteria usually involves three steps. First, the bacteria are attracted reversibly to the cationic chains, driven by electrostatic and hydrophobic interactions. Second, when irradiated with UV-Vis light, the conjugated polymers or oligomers absorb radiation and sensitize the formation of singlet oxygen ($^1O_2$). Last, this reactive oxygen species can penetrate the cell membrane, destroy membrane components and nuclei acids, and kill the bacteria.[23,76-78] The killing efficiency is well correlated with the singlet oxygen yield of poly(phenylene ethynylene)s (PPEs) and oligo(phenylene ethynylene)s (OPEs).[21] In general, end-functional OPEs are proven to be more efficient to kill bacteria, due to the better solubility and higher singlet oxygen yields.[21]

In a related work, Schanze and co-workers reported the preparation of silica particles that contained a graft layer of a poly(phenylene ethynylene) on the surfaces.[17] The surfaces of silica particles were first functionalized with aryl iodide groups, which served as graft points under Sonogashira polymerization conditions. However, the

application of this surface modification strategy was limited by the low grafting yield, difficult synthesis of the silane reagent and inhomogeneity of the polymer chain length.

In this work, a novel oligo(phenylene ethynylene) containing a trimethylsilyl-acetylene end group was designed and successfully synthesized. After deprotection, the oligomer can be readily attached to the azide modified surfaces of silica particles using “Click Reaction”. Surface modification of 300 nm diameter silica particles was first accomplished by the reaction of the silica surfaces with trimethoxysilane bearing a chloride group, followed by the substitution reaction with sodium azide. The alkyl azide units were further utilized as the graft points for the “Click Reaction”. This grafting process was easily monitored by infrared spectroscopy (FTIR) and thermogravimetric analysis (TGA). The surface modified silica beads fluoresced at 400 nm, corresponding to the oligomers emission. In oxygen-saturated deuterated methanol solution, the functional silica particles can generate singlet oxygen. This widely applicable method gives access to silica-based colloids with the important properties of oligo(phenylene ethynylene) for possible applications in antibacterial materials and fluorescence sensing.

Results and Discussion

Synthesis and Surface Modification

Oligomer synthesis

The novel oligomer (**OPEC1**) is functionalized with a cationic ammonium group at one end and a trimethylsilyl (TMS)-acetylene at the other end (Figure 2-1). The cationic group imparts the oligomer with water solubility and the interaction with bacteria. The acetylene will participate in the “Click Reaction” after deprotection. Compound **1** was prepared by the Sonogashira reaction of 1-iodo-4-bromobenzene with trimethylsilylacetylene, followed by the TMS-deprotection. Sonogashira reaction of

compound **1** with 4-(trimethylsilylacetylene)iodobenzene resulted in compound **2** with 85% yield. Compound **3** was synthesized by the substitution reaction of 4-iodophenol and dimethylaminopropyl chloride. Compound **4** was prepared by the Sonogashira reaction of compound **3** and trimethylsilyl-acetylene, followed by a deprotection reaction. The organic solvents soluble precursor **5** was synthesized by the Sonogashira reaction of compound **2** and compound **4**. The reaction of compound **5** and methyl iodide in dichloromethane gave **OPEC1** as white crystals. The final compound **OPEC1** was characterized by ^{1}H NMR, ^{13}C NMR and high resolution mass spectrometry.

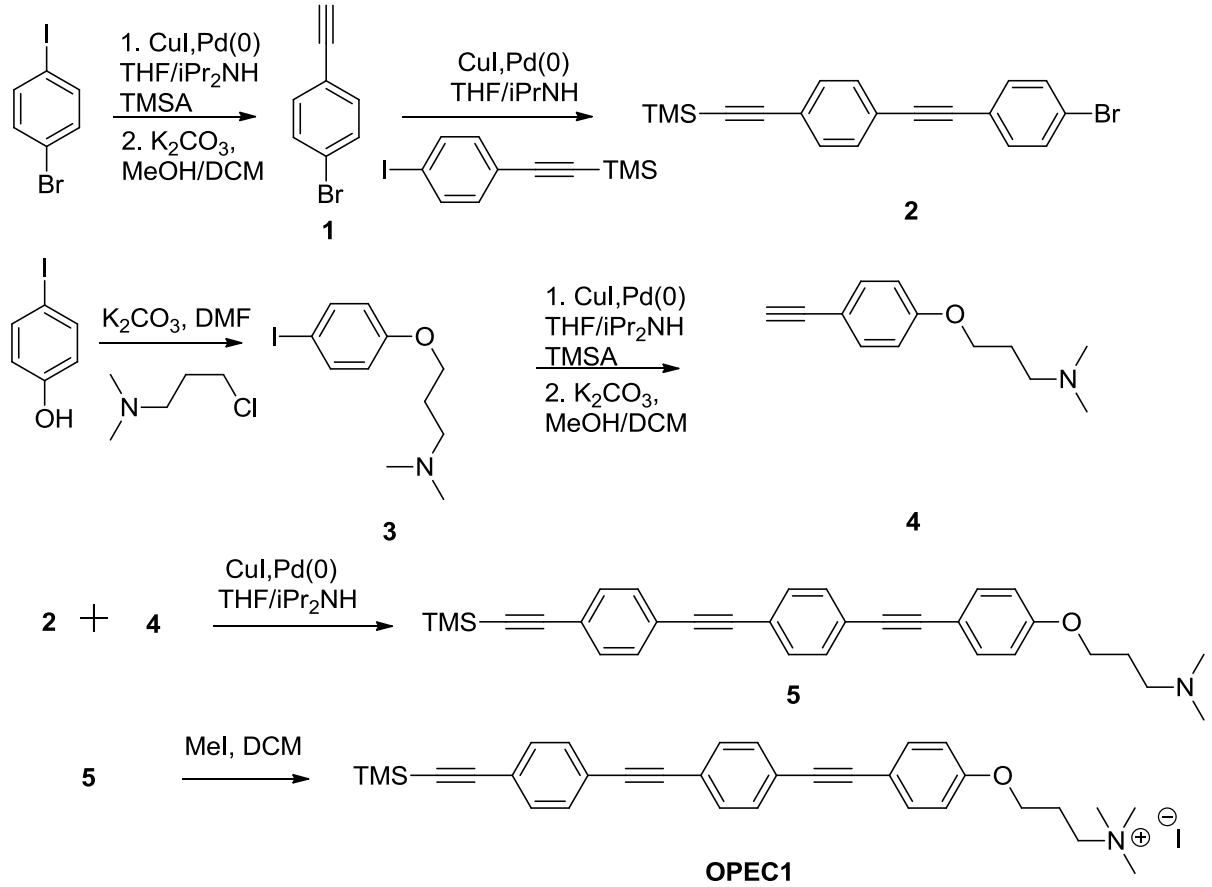

Figure 2-1. Synthesis of **OPEC1**.

Surface modification of silica particles

Conventional methods of silica surface modification involve reaction of surface hydroxyl groups with commercially available silane coupling reagents such as 3-(trimethoxysilyl)propyl amine. A similar approach was used to introduce the reactive alkyl chlorides onto the surface of silica particles (300 nm, Figure 2-2). Active points were introduced by the substitution of alkyl chlorides with sodium azide followed by the "Click Reaction" with alkynes. Then the "Click Reaction" of the deprotected **5** and azide functionalized silica particles was carried out in DMF with CuBr as catalyst to attach the fluorescent oligomer onto the silica surface. The final quarterized ammonium salts (**SiO_2-OPEC1**) was obtained in dichloromethane with methyl iodide.

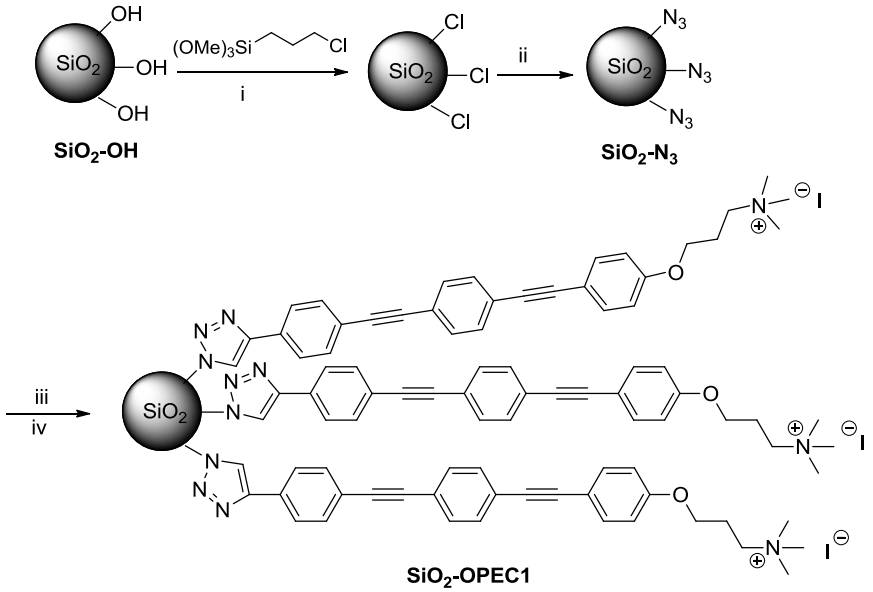

Figre 2-2. Surface modification strategy. (i) Toluene, reflux, 8 h; (ii) NaN_3, DMF, 70 ^{o} C, overnight; (iii) compound **5**, DMF, Tetrabutylammonium floride, CuBr, N,N,N',N'',N''-pentamethyldiethylenetriamine, rt, 24 h; (iv) MeI, DCM.

Characterization of Surface Modified Silica Particles

Infrared spectroscopy

In order to obtain the information of the graft process, infrared spectroscopy (FTIR) and thermogravimetric analysis (TGA) were applied. As shown in Figure 2-3, the

unmodified silica particles (**SiO_2-OH**) exhibited a strong peak at 1110 cm^{-1} which was assigned to the Si-O-Si asymmetric stretch. In addition, a broad peak centered at 3400 cm^{-1} was due to OH stretch from both the silanol and adsorbed water. The FTIR spectrum of **SiO_2-N_3** gave clear evidence for the presence of the azide groups. The peak at 2100 cm^{-1} corresponded to the stretch of the azide group. In addition, multiple weak peaks around 2900 cm^{-1} indicated the presence of sp^3 C-H bonds. After the "Click Reaction", the peak at 2100 cm^{-1} disappeared completely, confirming the success of the "Click reaction" with all the azide units reacted. In addition, the peaks around 1600 cm^{-1} confirmed the presence of aromatic compounds on the silica particles (**SiO_2-OPEC1**).

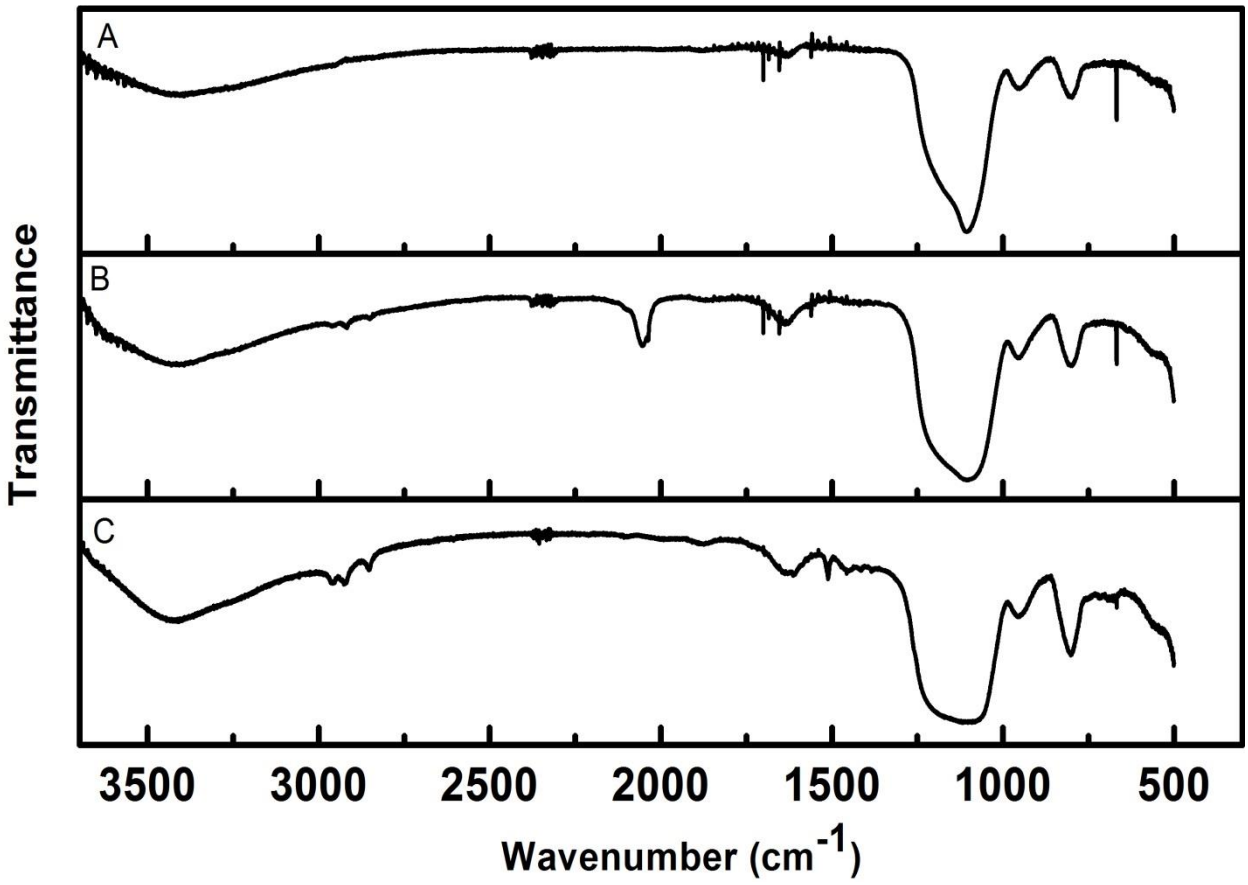

Figure 2-3. Comparison of infrared spectra of silica particles: (A) Unmodified silica particles (**SiO_2-OH**); (B) alkyl azide modified silica particles (**SiO_2-N_3**); (C) **OPEC1**-grafted silica particles (**SiO_2-OPEC1**).

Thermogravimetric analysis

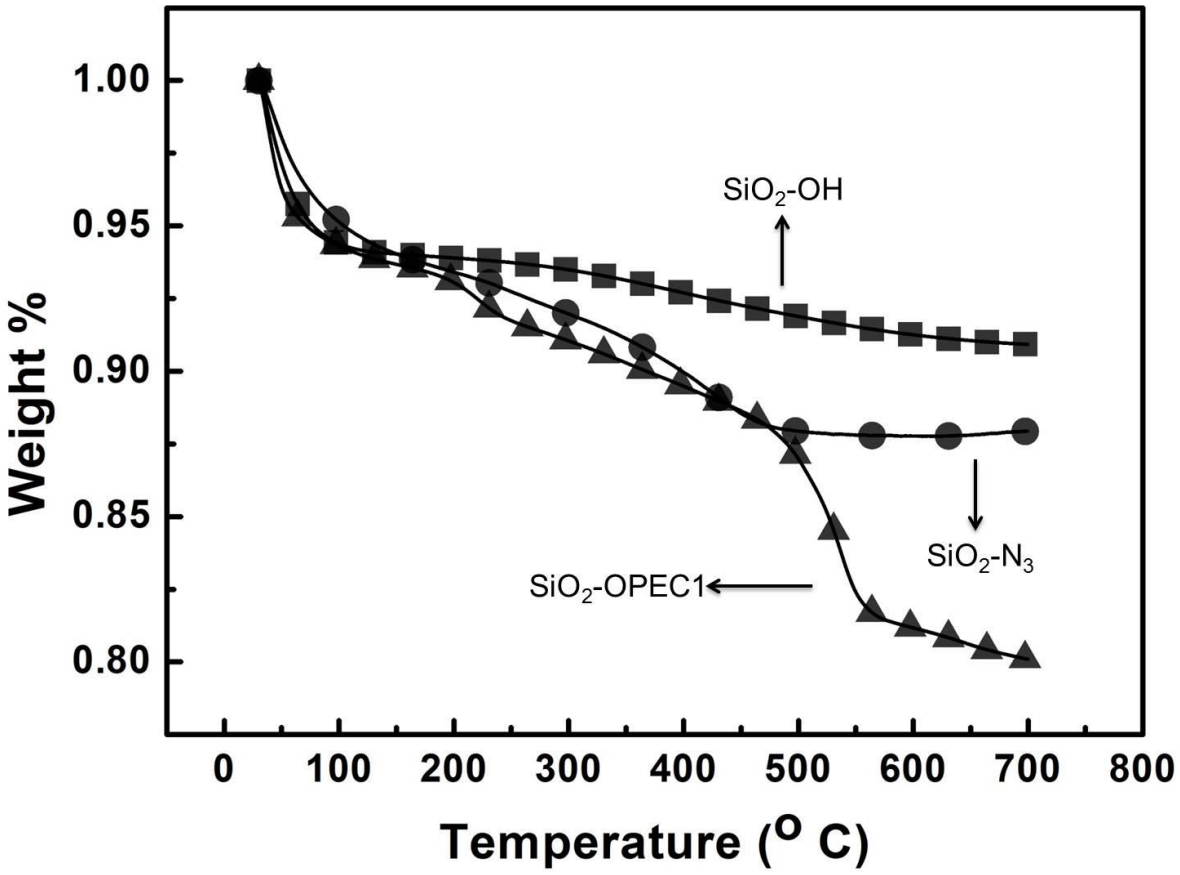

Figure 2-4. Thermogravimetric analysis of silica particles: unmodified silica particles **SiO_2-OH** (■); azide-modified silica particles **SiO_2-N_3** (●); **OPEC1**-grafted silica particles **SiO_2-OPEC1** (▲).

To obtain the information of loading levels of the oligomer on the silica particles, thermogravimetric analysis (TGA) was used. Figure 2-4 shows the TGA analysis of unmodified silica particles (**SiO_2-OH**), azide-modified silica particles (**SiO_2-N_3**) and OPE-grafted silica particles (**SiO_2-OPEC1**). The loss ~ 6.8% below 200 ^{o}C was due to the physisorbed water and residual organic solvent for all types of silica particles. The unmodified silica particles exhibited a further 2% weight loss within 200 – 700 ^{o} C. This decrease arose from the loss of the strongly adsorbed water and the dehydration of silanol units. Both surface modified silica particles (**SiO_2-N_3**, **SiO_2-OPEC1**) exhibited a

greater weight loss with increase of temperature; this additional loss was associated with the presence of organic material. The thermal induced weight loss in the TGA increased along the series **SiO_2-OH** < **SiO_2-N_3** < **SiO_2-OPEC1**, indicating that the amount of organic materials increased along the series.

Calculations were carried out to estimate the functionality density from the TGA data. At 700 ^{o}C, a weight loss of 3% for the azide-modified silica particles in the TGA curve was observed, which was attributed to the presence of spacer ~ propyl group. The residual mass percentage was 88% and the surface grafting density of azide groups was calculated to be ~ 9.3 chains/nm^2 according to Equation 2-1. The TGA curve of the **OPEC1**-grafted silica particles showed that the weight loss percentage corresponded to the decomposition of **OPEC1** chains was 8%, and the residue mass percentage was ~ 80% at 700 ^{o}C. The surface grafting density of **OPEC1** was calculated to be ~ 8.3 chains/nm^2.

$$\delta = \left(\frac{W_{org}}{W_{re}}\right) W_{SiO2} N_A / M_{org} SA \qquad (2\text{-}1)$$

where δ is the surface grafting density, W_{Org} is the weight loss percentage of the organic component, W_{re} is the residual weight percentage, N_A is Avogadro's number, M_{Org} is the molecular weight of the organic component, W_{SiO2} is the weight of silica particles (~3.69 x 10^{-14} g/sphere), and *SA* is the surface area of each silica particle (~3.42 x 10^5 nm^2). W_{SiO2} and *SA* were obtained from manufacturer.

Electron microscopy characterization

Transmission electron microscopy (TEM) was used to determine the morphology and texture of the silica particle surfaces. As shown in Figure 2-5A, unmodified silica particles had clean, smooth and spherical surfaces. After the attachment of alkyl azide

functional group on the surfaces, the azide-modified silica particles appeared about the same size and shape as the unmodified silica particles (Figure 2-5B). In contrast, the **OPEC1** grafted silica particles (**SiO_2-OPEC1**) showed a rough irregular surface, corresponding to the presence of organic material. The organic compounds formed a thin layer outside the surface of silica particles and thus changed the shape of the particles. It is of note that the TEM images did not show a significant change in the size of the silica particles after grafting of the oligomer.

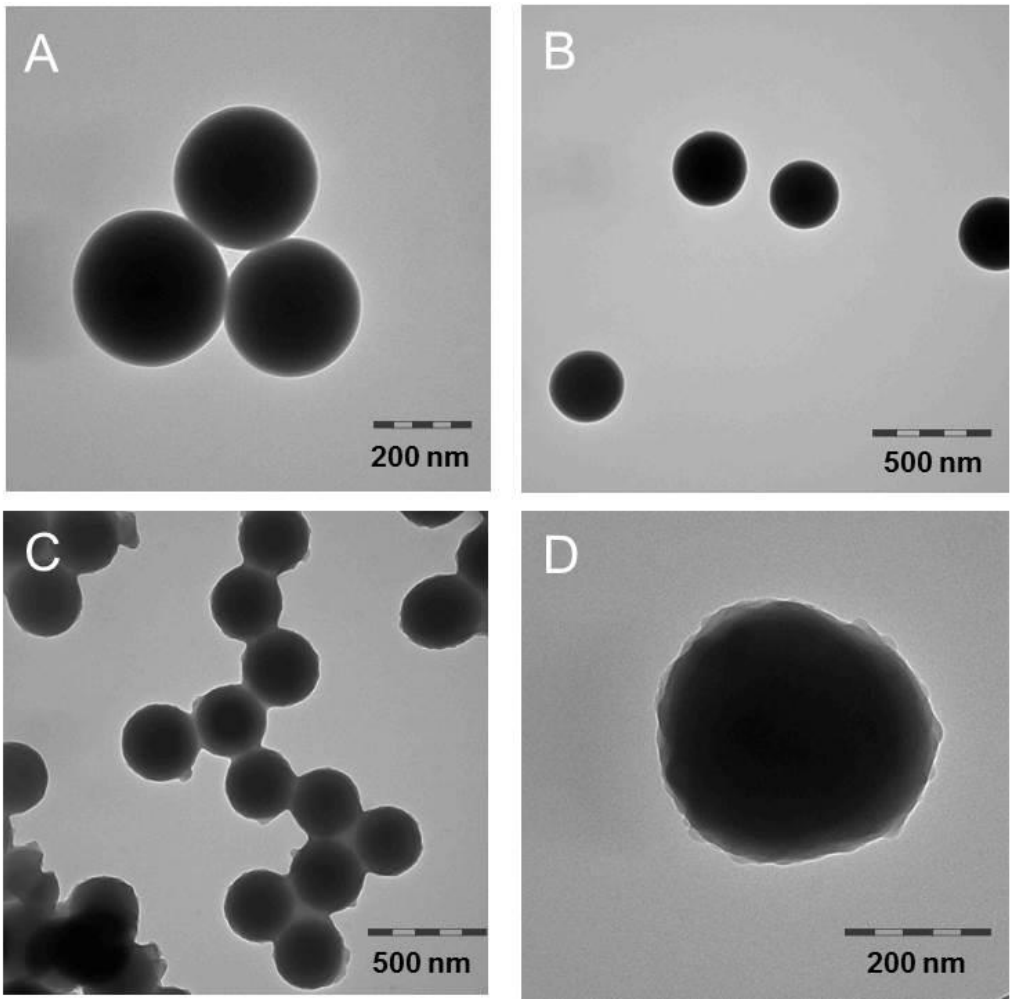

Figure 2-5. Transmission electron microscopy images of silica particles: (A) unmodified silica particles **SiO_2-OH**; (B) azide-modified silica particles **SiO_2-N_3**; (C), (D) **OPEC1**-grafted silica particles **SiO_2-OPEC1**.

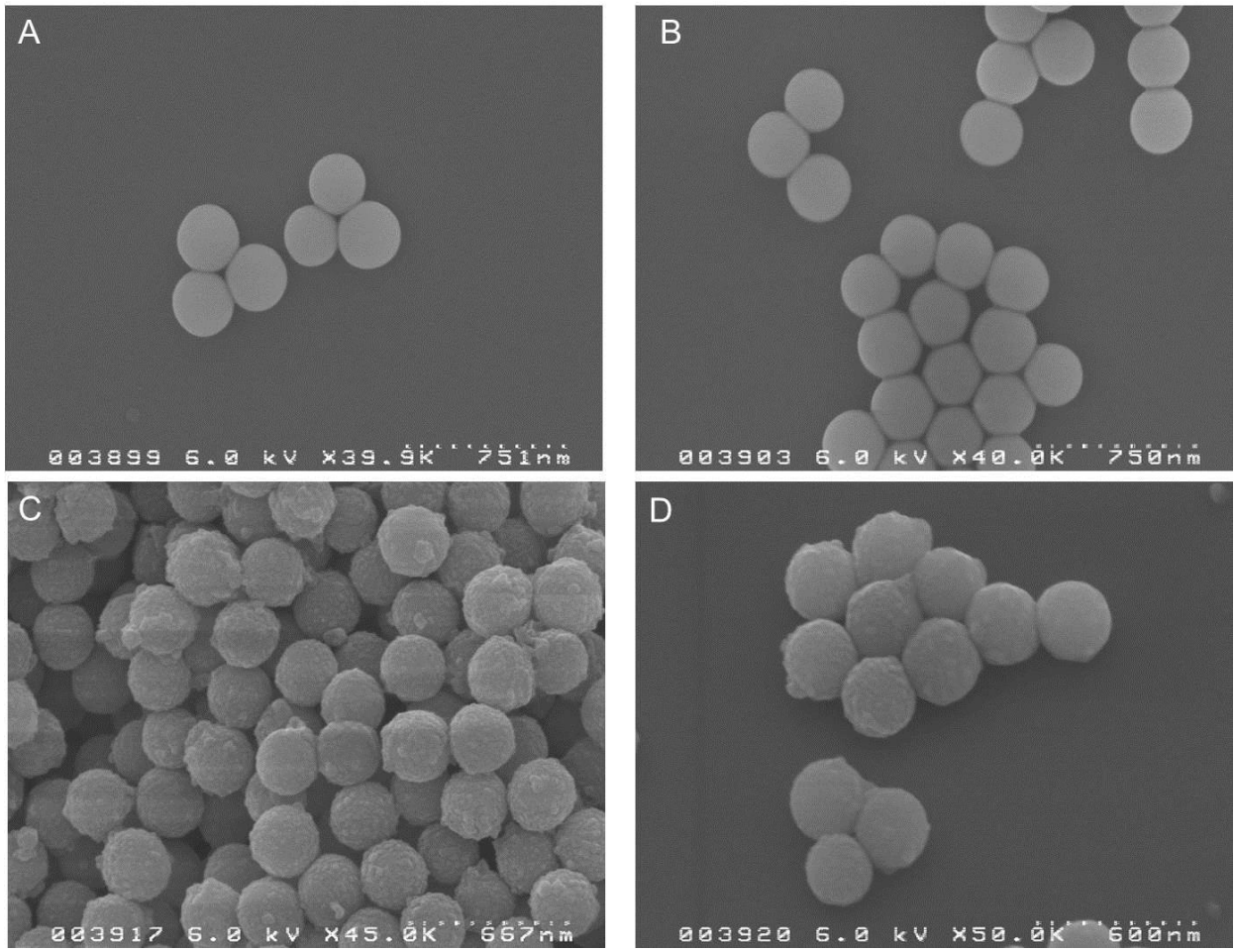

Figure 2-6. Scanning electron microscopy images of silica particles: (A) unmodified silica particles **SiO_2-OH**; (B) azide-modified silica particles **SiO_2-N_3**; (C), (D) **OPEC1**-grafted silica particles **SiO_2-OPEC1**.

In order to obtain more information about the shapes and features of the organic materials on the surfaces, scanning electron microscopy (SEM) was used. As shown in Figure 2-6A and B, the unmodified and azide-modified silica particles had smooth uniform surfaces. In contrast, the SEM image of **OPEC1**-grafted silica particles (Figure 2-6C and D) clearly showed the organic layer outside the surface. The SEM images revealed the fact that the coverage was not uniform. Most of the areas were covered by a thin layer of organic material, but there were evidence of large aggregates at some places. There are several reasons for these aggregates. One possibility is that the

oligomers form multiple layers coverage. Another possibility is that some organic material was chemically or physically adsorbed on the surfaces.

Photophysical Properties

Absorption and fluorescence properties of OPEC1

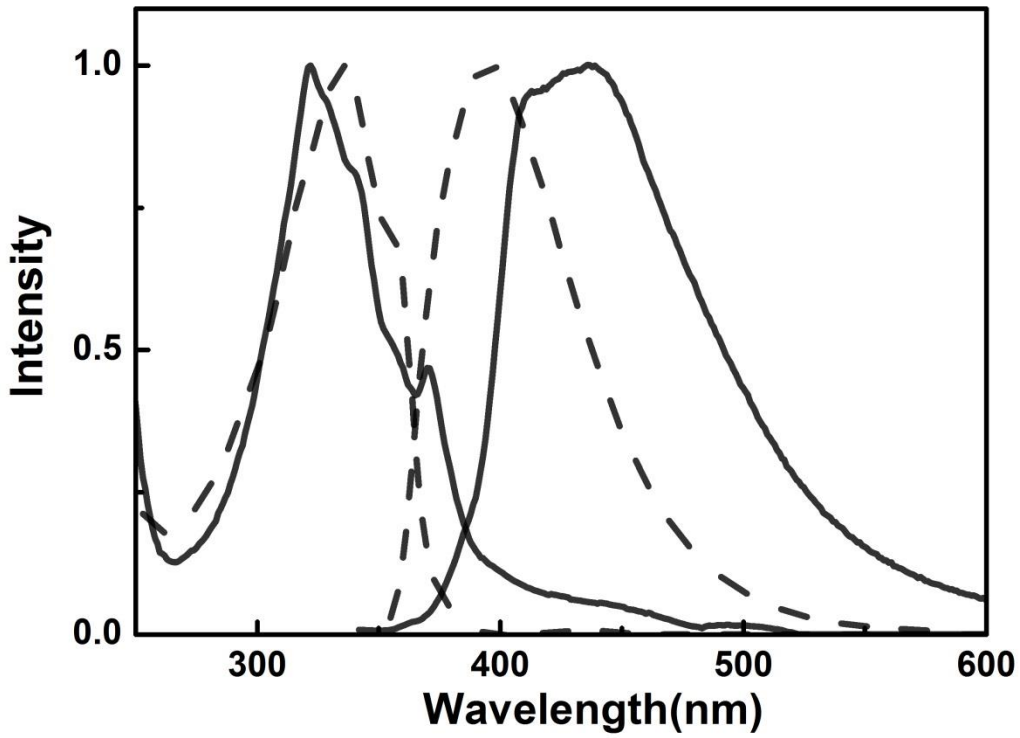

Figure 2-7. Normalized absorption and emission spectra of **OPEC1** in methanol (dash line) and water (solid line).

The photophysical properties of **OPEC1** were characterized in both water and methanol by absorption and fluorescence spectroscopy. Figure 2-7 shows the normalized absorption and fluorescence spectra of **OPEC1** in methanol and water. The absorption maximum in methanol was at 335 nm and the fluorescence maximum was ~ 400 nm. In aqueous solution, the maximum of the absorption spectrum was around 322 nm with a shoulder at 370 nm which may be assigned to the aggregate absorption. The emission peak in water was shifted by about 30 nm to the longer wavelength and broadened due to the formation of aggregates.

Fluorescence and singlet oxygen emission spectrum of SiO_2-OPEC1

The absorption and fluorescence of **SiO_2-OPEC1** were also investigated in methanol. However, the attempts to obtain an absorption spectrum were unsuccessful, because the silica particles were not transparent. Figure 2-8A shows the fluorescence spectra of **SiO_2-OPEC1** and **SiO_2-OH** in methanol (10 mg/mL). The surface modified silica particles **SiO_2-OPEC1** showed a strong fluorescence with a maximum ~ 400 nm. Compared to the fluorescence spectrum of **OPEC1** in methanol, the fluorescence spectrum of **SiO_2-OPEC1** was broader and weaker, likely due to the small amount of oligomers on the silica surfaces. In contrast, unmodified silica particles **SiO_2-OH** did not show any fluorescence but only a scattering peak at ~ 350 nm.

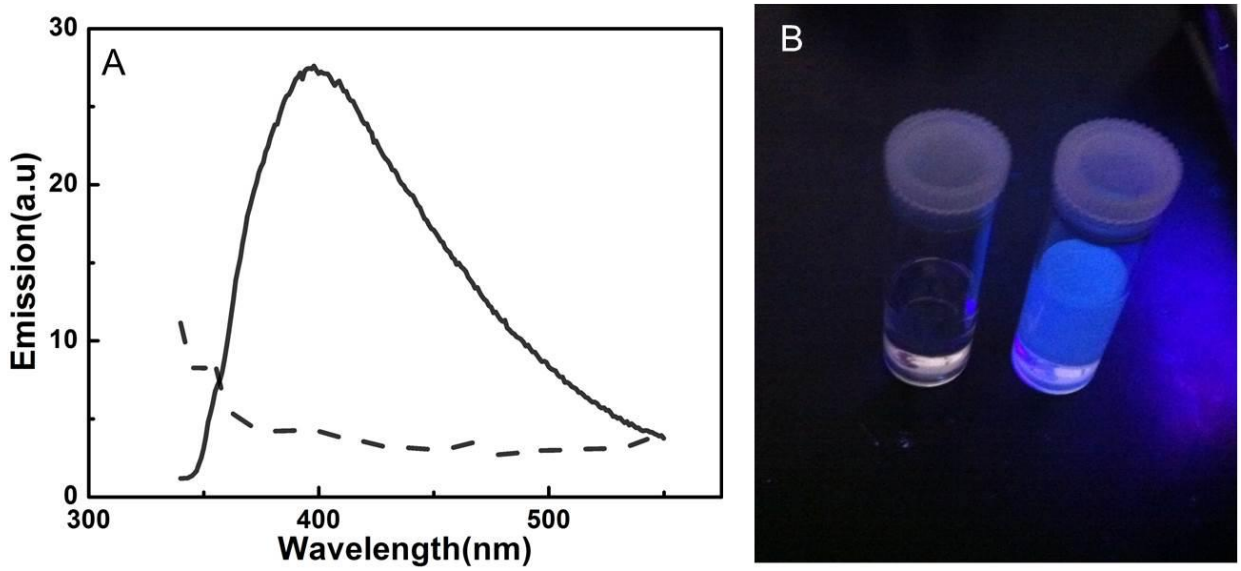

Figure 2-8. (A) Fluorescence spectra of **SiO_2-OH** and **SiO_2-OPEC1** in methanol. (B) Photography of **SiO_2-OH** and **SiO_2-OPEC1** in methanol under UV lamp irradiation. [SiO_2] = 10 mg/mL.

The presence of the organic material on the surfaces was confirmed by the strong fluorescence of **SiO_2-OPEC1** in methanol. Figure 2-8B shows photography of unmodified and **OPEC1**-grafted silica particles suspensions in methanol. The **OPEC1**

grafted silica particles solution emitted strong fluorescence, but no fluorescence was observed from the unmodified silica particles.

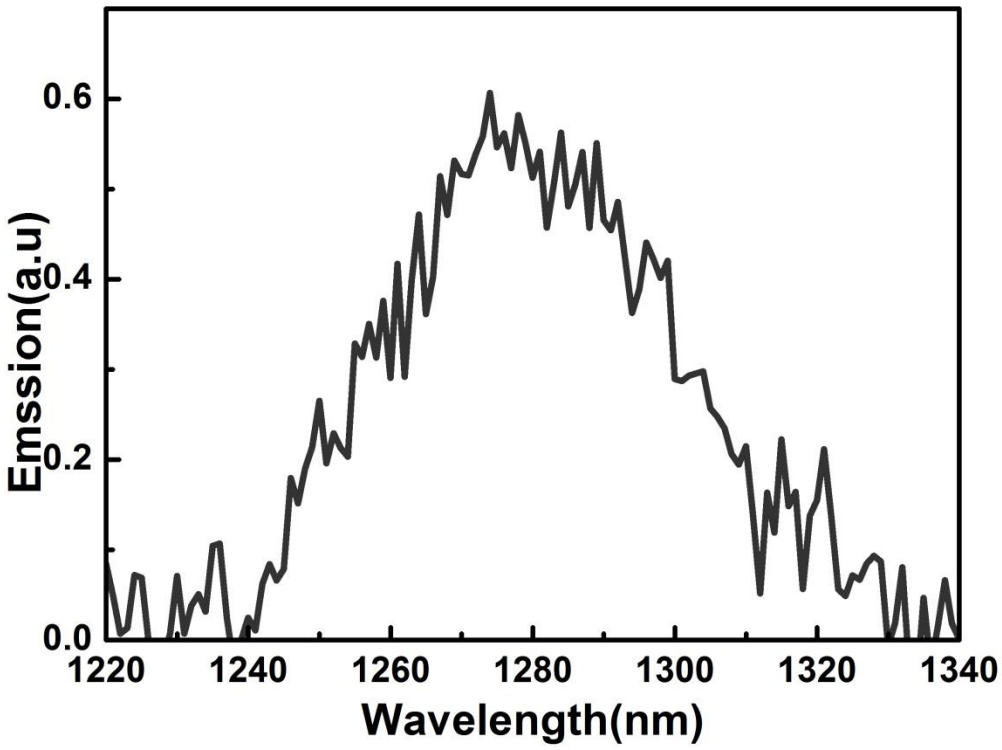

Figure 2-9. Singlet oxygen emission spectrum of **SiO_2-OPEC1** in deuterated methanol.

In order to prove the ability of **SiO_2-OPEC1** to generate singlet oxygen, singlet oxygen spectrum of **OPEC1**-grafted silica particles was measured in oxygen saturated deuterated methanol. After purging oxygen for half an hour, the **OPEC1**-grafted silica particles **SiO_2-OPEC1** were excited at 320 nm, and the emission signal of singlet oxygen appeared at ~ 1270 nm (Figure 2-9). This data suggested that **OPEC1**-grafted silica particles **SiO_2-OPEC1** can be explored as antibacterial materials. However, the singlet oxygen signal was weak and noisy compared to the singlet oxygen spectra of oligo(phenylene ethynylene)s and poly(phenylene ethynylene)s solutions.[18,19,21] One reason for this could be that the concentration of the **OPEC1** in the silica particle

surfaces is much lower. In addition, the formation of aggregates on the surfaces of silica particles may impair the ability to generate the singlet oxygen.

Fluorescence quenching experiments

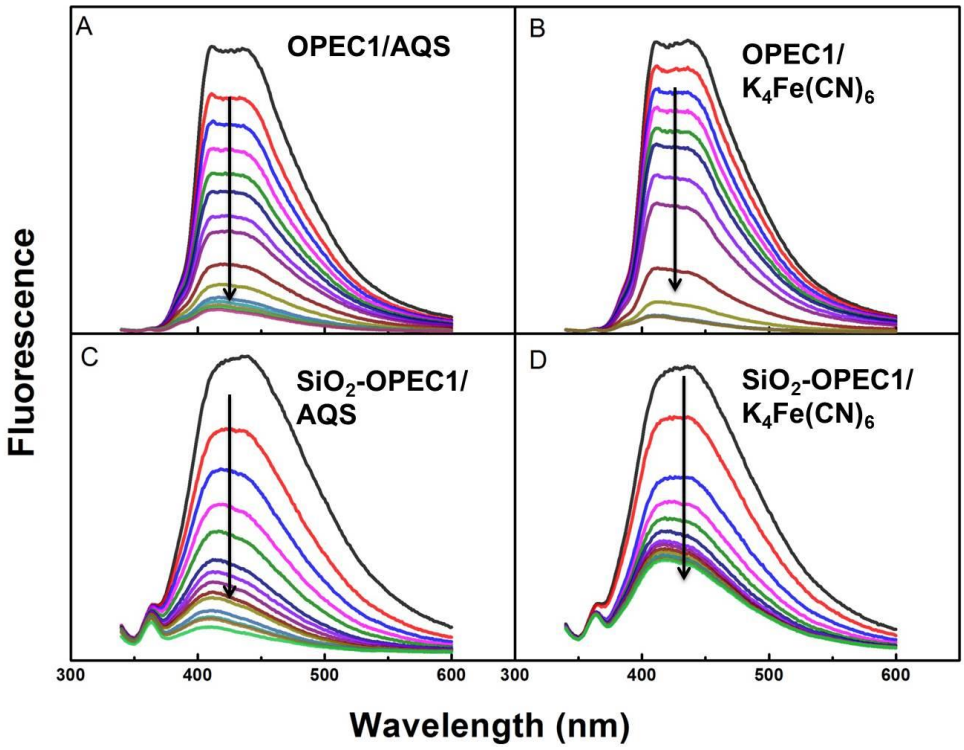

Figure 2-10. Fluorescence spectra of **OPEC1** and **SiO_2-OPEC1** upon addition of different quenchers in water: (A) **OPEC1** quenched by AQS; (B) **OPEC1** quenched by $K_4Fe(CN)_6$; (C) **SiO_2-OPEC1** quenched by AQS; (D) **SiO_2-OPEC1** quenched by$K_4Fe(CN)_6$. [**OPEC1**] = 10 μM. [**SiO_2-OPEC1**] = 3 mg/mL. Quencher concentrations are from 0 to 3 μM.

The quenching experiments of this oligomer (**OPEC1**) and the oligomer-coated silica particles (**SiO_2-OPEC1**) in water were investigated by AQS (9.10-anthraquinone-2,6-disulfonic acid disodium salt) and $K_4Fe(CN)_6$. Figure 2-10 shows the fluorescence spectra of **OPEC1** and **SiO_2-OPEC1** upon addition of different quenchers in aqueous solution. In each case, the fluorescence was efficiently quenched. However, the fluorescence intensity of **SiO_2-OPEC1** reached a saturation point where the further addition of quenchers induced little change to the spectra. This data suggests that

oligomers form multi-layer aggregates on the surfaces of silica particles in aqueous solution. The quenchers can efficiently quench the fluorescence of the outer layer of oligomer but cannot reach the internal layer of fluorescent molecules.

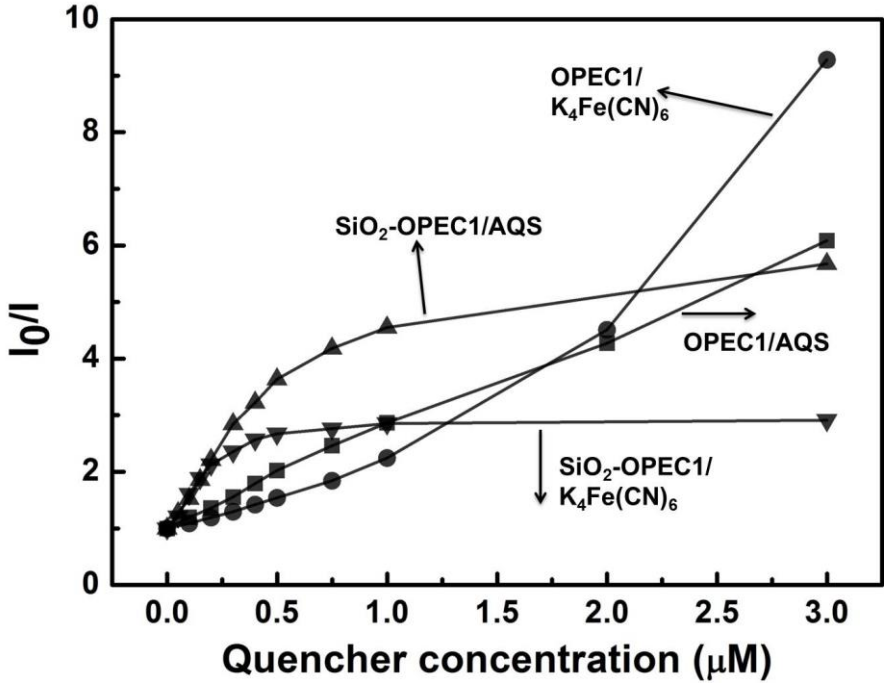

Figure 2-11. Stern-Volmer plots of **OPEC1** and **Si-OPEC1** upon addition of AQS and $K_4Fe(CN)_6$ in aqueous solution.

Figure 2-11 shows the Stern-Volmer plots of **OPEC1** and **SiO_2-OPEC1** upon addition of AQS and $K_4Fe(CN)_6$. The curves of **OPEC1** upon addition of AQS and $K_4Fe(CN)_6$ curves upward, and the Stern-Volmer constants are calculated as ~ 1.9 x 10^6 M^{-1} for AQS and 1.1 x 10^6 M^{-1} for $K_4Fe(CN)_6$, respectively. In contrast, the Stern-Volmer curves of **SiO_2-OPEC1** reaches a plateu at the quencher concentration ~ 0.5 μM with a larger Stern-Volmer constants (5.8 x 10^6 M^{-1} for AQS and 5.9 x 10^6 M^{-1} for $K_4Fe(CN)_6$). The formation of oligomer aggregates on the surfaces of silica particles enables the inter-chain exciton transfer pathway, resulting in a larger K_{sv} value. It may be also due to higher charge density of the silica particles.

Summary

In this chapter, a novel water soluble oligo(phenylene ethynylene) (**OPEC1**) was synthesized with a quaternized ammonium group at one end and a TMS-protected acetylene at the other end. Deprotected acetylene was used for grafting to silica particles by “Click” chemistry. The surface grafting process was monitored by infrared spectroscopy (FTIR) and thermogravimetric analysis (TGA). The presence of the functional organic material on the surfaces of silica particles was confirmed and the surface morphology was investigated by SEM and TEM. The absorption and fluorescence of **OPEC1** were characterized in both methanol and water. The modified silica particles **SiO_2-OPEC1** exhibited a comparable fluorescence spectrum to that of **OPEC1** and generated singlet oxygen in deuterated methanol. Steady state fluorescence quenching experiments of **OPEC1** and **SiO_2-OPEC1** were performed by AQS and $K_4Fe(CN)_6$ in aqueous solution. The data suggested that **OPEC1** was aggregated on the surfaces of silica particles. The oligomer and functionalized silica particles are believed to be promising candidates as biocidal materials.

Experimental

Materials

$Pd(PPh_3)_4$ was purchased from Strem Chemical Company and used as received. 9.10-Anthraquinone- 2,6-disulfonic acid disodium salt (AQS), dimethylaminopropyl chloride, 4-bromoiodobenzene and 4-iodophenol were purchased from Sigma-Aldrich and used without further purification. Potassium carbonate, hydrochloric acid and potassium ferrous cyanide ($K_4Fe(CN)_6$) were purchased from Fisher Scientific Company and used as received. THF and DMF were purified by solvent dispensing system. Uniformly sized silica microspheres were purchased from Bangs Lab

(http://www.bangslabs.com) as dry powders. All other chemicals were purchased from Sigma-Aldrich or Fisher Scientific companies and used without further purification. And for all experiments in water, the solutions were prepared using water (pH = 6.5).

Instrumentation

NMR spectra were recorded on either Varian Gemini (300 MHz) or Inova2 (500 MHz) spectrometer, and chemical shifts were reported in parts per million using $CDCl_3$ or DMSO-d_6 as solvents. Infrared spectra were taken using KBr pellets on a Perkin-Elmer Spectrum One FTIR spectrometer. Thermogravimetric analysis (TGA) data were obtained on a TA instruments Q5000 thermal analysis system. The samples were heated from room temperature to about 700 ^{o}C at a heating rate of 20 ^{o}C /min under a dry nitrogen atmosphere. UV-Vis spectra were collected on a Varian Cary-50 UV-Vis spectrophotometer. Photoluminescence measurements were carried out on a PTI fluorescence spectrophotometer. 1 cm square quartz cuvette was used for both absorption and emission measurements. Scanning electron microscope images were obtained on a Hitachi S-4000 FE-SEM instrument. Transmission electron microscope images were obtained on a Hitachi H-7000 TEM instrument. Singlet oxygen measurements were carried out on a PTI fluorescence spectrophotometer equipped with a near-IR detector. The sample solution was suspended in deuterated methanol and purged oxygen for half an hour before experiments. The sample was exited at 330 nm.

General Methods of Fluorescence Quenching

OPEC1 oligomer solution (2 mL, 10 μM) or a silica particles suspension (**SiO_2-OPEC1**, 2 mL, 3 mg/mL) was placed in a rectangular quartz cell and titrated with different quenchers (AQS, $K_4Fe(CN)_6$). The fluorescence spectra were measured after

addition of the quenchers. Fluorescence peak intensities were used for the construction of the Stern-Volmer (SV) plots if not specifically mentioned. The ratio of initial fluorescence intensity to observed fluorescence intensity (I_0/I) was plotted *versus* the quencher concentration. K_{sv} values were obtained by fitting of the linear region of Stern-Volmer plots.

Synthetic Procedures

4-(Trimethylsilyl-ethynyl)iodobenzene was synthesized following the literature procedure.[79]

4-Bromophenylacetylene (1). To a degassed mixture of 4-bromoiodobenzene (1 g, 3.5 mmol) and trimethylsilylacetylene (0.45 mL, 4.4 mmol) in 70 mL THF and 30 mL diisopropylamine, 1.5 mol% of $Pd(PPh_3)_4$ and 2 mol% of CuI were added. The reaction was allowed to run for 3 h, at room temperature. The resulting mixture was then filtered and the filtrates were evaporated and dissolved in hexane. The solution was then washed with saturated NH_4Cl once and then deionized water twice. Organic layers were combined, dried with anhydrous Na_2SO_4. The final compound **1** was purified by flash chromatograph in hexane and obtained as a white powder (yield: 80%). ^{1}H NMR (300 MHz, $CDCl_3$): δ 7.44 (d, 2H), 7.33 (d, 2H), 3.11 (s, 1H). ^{13}C NMR (75 MHz, $CDCl_3$): δ 133.55, 131.60, 123.15, 121.06, 82.59, 78.37.

1-Bromo-4-((4-trimethylsilylacetylenebenzyl)ethynyl)benzene (2). To a mixture of compound **1** (181 mg, 1 mmol) and 4-trimethylsilylacetylene-iodobenzene (40 mg, 1 mmol) in degased 100 mL THF and 30 mL diisopropylamine,1.5 mol% of $Pd(PPh_3)_4$ and 2 mol% of CuI were dispersed. The reaction was stirred for 8 h, at room temperature. The reaction mixture was then filtered and the filtrates were evaporated and dissolved in dichloromethane. The solution was then washed with saturated NH_4Cl

once and then DI water twice. Organic layers were combined, dried with anhydrous Na_2SO_4. Flash chromatograph in dichloromethane gave the desired compound (yield: 86%). ^{1}H NMR (300 MHz, $CDCl_3$): δ 7.50 (m, 6H), 7.40 (d, 2H), 0.28 (s, 9H). ^{13}C NMR (75 MHz, $CDCl_3$): δ 133.20, 133.13, 131.86, 131.56, 123.35, 123.11, 122.93, 122.15, 104.73, 96.67, 90.38, 90.37, 0.16.

4-(3-(N,N'-dimethylamino)propoxy)-iodobenzene (3). To a mixture of 4-iodophenol (2.20 g, 10 mmol) and dimethylaminopropyl chloride (1.22 g, 10 mmol) in 50 mL acetonitrile, 5 g K_2CO_3 and 0.1 g KI were added. The reaction was allowed to run for 6 h at 70 °C. The resulting mixture was then filtrated and filtrates were evaporated and redissolved in dichloromethane. Column chromatograph in DCM/ MeOH (9:1) gave the desired compound **3** (yield: 75%). ^{1}H NMR (300 MHz, $CDCl_3$): δ 7.5 5(d, 2H), 6.67 (d, 2H), 3.96 (t, 2H), 2.62 (t, 2H), 2.24 (s, 6H), 1.90 (m.2H). ^{13}C NMR (75 MHz, $CDCl_3$): δ 158.98, 130.23, 117.04, 82.69, 66.43, 56.41, 45.70, 27.60.

1-Ethynl-4-(3-(N,N'-dimethylamino)propoxy)benzene (4). To a degased solution of compound **3** (2 g, 4.96 mmol) in 50 mL THF and 30 mL diisopropylamine, $Pd(PPh_3)_4$ (30 mg) and CuI (60 mg) catalyst were added via spatula. Then trimethylsilylacetylene (0.75 mL, 6 mmol) was added via syringe. The reaction was allowed to run overnight, at room temperature. The reaction mixture was filtered and the filtrates were evaporated and redissolved in dichloromethane. The solution was then washed with saturated NH_4Cl once and then deionized water twice. Organic layers were combined, dried with anhydrous Na_2SO_4. The organic solvents were removed under vacuum to yield a yellow powder, which was dissolved in DCM/ MeOH (1:1). After degasing for 30 min, potassium carbonate (4 g) was added and the reaction was

allowed to run for 3 h. After removing the solvents under vacuum, column chromatograph in DCM/MeOH (9:1) gave the desired compound (yield: 60%). ^{1}H NMR (300 MHz, $CDCl_3$): δ 7.42 (d, 2H), 6.86 (d, 2H), 4.00 (t, 2H), 3.00 (s, 1H), 2.68 (t, 2H), 2.30 (s, 6H), 1.98 (m, 2H). ^{13}C NMR (75 MHz, $CDCl_3$): δ 159.48, 133.71, 114.61, 114.17, 83.88, 75.93, 66.32, 56.41, 45.52, 27.44.

Compound 5. To a degased solution of compound **4** (301 mg, 1 mmol) and compound **2** (500 mg, 1.41 mmol) in 40 mL THF and 20 mL diisopropylamine, $Pd(PPh_3)_4$ (20 mg) and CuI (30 mg) were added. The reaction was allowed to run overnight, followed by filtration. The filtrates were evaporated and the residue was dissolved in DCM. The solution was then washed with saturated NH_4Cl once and then deionized water twice. The organic layers were combined and dried with anhydrous Na_2SO_4. After removing the solvents under vacuum, column chromatography in DCM/MeOH (9:1) gave the desired compound as a white powder (yield: 78%). ^{1}H NMR (500 MHz, $CDCl_3$): δ 7.48 (d, 10H), 6.80 (d, 2H), 4.00 (t, 2H), 3.34 (t, 2H), 2.75 (s, 6H), 2.48 (m, 2H), 0.30 (s, 9H). ^{13}C NMR (125 MHz, $CDCl_3$): δ 159.49, 133.32, 132.14, 131.73, 131.60, 131.58, 123.07, 123.35, 123.28, 115.18, 114.82, 104.82, 96.62, 91.82, 91.32, 90.91, 88.02, 66.47, 56.51, 45.65, 27.59, 0.13. HRMS (APCI) *m*/*z*: $[M+H]^+$ calcd. for $C_{32}H_{34}NOSi$, 476.2404; found, 476.2417.

OPEC1. To a solution of compound **5** (200 mg) in 15 mL DCM, 1 mL MeI was added via syringe. After stirring overnight, the precipitates were collected and dried under vacuum. Yield: 90%. ^{1}H NMR (500 MHz, DMSO-d_6): δ 7.52 (m, 10H), 6.95 (d, 2H), 4.23 (t, 2H), 3.40 (t, 2H), 3.15 (s, 9H), 2.24 (m, 2H), 0.30 (s, 9H). ^{13}C NMR (125 MHz, DMSO-d_6): δ 159.41, 138.76, 133.87, 132.67, 132.47, 132.37, 132.21, 123.82, 123.19,

122.47, 118.04, 115.72, 115.00, 97.46, 92.40, 91.78, 91.37, 88.48, 65.67, 63.66, 53.03 23.21, 0.53. HRMS (ESI) *m*/*z*: $[M-I]^+$ calcd. for $C_{33}H_{36}NOSi$, 490.2561; found, 490.2567.

Surface Modification of Silica Particles

SiO_2-N_3. Silica particles (200 mg) and trimethoxysilylpropylchloride (2 mL) were mixed in 10 mL toluene and refluxed for 8 h. The surface-modified silica particles were collected via centrifugation and washed with acetone several times. Then the particles were added to a mixture of sodium azide (2 g) in 10 mL DMF. After stirring for overnight at 70 ^{o} C, the mixture was poured into 20 mL deionized water. The azide modified silica particles were collected by centrifugation and washed by water 4 times and MeOH twice. The azide modified particles were dried under vacuum for 1 day.

SiO_2-OPEC1. To a degassed mixture of surface modified silica particles (**SiO_2-N_3**, 50 mg) and compound **5** (50 mg, 0.1 mmol) in 10 mL DMF, TBAF solution (0.5 mL, 1M in THF) was added via syringe. The reaction was allowed to run for 3h. Then 5 mg CuBr and 2 mL N,N,N′,N″,N″-pentamethyldiethylenetriamine were added. The “Click Reaction” was allowed to run for 24 h under argon atmosphere. The silica particles were collected by centrifugation and washed by DMF 3 times, acetone 3 times and MeOH 3 times until no fluorescence in supernatant under UV light. The surface modified silica particles were dried under vacuum for 1 day. Then the particles were added to a solution of 1 mL MeI in 5 mL dichloromethane. After stirring for 12 h, the surface modified silica particles (**SiO_2-OPEC1**) were collected by centrifugation and washed by acetone several times. Then silica particles were dried under vacuum for 1 day.

CHAPTER 3
CONJUGATED POLYELECTROLYTES WITH GUANIDINIUM SIDE GROUPS: SYNTHESIS, PHOTOPHYSICS AND PYROPHOSPHATE SENSING

Background

Conjugated polyelectrolytes (CPEs) have attracted significant interest during the past decades and become one of the versatile polymer materials in photovoltaic devices, organic solar cells and biochemical sensors due to their exceptional physical and photophysical properties, such as high fluorescence quantum yield, electrostatic interaction and extraordinary high sensitivity to the fluorescence quenchers.[6,7,14,51,52,60,80] In particular, CPEs have been intensively explored as chemical and biological sensors owing to their high sensitivity and selectivity.[43,54,61,81] The amplified quenching is attributed to the delocalization and migration of the excitons along the polymer backbone, described as the molecular wire effect.[51] Three different mechanisms are proposed for the amplified quenching: photo-induced electron transfer, Förster resonance energy transfer and analyte-induced aggregation. Specially, the analyte-induced aggregation mechanism provides the fluorescence sensors with unique high sensitivity and selectivity through the specific interaction between the polymer side groups and the analytes.[24]

Pyrophosphate (PPi) anion plays an important role in numerous biological processes, including ATP hydrolysis and DNA hybridization.[82] The detection of PPi is investigated as a real-time DNA sequencing method.[82,83] Of all the PPi receptors, guanidinium has attracted considerable interest recently.[84-86] The guanidinium unit is naturally present in the side group of the amino acid (arginine) and able to form strong ion interactions with oxoanions such as carboxylates, sulfates and phosphates. The guanidinium molecule has unique planar Y-shaped configuration and very high pKa ~

13 which ensures protonation over a wide pH range.[87,88] The first example of a PPi sensor based on pyrene-funtionalized mono-guanidinium receptor was reported by Teramae's group.[89] It was found to self-assemble to form a 2:1 (host: guest) complex with pyrophosphate. The PPi worked as a spacer linking two host receptors. The binding constant was calculated as 9.8×10^7 M^{-1}.[89] However, this sensor system has obvious limitations and only applicable in non-aqueous solution such as methanol.

Herein, we report a novel family of water-soluble poly(phenylene ethynylene)s (PPEs) for PPi sensor, where guanidinium units are incorporated into the conjugated polymer system to impart both water solubility and molecular recognition properties. The photophysical properties of the series of PPEs were investigated in CH_3OH and H_2O solution by absorption, steady-state fluorescence spectroscopy and fluorescence lifetime measurement. Similar to other PPEs, these polymers undergo spontaneous aggregation in aqueous solution, resulting in a broad fluorescence spectra and a low fluorescence quantum yield.[6,90,91] The addition of the non-ionic surfactant (Triton X-100) into the weakly fluorescent aqueous solution of **GU-P1** increased fluorescence by forming polymer/surfactant complex. The fluorescence of the polymer/surfactant complex in aqueous solution was effectively quenched by the addition of pyrophosphate (PPi) with high selectivity over Pi; the quenching occurs because PPi binds to the guanidinium groups and induces the aggregation of polymer/surfactant complex. In addition, it was found that diffusion time of the aggregated complex increased by 9 times in comparison with free PPE/surfactant complex. Therefore, a PPi sensor is developed utilizing the significant fluorescence spectra change and size change. This

fluorescence sensor shows high selectivity for PPi over phosphate (Pi) in aqueous solution.

Results and Discussion

Synthesis of PPEs with Guanidinium Side Groups

In this chapter, we report the synthesis of water-soluble PPEs with novel guanidinium side chains as shown in Figure 3-1. **GU-P1** is a copolymer alternating with 1,4-(phenylene ethynylene), while **GU-P2** is the homopolymer. Both polymers have two guanidinium side chains for each repeat unit. The novel guanidinium side groups provide the good solubility in water and also molecular recognition capacity for the polymers.

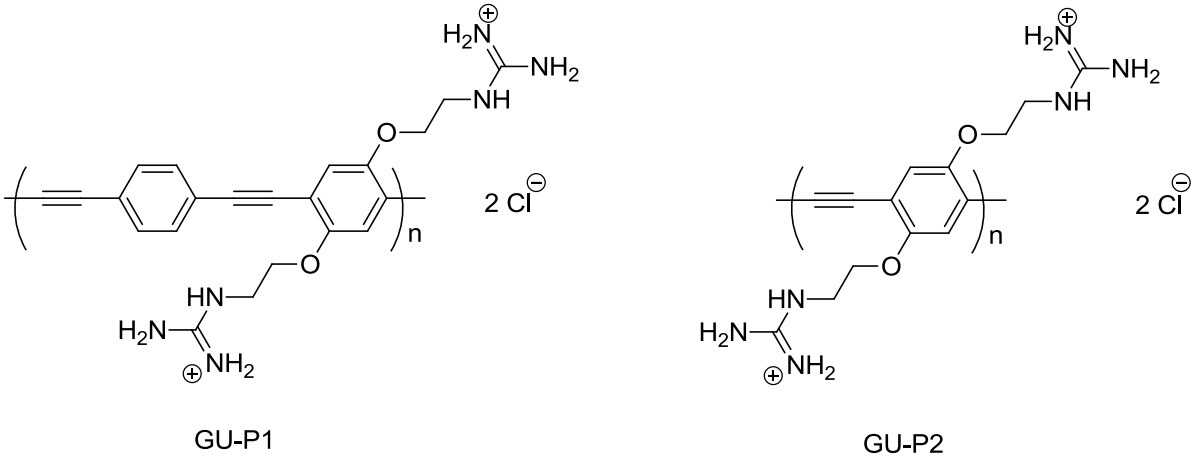

Figure 3-1. Structures of the PPEs with guanidinium side groups.

Monomer synthesis

Figure 3-2 shows the synthesis route for the monomer **5**. Starting from the commercial available 1,4-bis(hydroxyethoxy)benzene, compound **1** and **2** were synthesized according the literature.[90] Azide substitution of compound **2** afforded compound **3** in a modest yield. Compound **4** was prepared by the reduction of PPh_3

followed by the hydroxylation. The reaction of amine groups and N,N'-Boc_2-1H-pyrazole-1-carboxamidine provided the monomer **5** with 87% yield.

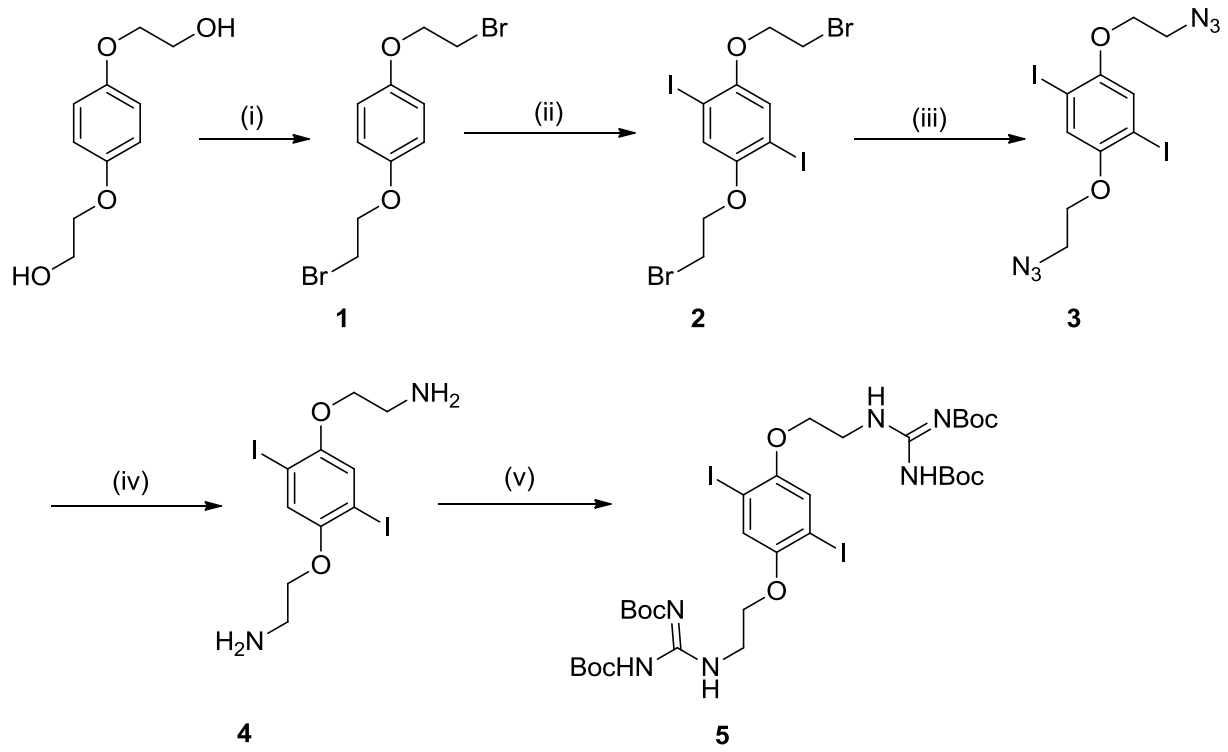

Figure 3-2. Synthesis route for monomer **5**. (i) CBr_4, PPh_3, MeCN, 0 ^{o} C, 4 h; (ii) I_2, bis(trifluoroacetoxy)iodobenezene, CH_2Cl_2, rt, 6 h; (iii) NaN_3, DMF, 40 ^{o} C, overnight; (iv) PPh_3, THF, H_2O; (v) N,N'-Boc_2-1H-pyrazole-1-carboxamidine, DMF, rt, 24 h.

Polymer synthesis and characterization

The polymers were synthesized following the "precursor route", in which the monomers used are uncharged and the polymerization leads to a precursor conjugated polymer that is uncharged. The ionic groups are unmasked in a subsequent reaction (e.g., base hydrolysis of the ester, or quaternization of the tertiary amine by methyl iodide). The synthesis routes for preparing the "precursor" organic-soluble polymers, the water-soluble target polymers are shown in Figure 3-3. The "precursor" polymers were prepared by Sonogashira coupling of a stoichiometric amount of the monomer **5** with BOC-protected guanidinium side chains and diethynylbenzene or trimethylsililacetylene

comonomer (**GU-P1-Boc** or **GU-P2-Boc**, respectively).[62] The polymerization was carried out in organic solution in order to avoid electrostatic repulsion of the ionic charged functional groups and to facilitate polymer characterization by gel permeation chromatography (GPC). Hydrolysis of the precursors was accomplished by treating the organic polymers with trifluoroacetic acid (TFA). The water-soluble PPEs were obtained as bright yellow solids in ~ 90% yield after lypholization. Each polymer was characterized by ^{1}H NMR.

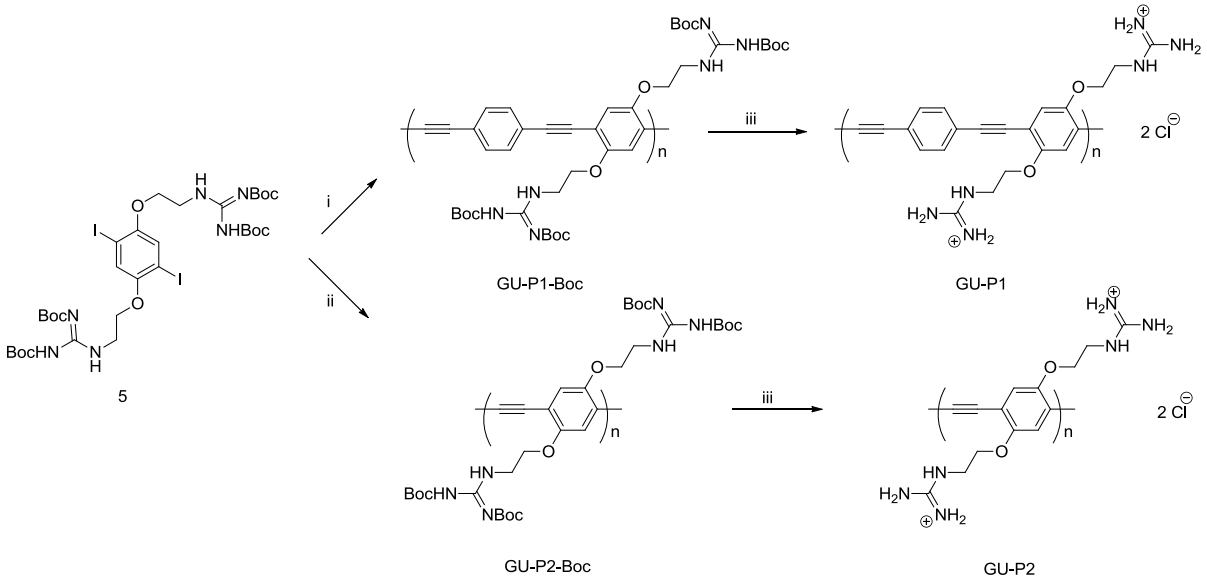

Figure 3-3. Synthesis route for polymer **GU-P1** and **GU-P2**. (i) $Pd(PPh_3)_4$, CuI, 1,4-diethynylbene, THF, iPr_2NH; (ii) $Pd(PPh_3)_4$, CuI, TMS-acetylene, THF, DBU; (iii) TFA, $CHCl_3$.

Table 3-1. GPC data of **GU-P1-Boc** and **GU-P2-Boc**.

Polymer	M_n (kD)	M_w (kD)	PDI
GU-P1-Boc	76	101	1.3
GU-P2-Boc	42	79	1.9

The number- and weight-average molecular weight (M_n and M_w, respectively) for the “precursor” polymers were characterized by GPC analysis against polystyrene

standards in THF. As shown in Table 3-1, **GU-P1-Boc** has a M_n ~ 76 kD and PDI ~ 1.3, while **GU-P2-Boc** has a M_n ~ 42 kD and PDI ~ 1.9.

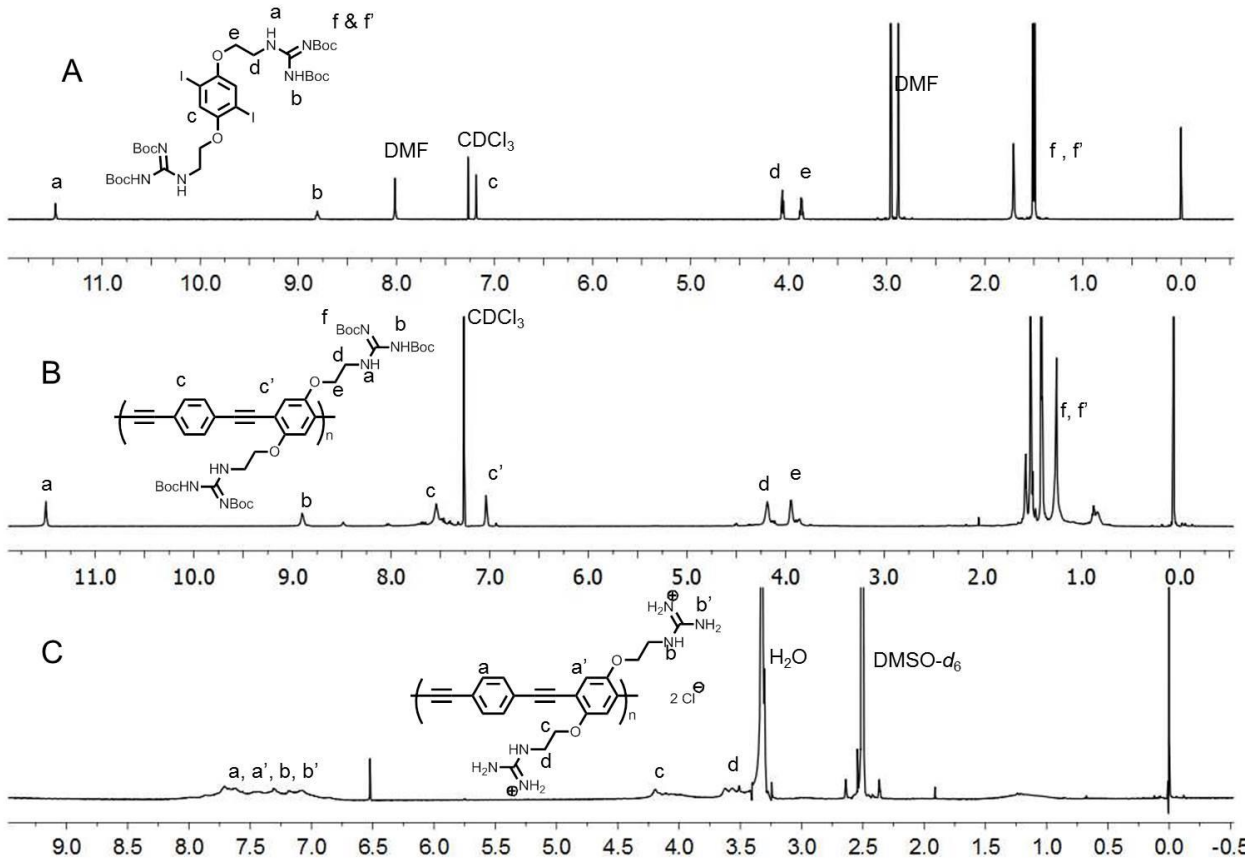

Figure 3-4. ^{1}H NMR spectra of (A) monomer **5**; (B) **GU-P1-Boc**; (C) **GU-P1**.

Figure 3-4 shows the representative ^{1}H NMR spectra of monomer **5**, the precursor polymer **GU-P1-Boc** and the water-soluble polymer **GU-P1**. Comparison between the spectra of monomer **5** and **GU-P1-Boc** revealed the appearance of the peaks at δ ~ 7.60 and 7.00 ppm, which were assigned to be the protons on the polymer backbone. The resonance peaks appeared to lose split pattern and become broader in the spectra of **GU-P1-Boc**. After hydrolysis, the ^{1}H NMR spectroscopy of **GU-P1** was accomplished in DMSO-d_6. Due to the low solubility, the solvent peak and water residue peak showed up strongly. No signals were observed in the range of 0.5 ~ 1.5 ppm and

the peak at 8.8 ppm and 11.5 ppm disappeared, indicating that the BOC groups were cleaved with an excellent yield (>95%). In addition, the protons of guanidinium in DMSO-d_6 showed up in the range of 7.0-8.0 ppm, close to the peaks of aromatic protons.[92]

Photophysical Properties

Absorption, fluorescence and fluorescence quantum yield

The photophysical properties of the PPEs were investigated by UV-visible absorption, fluorescence spectroscopy and fluorescence lifetime measurement. The absorption and fluorescence spectra are shown in Figure 3-5. Although **GU-P1-Boc** and **GU-P2-Boc** (Figure 3-5A) showed the similar pattern, **GU-P2-Boc** exhibited a red-shift in both absorption and emission spectra compared to **GU-P1-Boc**. This red-shift was consistent with the differences between the homopolymer O-p[61] and copolymer PPE-CO_2.[25] The solvent effects on water soluble polymers **GU-P1** and **GU-P2** were studied in CH_3OH and H_2O (Figure 3-5B and 3-5C). Methanol is typically considered to be a good solvent for PPEs because polymer aggregation is minimal.[6] In methanol, **GU-P1** exhibited an absorption maximum at 383 nm and a fluorescence maximum at 435 nm while **GU-P2** showed red-shifted spectra with an absorption maximum at 415 nm and a fluorescence maximum at 473 nm. Absorption spectra are red-shifted while fluorescence spectra show a broad, red-shifted “excimer-like” band, indicating that both **GU-P1** and **GU-P2** appeared to be aggregated in aqueous solution. Lacking of the bulky or highly charged side groups, **GU-P1** and **GU-P2** had a tendency to aggregate in aqueous solution driven by hydrophobic interactions of the polymer backbone, leading to low fluorescence quantum yields (~ 2%), which are similar to other PPEs with linear side groups including PPE-CO_2 and PPE-SO_3.[6,47,48,54]

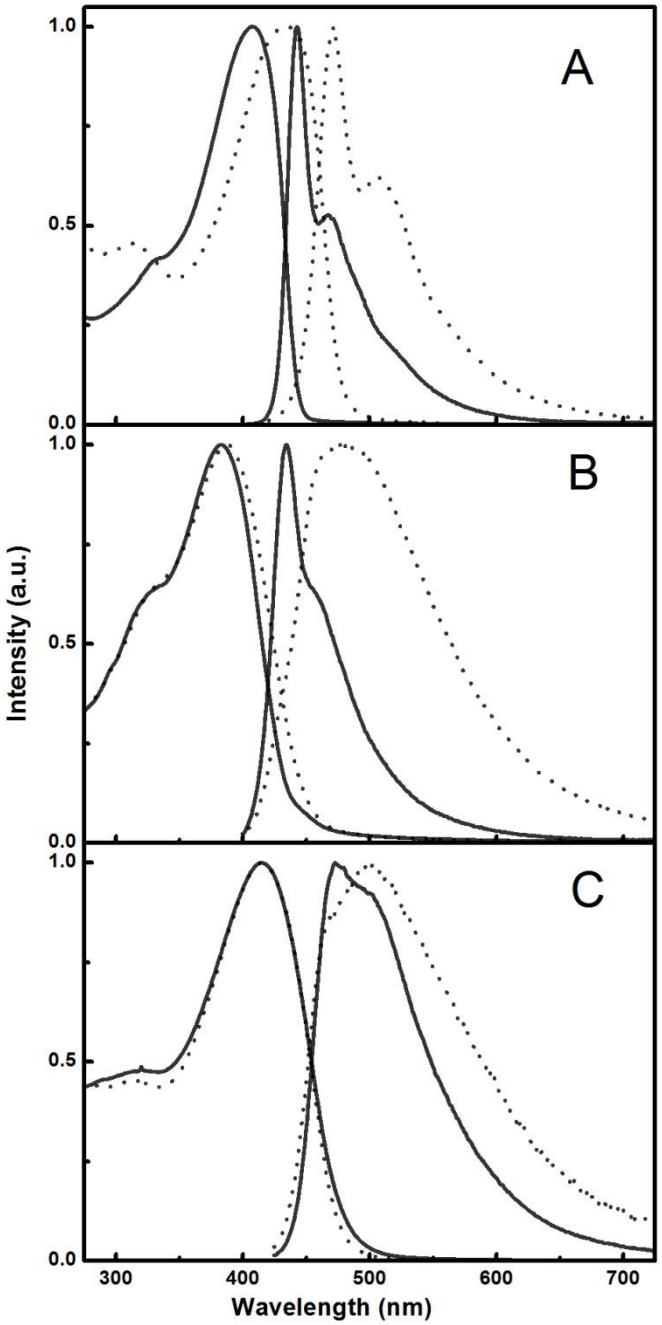

Figure 3-5. Normalized UV-Vis absorption and photoluminescence spectra of (A) **GU-P1-Boc** (solid line) and **GU-P2-Boc** (dash line) in $CHCl_3$; (B) **GU-P1** in MeOH (solid line) and H_2O (dash line); (C) **GU-P2** in MeOH (solid line) and H_2O (dash line). H_2O has pH = 5.

In summary, absorption and fluorescence studies suggested that both **GU-P1** and **GU-P2** existed as slightly aggregated states, with low fluorescence quantum yield

in water. In contrast, polymer **GU-P1** and **GU-P2** were more solvated in methanol with little evidence of the aggregation.

Table 3-2. Photophysical data of **GU-P1** and **GU-P2**.

Polymer	Solvent	λ_{max}^{ab} (nm)	λ_{max}^{fl} (nm)	Φ_{fl}^{b}
GU-P1	MeOH	383	435	0.16
	H_2O^{a}	391	476	0.02
GU-P2	MeOH	415	473	0.11
	H_2O^{A}	415	500	0.02

[a] H_2O pH = 5. [b] Quinine sulfate in 0.1 M H_2SO_4 solution as a standard (Φ_{fl} = 0.545).

pH Effects on the absorption and fluorescence spectra

Because **GU-P1** and **GU-P2** share the same solubilizing group (guanidinium), we focus on the pH effects on absorption and fluorescence spectra of **GU-P1**.

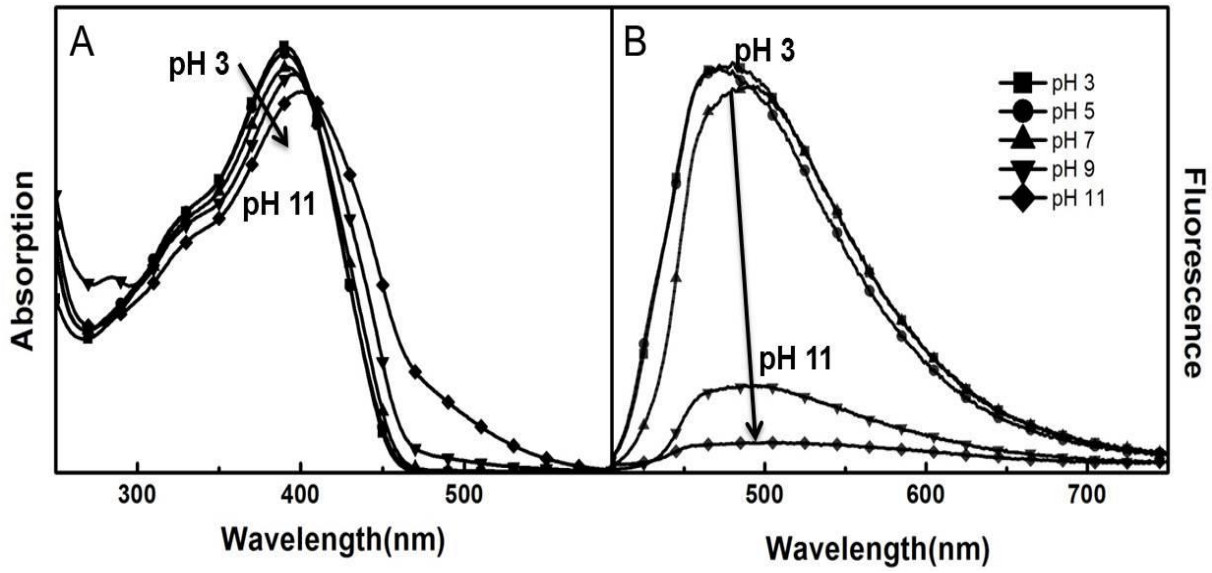

Figure 3-6. Absorption (A) and fluorescence (B) spectra of **GU-P1** in H_2O at different pH.

Figure 3-6 shows the effects of pH on the absorption and emission spectra of **GU-P1** in aqueous solutions. At pH lower than 7, the absorption and fluorescence spectra remained the same, indicating that the polymers were well solvated in H_2O.

Guanidinium group had a pK_a ~ 13,[87,88] and as the pH increased, the guanidinium side group began to partially lose proton, leading to a decreased solubility and formation of aggregates. As shown in Figure 3-6A, the absorption shifted to the red and the intensity decreased from pH 7 to pH 11, signaling the formation of aggregates. The fluorescence of the polymers was more sensitive to the conformational changes induced by the pH. As pH increased from 3 to11, the fluorescence shifted to red and became broad and weak. The largest change in fluorescence spectra occurred between pH 7 and pH 9. Partially deprotonation of the side groups of the polymer resulted in a conformational change to big aggregates.[18,19]

Fluorescence decay dynamics

The presence of aggregates in the PPEs causes the dynamic interaction between the excitons state in non-aggregated chains and excitons localized on aggregate (trap) chains. In order to get more information about the photophysical process in the PPEs with guanidinium side chains, we measured the fluorescence decay in both methanol and water using the time-correlated single photon counting (TCSPC).

The detailed fitting parameters for solutions of **GU-P1** and **GU-P2**, in pure methanol and in water at pH at 5.0 are shown in Table 3-3. All the CPEs showed three-exponential decay with components ranging from 0.15 ns to 2.12 ns. Here we provided a better phenomenological understanding of the decay kinetics including lifetimes (τ_i), and relative amplitude contributions (RA%) as a function of emission wavelengths and solvents (Figure 3-7). The non-exponential decay is due to the nature of inhomogeneous distribution of chromophores in the complex polymer system consisting of single-chain dissolved chains and aggregated chains. In addition, conformational

disorder of individual polymer chains gives arise to a distribution of conjugated segments with different chain lengths.

Table 3-3. Fluorescence lifetime of **GU-P1** and **GU-P2** in MeOH and water (pH = 5).

	MeOH					H_2O				
		RA (%)					RA (%)			
	τ_i (ns)	450 nm	500 nm	550 nm	600 nm	τ_i (ns)	450 nm	500 nm	550 nm	600 nm
GU-P1	τ_1 = 0.15	73	72	75	58	τ_1 = 0.17	88	82	76	75
	τ_2 = 0.46	27	27	23	36	τ_2 = 0.57	12	17	22	22
	τ_3 = 1.26	0	1	2	6	τ_3 = 1.98	0	1	3	3
	χ^2	0.99	0.99	1.00	1.02	χ^2	1.09	0.99	1.01	0.99
GU-P2	τ_1 = 0.17	82	74	68	67	τ_1 = 0.13	95	93	89	85
	τ_2 = 0.54	18	26	31	31	τ_2 = 0.61	5	6	10	13
	τ_3 = 1.73	0	0	1	2	τ_3 = 2.12	0	1	1	2
	χ^2	1.01	1.01	0.98	0.97	χ^2	1.00	0.97	0.97	0.93

Global analysis of the emission decay of **GU-P1** in methanol yielded three decay components, with the fastest two components (0.15 ns and 0.46 ns) contributing to more than 94% of the overall amplitude (Figure 3-7A). As the detection wavelength increased from 450 nm to 600 nm, the fastest component had a decreasing contribution while the second component (0.46 ns) slightly increased its contribution to the overall amplitude. Under acidic conditions in water (pH = 5.0), the fit of the fluorescence decay also featured three exponential decay. Similar results were obtained for **GU-P1** in H_2O with two fast components (0.17 ns and 0.57 ns) contributing more than 97% to the overall amplitude (Figure 3-7B). However, compared with Figure 3-7A, the shorter-

lifetime component had a larger contribution while the longer-lifetime components had relatively smaller contributions to the overall amplitude, resulting a shorter mean lifetime in water. This can be attributed to the fact that PPE chains adopted a more favorable aggregation state in H_2O, driven by the nature of hydrophobicity and those aggregates acted like energy traps. Table 3-2 shows that the fluorescence quantum yield of **GU-P1** in water is lower than that in methanol, a difference consistent with a larger fluorescence decay rate.

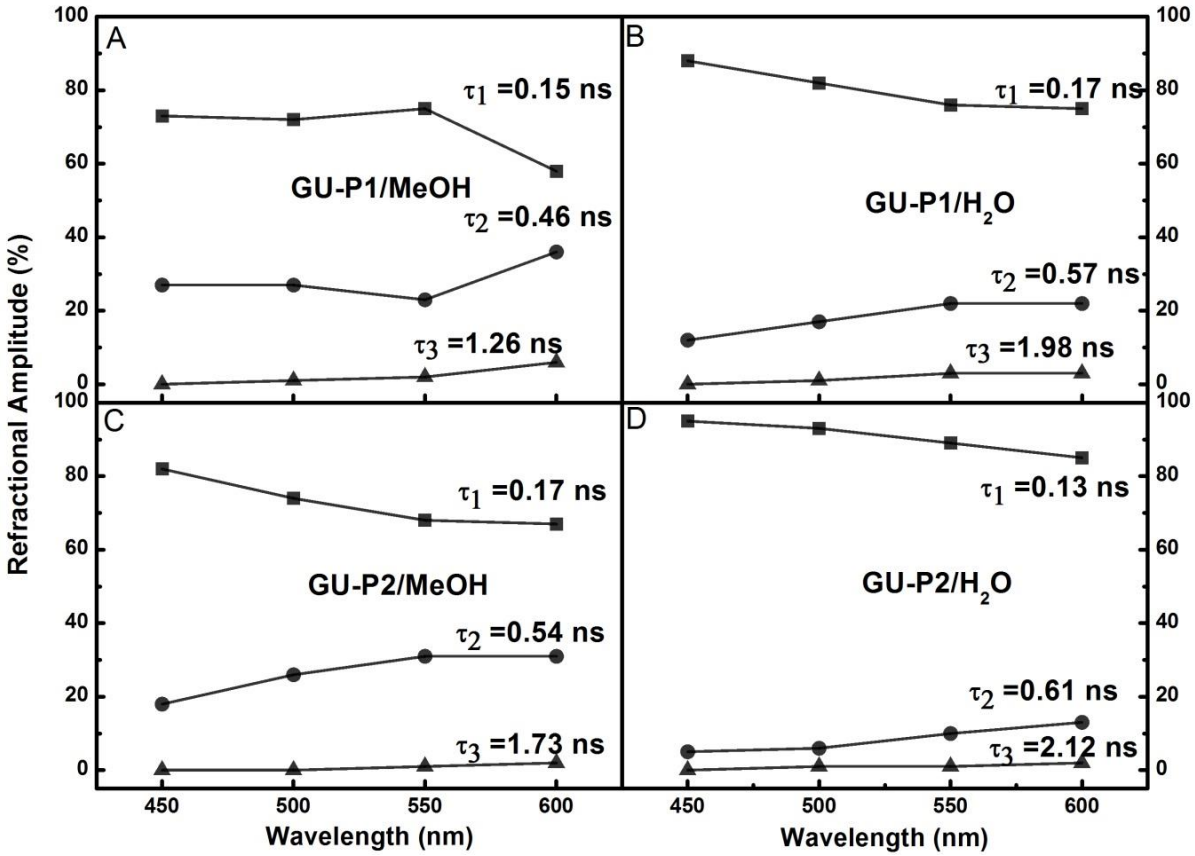

Figure 3-7. Fluorescence lifetime of (A) **GU-P1** in MeOH, (B) **GU-P1** in H_2O, (C) **GU-P2** in MeOH and (D) **GU-P2** in H_2O. H_2O has pH = 5 at various emission wavelengths.

The fluorescence decay of the **GU-P2** solution in methanol featured a similar three component decay with τ = 0.17 ns, 0.54 ns and 1.73 ns (Figure 3-7C). In the

aqueous solution, the decay of **GU-P2** was dominant by a short-lived component (τ = 0.13 ns, > 85%), indicating that PPE polymers had a stronger tendency to exist as aggregate states in water (Figure 3-7D).

There are two issues to consider with respect to the wavelength dependence of the amplitudes. First, this wavelength dependence may be due to multiple emissive segments, such as the aggregated chains in water. Second, the longer lifetime components have a larger contribution at a longer wavelength. It may be explained by the fact that the emission at longer wavelength has a slower decay rate, where the contribution from the aggregated polymer chains and longer chain segments is larger.

Overall, the emission decay kinetics revealed the fact that the fluorescence decay behavior of PPEs was complicated. The changes in the fluorescence decay dynamics indicated that energy was transferred to and quenched by aggregated states. At short wavelength the decay was rapid, likely due to energy transfer from single chains to aggregate traps. At longer wavelength the lifetime was longer, reflecting the lower radiative decay rate for the aggregated chains.[48] The shorter fluorescence lifetime in polar solvent was consistent with the lower fluorescence quantum yield, due to the fact that polymer was aggregated.

Steady-State Fluorescence Quenching of GU-P1 and GU-P2 in Methanol

The guanidinium unit was reported to self-assemble to form a 2:1 complex with biological relevant pyrophosphate ($P_2O_7^{4-}$, PPi) in MeOH.[87,89] In order to investigate the binding efficiency of PPi, fluorescence quenching experiments of **GU-P1** and **GU-P2** in methanol were performed using PPi, AQS, $K_4Fe(CN)_6$ and Pi as quenchers. Figure 3-8 shows the fluorescence of **GU-P1** in methanol upon addition of different quencher solutions. All quenchers quenched the fluorescence of **GU-P1** in methanol efficiently.

AQS and $K_4Fe(CN)_6$ are known efficient energy transfer quenchers, and the fluorescence of the polymer was quenched without any shape change as seen in Figure 3-8A and B. Strong fluorescence quenching were observed for PPi and Pi, accompanied by a slight broadening of the emission spectra and a loss of vibronic structure at higher quencher concentrations. This can be attributed to the fact that PPi and Pi can induce the aggregation of the polymer in MeOH.

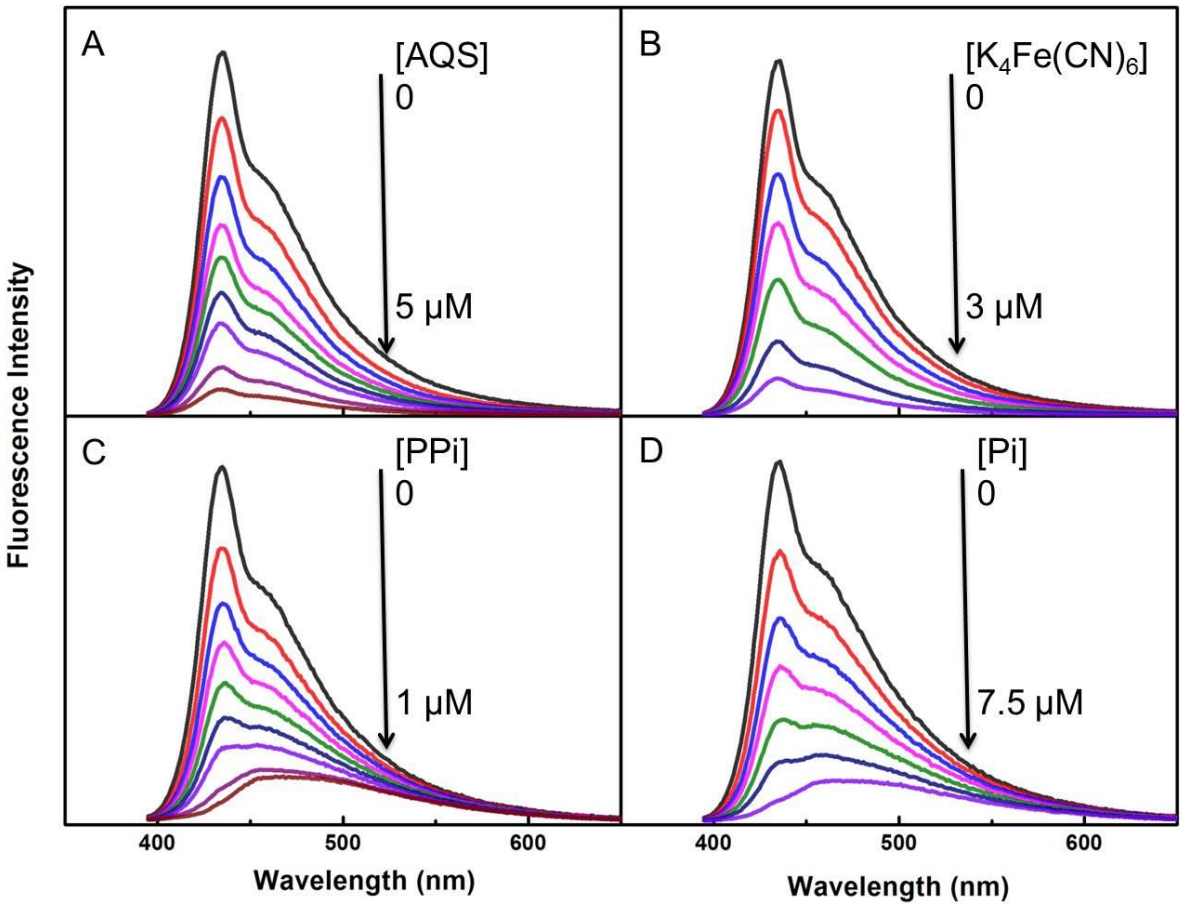

Figure 3-8. Fluorescence spectra of **GU-P1** in MeOH upon the addition of different quenchers. (A) AQS; (B) $K_4Fe(CN)_6$; (C) PPi; (D) Pi. [**GU-P1**] = 2 μM.

Figure 3-9 shows Stern-Volmer quenching plots of **GU-P1** (2 μM) in methanol by AQS, $K_4Fe(CN)_6$ PPi, and Pi. In each case the SV plots were curved upward and consequently we characterized each plot by a K_{sv} value calculated from the linear

portion of the curves at low quencher concentration, along with the [Q_{90}] value, which is defined as the quencher concentration that affords 90% fluorescence quenching. Fluorescence quenching data are summarized in Table 3-4.

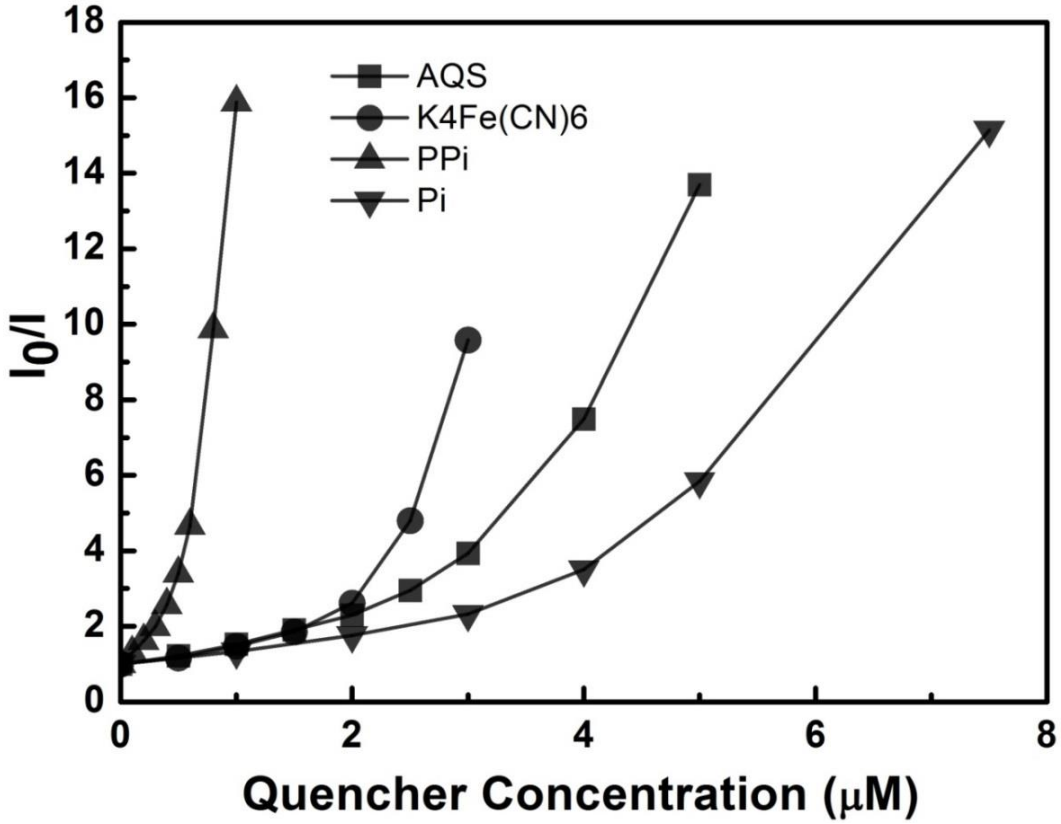

Figure 3-9**.** Stern-Volmer Plots of **GU-P1** (2 μM) with various concentration of the quenchers in MeOH. AQS(■); $K_4Fe(CN)_6$ (●); PPi (▲); Pi (▼).

Table 3-4. Stern-Volmer constant and [Q_{90}] for 2 μM **GU-P1** in MeOH with different quenchers.

Polymer	Quencher	K_{sv} (M^{-1})	[Q_{90}] (μM)
GU-P1	PPi	3.6×10^6	0.8
	$K_4Fe(CN)_6$	6.8×10^5	3.0
	AQS	6.1×10^5	4.4
	Pi	5.3×10^5	6.0

Among all the quenchers, PPi exhibited the strongest quenching with the highest K_{sv} value of 3.6×10^6 M^{-1} and the lowest [Q_{90}] value of 0.8 μM. AQS and $K_4Fe(CN)_6$,

known as widely used electron deficient quencher molecules, had Stern-Volmer coefficients of 6.8 x 10^5 M^{-1} and 6.1 x 10^5 M^{-1} respectively. In addition, the **GU-P1** showed a good selectivity for PPi over Pi; Pi had much weaker ability to quench the fluorescence with a K_{sv} value of 5.3 x 10^5 M^{-1} and a [Q_{90}] value of 6.0 μM. The significant fluorescence quenching by PPi was presumably a consequence of aggregation induced by the complexation of two guanidinium side groups of the polymer **GU-P1** with PPi. Although AQS had two sulfate groups, there was no evidence that AQS can cause the aggregation under the experimental conditions, likely due to the low binding affinity to guanidinium and less basic nature.

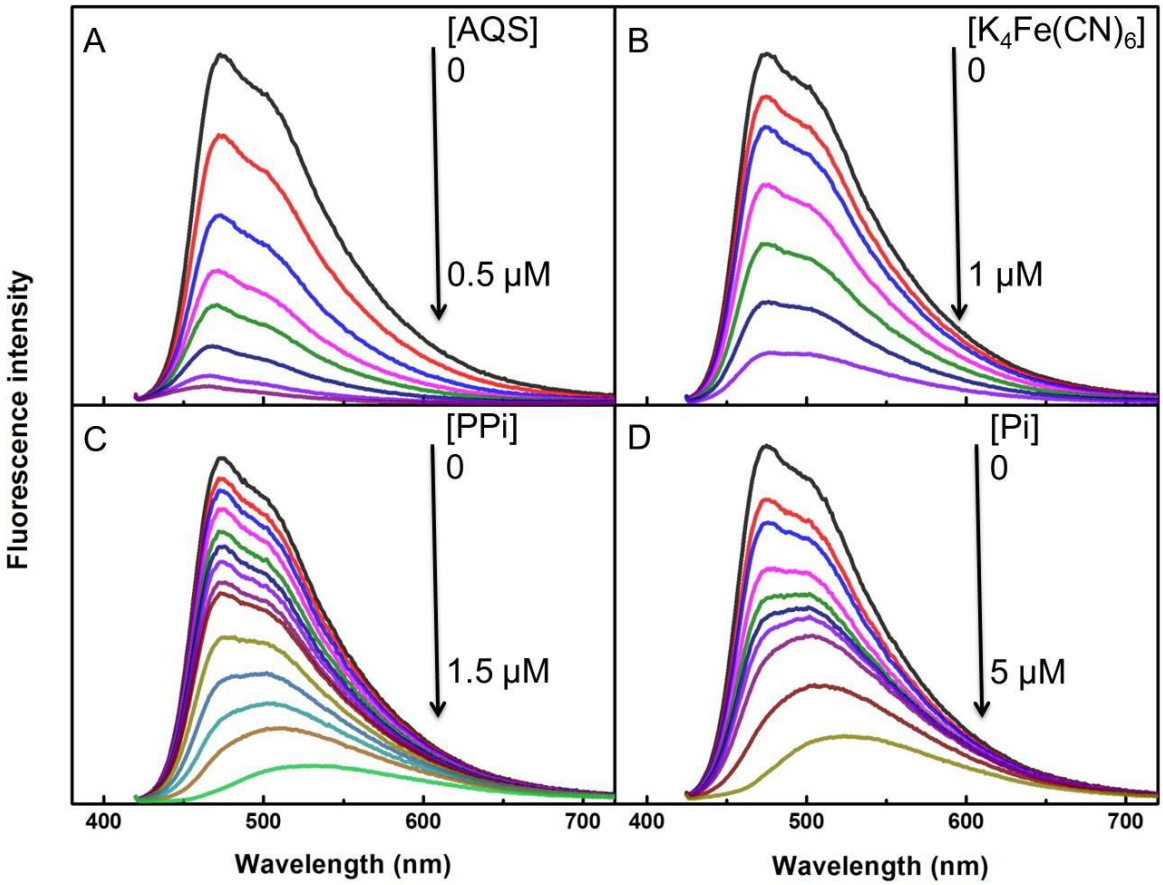

Figure 3-10. Fluorescence spectra of **GU-P2** in MeOH upon addition of different quenchers. (A) AQS; (B) $K_4Fe(CN)_6$; (C) PPi; (D) Pi. [**GU-P2**] = 2 μM.

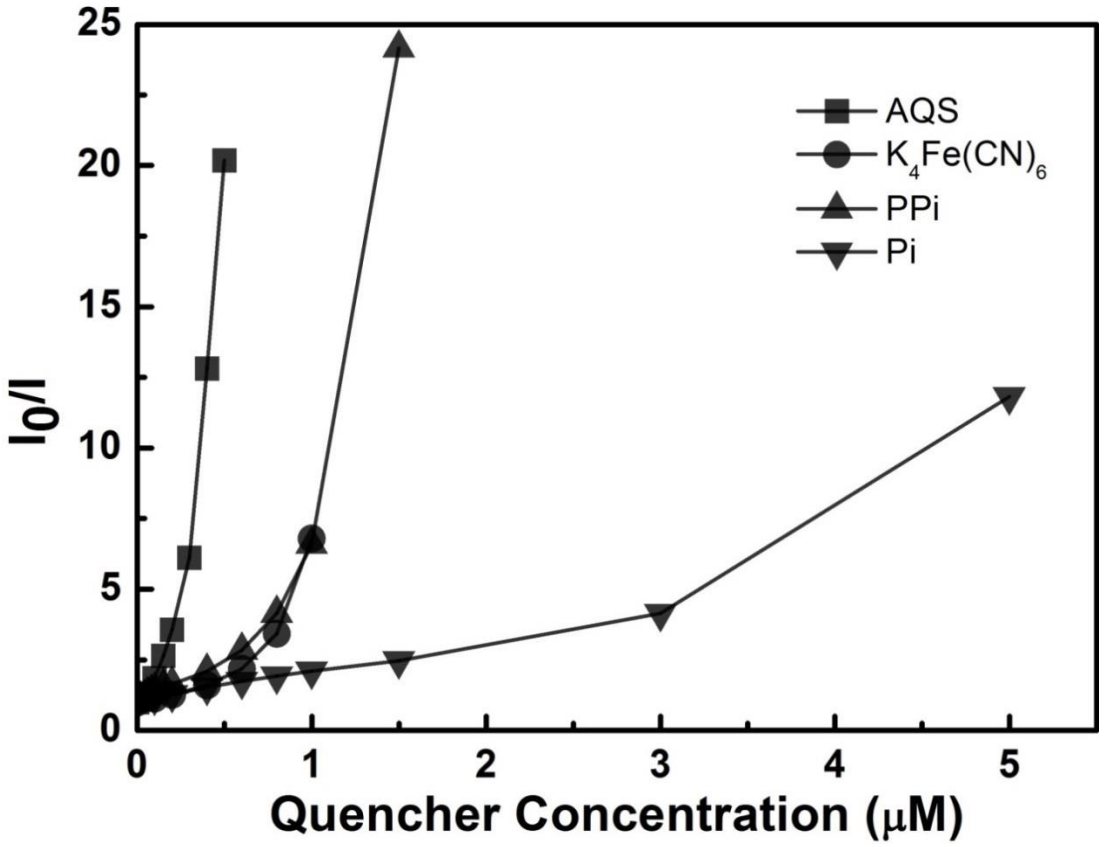

Figure 3-11. Stern-Volmer Plots of **GU-P2** (2 μM) with different quenchers in MeOH. AQS(■); $K_4Fe(CN)_6$ (●); PPi (▲); Pi (▼).

Table 3-5. Stern-Volmer constant and [Q_{90}] for 2 μM **GU-P2** in MeOH with different quenchers.

Polymer	Quencher	K_{sv} (M^{-1})	[Q_{90}] (μM)
GU-P2	PPi	4.6×10^6	1.2
	$K_4Fe(CN)_6$	1.5×10^6	1.1
	AQS	8.0×10^6	0.4
	Pi	1.3×10^6	4.5

Fluorescence quenching of **GU-P2** by different quenchers were conducted in MeOH and shown in Figure 3-10. Figure 3-11 shows the Stern-Volmer plots of **GU-P2** in MeOH, where the Stern-Volmer constants were calculated from the linear range at low concentration and the [Q_{90}] values were obtained. Compared with **GU- P1**, all the

quenchers had a higher K_{sv} value, due to the fact that **GU-P2** had a higher charge density. AQS and $K_4Fe(CN)_6$ exhibited K_{sv} values, 8 x 10^6 M^{-1} and 1.5 x 10^6 M^{-1}, respectively. In MeOH, **GU-P2** also had a good selectivity for PPi over Pi, as seen in Table 3-5. The Stern-Volmer constant for PPi was 4.6 x 10^6 M^{-1}, 3 times higher than that for Pi ~ 1.3 x 10^6 M^{-1}. However, the [Q_{90}] of PPi for **GU-P2** was 1.2 μM, which was larger than the [Q_{90}] for **GU-P1**. The differences can be explained by the possibility for formation of an intra-chain complex, where two neighbor guanidinium units bind with only one PPi molecule.

In general, it was shown that PPi can quench the fluorescence of polymers much more efficiently than Pi. In part the enhanced quenching efficiency arose because the association constant for the guanidinium/PPi complex was larger compared with the other anions. In addition, another effect contributed to the significantly enhanced fluorescence quenching: analyte-induced aggregation of the polymer chains. As the concentration increased, PPi acted like a bridge, inducing polymer aggregation. In particular, analyte induced polymer aggregation turned on pathways for three dimensional exciton migration and significantly increased the quenching ability of the quencher.[93-95]

Application of GU-P1 to PPi Sensing

Interaction of **GU-P1** with PPi in water gave unexpected results, the fluorescence intensity of **GU-P1** increased first and decreased afterward. This was likely due to fact that polymer alone was aggregated in aqueous solution. Previous work showed that addition of surfactant to CPEs caused “de-aggregation”, resulting in the fluorescence recovery.[96] A similar result was observed that the addition of non-ionic surfactant Triton X-100 to a solution of **GU-P1** in water gave a substantial increase in fluorescence

intensity. The significantly enhanced fluorescence intensity and blue-shifted spectrum signaled the changes in polymer conformation and aggregation state due to “wrapping” of polymer chains by surfactant molecules. A titration was carried out to quantify the effects of Triton X-100 concentration on the polymer fluorescence. As shown in Figure 3-12A, upon the addition of Triton X-100 from 0 to 200 μM, the fluorescence intensity of **GU-P1** increased by about 15 fold at 435 nm. The significant change of the fluorescence intensity suggested that surfactant molecules inhibited the aggregation of the polymer chains as reported.[97,98] The improved properties can be used in PPi sensor development in aqueous solution.

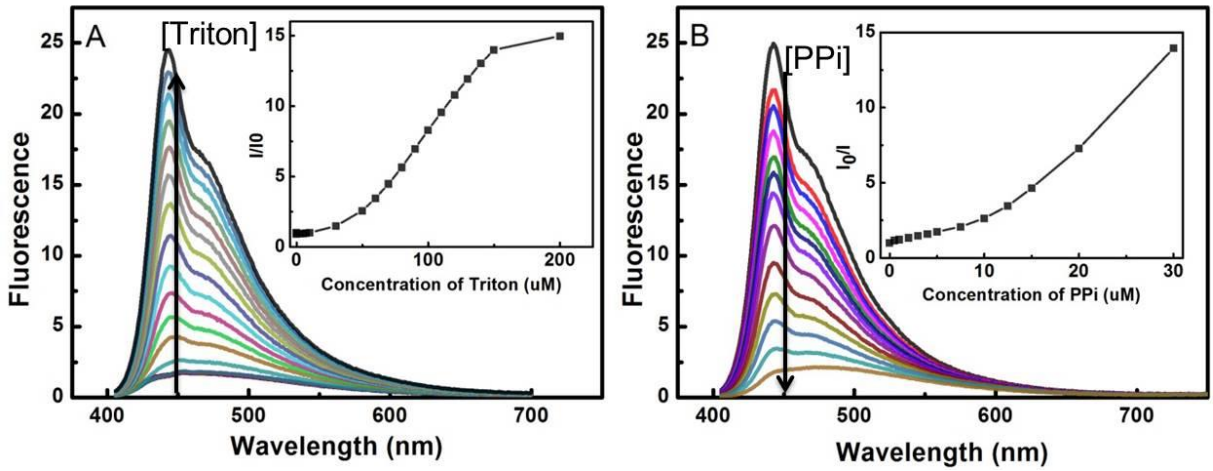

Figure 3-12. (A) Fluorescence spectra and emission change of **GU-P1** (3 μM) in H_2O (pH = 6.5) upon the addition of Triton X-100 from 0 to 200 μM; (B) fluorescence spectra of **GU-P1**/triton complex and emission change upon the addition of PPi from 0 to 30 μM, [**GU-P1**] = 3 μM, [Triton X-100] = 200 μM. Insets are the Stern-Volmer plots.

As an effort to develop a PPi sensor, a fluorescence quenching experiment of the mixture of **GU-P1**/Triton ([**GU-P1**] = 3 μM, [Trixton X-100] = 200 μM, pH = 6.5) in water was carried out upon addition of various concentration of PPi. As shown in Figure 3-12B, addition of PPi induced significant fluorescence quenching via analyte-induced aggregation mechanism, with a modest Stern-Volmer value of 1.7 x 10^5 M^{-1} and a [Q_{90}]

~ 22 μM. As a comparison, the effect of Pi was studied by addition of Pi to the **GU-P1**/Trixton X-100 mixture. Very little or no quenching was observed, indicating that **GU-P1**/Triton mixture had a high selectivity of PPi over Pi (Figure 3-13). Although Pi can neutralize the polymer charges, clearly it is unable to induce the polymer aggregation.

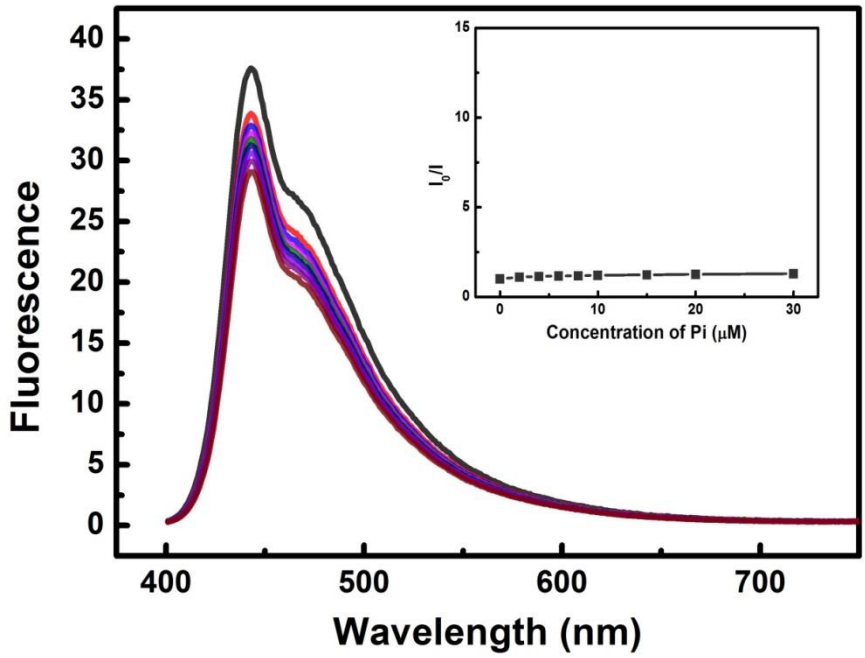

Figure 3-13. Fluorescence spectra of **GU-P1**/triton complex and emission change upon the addition of Pi from 0 to 30 μM, [**GU-P1**] = 3 μM, [Triton X-100] = 200 μM. Inset is the Stern-Volmer plots.

Table 3-6**.** Diffusion time and hydrodynamic radius calculation.

Number	**GU-P1** (μM)	Triton X-100 (μM)	PPi (μM)	τ (s)	R_H (nm)
1	2	0	0	1.46×10^{-4}	3.14
2	2	200	0	2.98×10^{-4}	6.41
3	2	200	50	2.57×10^{-3}	55.3

In order to determine the size change in our PPE system, fluorescence correlation spectroscopy (FCS) was applied to measure the diffusion behavior of

aqueous **GU-P1**, **GU-P1**/Trition complex and **GU-P1**/Trition/PPi complex. Diffusion time and subsequently calculated hydrodynamic radius are summarized in Figure 3-14 and Table 3-6.

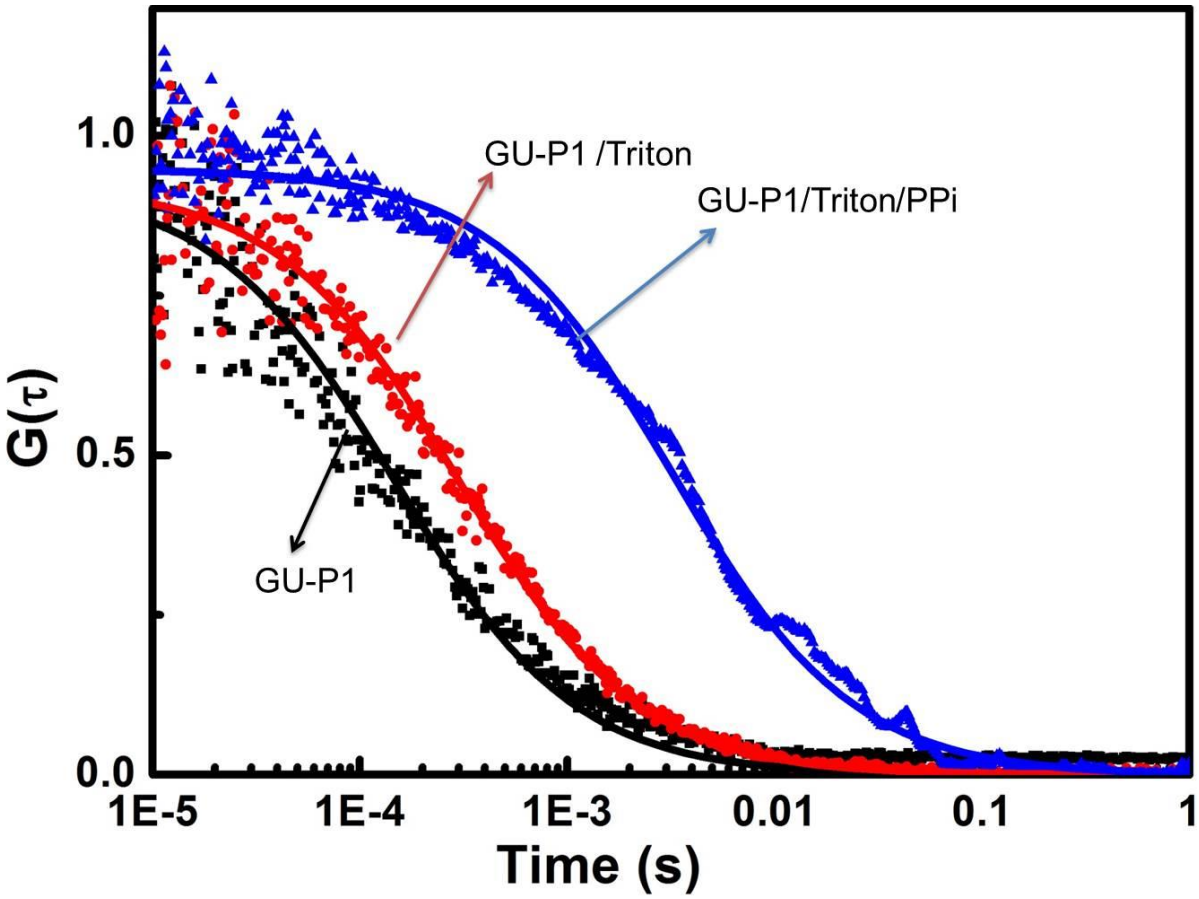

Figure 3-14. Normalized correlation curves for **GU-P1** (black), **GU-P1**/Triton X-100 (Red) and **GU-P1**/Triton X-100/ PPi (blue) in aqueous solutions (pH = 6.5). The solid lines are single specific fitting curves. Black: **GU-P1** (2 μM); Red: **GU-P1** (2 μM)/Triton X-100 (200 μM); Blue: **GU-P1** (2 μM)/Triton X-100 (200 μM)/PPi (50 μM).

The results indicated that **GU-P1**/Trition complex showed a slightly longer diffusion time (29.8 ms) compared to **GU-P1** alone (14.6 ms). The increase of the diffusion time was probably attributed from the hydrophobic interaction between surfactants and polymer chains that led to the formation of PPE/surfactant complex. After PPi was introduced, a significant further increase of the diffusion time (55.3 ms)

was observed, indicating the formation of very large aggregates. The size change of the polymer contributed to its fluorescence quenching, which was consistent with the idea that PPEs were cross-linked together by PPi to form inter-chain aggregates.

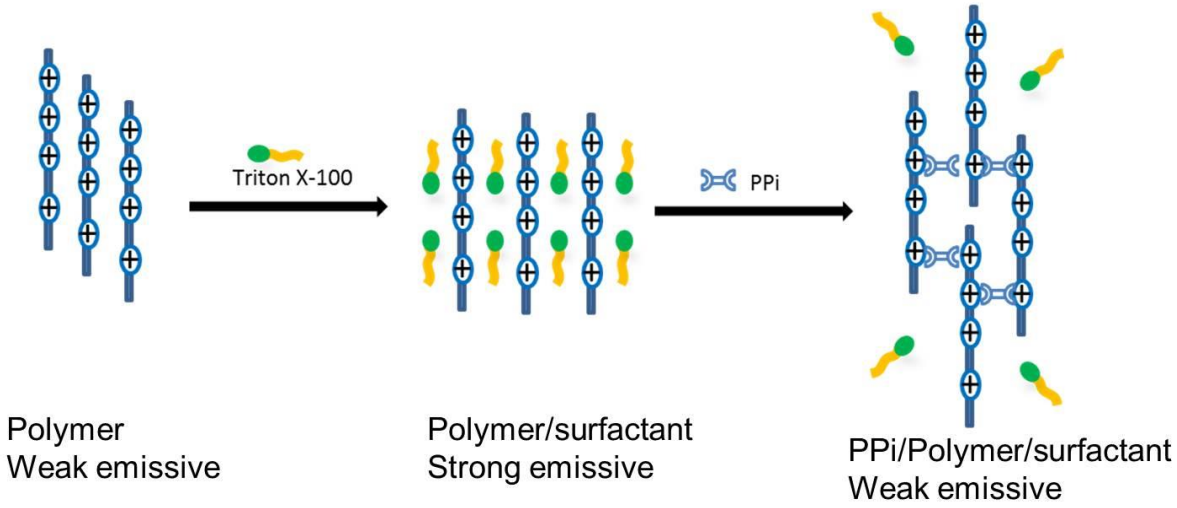

Figure 3-15. Proposed PPi sensing mechanism.

Therefore, a PPi sensing strategy is established based on the interaction between the natural substrate PPi, surfactant and a fluorescent water-soluble conjugated polyelectrolyte as illustrated in Figure3-15. The fluorescence intensity of the PPE in water was increased significantly by the addition of Triton X-100, due to the formation of a CPE-surfactant complex. Pyrophosphate-induced aggregation caused substantial fluorescence quenching, which in turn allowed sensing of dissolved PPi in aqueous solution.

Summary

We have successfully prepared and characterized a new series of conjugated polyelectrolytes based on the poly(phenylene ethynylene) backbone featuring guanidinium side groups. These polymers were prepared using a “precursor” route.

Hydrolysis of the precursor polymers followed by dialysis against pure water affords water soluble cationic PPEs.

Investigations of the photophysical properties of the PPEs led to the conclusion that both **GU-P1** and **GU-P2** were aggregated in water, with lower fluorescence quantum yield, red-shifted broad fluorescence spectra, and shorter fluorescence lifetime. Steady state fluorescence quenching of **GU-P1** and **GU-P2** with a series of quenchers revealed the fact that two guanidinium side units can form a complex with PPi, which in turn induced the aggregation of polymer chains and dramatically decreased the fluorescence intensity.

A fluorescence turn-off sensor for pyrophosphate was developed by taking advantage of the interaction between water-soluble PPE, surfactant and PPi. In aqueous solution, the spectroscopic properties of the polymer/surfactant were sensitive to the concentration of PPi with high selectivity over Pi due to analyte-induced aggregation mechanism. The change in the polymer aggregation state was readily examined by fluorescence correlation spectroscopy, which directly provided the size of polymer chains. We are currently developing biological assays for enzymes with PPi as substrates using this system and we believe the design principles can be applied to other anion species of interest.

Experimental

Materials

$Pd(PPh_3)_4$ was purchased from Strem Chemical Company and used as received. Triton X-100, sodium pyrophosphate, sodium phosphate, N,N'-Boc_2-1H-pyrazole-1-carboxamidine, 9,10-anthraquinone- 2,6-disulfonic acid disodium salt (AQS), and 1,8-diazabicyclo[5.4.0]undec-7-ene (DBU) were purchased from Sigma-Aldrich and used

without further purification. Sodium azide, trifluoroacetic acid, hydrochloric acid and potassium ferrous cyanide ($K_4Fe(CN)_6$) were purchased from Fisher Scientific Company and used as received. THF and DMF were purified by solvent dispensing system. All chemicals were from commercial sources unless specially mentioned. Stock solutions (1.0 mM, polymer repeat unit) of all PPEs were prepared in H_2O (pH = 5) and were stored at 4 ^{o} C.

Instruments and General Methods

NMR spectra were recorded using a Gemini-300 NMR operating at 300 MHz for ^{1}H NMR and at 75 MHz for ^{13}C NMR for small organic compounds. ^{1}H NMR spectra of the polymers were measured in Inova2-500 NMR operating at 500 MHz for ^{1}H NMR. Gel permeation chromatography (GPC) analysis was carried out on a system comprised of a Shimadzu LC-6D pump, Agilent mixed-D column and a Shimadzu SPD-20A photodioide array (PDA) detector, with THF as eluent at 1 mL/min flow rate. The system was calibrated against linear polystyrene standards in THF. UV-Vis absorption spectra were measured on a Shimadzu UV-1800 spectrophotometer. Luminescence spectra were measured on a PTI (Photon Technology International) fluorescence spectrometer. Fluorescence lifetimes were determined by time-correlated single photon counting on a FluoTime 100 spectrometer (Pico Quant) equipped with 370 nm diode laser as excitation source. Fluorescence quantum yields were reported relative to known standards. The optical density of solutions at the excitation wavelength was <0.1 and corrections were applied for differences in the refractive index of standard and sample solutions. Fluorescence correlation spectroscopy (FCS) measurements were taken on a homemade setup using a 405 nm diode laser as the excitation light. Fluorescein (30 nM)

in 10 mM phosphate buffer (pH = 8) was used as the calibration standard for the system.

Synthetic Procedures

1,4-Bis(2-bromoethoxy)benzene (**1**) and 2,5-diiodo-1,4-bis(2-bromoethoxy) benzene (**2**) were synthesized according to literature procedures.[90]

2,5-Diiodo-1,4-bis(2-azidoethoxy)benzene (3). To a solution of compound **2** (3.0 g, 5.2 mmol) in 50 mL of dry DMF, sodium azide (6.77 g, 0.1 mol) was charged. The mixture was allowed to stir at 40 ^{o} C overnight. Upon the completion of reaction, the mixture was poured into 100 mL of cold water. The white precipitate was collected by filtration and dried under vacuum (yield: 2.5 g, 82%). ^{1}H NMR (300 MHz, $CDCl_3$): δ 3.64 (t, 4H), 4.10 (t, 4H), 7.22 (s, 2H). ^{13}C NMR (75 MHz, $CDCl_3$): δ 50.49, 69.24, 86.32, 123.36 153.23.

2,5-Diiodo-1,4-bis(2-aminoethoxy)benzene (4). To a solution of compound **3** (2.5 g, 10 mmol) in 180 mL of THF and water mixture (v/v, 2/1), triphenylphosphine (8.18g, 31.2 mmol) was charged. The mixture was heated to reflux for 2 h. The solvent was removed under vacuum and the residue was taken by 20 mL acetone. Concentrated HCl (5 mL) was added slowly to the solution, whereupon a white precipitate was formed. The precipitate was collected by vacuum filtration and re-dissolved in 30 mL water and basified with 20 mL of 1N NaOH solution. The white solid was collected by vacuum filtration and dried under vacuum (yield: 1.2 g, 52%). ^{1}H NMR (300 MHz, DMSO-d_6): δ 1.50 (s, 4H), 2.84 (t, 4H), 3.92 (t, 4H), 7.35 (s, 2H). ^{13}C NMR (75 MHz, DMSO-d_6): δ 40.74, 41.72, 73.38, 87.90, 123.41, 153.13.

Compound 5. To a stirred solution of compound **4** (1 g, 2.23 mmol) in DMF (20 mL) was added N,N'-Boc_2-1H-pyrazole-1-carboxamidine (1.52 g, 4.90 mmol). The

resulting solution was stirred at room temperature for 24 h. The white precipitates were collected by vacuum filtration and washed thoroughly by large amount of water (yield: 1.8 g, 87%). ^{1}H NMR (500 MHz, $CDCl_3$): δ 1.49 (s,18H), 1.51 (s, 18H), 3.88 (t, 4H), 4.06 (t, 4H), 7.19 (s, 2H), 8.81 (m, 2H), 11.48(s, 2H). ^{13}C NMR (125 MHz, $CDCl_3$): 28.32, 28.55, 40.33, 69.07 , 79.60, 83.37, 86.57, 123.55, 153.01, 153.17, 156.67, 163.74. HRMS (ESI) *m*/*z*: $[M+Na]^+$ calcd. for $C_{32}H_{50}I_2N_6O_{10}Na$, 955.1570; found, 955.1572.

Synthesis of GU-P1-Boc. To a degassed solution of compound **5** (93.3 mg, 0.1 mmol) and 1,4-diethynylbenzene (12.6 mg, 0.1 mmol) in 25 mL THF/iPr_2NH (v/v 4/1), tetrakis(triphenylphosphine)palladium(0) (10 mg, 8.7 μmol) and CuI (10 mg, 52 μmol) were added. The solution was stirred at 60 ° C for 48 h. The solvent was removed under vacuum. The residue was re-dissolved in 20 mL $CHCl_3$ and then passed through a short alumina column to remove all the catalyst. The resulting solution was concentrated to 3 mL and then poured into a large volume of hexane. The polymer precipitates were collected as yellow fine powder and the polymer was further purified by multiple precipitation in hexane (yield: 70%). ^{1}H NMR (500 MHz, $CDCl_3$): δ 1.30 (s, 18H), 1.45 (s, 18H), 3.90 (br, t, 4H), 4.20 (br, t, 4H), 7.01 (s, 2H), 7.55 (s, 4H), 8.90 (br, 2H), 11.52 (s, 2H). GPC (THF, Polystyrene standards): M_n = 76.2 kD, M_w = 101 kD, PDI = 1.33.

Synthesis of GU-P2-Boc. To a solution of compound **5** (142 mg, 0.15mmol) in 15 mL THF, 0.8 mL DBU and 0.2 mL deionized water were added. After degassing for 30 mins, CuI (10 mg, 52 μmol) and $Pd(PPh_3)_4$ (10 mg, 8.7 μmol) were added under the protection of argon. Then 22 μL trimethylsilylacetylene was added to the solution by syringe. The solution was stirred at room temperature for 3 days before directly passing through a short alumina column. The resulting solution was concentrated and poured

into a large volume of hexane. The polymer precipitated as a fine powder and then further purified by several steps of dissolution in $CHCl_3$ followed by precipitation from hexane (yield: 50%). ^{1}H NMR (500 MHz, $CDCl_3$): δ 1.25 (s, br, 18H), 1.45 (s, 18H), 3.90 (br, 4H), 4.20 (br, 4H), 7.00 (s, 2H), 8.80 (br, 2H), 11.45 (br, 2H). GPC (THF, Polystyrene standards): M_n = 41.5 kD, M_w = 79.4 kD, PDI = 1.91.

Hydrolysis. GU-P1-Boc (80 mg, 0.1 mmol) or **GU-P2-Boc** (65 mg, 0.1 mmol**)** was dissolved in 20 mL $CHCl_3$ and cooled down in an ice/water bath. Trifluoroacetic acid (TFA, 20 mL) was added to the polymer solution drop-wise. Upon the completion of the addition, the reaction mixture was allowed to warm to room temperature and stirred for another 24 h. The excess TFA and the solvent were removed under vacuum and the residue was taken by 3 mL ethanol followed with addition of 3 mL hydrochloric acid. Then the polymer solution was poured into a large volume of acetone and precipitated as a yellow powder. The polymer was further purified by several steps of dissolution in water followed with precipitation from acetone. The polymer was dissolved in 20 mL water and filtered through a cellulose membrane (pore size: 0.22 um). Final purification of the polymer was accomplished by dialysis of aqueous solution of the polymer against water (pH = 5) using Fisher Brand cellulose membrane (12 kD molecular weight cut-off) for 3 days. Light yellow solid was obtained in a yield of 80~90 % after lypholization.

GU-P1: ^{1}H NMR (500 MHz, DMSO-d_6): δ 3.65 (br, 4H), 4.20 (br, 4H), 7.00 – 8.00 (br, 16H).

GU-P2: ^{1}H NMR (500 MHz, DMSO-d_6): δ 3.60 (br, 4H), 4.25 (br, 4H), 7.20 – 7.70 (br, 10H), 7.75 – 8.10 (br, 2H).

CHAPTER 4
VARIABLE BAND GAP POLY(ARYLENE ETHYNYLENE)S FEATURING METHYLENE CARBOXYLATE SIDE CHAINS

Background

Over the past decades, significant efforts have been devoted to synthesize new conjugated polyelectrolytes (CPEs) and explore their applications in photovoltaic devices, solar cells,[49] and chemical and biosensors.[24] In particular, PAE-type CPEs have attracted more and more attention, owing to their extraordinary properties, such as high fluorescence quantum yield, water solubility, and high sensitivity to fluorescence quenchers due to exciton migration.[52,99,100] In addition, the amplified fluorescence quenching effects are enhanced in aggregated states when exciton inter-chain migration is accessible.[54,91,101] However, the applications of poly(arylene ethynylene)s (PAEs) is sometimes limited by low quantum yield, bad solubility and unexpected sensing behavior caused by the self-assembly into aggregates in aqueous solutions.[52,94]

As mentioned earlier in chapter 3, methanol is typically considered as a good solvent for conjugated polyelectrolytes, which preserve their good optical properties such as the high fluorescence quantum yields, sharp structured fluorescence spectra, and low Stokes shift from absorption maximum to emission maximum. In aqueous solution, PAEs exhibit a red-shift in UV-Vis spectra with a pronounced shoulder and a broad “excimer like” band in fluorescence spectra. It was found that the differences in photophysical properties were attributed to a strong tendency to aggregate in “poor solvent” water.[6,7] For this reason, sizable efforts have been made to reduce aggregation tendencies by adding surfactants, attaching bulky ionic side groups or twisting the polymer backbone.[48,64,96]

The traditional PPE-type CPEs always had an oxygen on the linker directly attached to the polymer backbone and in a related work reported by Schanze and coworkers, three OPEs without oxygen linkers exhibited extraordinary photophysical properties in aqueous solution.[102] The remarkable photophysical properties were attributed to the introduction of methylene carboxylate side groups, resulting in unaggregated OPEs in aqueous solution. Therefore, a new series of poly(arylene ethynylene)s (PAEs) conjugated polyelectrolytes featuring methylene carboxylate side chains have been prepared. The series consist of four members of polymers which share the same anionic side groups: methylene carboxylate ($-CH_2-CO_2Na$).The repeat unit of the poly(arylene ethynylene) backbone comprises of a bis(methylene carboxylate)phenylene ethynylene unit alternating with a second arylene ethynylene moiety and four different aryls were used, Ar = 1,4-phenyl (**P1**), 2,5-thienyl (**P2**), 2,5-(3,4-ethylenedioxy)thienyl (**P3**) and 1,4-(2,3,5,6-tetrafluoro)phenyl (**P4**) (Figure 4-1). The photophysical properties of the PAEs were studied in both methanol and water by absorption, fluorescence spectroscopy and fluorescence lifetime measurements. Stern-Volmer fluorescence quenching studies were carried out using methyl viologen (MV^{2+}) as an electron acceptor in aqueous solution. The photophysical data suggested that the aggregation tendency was significantly suppressed, resulting in non-aggregated PAEs in aqueous solution.

Some applications based on this set of PAEs were developed. Fluorescence quenching and fluorescence correlation spectroscopy were applied to study the interaction between polymer **P1** and different metal ions. As an effort to develop new dye sensitized solar cell, **P2-H** (acid form polymer) was deposited on the surfaces of

ZnO single crystal. AFM images indicated that most of the polymers existed as a single chain with a height around 3 nm. Finally, a fluorescent sensor based on **P4**/rhodamine system was developed to detect mercury (II) ion in water, with a high selectivity over other metal ions.

Results and Discussion

Synthesis of PAEs with Methylene Carboxylate Side Chains

In this study, we report new water-soluble PAEs with novel methylene carboxylate side chains as shown in Figure 4-1. Each polymer contains a bis(methylene carboxylate) phenylene ethynylene unit and different arylene ethynylene units have been introduced into the polymer backbone to tune the band gap. Four different arylene units were used, Ar = 1,4-phenyl, 2,5-thienyl, 2,5-(3,4-thylenedioxy)thienyl and 1,4-(2,3,5,6-tetrafluoro)phenyl.

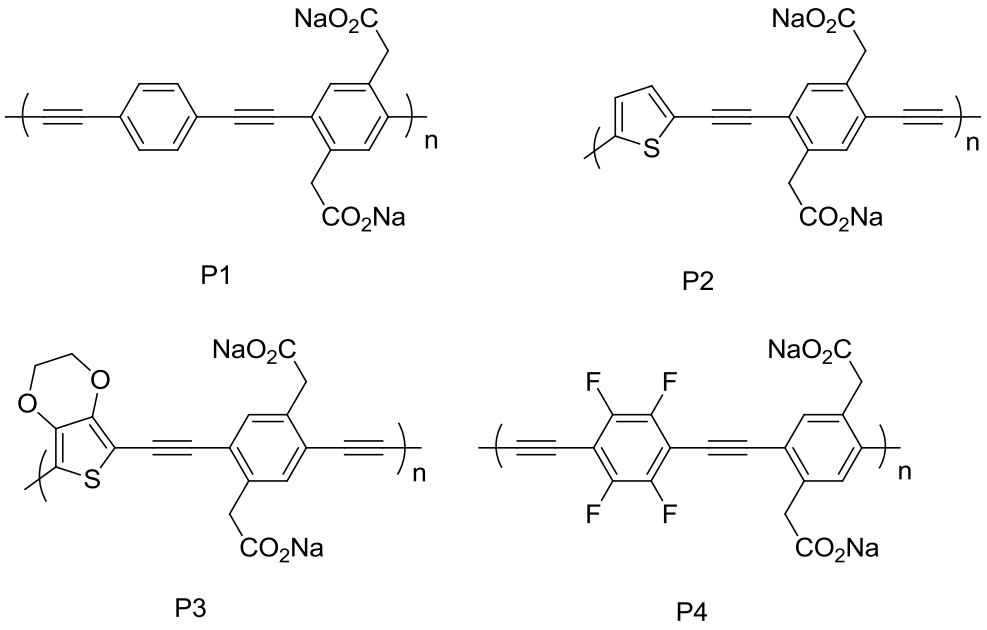

Figure 4-1. Structures of poly(arylene ethynylene)s with methylene carboxylate side groups.

Monomer synthesis

The monomer, didodecyl-2,2'-(2,5- diiodo-1,4-phenylene)diacetate (**C1**) was synthesized as shown in Figure 4-2. In this route, the monomer was prepared from commercial available dichloro-*p*-xylene in 6 steps with the overall yield of 14%.

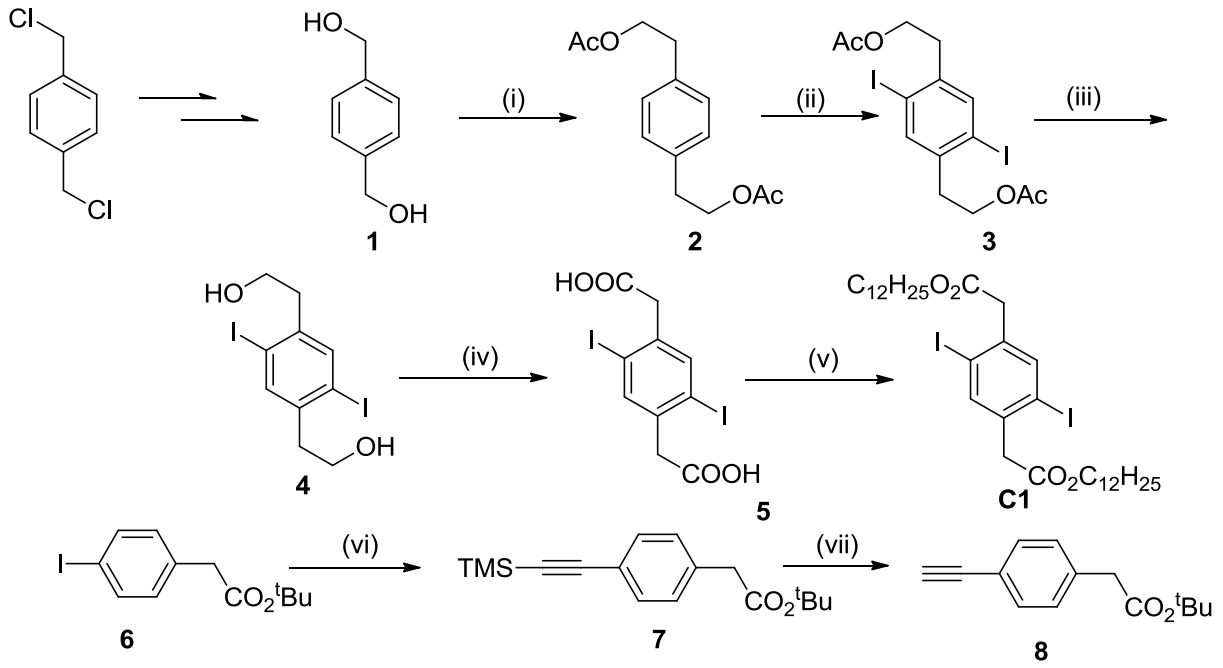

Figure 4-2. Synthesis of monomer **C1**. (i) Ac_2O, pyridine, overnight; (ii) I_2, $NaIO_4$, AcOH, Ac_2O, rt, 6 hrs; (iii) K_2CO_3, CH_2Cl_2, CH_3OH, rt, overnight; (iv) PCC, $NaIO_4$,rt, 6 hrs; (v) $C_{12}H_{25}OH$, H_3PO_4, 150 ^{o}C, 6 hrs; (vi) TMSA, $Pd(PPh_3)_2Cl_2$, CuI, rt, overnight; (vii) tetrabutylammonium floride (TBAF), $CHCl_3$, rt, 1h.

The 2,2'-(1,4-phenylene)diethanol (**1**) was prepared following the literature procedure.[103] Esterification of 2,2'-(1,4-phenylene) diethanol (**1**) with excess of acetic anhydride afforded compound **2** in quantitative yield. Iodination of compound **2** with iodine and sodium periodinate in acetic acid and acetic anhydride mixture gave compound **3** in 80% yield. Subsequent deprotection of the ester **3** with K_2CO_3 afforded compound **4** in 85% yield. Diacid compound **5** was prepared by oxidation of compound **4** with pyridinium chlorochromate (PCC) and periodic acid. Then Fisher esterification of

compound **5** with dodecyl alcohol in the presence of a catalytic amount of H_3PO_4 gave the desired monomer **C1**, which was easily isolated as white solids in 85% yield. The purities of intermediates and the monomer were proven by ^{1}H NMR, ^{13}C NMR spectroscopy and mass spectrometry. Compound **6** was synthesized according to the procedures described in literatures.[104,105] Sonogashira reaction with trimethylsilyl acetylene (TMSA) and subsequent deprotection provided compound **8** with a good yield ~ 85%.

Polymer synthesis and characterization

In order to prevent electrostatic repulsion of ionic charged groups in aqueous media and facilitate gel permeation chromatography (GPC) analysis to measure accurate molecular weight, the polymerization was carried out in organic solvents using a “precursor route”. As shown in Figure 4-3, a set of anionic PAE-based conjugated polyelectrolytes with variable band gap were synthesized using palladium-catalyzed Sonogashira coupling chemistry, which consist of four polymers that share the same anionic side groups, methylene carboxylate ($-CH_2-CO_2Na$). The tuning of the band gap was accomplished by copolymerizing monomer **C1** with different trimethylsilyl (TMS) protected diacetylene arylene compounds. After the reaction was stirred at 60 ^{o} C for 24 hours, compound **6** (1 mg) and compound **8** (1 mg) were added as end cappers. After additional 24 hours, the organic precursors were isolated as solids and purified by multiple precipitations in methanol. Each polymer was characterized by ^{1}H NMR spectroscopy. The GPC analysis was carried out in THF against polystyrene standards and the number average molecular weight and polydispersity data for **P1-E** - **P4-E** are listed in Table 4-1.

The hydrolysis of the precursor polymers was easily accomplished by treating the ester precursors with trifluoroacetic acid followed by NaOH in THF/H_2O mixture. The resulting polymers were precipitated in acetone containing 5 ~ 20% MeOH and collected by centrifugation. Further purification was carried by out by multiple precipitation in acetone followed by the dialysis using 12 kD molecular weight cut-off (MWCO) dialysis membranes for 3 days. The water soluble PAEs (**P1** - **P4**) were obtained as solids in 90 ~ 100% yields after lyophilization.

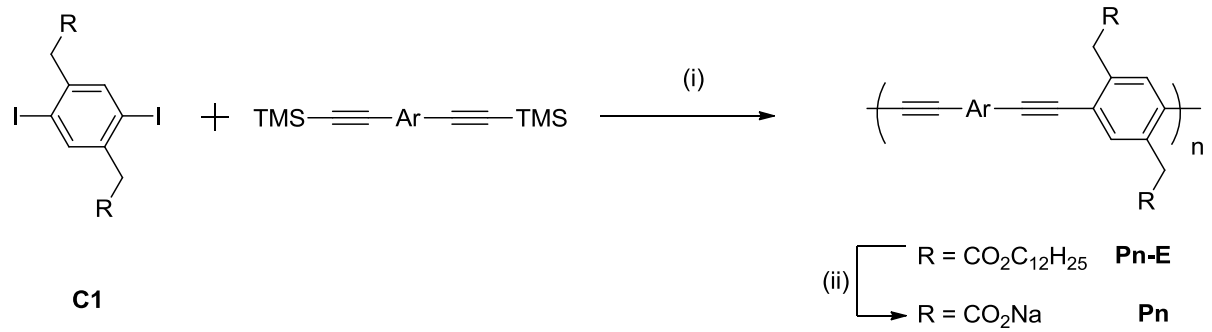

Figure 4-3. Synthesis of PAEs through precursor route. (i) $Pd(PPh_3)_4$, CuI, TBAT, compound **6**, compound **8**, THF, i-Pr_2NH, 60 ^{o}C, 48 h; (ii) TFA, $CHCl_3$, 5 h; NaOH, THF, H_2O, 60 ^{o}C, 2 days.

Table 4-1. GPC analysis for precursor polymers (**Pn-E**).

Structures	Names	Ar	M_n (kD)	PDI
	P1-E	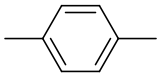	19	1.8
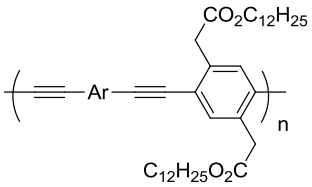	**P2-E**	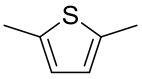	42	1.9
	P3-E	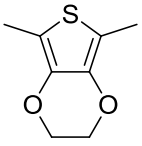	19	1.8
	P4-E	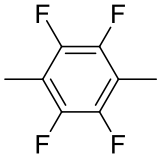	65	2.6

Figure 4-4 shows the representative ^{1}H NMR spectra of monomer **C1**, the precursor polymer **P1-E** and the water-soluble polymer **P1**. ^{1}H NMR spectra analysis revealed that there was only one difference between the spectra of monomer **C1** and **P1-E**: the resonance peak at δ = 7.60 ppm, which was assigned to all aromatic protons of the polymer backbone. In addition, the resonance peaks become broader and weaker in the spectra of **P1-E**.

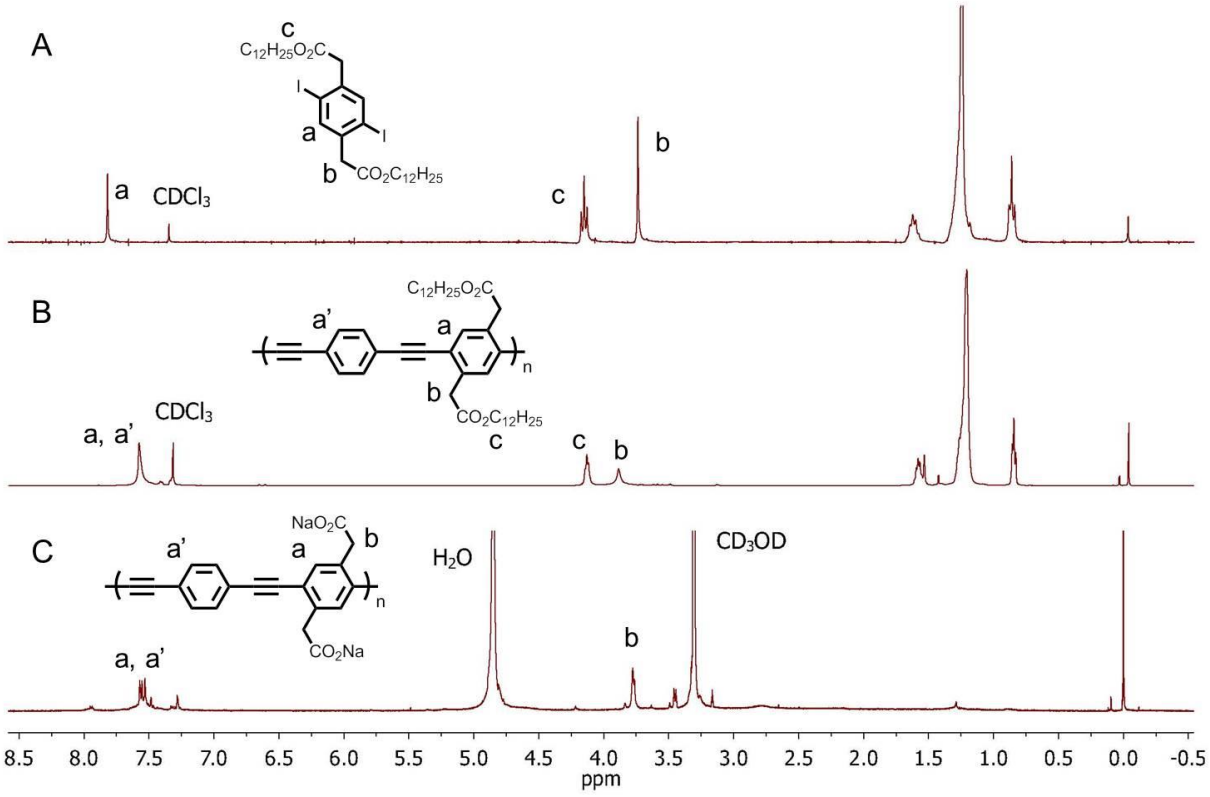

Figure 4-4. ^{1}H NMR spectra of (A) monomer **C1**; (B) **P1-E**; (C) **P1**.

After ester hydrolysis, the ^{1}H NMR spectrum of **P1** was measured in CD_3OD. The solvent peak and water residue peak showed up strongly because of the low solubility of **P1**. No signals were observed in the range of 0.5 ~ 1.5 ppm and the peak at 4.3 ppm

disappeared, indicating that the dodecyl groups were cleaved with an excellent yield (>95%).

Photophysical Properties

Absorption and fluorescence spectroscopy

The photophysical properties of precursor polymers were studied in $CHCl_3$ by UV-Vis absorption and fluorescence spectroscopy. Figure 4-5 shows a systematically red-shift in UV-Vis absorption and fluorescence spectra of dodecyl ester precursor polymers in the order of **P1-E** < **P4-E** < **P2-E** < **P3-E** in $CHCl_3$. Across the entire series, the absorption maximum shifted from 375 nm (**P1-E**) to 434 nm (**P3-E**), whereas the fluorescence maximum shifted from 418 nm (**P1-E**) to 484 nm (**P3-E**). The origin of the red-shifts is likely due to the difference in HOMO-LUMO levels of the polymers. Specially, the shifts of **P2** and **P3** polymers arose from the electron-donor character of thienyl and 3,4-ethylenedioxy-2,5-thienyl units. It is of note that incorporation of tetrafluorophenyl into the polymer backbone only induces a small red-shift in absorption and fluorescence spectra compared with phenyl, indicating that tetrafluorophenyl is not a good pi-electron acceptor unit.

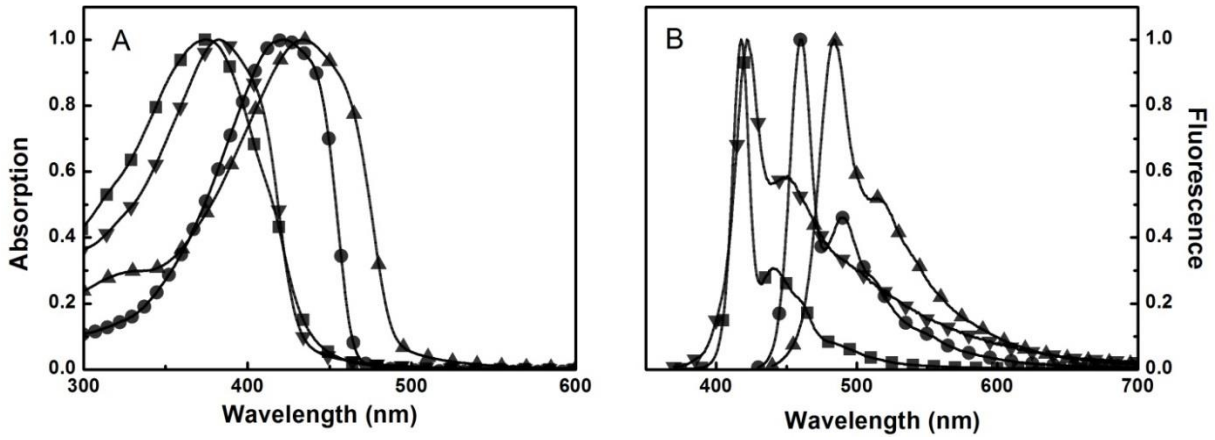

Figure 4-5. Normalized absorption (A) and fluorescence (B) spectra of **P1-E** (■), **P2-E** (●), **P3-E** (▲), **P4-E** (▼) in $CHCl_3$.

In our previous studies, it was found that the optical properties of these water-soluble PAEs were strongly dependent on solvents.[6,48] Here the photophysical properties of PAEs with methylene carboxylate side chains were investigated by UV-Vis and fluorescence spectroscopy in MeOH and H_2O. Normalized absorption and fluorescence spectra of PAEs in MeOH and H_2O are shown in Figure 4-6.

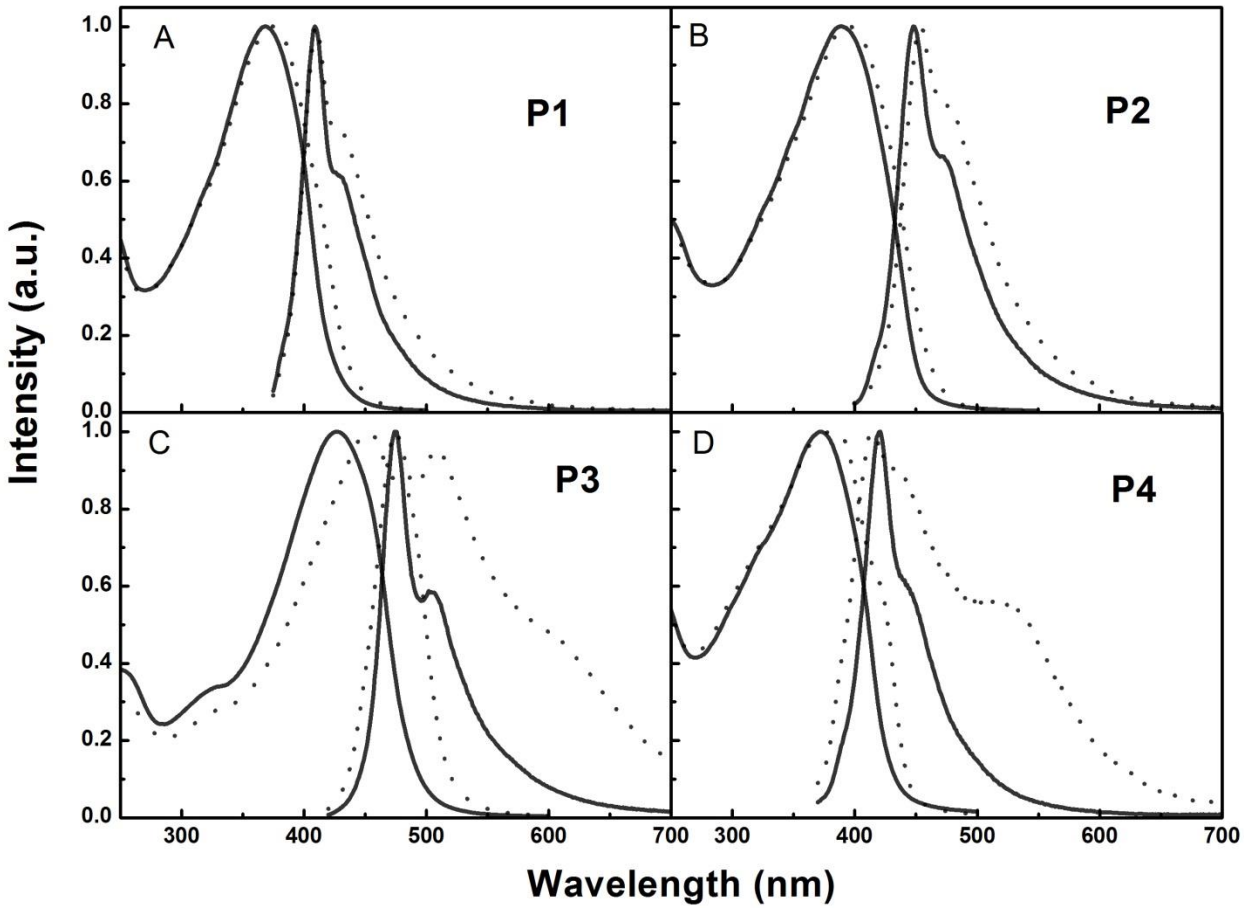

Figure 4-6. Normalized absorption and emission spectra of PAEs containing methylene carboxylate side chains in MeOH (solid line) and H_2O (dash line). (A) **P1**; (B) **P2**; (C) **P3**; (D) **P4**. MeOH contains 10 mM NaOH; H_2O at pH = 8.0.

In general, the absorption and fluorescence spectra of PAEs in aqueous solution were broader and red-shifted compared with the spectra in MeOH. The absorption and fluorescence spectra of **P1** and **P2** had very small red-shifts (<6 nm) and the fluorescence spectra retained the sharp structure, indicating that **P1** and **P2** did not

aggregate in H_2O. In contrast, the absorption spectra of **P3** and **P4** showed bigger red-shifts (9 nm and 16 nm, respectively) and the structured fluorescence bands were replaced by a combination of the molecularly dissolved polymer emission and a pronounced “excimer-like” fluorescence band at higher wavelengths. This photophysical data implied that **P3** and **P4** polymers in H_2O were partially aggregated.

Table 4-2. Photophysical data of PAEs (**P1**-**P4**).

	MeOH[a]			H_2O[b]		
Polymers	λ_{max}^{abs}/nm	λ_{max}^{em}/nm	Φ_{FL}[c]	λ_{max}^{abs}/nm	λ_{max}^{em}/nm	Φ_{FL}
P1	368	409	0.19	374	411	0.16
P2	388	448	0.26	394	454	0.17
P3	427	475	0.14	453	475	0.03
P4	373	421	0.26	382	415	0.16

[a] MeOH contains 10 mM NaOH; [b] H_2O has pH = 8.0; [c] Quinine sulfate in 0.1 M H_2SO_4 was used as a standard, Φ_{FL} = 0.454.

The fluorescence quantum yields of the series of PAEs (**P1** - **P4**) were measured in MeOH and H_2O and summarized in Table 4-2. In general, all polymers (**P1** - **P4**) were fluorescent in MeOH with a fluorescence quantum yield ~ 0.20. In aqueous solution polymers (**P1**, **P2** and **P4**) exhibited a comparable high quantum yield (~0.16). The high fluorescence quantum yields were likely due to the relieved aggregation by attaching the novel methylene carboxylate side chains. However, the emission quantum yield of the polymer (**P3**) dropped to 0.03. It is likely due to the fact that **P3** has oxygen atoms on linkers directly attached to the polymer backbone, which may promote aggregation and quench the excited states. Regarding to the oxygen effects, see more discussions in the last chapter (chapter 6).

pH Effects on the absorption and fluorescence

In order to probe the pH effects on photophysical properties, the absorption and fluorescence spectra of **P1** and **P2** in water were measured as a function of pH (Figure 4-7). The pH of the polymer solution was adjusted by addition of dilute HCl solution or NaOH solution according to a pH-meter.

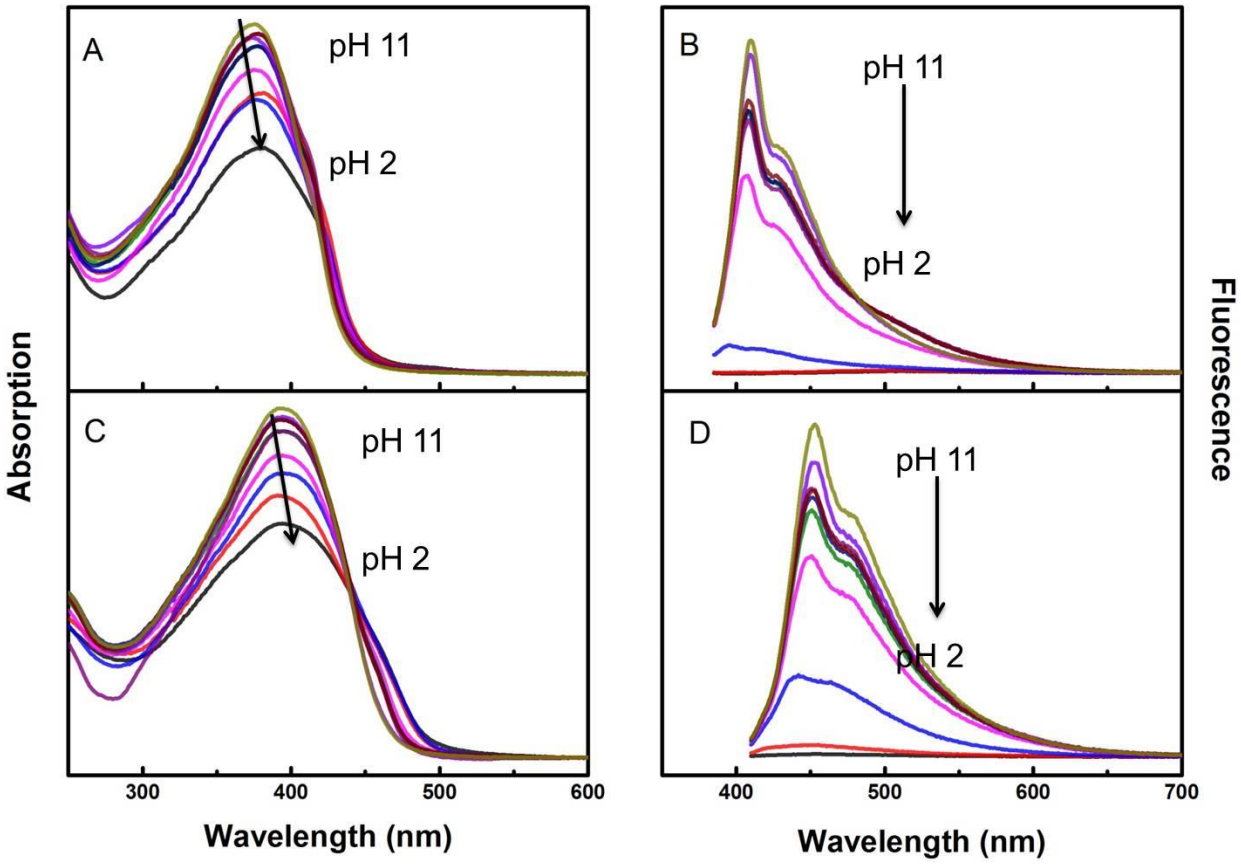

Figure 4-7. Absorption (A) and emission spectra (B) of **P1** in aqueous solutions as a function of pH. [**P1**] = 2 μM. Absorption (C) and emission spectra (D) of **P2** in aqueous solutions as a function of pH. [**P2**] = 2 μM.

In general, the absorption and emission of both polymers showed a strong dependence on pH. At pH 11, the absorption of **P1** showed a maximum at 374 nm and the emission showed a structured emission with a maximum at 411 nm. As the pH decreased, the absorption spectra of **P1** exhibited a bathochromic shift with a shoulder

band at 410 nm and the fluorescence spectra intensities decreased. The largest change in the fluorescence spectra was visible at pH = 4, in line with the pK_a values of phenylacetic acid ~ 4.31.[106] At this point, 67% of the carboxylate groups on the polymer chains were protonated. As a result of carboxylate protonation, the interaction with solvent molecules and the repulsions between side chains were decreased, leading to the aggregation or precipitation of polymer chains. A similar change in absorption and fluorescence spectra was observed for **P2** as the pH decreased from 11 to 2. It was found that the protonation of the carboxylate side groups caused the aggregation or precipitation, leading to a decrease in absorption spectra and fluorescence intensities. The biggest change in fluorescence spectra happened when pH decreased form pH = 5 to pH = 4. At the same time (pH = 4), the absorption spectra began to show the shoulder.

Fluorescence lifetime measurement

In order to gain more information about photophysical properties of the precursor polymers **Pn-E**, fluorescence lifetimes were measured in $CHCl_3$. In general, all four precursor polymers exhibited biexponential decays with the same short lifetime component (τ ~ 0.3 ns). As the detection wavelength increased, the longer lifetime species had more contribution to the overall amplitudes. The non-exponential decay can be explained by the polymer polydispersity and different emissive segments with different chain lengths. As seen in Table 4-3, the global analysis of the emission of **P1-E** yielded two decay components (τ_1 = 0.30 ns, τ_2 = 0.76 ns). As the detection wavelength increased from 420 nm to 500 nm, the contribution of the first component decreased, while the second component increased contribution to the overall emission lifetime. This may be explained by the fact that the emission at the longer wavelength had a slower

decay rate because the contributions from the longer polymer chains and longer chain segments were larger. Similar fluorescence lifetimes were observed for **P2-E**, and **P3-E**. Despite the similar features, **P4-E** had a much longer lifetime component (τ ~ 1.36 ns), which typical in the donor-acceptor type CPEs.[48]

Table 4-3. Fluorescence lifetime (τ_i , ns) and relative amplitudes (RA, %) for precursor polymer **Pn-E** in $CHCl_3$.

		RA (%)[a]								
	τ (ns)[b]	420 nm	450 nm	470 nm	500 nm		τ (ns)	450 nm	470 nm	500 nm	520 nm
P1-E	τ_1 = 0.30	100	97	94	88	**P2-E**	τ_1 = 0.34	91	90	83	74
	τ_2 = 0.76	0	3	6	12		τ_2 = 0.73	9	10	17	26
	χ^2	1.03	1.00	0.97	1.01		χ^2	0.99	0.99	1.01	1.03
	τ (ns)	470 nm	500 nm	550 nm	600 nm		τ (ns)	420 nm	450 nm	500 nm	550 nm
P3-E	τ_1 = 0.38	86	88	82	74	**P4-E**	τ_1 = 0.36	98	93	76	57
	τ_2 = 0.71	14	12	18	26		τ_2 = 1.36	2	7	23	36
	χ^2	1.03	1.02	1.05	1.01		χ^2	1.08	1.01	1.01	1.00

[a] Data were processed by global fitting algorithm. [b] Typical limits of error on τ_i are less than 3%.

In order to understand the relationship between the optical properties, chemical structures and aggregation behavior, the fluorescence decay of the PAEs with methylene carboxylate side chains were measured in MeOH and H_2O using the time-correlated signal photon counting (TCSPC). To keep the carboxylate side chains un-protonated, MeOH solutions contained 10 mM NaOH and aqueous solutions were adjusted to pH = 8.0. As seen in Table 4-4, all the PAEs showed relatively complicated multi-exponential lifetimes, which were attributed to the existence of aggregation, inhomogeneity of polymer chains length and emissive segments with different lengths.

In general, the fluorescence decays of PAEs in MeOH featured two exponential decays. The lifetimes of PAEs in MeOH were similar to the precursor polymer in $CHCl_3$ and the fluorescence decay of PAEs in H_2O was more complicated.

For all polymers in MeOH, the global analysis of the fluorescence decay provided two exponential decays as shown in Figure 4-8. The first component had shorter lifetime and the second component had longer lifetime. As the detection wavelength increased, the contribution from the first component gradually decreased, while the second one increased its contribution to the overall amplitude. This resulted in larger lifetimes at longer wavelengths. For polymers (**P1** and **P2**) in aqueous solution, global analysis of the fluorescence decays gave bi-exponential decays with two components similar to those in MeOH. The shorter-lifetime component decreased its contribution as the detection wavelength increased. The similar florescence decay in aqueous solution suggested that those polymers (**P1** and **P2**) were as well solvated as in MeOH, indicating that those polymers were not aggregated. Although the fluorescence decay of **P4** in aqueous solution exhibited three decay components, the first two components had similar lifetimes and similar behaviors to those in MeOH. The third component (τ_3 = 8.72 ns) had an essential role at wavelength 550 nm (~25% contribution), whereas the broad excimer band showed up. **P4** exhibited a slight aggregation behavior but the fluorescence quantum yield was much higher (~16%), suggesting that only a small amount of **P4** was aggregated.

In the previous studies, it was found that some PPEs aggregated in H_2O and the aggregates acted like an energy trap and quencher, resulting in a shorter lifetime in water than in MeOH.[48] A similar result was observed for the fluorescence decay of **P3**.

First, the global analysis of the fluorescence decay of **P3** in aqueous solution yielded three-exponential decays with a much longer lifetime component (τ_3 = 2.20 ns). This longer time component had ~10% contribution at 600 nm, where the “excimer-like” band was observed, indicating that the aggregates had a longer lifetime. In addition, the shortest lifetime had a dominant role in the overall amplitude, resulting in a much shorter mean lifetime in aqueous solution.

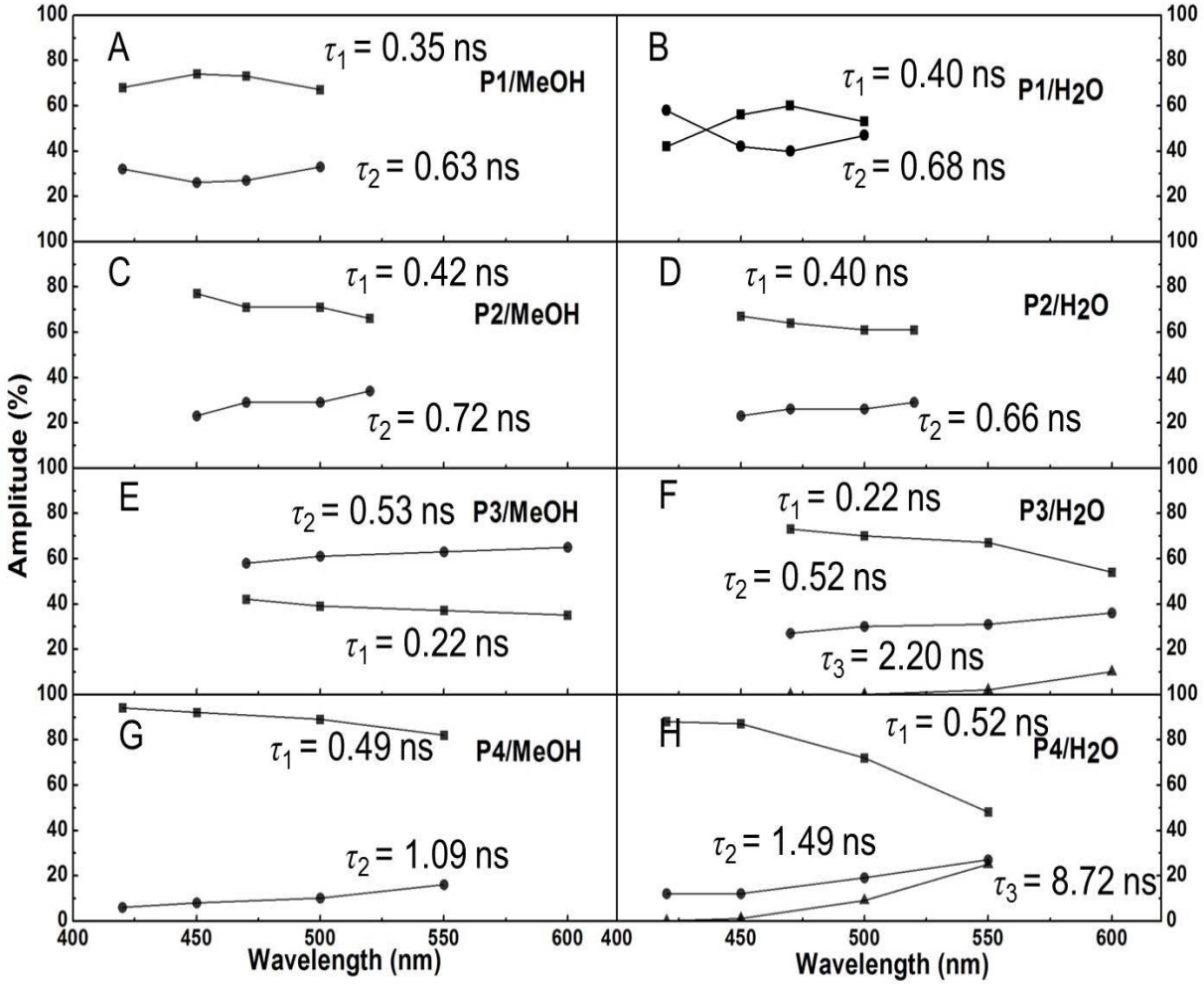

Figure 4-8. Fluorescence lifetime at different detection wavelengths: (A) **P1** in MeOH; (B) **P1** in H_2O; (C) **P2** in MeOH; (D) **P2** in H_2O; (E) **P3** in MeOH; (F) **P3** in H_2O; (G) **P4** in MeOH; (H) **P4** in H_2O. MeOH contains 10 mM NaOH. H_2O has pH = 8.0.

Table 4-4. Fluorescence lifetime (τ_i, ns) and relative amplitudes (RA, %) for **Pn** in basic MeOH and H_2O (pH = 8.0).

		RA (%)[a]								
		MeOH					H_2O			
	τ (ns)[b]	420 nm	450 nm	470 nm	500 nm	τ (ns)	420 nm	450 nm	470 nm	500 nm
P1	τ_1 = 0.35	68	74	73	67	τ_1 = 0.40	42	56	60	53
	τ_2 = 0.63	32	26	27	33	τ_2 = 0.68	58	42	40	47
	χ^2	1.05	1.00	1.03	1.07	χ^2	1.03	1.01	1.00	1.02
	τ (ns)	450 nm	470 nm	500 nm	520 nm	τ (ns)	450 nm	470 nm	500 nm	520 nm
P2	τ_1 = 0.42	77	71	71	66	τ_1 = 0.40	67	64	64	61
	τ_2 = 0.72	23	29	29	34	τ_2 = 0.66	23	26	26	29
	χ^2	1.01	0.99	1.00	1.01	χ^2	1.08	1.00	1.00	1.10
	τ (ns)	470 nm	500 nm	550 nm	600 nm	τ (ns)	470 nm	500 nm	550 nm	600 nm
	τ_1 = 0.22	42	39	37	35	τ_1 = 0.22	73	70	67	54
P3	τ_2 = 0.53	58	61	63	65	τ_2 = 0.52	27	30	31	36
						τ_3 = 2.20	0	0	2	10
	χ^2	1.02	1.04	1.05	1.01	χ^2	1.04	0.98	0.98	1.03
	τ (ns)	420 nm	450 nm	500 nm	550 nm	τ (ns)	420 nm	450 nm	500 nm	550 nm
	τ_1 = 0.49	94	92	89	82	τ_1 = 0.52	88	87	72	48
P4	τ_2 = 1.09	6	8	10	16	τ_2 = 1.49	12	12	19	27
						τ_3 = 8.72	0	1	9	25
	χ^2	1.00	1.00	1.00	0.96	χ^2	1.04	1.04	1.01	1.08

[a] Data were processed by global fitting algorithm. [b] Typical limits of error on τ_i are less than 3%.

In conclusion, the introduction of the methylene carboxylate side groups successfully suppressed the aggregation of PAEs in aqueous solution, since polymers (**P1**, **P2** and **P4**) showed similar decay behavior in aqueous solution to that in methanol solution. The oxygen on the linker to the polymer backbone of **P3** may induce some aggregation and thus have a much shorter lifetime in aqueous solution.

Fluorescence correlation spectroscopy

The photophysical data suggested that **P1** and **P2** did not aggregate while **P3** and **P4** were partially aggregated. In order to gain more information regarding the solution properties of PAEs, fluorescence correlation spectroscopy was applied to detect the diffusion time of each polymer and calculate the hydrodynamic radius. The experiments were carried out in aqueous solutions (pH = 8.0) with 2 μM of each polymer using fluorescein (30 nM) as standard. The hydrodynamic radius of the PAEs in aqueous solution was estimated from the FCS diffusion time according to the equations listed below. The diffusion time and hydrodynamic radius for the polymers are summarized in Figure 4-8 and Table 4-5.

$$W_r^2 = 4D_0\tau_0 \quad (4\text{-}1)$$

$$D = W_r^2/4\tau_d \quad (4\text{-}2)$$

$$D = KT/(6\pi\eta R_H) \quad (4\text{-}3)$$

where D_0 is the diffusion coefficient of the standard, τ_0 is the diffusion time of the standard, W_r is the focus volume of the fluorescence microscope, τ_d is the sample diffusion time, D is the diffusion coefficient of samples, T is the temperature, K is the Boltzmann constant, η is the viscosity of water, and R_H is the hydrodynamic radius.

Table 4-5. Diffusion time and hydrodynamic radius of PAEs in aqueous solution (pH = 8.0).

Polymer	Concentration (μM)	**Pn-E** M_n (kD)	τ (x 10^{-5} s)	R_H (nm)
P1	2	19	6.17	1.49
P2	2	48	6.72	1.63
P3	2	19	4.77	1.15
P4	2	65	7.55	1.83

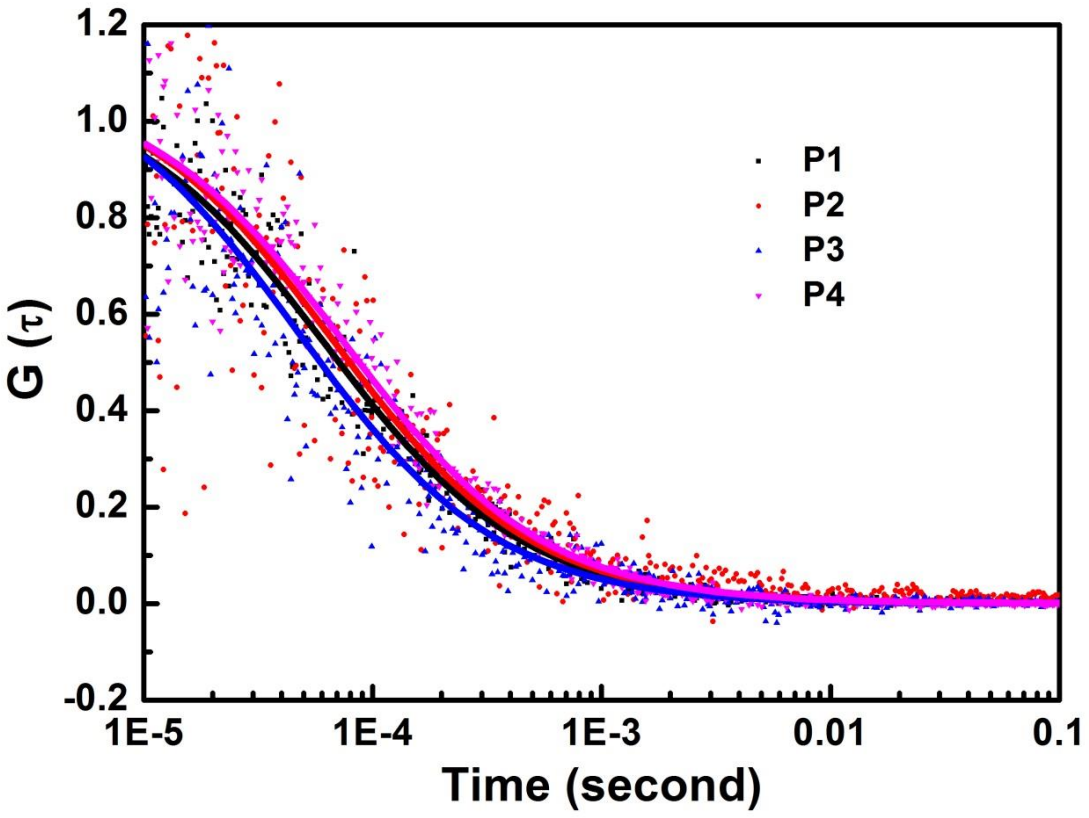

Figure 4-9. Normalized correlation curves for PAEs in aqueous solutions. Balck: **P1**; Red: **P2**; Blue: **P3**; Pink: **P4**. pH = 8.0. [PAE] = 2 μM. The solid lines are single specific fitting curves.

In general, the diffusion times of all PAEs were in the range of 10^{-5} s and the diffusion curve in Figure 4-9 was quite smooth and similar to each other. Polymer **P4** gave the largest diffusion time (7.55 x 10^{-5} s) and radius (1.83 nm), because **P4** had the

highest molecular weight. **P3** showed the smallest particle size (radius ~ 1.15 nm). The diffusion time for **P1** and **P2** were 6.17 x 10^{-5} s and 6.72 x 10^{-5} s, respectively. Typically, larger molecular weight polymers give longer diffusion times. However, the diffusion time and the radius of **P3** were smaller than **P1**, despite similar molecular weight. This can be explained by the polymer structure differences: the polymer backbone of **P1** was more rigid and linear while the polymer backbone of **P3** had some flexibility for rotation because of the more flexible 2,5-(3,4-ethylenedioxy)thienyl unit. Overall, the relatively small diffusion time and hydrodynamic radius suggested that all PAEs did not form large aggregates in aqueous solution. However, there was also possibility that some of them (**P3** and **P4**) formed some loose aggregates, which cannot be detected by FCS techniques.

Steady state fluorescence quenching with methyl viologen (MV^{2+})

In the previous studies, it was found that unaggregated PPEs usually had a smaller K_{sv} values (~ 10^5 M^{-1}) compared with the aggregated PPEs in aqueous solution including PPE-CO_2 and PPE-SO_3. The aggregated polymers had a much larger Stern-Volmer constant (10^6 M^{-1} ~ 10^7 M^{-1}), when quenched by a quencher like methyl viologen (MV^{2+}). [48,54,91,101] Steady state fluorescence quenching of PAEs were conducted in aqueous solution with methyl viologen. MV^{2+} is known as an efficient quencher via the photo-induced electron transfer mechanism. The detailed fluorescence spectra of PAEs (2 μM) upon the addition of MV^{2+} were shown in Figure 4-10. The fluorescence of all PAEs was efficiently quenched by MV^{2+} in aqueous solution. Figure 4-11 shows the Stern-Volmer plots of PAEs upon addition of MV^{2+}. In each case the Stern-Volmer plot showed a linear dependence on the quencher concentrations. Consequently we

characterized the plots using K_{sv} values calculated at low quencher concentrations according to Stern-Volmer equation (Equation 4-4).

$$I_0/I = 1 + Ksv[Q] \quad (4\text{-}4)$$

where I_0 is the emission intensity in the absence of the quencher, and I is the emission intensity in the presence of the quencher, [Q] is the quencher concentration, and the K_{sv} is the effective association constant for the complex formed between the polymer and the quencher.

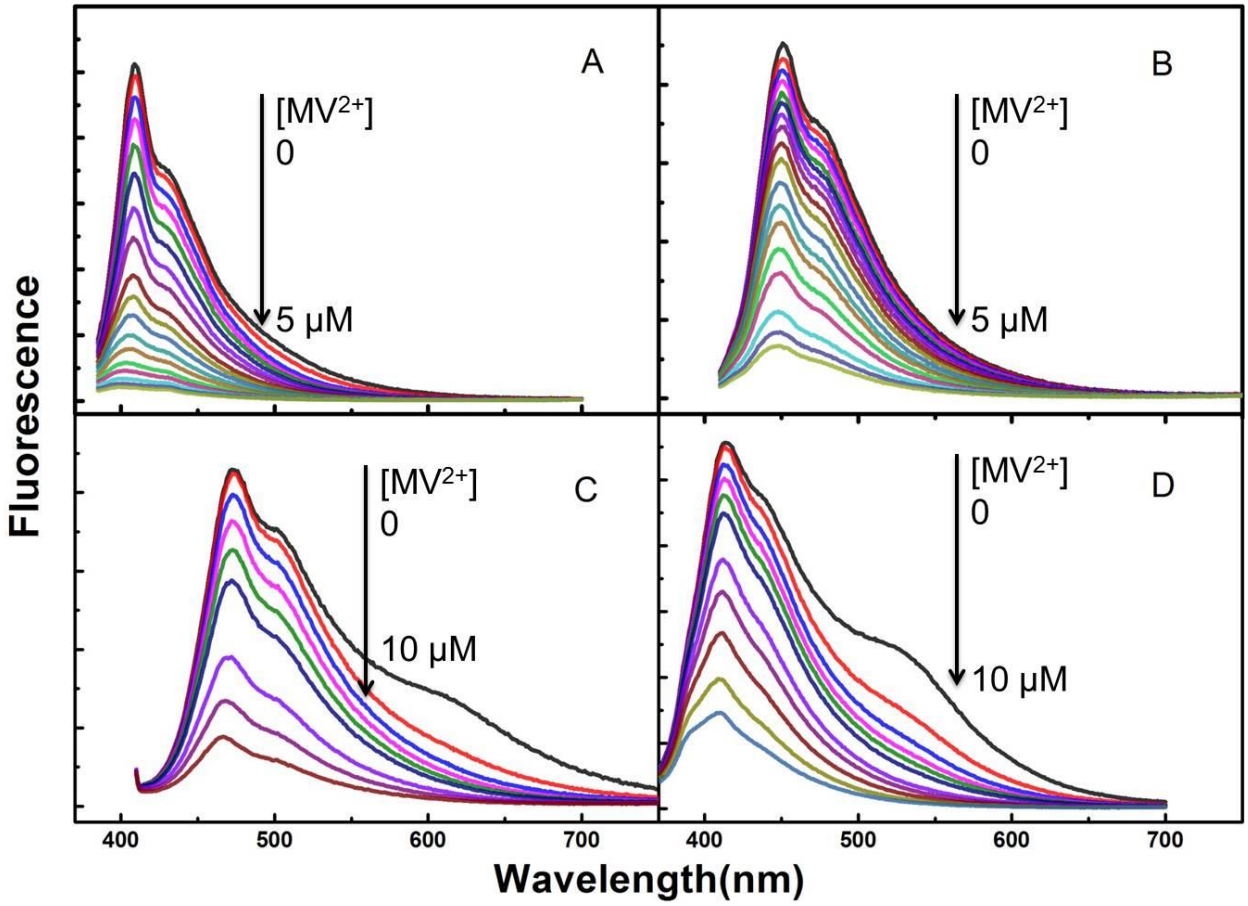

Figure 4-10. Fluorescence spectra of PAEs upon the addition of MV^{2+} quencher. (A) **P1**; (B) **P2**; (C) **P3**; (D) **P4**. [PAE] = 2 μM; pH = 8.0.

The K_{sv} values for **P1**, **P2**, **P3** and **P4** were 3.9 x 10^5 M^{-1}, 2.5 x 10^5 M^{-1}, 3.4 x 10^5 M^{-1} and 1.9 x 10^5 M^{-1}, respectively. The K_{sv} values for all PAEs were much smaller at

the range of 10^5 M^{-1}, suggesting that no strong aggregation in aqueous solution was observed. However, in the quenching experiments of **P3** and **P4**, the excimer bands at longer wavelengths were efficiently quenched within the first titration of MV^{2+}, indicating that only a small amount of polymers were aggregated and they were quenched by MV^{2+} with a higher efficiency.

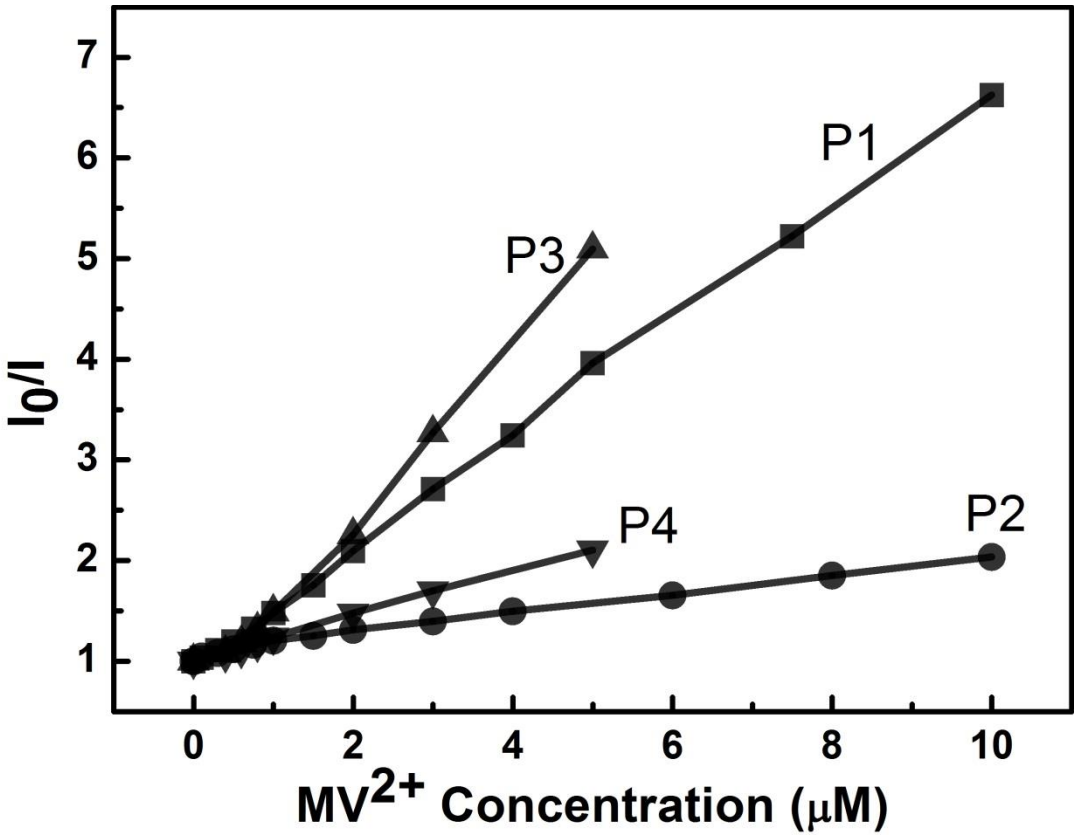

Figure 4-11. Stern-Volmer plots of PAEs upon the addition of MV^{2+} quencher. **P1** (■); **P2** (●); **P3** (▲); **P4** (▼). [PAE] = 2 μM; pH = 8.0.

Application of P1 to Metal Ion Sensing in Aqueous Solution

The interaction of **P1** with different metal ions was studied in aqueous solution. This experiment was carried out in water (pH = 8.0) with a series of 6 different metal ions: Na^+, Zn^{2+}, Hg^{2+}, Cu^{2+}, Fe^{2+} and Fe^{3+}. From the study of pH dependence, pure polymer **P1** was not aggregated at pH = 8. The fluorescence quenching experiment with

Na^+ was used as a control to reflect the influences of photo bleaching and ion strength. Figure 4-12 shows the fluorescence spectra of **P1** (2 μM) upon addition of various concentrations of different metal ions. As shown in Figure 4-12, the addition of 25 μM Na^+ and Zn^{2+} to **P1** solution failed to induce any fluorescence quenching, while 25 μM of Cu^{2+}, Fe^{2+} and Hg^{2+} can induce modest quenching. In contrast, the strongest quenching of polymer fluorescence was induced by 7.5 μM of Fe^{3+} with a loss of the vibronic structure in fluorescence spectra.

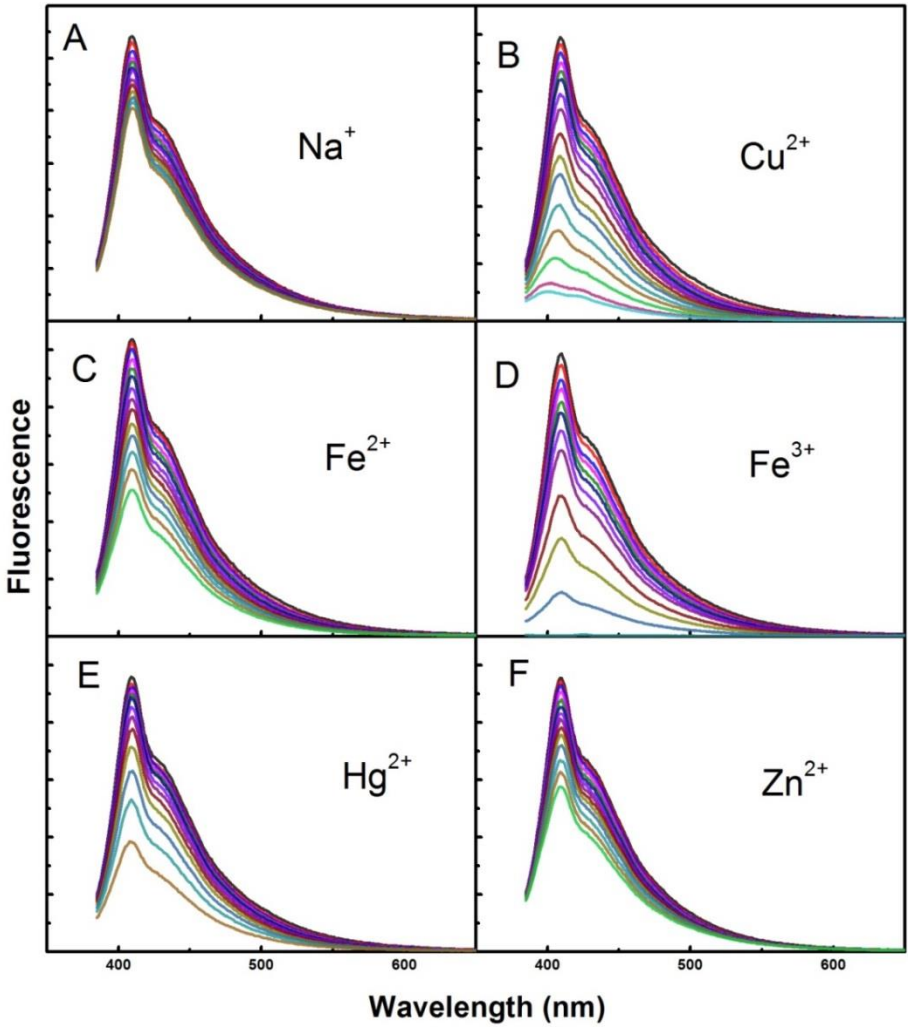

Figure 4-12. Fluorescence spectra of **P1** in H_2O (pH = 8.0) upon addition of different metal ions. (A) Na^+; (B) Cu^{2+}; (C) Fe^{2+}; (D) Fe^{3+}; (E) Hg^{2+}; (F) Zn^{2+}. [**P1**] = 2 μM; Fe^{3+} concentration ranged from 0 – 7.5 μM; other metal ions concentrations ranged from 0 – 25 μM.

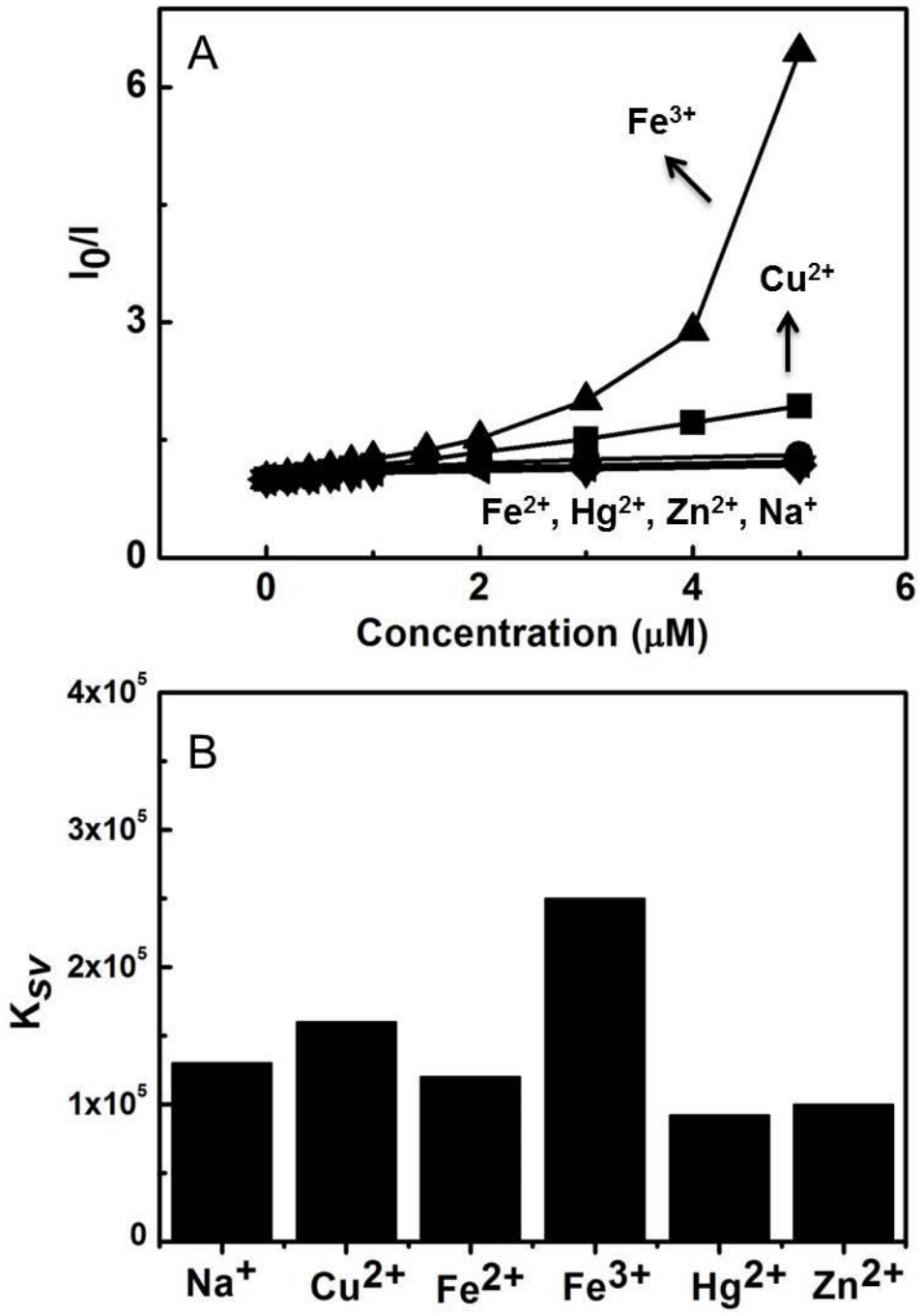

Figure 4-13. (A) Stern-Volmer plots (A) of **P1** with different metal ions in aqueous solution (pH = 8.0). (B) Comparison of K_{sv} values for different metal ions.

The Stern-Volmer (SV) plots for all the 6 metal ions are shown in Figure 4-13A. In the experiment concentration range, a linear curve was observed for all metals except Cu^{2+} and Fe^{3+}, which showed an upward curvature above1 μM concentration.

Stern-Volmer quenching constants (K_{sv}) for all the metal ions were extrapolated by fitting the linear regions of their SV plots and were compared in the bar graph shown in Figure 4-13B. For all the metal ions, K_{sv} values were observed in the range of 10^4 M^{-1} ~ 10^5 M^{-1} and the largest K_{sv} value was obtained for Fe^{3+} (2.5 x 10^5 M^{-1}).

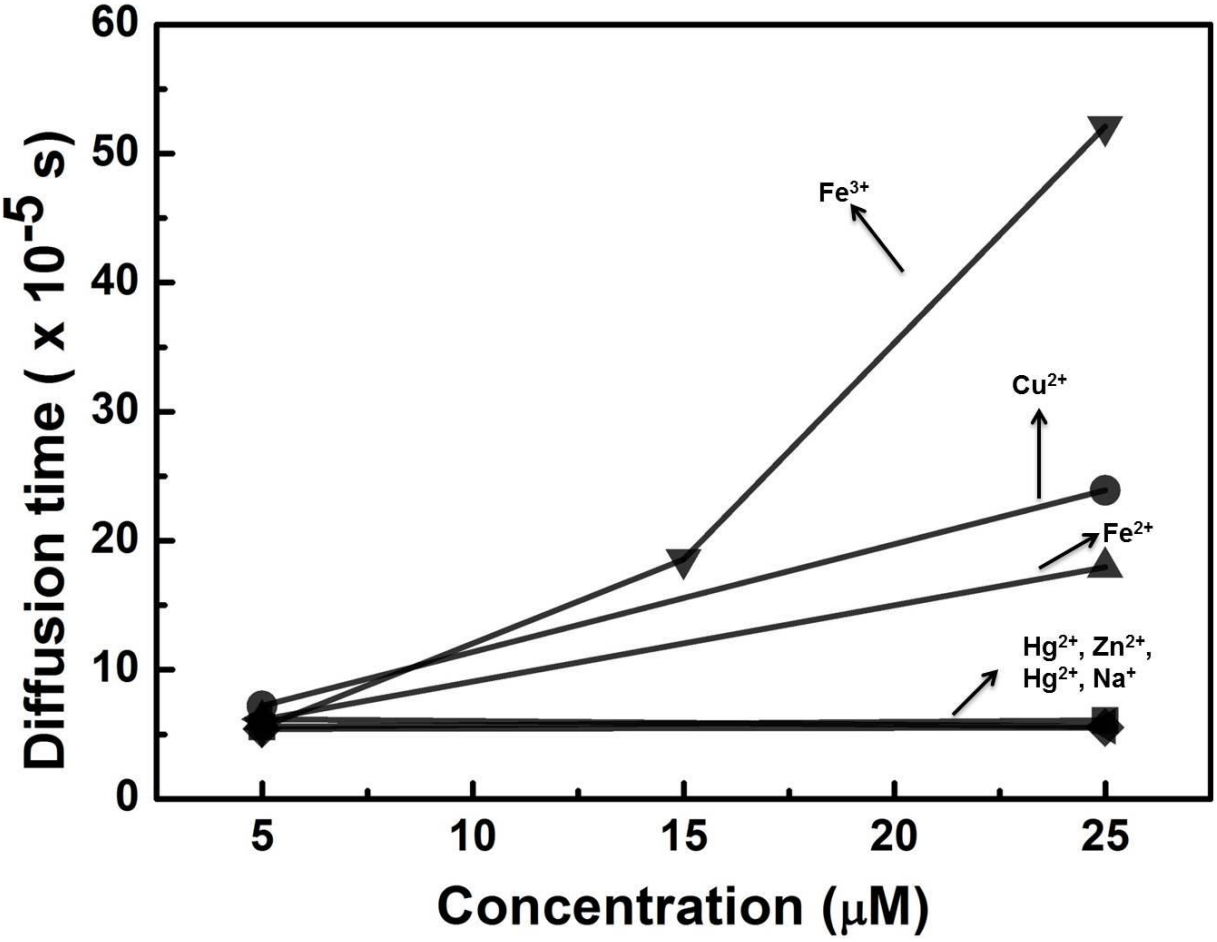

Figure 4-14. Diffusion time of **P1** in the presence of different metal ions in H_2O (pH = 8.0) obtained by the fluorescence correlation spectroscopy using the fluorescein standard. [**P1**] = 2 μM.

In order to study the aggregation behavior of the polymer in the presence of different metal ions, fluorescence correlation spectroscopy was applied to detect the diffusion time and the data were shown in Figure 4-14. For metal ions such as Zn^{2+}, Na^+ and Hg^{2+}, the diffusion times of **P1**/metal ions were ~ 5.5 x 10^{-5} s, close to the diffusion

time of pure **P1** in aqueous solution. The addition of 25 μM Cu^{2+}, Fe^{2+} and Fe^{3+} were able to induce significant aggregation, and the diffusion times were increased more than 3 fold. In particular, Fe^{3+} can induce the aggregation very efficiently, due to the fact that Fe^{3+} is trivalent and has more charge density. The formation of polymer aggregates enables the interchain exciton transfer, resulting in a much more efficient quenching.

In conclusion, the fluorescence of polymer **P1** was most sensitive to Fe^{3+}, which can be explained by the fact that Fe^{3+} can significantly induce the polymer aggregation and also quench the exited state of the polymer. The total quenching effect was a combination of the metal-ion induced aggregation and electron transfer mechanism. This system can be explored for fluorescence sensing of Fe^{3+} with high sensitivity and selectivity.

Application of P2 in Dye Sensitized Solar Cells

In a previous study, our group collaborated with Dr. Parkinson group on investigation of interfacial morphology and photoelectrochemistry of CPEs on metal oxide semiconductor. It was found that the magnitude of sensitized photocurrent was related to the surface coverage and the degree of aggregation of CPEs.[16] Therefore, we decided to continue our collaboration with Dr. Alexander Nepomnyashchii in Dr. Parkinson group using polymer **P2**, since **P2** was not aggregated in solution and may stay unaggregated in film.

Conjugated polyelectrolytes (CPEs) have been extensively studied as sensitizers in dye sensitized solar cells (DSSCs), owing to their high absorption, tunable band gap, good charge transport properties and low cost.[7,49,107,108] The binding to oxide semiconductor surfaces can be also controlled for CPEs through the degree of

carboxylate substitution on the polymer backbone. The morphology of the CPEs at the interface where charge separation occurs plays a pivotal role in the solar-electrical power conversion and wavelength response of the photocurrents.[109,110] For instance, inefficient exciton transport may occur for aggregated polymer whose photo-generated excitons must hop several chains to reach the semiconductor interface.[111,112] Aggregation may also decrease the efficiency of light harvesting, charge injection and charge collection depending on the structure and physical properties of the aggregates.[113,114] In contrast, non-aggregated CPE chains are expected to inject electrons more efficiently.

As described in the previous section, polymer **P2** did not aggregate in solution. Therefore, we hypothesized that the unaggregated polymer in solution may be a promising candidate to stay unaggregated as film on the surfaces of semiconductors. The acid-form of the polymer (**P2-H**) was prepared by adding HCl solution (1 N, 3 mL) to 10 mg of **P2** in H_2O solution (3 mL) and collected by centrifugation (Figure 4-15). After the deposition of the acid form **P2-H** on the surfaces of ZnO single crystals, atomic force microscopy (AFM) and photoelectrochemical measurements were carried out to investigate the aggregation behavior.

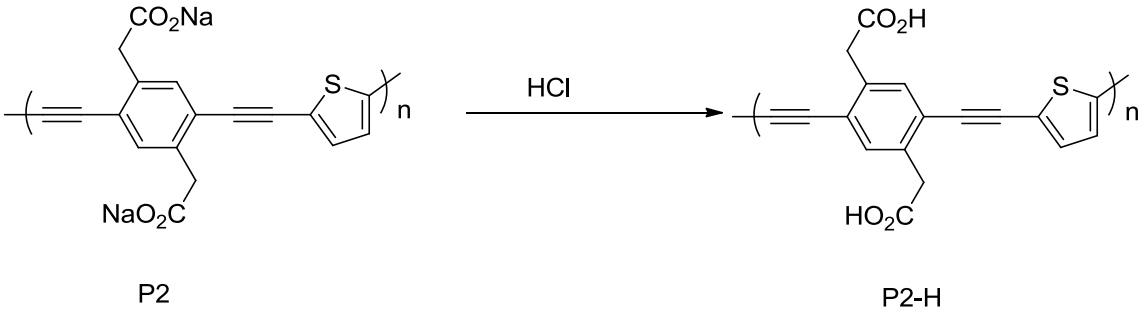

Figure 4-15. Synthesis of **P2-H**.

The photophysical properties of **P2** and **P2-H** were initially investigated and compared in Figure 4-16. The absorption and fluorescence spectra in different solvents showed no substantial solvent effect. In particular, the high fluorescence quantum yields (16% in water, 26% in MeOH and 30% in DMF, respectively) indicated polymer **P2** and **P2-H** did not aggregate in solution and may have the potential to form films without aggregation.

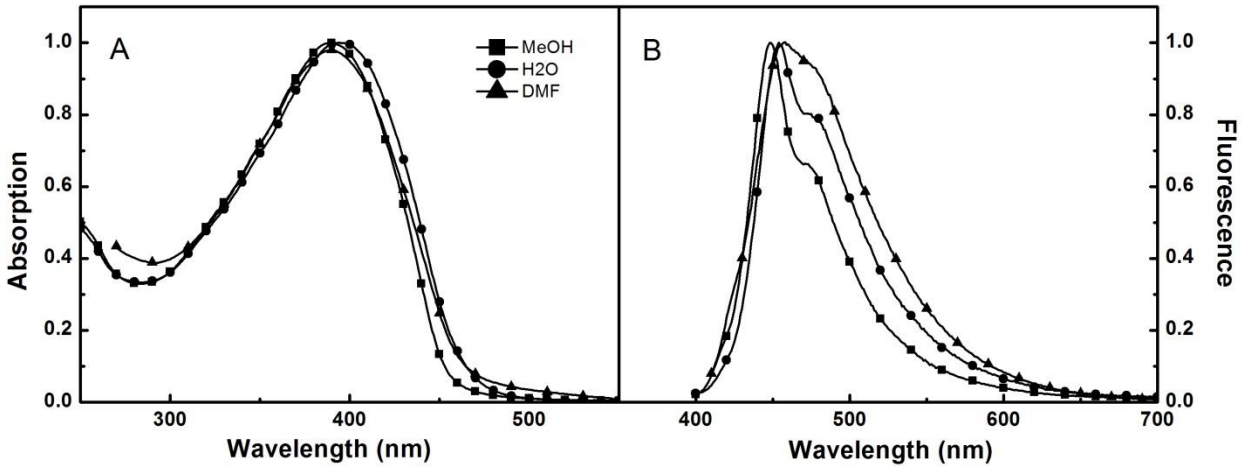

Figure 4-16. Normalized absorption (A) and fluorescence spectra (B) of **P2** in MeOH (■), **P2** in H_2O (●) and **P2-H** in DMF (▲). MeOH contains 10 mM NaOH. H_2O has pH = 8.

It is known that obtaining topographic information of the deposited PPEs polymer chains within a mesporous oxide film is challenging. Therefore, in this work atomically flat n-type zinc oxide (0001) single crystal surfaces were used as a substrate to allow detailed structure determination with atomic force microscopy (AFM) and to correlate photocurrent response with the sensitizer concentration in the solution. In addition, zinc oxide is a semiconductor material with a wide band gap of 3.2 - 3.4 eV,[115] which is suitable for studying sensitization by organic dyes.[116] According to the absorption spectrum, **P2-H** had an absorption maximum at around 390 nm or 3.0 eV, which was

below the ZnO band gap. The driving force of 0.2 – 0.4 V was big enough to enable the photoexcited electron injection from **P2-H** into ZnO.

Figure 4-17A shows clear atomically flat terraces of around 250 nm across obtained for polished and annealed ZnO crystals. A dipping method, submerging the ZnO into various concentrations of **P2-H** in DMF solutions for 5 mins, was used for the surface coverage studies. This process was found to be the most reliable and reproducible for the formation of uniform coverage of the carboxylate polymer on the single crystal surfaces.

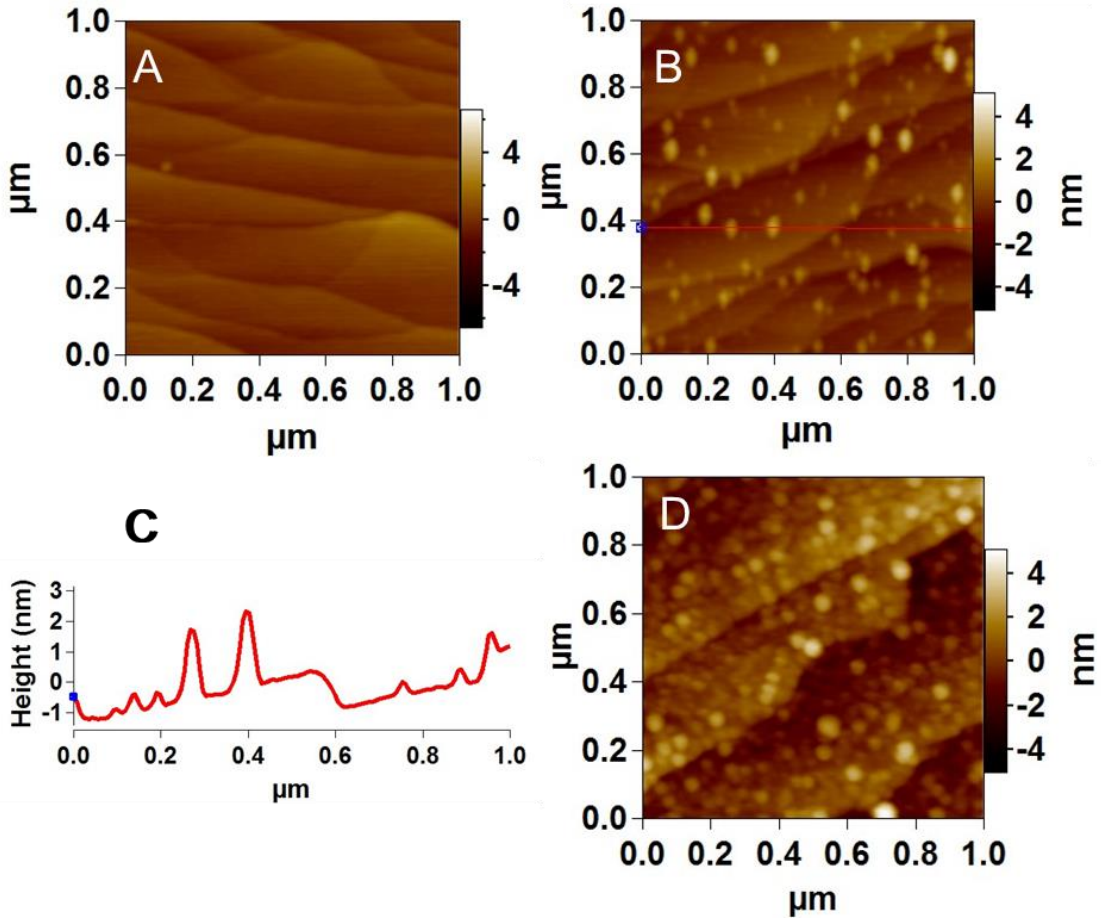

Figure 4-17. Non-contact tapping mode AFM images of **P2-H** deposited on ZnO (0001) surface from DMF solutions of different concentrations: (A) 0, (B) 6, and (D) 60 µg/mL. (C) Cross section analysis for the red line in (B). DMF solution was the solvent used for deposition with a dipping time of 5 minutes. Data obtained by Dr. Nepomnyashchii.

Polymer deposition at a low concentration of **P2-H** led to sub-monolayer coverage of the particles in AFM images (Figure 4-17B). The cross section analysis for the red line in Figure 4-17B revealed that most of the particles were around 2 to 3 nm in height, which seemed to be a single polymer chain (Figure 4-17C). It is of note that the particle heights are used to estimate their sizes since the AFM microscope has the highest resolution on height. Exposure to solution with a higher concentration resulted in an increase of surface coverage without a sign of aggregation (Figure 4-17D).

To verify our premise that the “blobs” in the AFM images corresponded to individual polymer chains, all the particles in Figure 4-17B were measured and a histogram showing the distribution of heights was compared with the distribution of calculated radius in Figure 4-18. For each polymer chain, the radius of the solid particle was calculated from the molecular weight obtained from GPC analysis using the equations listed below and the hemispherical model. Therefore, the GPC curve can be transferred into a distribution curve of calculated radius. The distribution of calculated radius of polymer chains was in close agreement with the distribution of heights. The only difference was that the calculated radius was ~ 1 nm bigger, which can be attributed to the fact that particles in solid state were flatter than hemispherical model. The good correlation between the real particles heights and the calculated radius supported our premise and suggested that this novel polymer did not aggregate on surface.

$$M_{acid} = M_1 M_{ester}/M_2 \quad (4\text{-}5)$$

$$m = M_{acid}/NA \quad (4\text{-}6)$$

$$\mathrm{V} = m/\rho \quad (4\text{-}7)$$

$$V = 2\pi r^3/3 \quad (4\text{-}8)$$

where, M_{ester} is the molecular weight of the ester polymer, M_1 is the molecular weight of each repeat unit of acid polymer, M_2 is the molecular weight of each repeat unit of ester polymer, M_{acid} is the molecular weight of the acid polymer, NA is Avogadro number, m is the mass of each acid polymer chain, the density ρ is assumed to be 1.1 g/cm^3 according to density of P3HT solid.[117] The hemispherical model is chosen and r is the radius of each polymer particle.

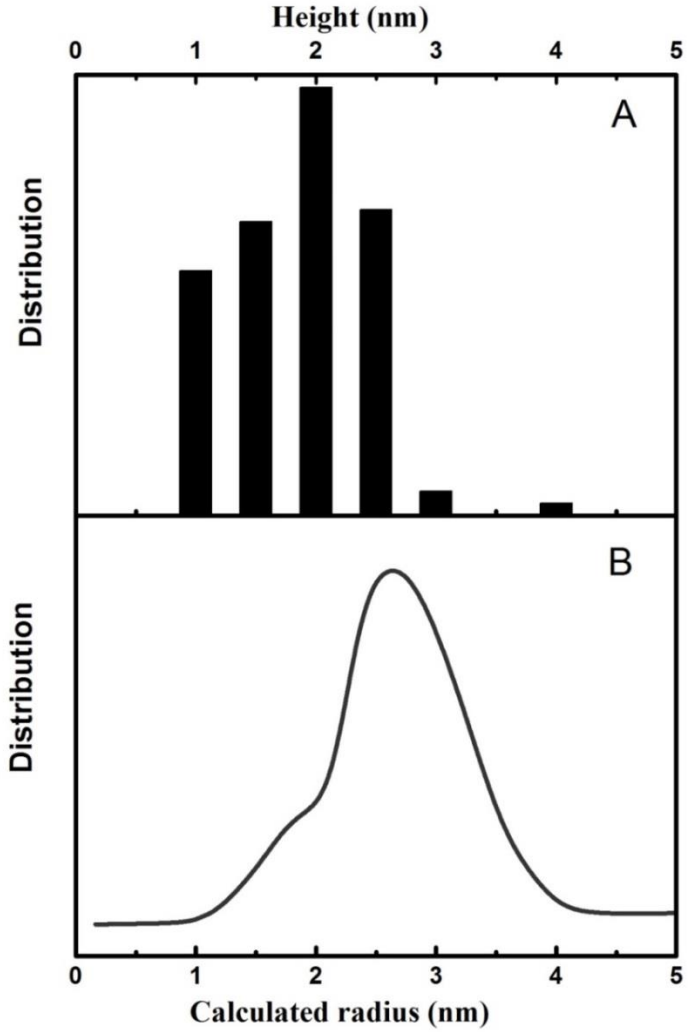

Figure 4-18. (A) Distribution of the particles with different heights obtained from Figure 4-17B. Data obtained by Dr. Nepomnyashchii. (B) Distribution of the polymer chains over calculated radius.

Figure 4-19A shows the incident photon to current efficiency (IPCE) spectra for adsorbed **P2-H** on the surfaces of ZnO single crystals as a function of polymer concentration, using iodide/iodine couple as mediator. Efficient electron injection from polymer to ZnO crystals was observed. The sensitized photocurrent from **P2-H** started at 480 nm and reached a maximum value at ~ 410 nm, close to adsorption maxima in film and DMF solution. The increases of the photocurrent with the coverage showed an adsorption-isotherm-like behavior where a saturation point was reached at ~ 30 μg/mL in Figure 4-19B.

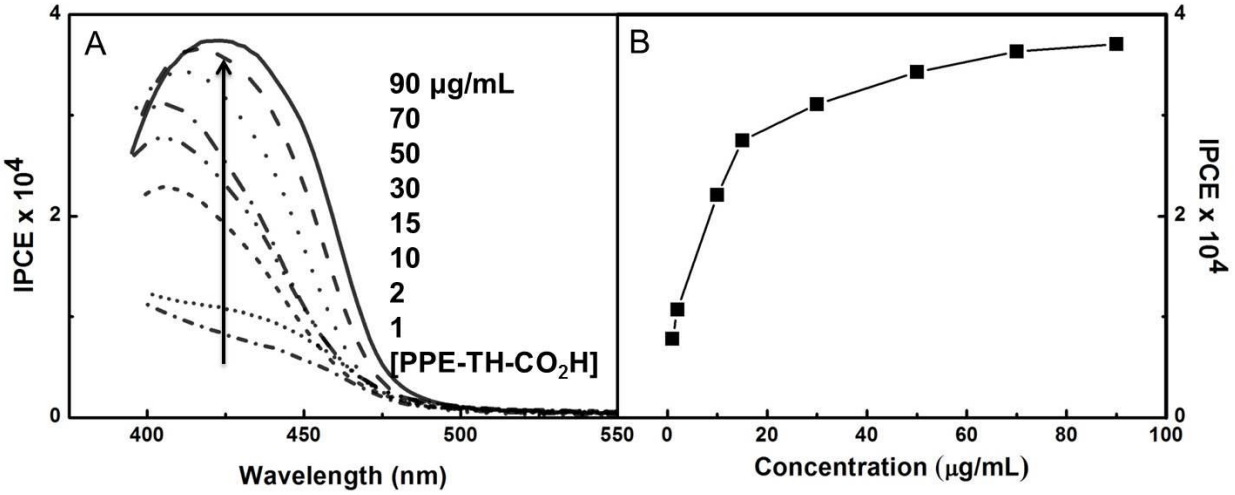

Figure 4-19. (A) IPCE spectra for a ZnO electrode dipped into various concentration of **P2-H** in DMF solution. (B) IPCE values as a function of the dipping solution concentration for curves shown in A. Data obtained by Dr. Nepomnyashchii.

The isotherm behavior was similar to the isotherms obtained for monomeric ruthenium dyes, monomeric and h-aggregated cyanine dyes on the TiO_2 single crystal surfaces (anatase and rutile).[118] The plateauing of the "isotherm" and the lack of multilayers in the AFM images suggested that the individual chains were covalently bonded to the oxide surface and not aggregated into multilayers. Otherwise, decreases in the IPCE values can be observed for other polymeric sensitizers with increasing coverage, due to the formation of thick polymer layers where photoexcited carriers or

excitons created near the polymer surface cannot reach the interface to be separated by electron injection into the semiconductor conduction band.[113,114] The maximum IPCE for **P2-H** on the surfaces of ZnO was ~ 0.04%. There are several explanations for the low IPCE values. One is that the dye coverage is sub-monolayer coverage. The other is that ZnO crystals absorb light starting from ~ 400 nm overlapping with the absorption maximum of the polymer. In addition, the relative low band gap between the polymer and the ZnO leads to lower electron injection efficiency.

In conclusion the synthetic strategy to produce a sensitizing polymer that was unlikely to aggregate was successful. The absence of aggregations in solution and at surfaces was verified by photophysical measurements, AFM imaging, and photocurrent spectroscopy. Non-aggregating polymeric sensitizers may be useful in designing more efficient solar cells as it allows for more control of surface-polyelectrolyte binding.

Application of P4 in Mercury (II) Ion Sensing

Mercury ion (Hg^{2+}) is a toxic heavy metal ion, available in many natural sources such as coal and gold mining, fossil fuel, solid waste.[119] Owing to its notorious biological membrane disruption, accumulation and long residence in nervous systems, mercury pollution causes serious nervous diseases such as Acrodynia, Menimata and Hunter-Russel syndrome.[120,121] Therefore, great efforts have been devoted to the design and development of an easy, rapid and effective sensor to detect and quantitatively measure the mercury ion sensors in aqueous solution. Among all the sensors, the fluorescence sensors based on conjugated polyelectrolytes (CPEs) seem to be the ideal candidate for both sensing and bio-imaging of the metal ions in various samples, due to theirs high sensitivity, fast analysis, non-destructive sample preparation and the highly effective quenching effects known as amplified quenching effects.[52,122-125] Recently, Ma and

coworkers reported that rhodamine B thiolactone (**S-Rho**) can form a complex with Hg^{2+}.[123] The rhodamine-Hg^{2+} complex (**S-Rho-Hg^{2+}**) exhibited an absorption maxima at ~ 560 nm, which was overlapping with the fluorescence spectra of the polymer **P4** (Figure 4-21). Also the positive charged **S-Rho-Hg^{2+}** ion complex will be attracted to the negative charged **P4** by the electrostatic interaction. Here, we report a novel and highly sensitive Hg^{2+} sensor based on **P4** and rhodamine B thiolactone, by taking advantage of the Förster energy transfer (FRET) between the polymer and rhodamine B thiolactone-Hg^{2+} complex.

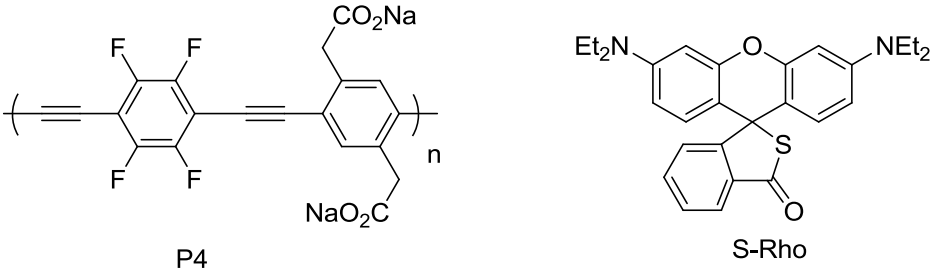

Figure 4-20. Structures of **P4** and **S-Rho**.

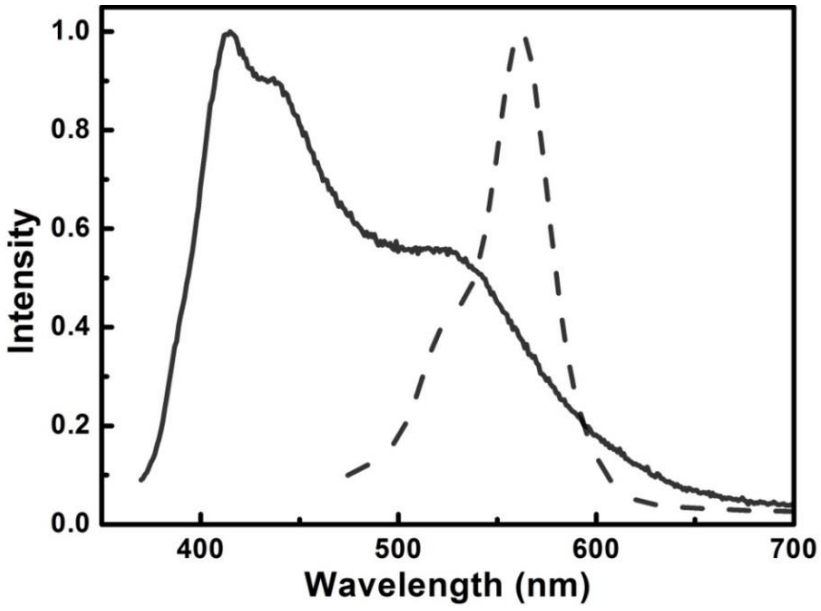

Figure 4-21. Normalized fluorescence spectrum of **P4** (solid line) and absorption spectrum of **S-Rho-Hg^{2+}** (dashed line).

As discussed before, the conjugated polymer **P4** was synthesized through a "precursor" route using a Sonogashira reaction, in which both monomers were soluble in organic solvent. Subsequent deprotection of the ester groups afforded the water-soluble highly emissive polymer **P4**.

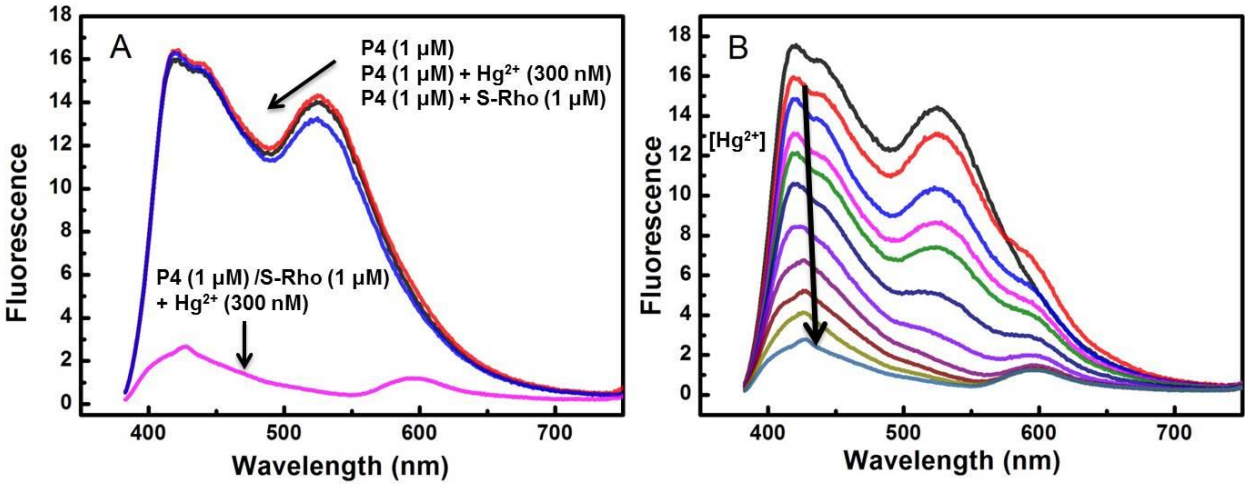

Figure 4-22. (A) Fluorescence spectra of **P4** (1 μM) and **P4** (1 μM)/**S-Rho** (1 μM) upon the addition of Hg^{2+} (300 nM) in H_2O /DMSO (99/1, v/v). (B) Fluorescence spectra of **P4** (1μM)/**S-Rho** (1μM) upon the addition of various concentration of Hg^{2+} in H_2O /DMSO (99/1, v/v). Excitation at 373 nm.

Figure 4-22A shows the fluorescence spectra of **P4** (1 μM), **P4** (1 μM)/**S-Rho** (1 μM) mixture and **P4** (1 μM)/Hg^{2+} (300 nM) mixture in H_2O /DMSO (99/1, v/v). The addition of **S-Rho** (1 μM) to the **P4** (1 μM) did not affect the fluorescence spectra, indicating that the interaction between **S-Rho** and **P4** was negligible without Hg^{2+} ion. In addition, the fluorescence spectrum of **P4** remained the same upon the addition of Hg^{2+} (300 nM). In contrast, the addition of Hg^{2+} ion into the **P4** (1 μM)/**S-Rho** (1 μM) mixture caused significant quenching to the fluorescence spectra, indicating the combination of **S-Rho** and Hg^{2+} played the important role. More than 95% of the emission intensity at 525 nm was quenched upon the addition of 300 nM Hg^{2+}. Formation of the positive charged **S-Rho**/Hg^{2+} ion complex through a ring opening process[123] resulted in efficient

fluorescence quenching of **P4** via the Förster energy transfer mechanism. The Stern-Volmer plots of **P4** (1μM)/**S-Rho** (1μM) upon the addition of different metal ions in H_2O /DMSO (99/1, v/v, pH 8) were shown in Figure 4-23A. The Stern-Volmer plot for Hg^{2+} curved upward at higher concentration and exhibited a linear profile at the low concentration (<50 nM). The K_{sv} value was derived from the linear range to be ~ 2.3 x 10^7 M^{-1}, which was the highest value among all reported Hg^{2+} sensors based on CPE. In addition, the selectivity of this sensor is remarkably high for Hg^{2+}. The fluorescence intensity change of **P4** (1 μM)/**S-Rho** (1 μM) upon addition of different metal ions (300 nM) was shown in Figure 4-23B. Metal ions such as Ca^{2+}, Cu^{2+}, Fe^{2+}, Fe^{3+} and Zn^{2+} failed to induce significant change, while Hg^{2+} quenched most of the fluorescence intensity.

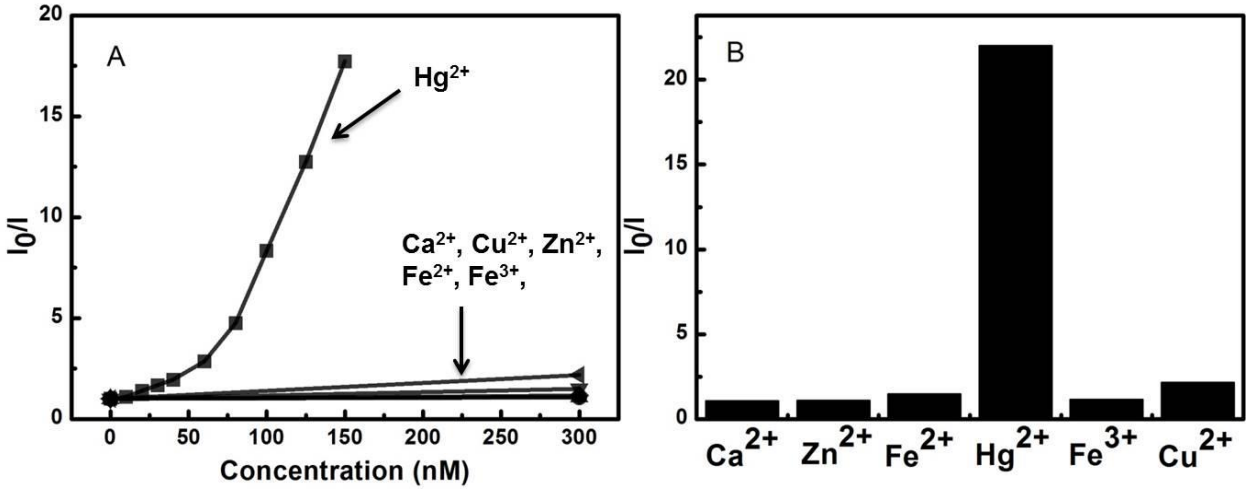

Figure 4-23. (A) Stern-Volmer plots of **P4** (1 μM)/**S-Rho** (1 μM) upon the addition of different metal ions in H_2O /DMSO (99/1, v/v); (B) fluorescence intensity changes of **P4** (1 μM)/**S-Rho** (1 μM) upon the addition of different metal ions (300 nM) in H_2O /DMSO (99/1, v/v), pH = 8. Excitation at 373 nm, fluorescence intensity was monitored at 525 nm.

The proposed sensing mechanism was displayed in Figure 4-24. The rhodamine B thiolactone undergoes a ring opening process and forms a complex with Hg^{2+}. The

positive charges on the complex played an essential role in binding to the carboxylate groups of **P4**. The overlapped spectra between donor fluorescence and acceptor absorption provided the fundamental pathway to the Förster energy transfer effects.

Overall, a novel fluorescence turn-off sensor for Hg^{2+} ion has been developed based on **P4** and **S-Rho**. The fluorescence of **P4**/**S-Rho** was selectively quenched by Hg^{2+} with an outstanding efficiency. The quenching mechanism was proposed and rationalized as Förster energy transfer mechanism. In addition, the fluorescence sensor provided an easy and fast way to detect Hg^{2+} in aqueous solution.

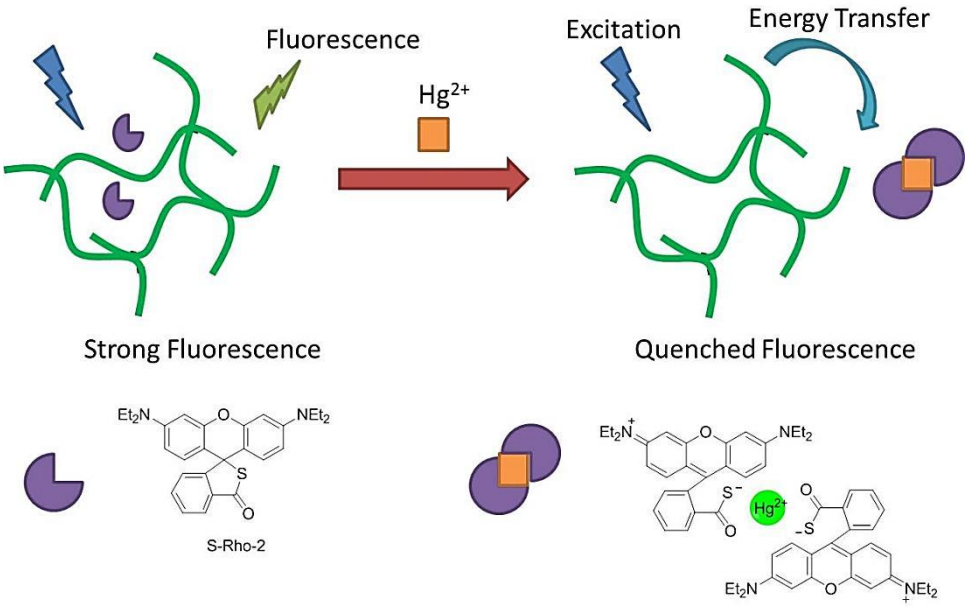

Figure 4-24. Proposed sensing mechanism for Hg^{2+}.

Summary

In this chapter, a new family of anionic poly(arylene ethynylene)s (PAEs) featuring methylene carboxylate side groups have been prepared. The polymerization was carried out in organic solvents by Sonogashira coupling reaction according to the "precursor" route. Subsequent base-promoted ester hydrolysis and purification provided the water-soluble conjugated polyelectrolytes (CPEs). The repeat unit of the PAEs

backbone consisted of a phenylene ethynylene unit alternating with a second arylene ethylene moiety and four different arylenes were used, Ar = 1,4-phenyl, 2,5-thienyl, 2,5-(3,4-ethylenedioxy)thienyl and 1,4-(2,3,5,6-tetrafluoro)phenyl. The different arylene units induced variation in the HOMO-LUMO band gap across the series of polymers, resulting in an absorption maximum ranging from 360 nm to 450 nm and a fluorescence maximum ranging from 409 nm to 475 nm. The photophysical properties such as absorption, fluorescence and fluorescence lifetime were investigated in MeOH and H_2O. All polymers except **P3** showed comparable optical properties in aqueous solution to those in MeOH. Through the careful structure-property relationship analysis, the weak fluorescence and low fluorescence quantum yield were attributed to the oxygen attached to the polymer backbone, which induced aggregation and quenching. The synthetic route for the alternative polymer without oxygen linkage was much more challenging, but as a result, the photophysical properties were improved drastically. Most of the polymers had a fluorescence quantum yield ~ 16% in aqueous solutions. The steady state fluorescence quenching of the PAEs were conducted by MV^{2+} in aqueous solution. The fluorescence of the PAEs was quenched efficiently with K_{sv} values ~ 10^5 M^{-1}, indicating that most of the polymers chains were existed as single chains. And the small diffusion times measured by fluorescence correlation spectroscopy supported the same conclusion that polymers did not aggregate in water.

Beyond the basic photophysical studies, several applications based on the PAEs were successfully developed. First, the interaction of **P1** with the metal ions were investigated and the results suggested that **P1** was remarkable sensitive to Fe^{3+} and a promising Fe^{3+} sensor could be built. The AFM images of the acid polymer **P2**-**H** on the

surface of ZnO single crystal were obtained. By comparison of the particles heights in the AFM images and the calculated radius from GPC data, it was found that the “blobs” in the AFM images represented the single chains which formed a globular structure. Further photoelectrochemical experiments of the **P2-H** were carried out for the application of Dye Sensitized Solar Cell (DSSC). Finally, a novel highly sensitive fluorescence sensor for mercury (II) ion was designed and developed based on **P4**/**S-Rho** complex with a high selectivity. This sensor takes advantages of the Förster energy transfer mechanism and the overlap between the fluorescence of **P4** and absorption of **S-Rho-Hg^{2+}** complex ions. The fluorescence of the **P4** was quenched by the **S-Rho-Hg^{2+}** metal ions with a K_{sv} value ~ 2.5 x 10^{7} M^{-1}.

Experimental

Materials

$Pd(PPh_3)_4$ and $Pd(PPh_3)_2Cl_2$ were purchased from Strem Chemical Company and used as received. 1,4-Bis(chloromethyl)benzene, sodium perchlorate, 1-dodecanol, diisopropylamine, tetrabutylammonium hexafluorophosphate ($TBAPF_6$) and copper iodide were purchased from Sigma-Aldrich Chemical Company. Acetic acid, acetic anhydride, sulfuric acid, potassium carbonate, ferric chloride, mercury (II) chloride, ferrous chloride, zinc chloride and sodium chloride were purchased from Fisher Scientific Company and used as received. Tetrabutylammonium difluorotriphenylsilicate (TBAT) was purchase from TCI America Company. THF and DMF were purified by solvent dispensing system. All other chemicals and solvents were purchased from Sigma-Aldrich, Fisher Scientific and used as received. Stock solutions (1.0 mM) of all PAEs were prepared in deionized H_2O (pH = 9) and have been stored at 4 ^{o} C. For all experiments with the PAEs in aqueous solution, the pH was adjusted to 8.0 by addition

of a dilute solution of sodium hydroxide. And for all experiments with the PAEs in MeOH, the methanol solution contains 10 mM NaOH to keep the solution basic.

Instrumentation

NMR spectra were recorded using a Gemini-300 NMR operating at 300 MHz for ^{1}H NMR and at 75 MHz for ^{13}C NMR for small organic compounds. ^{1}H NMR spectra of the polymers were measured in Inova2-500 NMR operating at 500 MHz for ^{1}H NMR. Gel permeation chromatography (GPC) analysis was carried out on a system comprised of a Shimadzu LC-6D pump, Agilent mixed-D column and a Shimadzu SPD-20A photodioide array (PDA) detector, with THF as eluent at 1 mL/min flow rate. The system was calibrated against linear polystyrene standards in THF. UV absorption spectra were measured on a Shimadzu UV-1800 spectrophotometer. Luminescence spectra were measured on a PTI (Photon Technology International) fluorescence spectrometer. Fluorescence lifetimes were determined by time-correlated single photon counting on a FluoTime 100 spectrometer (Pico Quant) equipped with 370 nm diode laser as excitation source. Detection filters were used with a width ~ 10 nm. A 1 cm square quartz cuvette was used for solution spectra, and emission was collected at 90 ^{o} relative to excitation beam. Fluorescence quantum yields are reported relative to known standards quinine sulfate in 0.1 M H_2SO_4 solution. The optical density of solutions at the excitation wavelength was < 0.1, and corrections were applied for differences in the refractive index of standard and sample solutions. FCS measurements were taken on a homemade setup using a 405 nm diode laser (Coherent, CUBE) as the excitation light. Fluorescein (30 nM in 10 mM phosphate buffer, pH = 8) was used as the calibration for the system. The concentrations of oligomer and polymer samples were 2 uM for all experiments.

General Methods for Surface and Photoelectrochemical Characterization

Sample preparation: ZnO (0001) single crystals were obtained from MTI Corporation (Richmond, CA). Atomically flat surfaces without substantial pits present were achieved by polishing with 30 and 50 nm diameter silica (Buehler, Lake Bluff, IL) and further annealing at 1000 ^{o}C for 12 hours. The initial solution with CPEs was filtered using 200 M syringe filter (Nalgene, Rochester, NY) prior the photoelectrochemical and AFM measurements. ZnO (0001) single crystal electrodes were dipped inside the solutions and covered with CPEs. Then the crystals were attached with plastic screws to specially built cell to assure presence of electrical contact.

Atomic force microscopy (AFM) investigations: AFM measurement has been carried out using non-contact AC mode of AFM and Asylum Research (Santa Barbara, CA) microscope. Olympus silicon rectangular probes with a 42 N/m force constant, tip radius of 9+/-2 nm and resonant frequency of approximately 300 kHz were used to probe the crystal surface. Cross section analysis was applied to determine the size (height) of the particles. Exactly the same crystals as used for the photoelectrochemical measurements were applied to achieve direct correlation between photoelectrochemical and surface properties. Different areas of ZnO (0001) single crystals were analyzed to obtain reproducible results.

Photoelectrochemical measurements: Photoelectrochemical measurements were carried out in aqueous solutions containing 0.1 M KNO_3 and 20 mM KI. Three-electrode setup with ZnO (0001) as a working electrode, platinum wire as a counter electrode and Ag/AgCl as a reference electrode was used in all experiments. Princeton Instruments (Princeton, NJ) 174A potentiostat was applied in IPCE measurements. IPCE spectra

were collected using a Stanford Research Systems (Sunnyvale, CA) model SR830 DSP lock-in preamplifier. The collected signal from preamplifier was transmitted to a SRS-model SR830 DSP lock-in amplifier. 100 W Oriel tungsten lamp (Newport Corp., Santa Clara, CA) (cut off filter 350 nm) was used as a source of excitation. The light was passed through a computer controlled monochromator (2 nm step interval) and further chopped at 14 Hz to provide a modulated photocurrent signal (model SR540 chopper, Stanford Research Instruments). The collected photocurrent signal was then corrected for photon flux by collecting lamp power spectrum with thermopile detector (Pomona Electronics, Way Everett, WA). Incident power through monochromator for certain wavelength was collected using Thorlabs C-Series photodiode (Newton, NJ). I-V curves were collected for the same crystals using 120 mW purple laser and IVIUM potentiostats (Eindhoven, The Netherlands).

Synthetic Procedure

Compound **1**,[103] **6**,[104,105] 1,4-bis(trimethylsilyl)ethynyl)tetrafluorobenzene,[126] and 5,7-bis((trimethylsilyl)ethynyl)-2,3-dihydrothieno[3,4-b][1,4]dioxine[47] were prepared according to the literature procedures. The rhodamine B thiolactone was synthesized from commercial available rhodamine B according to the literature.[123]

1,4-bis(2-acetoxy-ethyl)benzene (2). To a mixture of acetic anhydride (50 mL), pyridine (200 mL) and 4-dimethylamino pyridine (20 mg), compound **1** (10 g, 60 mmol) was added and the mixture was allowed to stir at room temperature for overnight. The solvents and excess of acetic anhydride were removed under vacuum. The residue was purified by silica chromatography to give **2** as a white solid (yield: 15 g, 100%). ^{1}H NMR (300 MHz, $CDCl_3$): δ 7.15 (s, 4H), 4.26 (t, 4H), 2.91 (t, 4H), 2.03 (s, 6H). ^{13}C NMR (75

MHz, $CDCl_3$): δ 171.19, 136.28, 129.24, 65.12, 34.89, 21.18. HRMS (ESI) *m/z*: $[M+Na]^+$ calcd. for $C_{14}H_{18}O_4Na$, 273.1097; found, 273.1283.

2,5-Diiodo-1,4-bis(2-acetoxy-ethyl)benzene (3). Sodium periodate (7.3 g, 34 mmol, 40% excess) and iodine (26.2 g, 104 mmol, 40% excess) were stirred into a mixture of glacial acetic acid (129 mL) and acetic anhydride (64.5 mL) at 0 ^{o} C. Concentrated sulfuric acid (43 mL, 860 mmol) was then added slowly to the stirring suspension. Compound **2** (21.5 g, 86 mmol) was added to this solution and stirred continuously for 6 h at room temperature. The reaction mixture was then poured into an ice-water mixture containing previously dissolved Na_2SO_3. The precipitate was collected and recrystallized in ethanol to give compound **3** as a white solid (yield: 34.5 g, 80%). ^{1}H NMR (300 MHz, $CDCl_3$): δ 7.67 (s, 2H), 4.24 (t, 4H), 3.00 (t, 4H), 2.06 (s, 6H). ^{13}C NMR (75 MHz, $CDCl_3$): δ 171.13, 141.26, 140.57, 100.43, 63.34, 38.89, 21.16. HRMS (ESI) *m/z*: $[M]^+$ calcd. for $C_{14}H_{18}I_2O_4$, 503.9289; found, 502.9225.

2,2'-(2,5-Diiodo-1,4-phenylene)dienthanol (4). To the solution of **3** (8.4g, 16.7 mmol) in dichloromethane (50 mL) and methanol (200 mL) was added potassium carbonate (25 g, 181 mmol). The mixture was stirred at room temperature overnight. The solvent was removed under vacuum. Water (300 mL) was added and the suspension was vigorously stirred at room temperature for 2 h. The solid was collected by vacuum filtration to give **4** as a white solid (yield: 5.9 g, 85%). ^{1}H NMR (300 MHz, Acetone-d_6): δ 7.71 (s, 2H), 3.86 (m, 4H), 2.94 (t, 4H), 1.38 (t, 2H). ^{13}C NMR (75 MHz, Acetone-d_6): δ 142.26, 140.50, 100.25, 61.15, 42.84. HRMS ESI *m/z*: $[M+Na]^+$ calcd. for $C_{10}H_{12}I_2O_2Na$, 440.8819, found 440.8827.

2,2'-(2,5-Diiodo-1,4-phenylene)diacetic acid (5). To acetonitrile (80 mL), periodic acid (4.8 g, 21 mmol) was added and the mixture was stirred at room temperature for 15 min. The mixture was cooled down to 0 ^{o}C, and compound **4** (2.0 g, 4.8 mmol) was then added, followed by the addition of freshly prepared pyridinium chlorochromate (44 mg, 2 mol%) in acetonitrile (10 mL). The reaction mixture was stirred at room temperature for 6 h. After removal of most solvent under vacuum, the residue was poured into water (100 mL). The precipitate was collected and recrystallized in toluene to afford **5** as a white solid (yield: 1.7 g, 80%). ^{1}H NMR (300 MHz, DMSO-d_6): δ 12.50 (s, 2H), 7.80 (s, 2H), 3.68 (s, 4H). ^{13}C NMR (75 MHz, DMSO-d_6): δ 171.98, 141.33, 139.99, 102.18, 45.12. HRMS ESI *m/z*: $[M+Na]^+$ calcd. for $C_{10}H_8I_2O_4Na$, 468.8404, found, 468.8404.

Didodecyl 2,2'-(2,5-diiodo-1,4-phenylene)diacetate (C1). A mixture of compound **5** (9.0 g, 20 mmol), dodecyl alcohol (80.0 g, 465 mmol) and 85% phosphoric acid (0.5 mL) was placed in a flask equipped with a Dean-Stark trap. After reaction at 150 ^{o} C for 6 h, the solvent was removed by vacuum distillation. The residue was recrystallized in isopropanol to give **C1** as a white solid (yield: 13.4 g, 85%). ^{1}H NMR (300 MHz, $CDCl_3$): δ 7.73 (s, 2H), 4.12 (t, 4H), 3.71 (s, 4H), 1.63 (m, 4H), 1.26 (m, 36H), 0.88 (t, 6H). ^{13}C NMR (75 MHz, $CDCl_3$): δ 170.09, 140.84, 138.85, 100.81, 65.64, 45.31, 32.14, 29.88, 29.81, 29.59, 29.43, 28.75, 26.12, 22.93, 14.36. HRMS ESI *m/z*: $[M+Na]^+$ calcd. for $C_{34}H_{56}I_2O_4Na$, 805.2160; found, 805.2160.

Compound **7**: Compound **6** (6.4 g, 20 mmol) was dissolved in a mixture of THF (50 mL) and isopropylamine (150 mL), and combined with $Pd(PPh_3)_2Cl_2$ (28 mg, 0.4 mmol) and CuI (15 mg, 0.8 mmol). After bubbling Ar for 40 mins, trimethylsilylacetylene

(4.8 g, 50 mmol) was added, and stirred overnight at room temperature. The solvent was removed and the residue was extracted with dichloromethane/water. The organic layer was washed with saturated ammonium chloride, water and brine, and then dried over anhydrous sodium sulfate. The solvent was removed under vacuum and the crude product was purified by silica chromatography (hexane/dichloromethane, 2/1) to give compound **7** as light yellow solid (yield: 5.5 g, 95%). ^{1}H NMR (300 MHz, $CDCl_3$): δ 7.43 (d, 2H), 7.21 (d, 2H), 3.50 (s, 2H), 1.43 (s, 9H), 0.24 (s, 9H). ^{13}C NMR (75 MHz, $CDCl_3$): δ 170.45, 135.45, 132.28, 129.33, 42.87, 28.23, 0.24. HRMS ESI *m*/*z*: $[M+Na]^+$ calcd. for $C_{17}H_{24}O_2SiNa$, 311.1438; found, 311.1448.

Compound **8**: To the solution of compound **7** (2.9 g, 10 mmol) in chloroform (50 mL) was added tetra-n-butylammonium floride (TBAF, 12 mL, 12 mmol, 1M in THF). After reaction over 1 h, the reaction mixture was passed through a silica column and gave **8** as light yellow solid (yield: 2.0 g, 95%). ^{1}H NMR (300 MHz, $CDCl_3$): δ 7.46 (d, 2H), 7.24 (d, 2H), 3.52 (s, 2H), 3.06 (s, 1H), 1.43 (s, 9H). ^{13}C NMR (75 MHz, $CDCl_3$): δ 170.55, 135.71, 132.38, 129.40, 83.69, 81.29, 42.77, 28.22. HRMS ESI *m*/*z*: $[M+Na]^+$ calcd. for $C_{14}H_{16}O_2Na$, 239.1042, found, 239.1043.

General polymerization procedure for PPEs. Monomer **C1** (0,1 mmol) and 0.1 mmol of the co-monomers (1,4-bis(trimethylsilyl)ethynyl)benzene for **P1**, 2,5-bis((trimethylsilil)- ethynyl)thiophene for **P2**, 5,7-bis((trimethylsilyl)ethynyl)-2,3-dihydrothieno[3,4-b][1,4]dioxine for **P3**, 1,4-bis(trimethylsilyl)ethynyl)tetrafluorobenzene for **P4**, respectively) were dissolved in a mixture of THF (20 mL) and diisopropylamine (5 mL). The solution was degassed for 1 hour, followed by the addition of tetrabutylammonium difluorotriphenylsilicate (TBAT, 108 mg, 0.2 mmol). The reaction

was allowed to stir at room temperature for 3 hours. Then $Pd(PPh_3)_4$ (15 mg) and CuI (10 mg) were added under the protection of argon. The reaction was stirred at 70 ^{o}C for 24 hours, followed by the addition of the Endcap **6** (1 mg). After 6 hours, the Endcap **8** (1mg) was added. After another 18 hours, the solvent was removed under vacuum and the residue was dissolved in $CHCl_3$. The resulting solution was passed through a short column of alumina to remove all catalyst and concentrated to 2 mL. Then the polymer was precipitated in a large amount of methanol (100 mL) and collected by centrifugation. The polymer was further purified by multiple cycles of dissolving in $CHCl_3$ and precipitation in methanol.

Hydrolysis. The precursor **Pn-E** (~ 40 mg) was dissolved in chloroform (15 mL) and treated with excess of TFA (15 mL) over 5 hours at ambient temperature. The solvents were completely removed under vacuum. The residue was dissolved in THF (20 mL) and then a solution of sodium hydroxide (10 equivalents to ester group) in methanol/water (3 mL, 2/1, v/v) was added. The mixture was stirred at 50 ^{o} C overnight. The solvents THF and methanol were removed under vacuum, and water (10 mL) was added to the residue, followed by heating at 50 ^{o} C for 1 day. The mixture was concentrated to about 2 mL, precipitated in acetone (25 mL), and centrifuged. The precipitate was dissolved again in water (pH 9, 2 mL). Multiple precipitation was repeated 3 ~ 5 times in acetone (containing 5 ~ 20% methanol). Any insoluble in water was removed by centrifuge before precipitation operation. After filtration on a membrane filter with a 0.22 μm pore size, the polymers were subjected to dialysis using Fisher Brand dialysis membrane (molecular weight cutoff 8 kD) against water (pH 8) over 3

days. Light yellow to brown solids were obtained in a yield of 80 ~ 90% after lypholization.

Acid polymer P2-H. To a solution of **P2** (10 mg) in 3 mL water (pH 8), 3 mL of dilute HCl solution (3 N) was added. The precipitate was collected by centrifugation and dried under vacuum for 3 days. The acid polymer was used without any further purification.

P1-E. ^{1}H NMR (500 MHz, $CDCl_3$): δ 7.50 (br, s, 6H), 4.14 (br, m, 4H), 3.85 (br, s, 4H), 1.68 (br, m, 4H), 1.25 (br, m, 36H), 0.85 (br, t, 6H). GPC (THF, polystyrene standard): M_n = 19 kD, M_w = 34 kD, PDI = 1.8.

P2-E. ^{1}H NMR (500 MHz, $CDCl_3$): δ 7.50 (br, s, 2H), 7.18 (br, s, 2H), 4.15 (br, t, 4H), 3.83 (br, s, 4H), 1.65 (br, m, 4H), 1.27 (br, m, 36H), 0.88 (br, t, 6H). GPC (THF, polystyrene standard): M_n = 42 kD, M_w = 80 kD, PDI = 1.9.

P3-E. ^{1}H NMR (500 MHz, $CDCl_3$): δ 7.50 (br, s, 2H), 4.38 (br, s, 4H), 4.16 (br, t, 4H), 3.84 (br, s, 4H), 1.65 (br, m, 4H), 1.25 (br, m, 36H), 0.90 (br, 6H). GPC (THF, polystyrene standard): M_n = 19 kD, M_w = 34 kD, PDI = 1.8.

P4-E. ^{1}H NMR (500 MHz, $CDCl_3$): δ 7.65 (br, s, 2H), 4.18 (br, m, 6H), 3.90 (br, m, 2H), 1.66 (br, m, 4H), 1.28 (br, m, 36H), 0.83 (br, t, 6H). GPC (THF, polystyrene standard): M_n = 65 kD, M_w = 169 kD, PDI = 2.6.

P1. ^{1}H NMR (500 MHz, CD_3OD): δ 7.55 (br, 6H), 3.78 (br, 4H).

P2. ^{1}H NMR (500 MHz, CD_3OD): δ 7.50 (br, 2H), 7.20 (br, 2H), 3.75 (br, 4H).

P3. ^{1}H NMR (500 MHz, CD_3OD): δ 7.53 (br, 2H), 4.38 (br, 4H), 3.78 (br, 4H).

P4. ^{1}H NMR (500 MHz, CD_3OD): δ 7.60 (br, 2H), 4.10 (br, 2H), 3.85 (br, 2H).

CHAPTER 5
HIGHLY FLUORESCENT CONJUGATED POLYELECTROLYTES FEATURING METHYLENE AMMONIUM SIDE GROUPS

Background

Over past decades, conjugated polyelectrolytes (CPEs) have attracted considerable attention as chemical and biosensors for the detection and analysis of a variety of molecules of environmental and biological interest, including small molecules, ions and biological targets.[7,52] Among all the sensors, fluorescent sensors based on cationic CPEs are of particular interest. First, most biologically important species are negatively charged such as DNA, protein and Gram-negative bacteria. Second, the amplified quenching effects of CPEs allow developing the sensors with extremely high sensitivity and rapid detection. However, despite the advantages of CPEs, their solution processing is sometimes limited by bad solubility, low quantum yield and unexpected sensing behavior induced by a strong tendency to self-aggregate in aqueous solution.[64,127,128]

In chapter 4, it was shown that PPEs with methylene carboxylate side groups had much less tendency to aggregate in aqueous solution. Through the structure-property studies, we found that the enhanced fluorescence quantum yield was correlated with the absence of oxygen on the linker to phenylene rings. In this chapter, a novel family of water-soluble poly(phenylene ethynylenes) (PPEs) with cationic methylene ammonium side groups were synthesized by Sonogashira reaction. The backbone of this PPE series shares a same bis(methylene trimethylammonium) phenylene ethynylene unit alternating with a second arylene ethynylene unit (phenylene for **P1-N** and thiophene for **P2-N**, respectively). The photophysical properties of the series of PPEs were investigated in methanol and aqueous solution by absorption,

fluorescence spectroscopy and fluorescence lifetime measurement. The photophysical data suggested that both polymers existed as single polymer chains in aqueous solution with remarkably high fluorescence quantum yields (0.16 for **P2-N** and 0.30 for **P1-N**, respectively). Steady-state fluorescence quenching of this series of PPEs were performed by AQS and $K_4Fe(CN)_6$ in aqueous solution. A fluorescence sensor for ATP has been successfully developed based on the highly fluorescent cationic PPE (**P1-N**). The fluorescence of **P1-N** in MES buffer solution was efficiently quenched by ATP with a high selectivity over ADP, AMP, PPi and Pi. This sensor can be applied to build a fluorescence assay for alkaline phosphatase (ALP), which catalyzes the dephosphorylating of ATP in cells.[129]

Results and Discussion

Synthesis of PPEs with Cationic Methylene Ammonium Side Groups

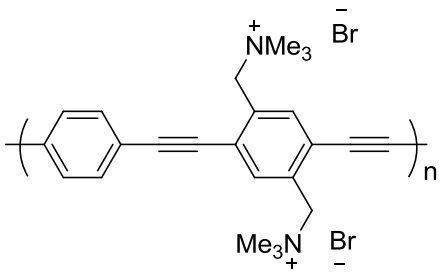

P1-N

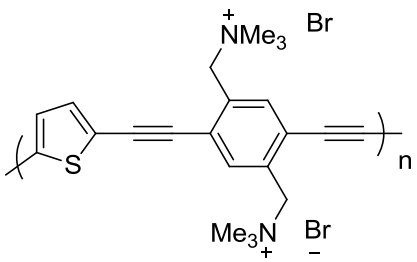

P2-N

Figure 5-1. Structures of **P1-N** and **P2-N**.

In this chapter, a series of water-soluble PPEs with cationic methylene ammonium side groups were synthesized through Sonogashira reaction. The backbone of this series of PPEs consists of a bis(methylene ammonium)phenylene ethynylene unit alternating with a second arylene ethynylene unit. For **P1-N**, the second arylene unit was phenylene, while the arylene was thiophene for **P2-N** (Figure 5-1).

Monomer synthesis

Figure 5-2 shows the synthetic route for the monomer **N1**. Compound **1** was prepared by the substitution reaction of the commercial available dichloro-*p*-xylene and potassium acetate. Iodination reaction of compound **1** in a mixture of acetic acid and acetic anhydride resulted in compound **2** in 80% yield. Compound **3** was synthesized by the base assisted hydrolysis with quantitative yield. Compound **4** was obtained by the reaction of PBr_3 and compound **3**. Monomer **N1** was synthesized by refluxing trimethylamine with compound **4** for 24 hours.

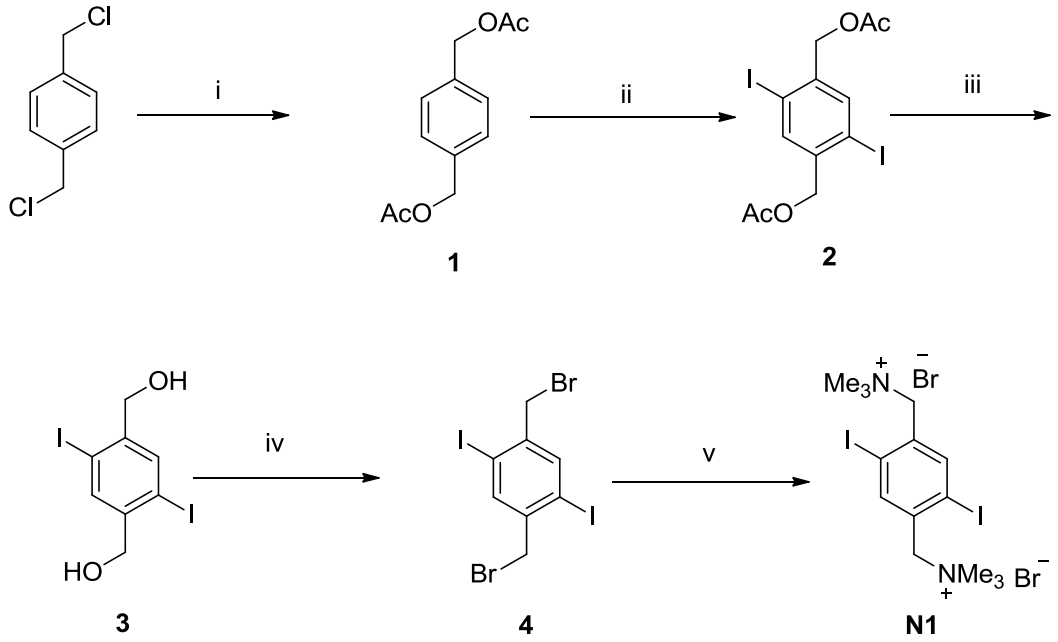

Figure 5-2. Synthetic route for the monomer **N1**. (i) KOAc, DMF, 60 ^{o} C, overnight; (ii) I_2, $NaIO_4$, AcOH, $(Ac)_2O$, H_2SO_4, 60 ^{o} C, overnight; (iii) K_2CO_3, $CHCl_3$, MeOH, rt overnight; (iv) PBr_3, THF, rt, 24 h; (v) NMe_3, $CHCl_3$, reflux, 24 h.

Polymer synthesis and characterization

The polymers (**P1-N** and **P2-N**) were synthesized in a “direct route”, where the monomers used were soluble in DMF/H_2O mixture. The polymerization directly led to water-soluble conjugated polyelectrolytes.

Figure 5-3 shows the synthesis route for water-soluble polymers **P1-N** and **P2-N**. The polymers were prepared by Sonogashira coupling of a stoichiometric amount of the monomer **N1** and diethynylbenzene or diethynylthiophene (**P1-N** or **P2-N**, respectively). The polymers were purified by multiple precipitations in acetone, followed by the dialysis against deionized water using Fisher brand dialysis membrane (12 kD Molecular Weight Cut-off) for three days. The final polymers were obtained after lypholization as brown yellow solids in ~ 70% yield. Each polymer was characterized by ^{1}H NMR.

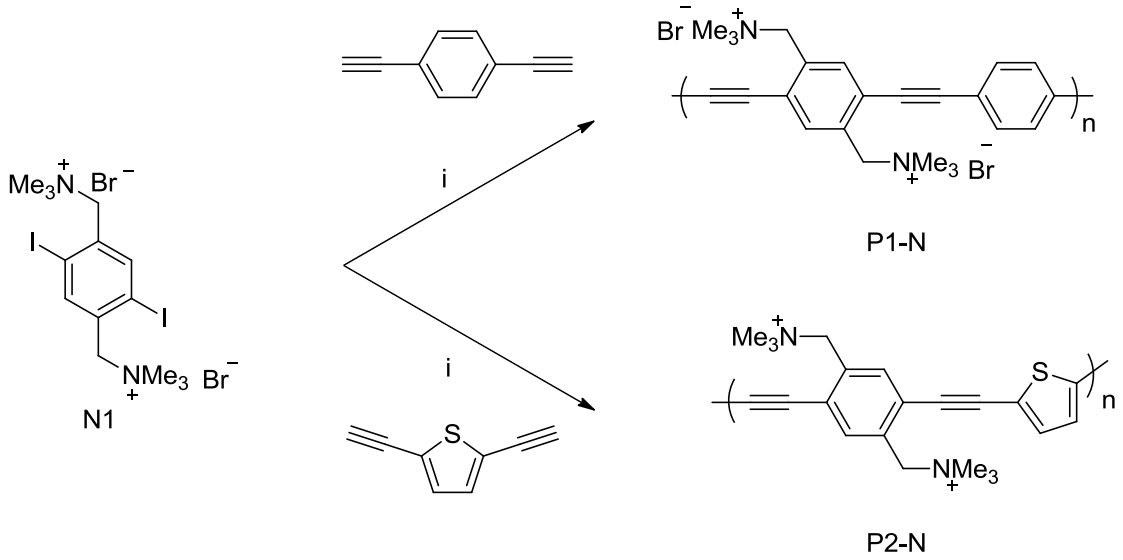

Figure 5-3. Synthesis route for **P1-N** and **P2-N**. (i) $Pd(PPh_3)_4$, CuI, DMF, H_2O, 70 ^{o} C, 2d.

Figure 5-4 shows the ^{1}H NMR spectra of monomer **N1** and the water-soluble polymers **P1-N** and **P2-N**. The ^{1}H NMR spectra of **P1-N** and **P2-N** were obtained in D_2O at 50 ^{o} C after H_2O signal suppression. In Figure 5-4B, the peaks from 7.4 ppm to 8.2 ppm were the protons of the aromatic rings. In Figure 5-4C, the peak ~ 8.2 ppm was from the protons of the benzene ring and the peak ~ 7.6 ppm was from the protons of the thiophene. The peaks ~ 5.0 ppm in both Figure 5-4B and C were assigned to the benzyl protons.

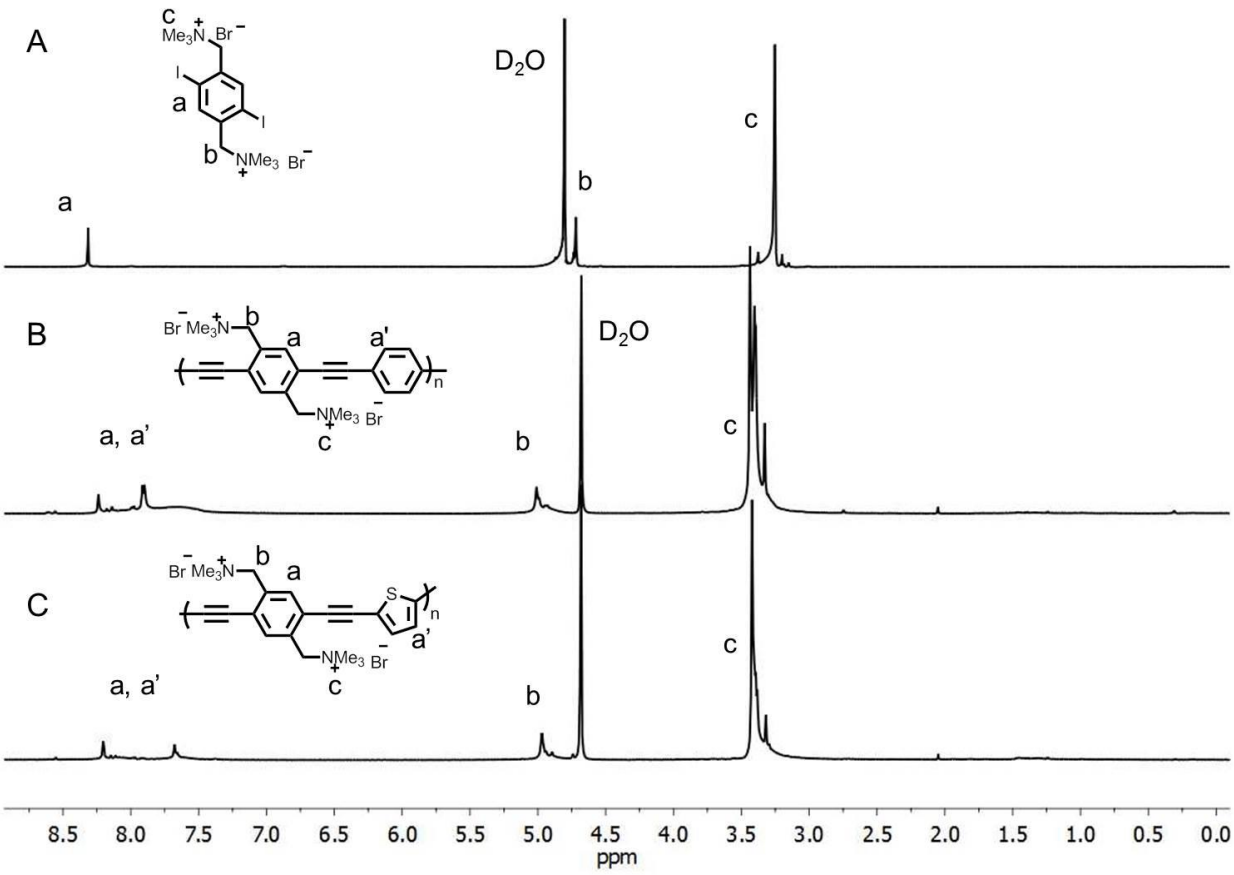

Figure 5-4. ^{1}H NMR spectra (500 MHz) of (A) monomer **N1**; (B) **P1-N**; (C) **P2-N** in D_2O. Polymer NMR spectra were obtained in D_2O at 50 ^{o} C after water signal suppression by Dr. Ion.

Fluorescence correlation spectroscopy

Obtaining accurate molecular weights of CPEs by GPC in aqueous solution was challenging because of the need of special instruments. Therefore, fluorescence correlation spectroscopy was applied to detect the diffusion time of each polymer and calculate the hydrodynamic radius. The experiments were carried out in aqueous solutions (pH = 6.5) with 2 μM of **P1-N** and **P2-N** using fluorescein (30 nM) as standard. The diffusion times and calculated hydrodynamic radius are shown and compared with polymer **P1** and **P2** (chapter 4) in Table 5-1. It is of note that the diffusion time of the polymer sample is related to the focus volume of the FCS instrument and the focus

volume may vary slightly with each experiment. The diffusion time of **P1-N** was smaller (10.02 x 10^{-5} s) compared with the diffusion time of **P2-N** (12.54 x 10^{-5} s). The hydrodynamic radius of **P1-N** was 1.86 nm and the hydrodynamic radius of **P2-N** was 2.32 nm. Considering that **P1-N** and **P1** had the same polymer backbone, the molecular weight of **P1-N** was calculated according to the equations below. If we used the spherical model, Equation 5-1 was chosen; if we consider our polymer to be a rod-like particle, we should use Equation 5-2. See the details of FCS calculation in Appendix C.

$$\frac{M_2}{M_1} = (\frac{R_2}{R_1})^3 \quad (5\text{-}1)$$

$$\frac{M_2}{M_1} = \frac{L_2}{L_1} \quad (5\text{-}2)$$

where *M* is the molecular weight of the ionic polymer, *R* is the hydrodynamic radius of the polymer (spherical model) and *L* is the length of the polymer sample (rod model). **P2** and **P2-N** had the same polymer backbone and same conformation in aqueous solution, thus the molecular weight of **P2-N** was estimated based on the molecular weight of **P2**. Then molecular weight of **P1-N** was estimated to be 13 ~ 20 kD and the molecular weight of **P2-N** was 38 ~ 77 kD.

Table 5-1. Diffusion time and hydrodynamic radius of PPEs in aqueous solution.

Polymer	τ (x 10^{-5} s)	D (x 10^{-10} m^2s^{-1})	R_H (nm)	L (nm)	M_n (kD)
P1-N[a]	10.02	1.30	1.86	14.9	20[c] 13[d]
P1[b]	6.17	1.62	1.49	11.9	19 (**P1-E**)
P2-N[a]	12.54	1.04	2.32	18.6	77[c] 38[d]
P2[b]	6.72	1.48	1.63	13.0	48 (**P2-E**)

[a] **P1-N** and **P2-N** solution had pH = 6.5. [b] **P1** and **P2** solution had pH = 8.0. [c] Molecular weight calculated by spherical model. [d] Molecular weight calculated by rigid rod model.

Photophysical Properties

Absorption, fluorescence and quantum yield

The photophysical properties of the PPEs were investigated by UV-Vis absorption, fluorescence spectroscopy and fluorescence lifetime measurements in MeOH and H_2O. Figure 5-5 shows the normalized absorption and fluorescence spectra of **P1-N** and **P2-N** in both methanol and water. In general, both polymers were well solvated in MeOH with structured emission and very small Stokes shift between absorption maximum and fluorescence maximum. Unlike traditional PPEs, solvents effects were much suppressed for both **P1-N** and **P2-N**. In methanol, **P1-N** exhibited an absorption maximum at 385 nm and a fluorescence maximum at 415 nm. The spectra of **P1-N** in aqueous solution were very similar to those in methanol, indicating that **P1-N** was molecularly dissolved in H_2O. A similar result was observed for polymer **P2-N.** The spectra of **P2-N** in methanol and water were almost the same with an absorption maximum around 425 nm and a fluorescence maximum around 464 nm.

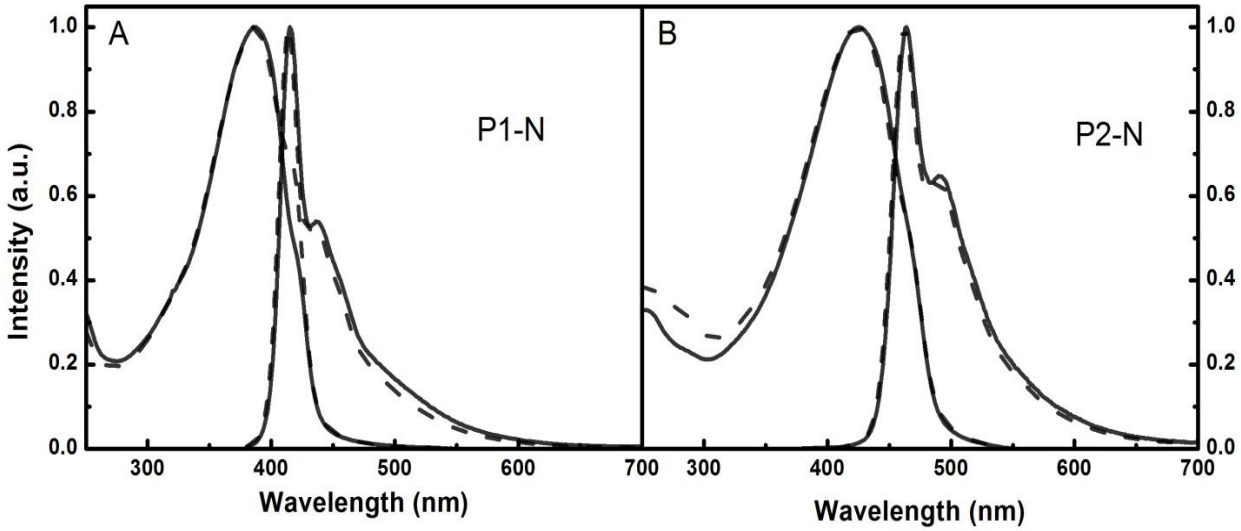

Figure 5-5. Normalized absorption and fluorescence spectra of **P1-N** (A) and **P2-N** (B) in MeOH (solid line) and H_2O (dash line). H_2O at pH = 6.5.

Table 5-2. Photophysical data of **P1-N** and **P2-N**.

Polymer	Solvent	λ_{max}^{abs} (nm)	λ_{max}^{fl} (nm)	Φ_F[b]
P1-N	MeOH	386	415	0.30
	H_2O[a]	385	414	0.30
P2-N	MeOH	425	464	0.17
	H_2O[a]	424	462	0.14

[a] H_2O at pH = 6.5. [b] Quinine sulfate in 0.1 M H_2SO_4 solution as a standard (Φ_F = 0.545).

The absence of aggregation was confirmed by the remarkably high fluorescence quantum yield in aqueous solution. Table 5-2 summarizes the photophysical properties of **P1-N** and **P2-N** in both methanol and water. The fluorescence quantum yield of **P1-N** was ~ 0.30 in aqueous solution, the same as that in methanol. The fluorescence of quantum yield of **P2-N** in methanol was ~ 0.17, due to the presence of thiophene unit which increased the rate of intersystem crossing. The quantum yield of **P2-N** in aqueous solution was still quite high ~ 0.14.

In conclusion, the shape and structure of the fluorescence spectra combined with the high fluorescence quantum yields supported our premise that the positively charged methylene trimethylammonium side groups can significantly suppress the aggregation of PPEs in aqueous solution.

Fluorescence lifetime measurement

In the previous studies, it was found that the presence of aggregates in CPEs caused the dynamic interaction between the excitons state in non-aggregated chains and excitons located on the aggregated chains.[48] The aggregates in those cases acted as an energy trap and quencher, resulting in a much shorter lifetime in aqueous solution. In order to support the idea that the aggregated chains were absent, the fluorescence

decay of **P1-N** and **P2-N** in both methanol and water were measured using the time-correlated single photon counting (TCSPC). Table 5-2 and Figure 5-6 show the average fluorescence lifetime of **P1-N** and **P2-N** in MeOH and H_2O (pH = 6.5) at each detection wavelength with ~ 10 nm band width.

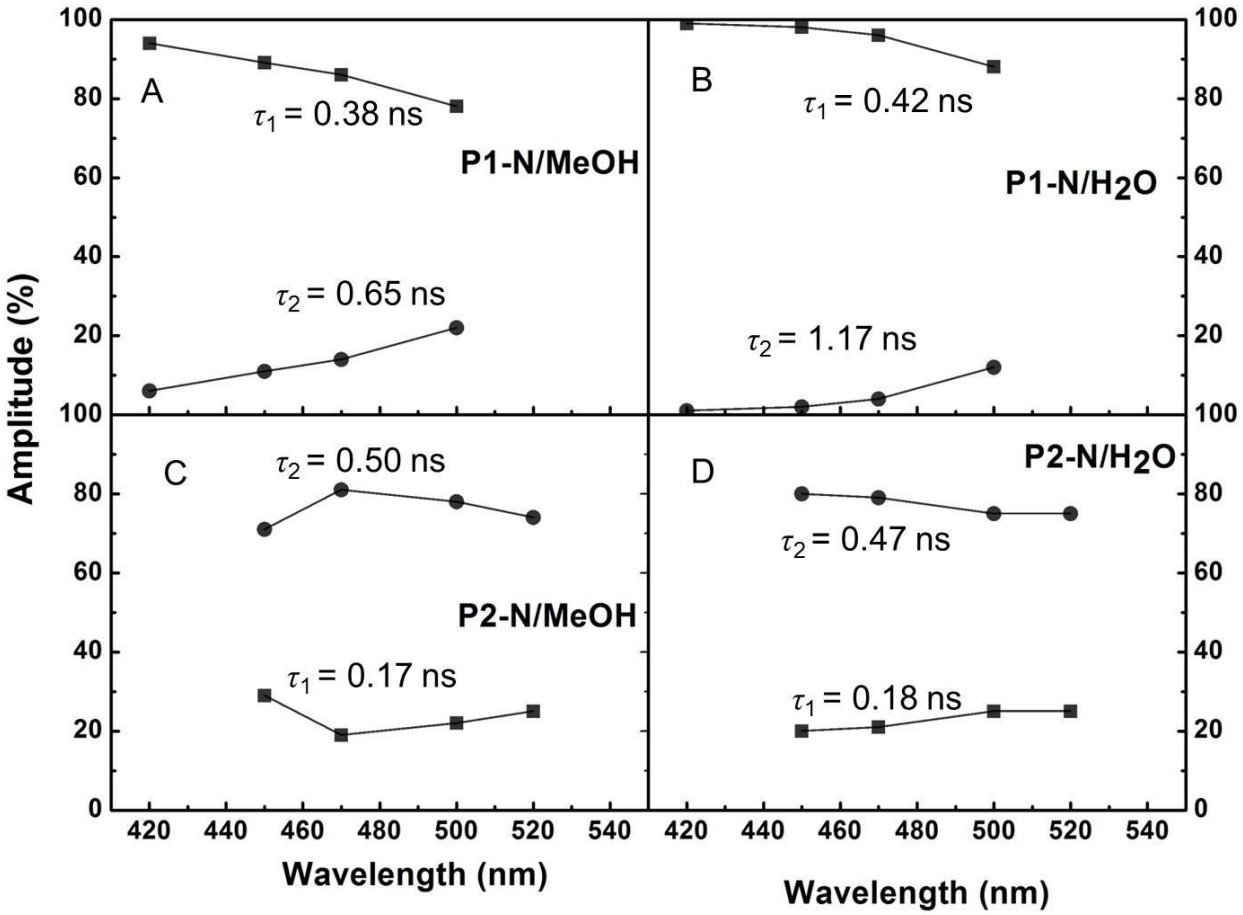

Figure 5-6. Fluorescence lifetime at different wavelengths: (A) **P1-N** in MeOH; (B) **P1-N** in H_2O; (A) **P2-N** in MeOH; (B) **P2-N** in H_2O.

In general, the fluorescence decays of **P1-N** and **P2-N** in both MeOH and H_2O featured bi-exponential decays. The global analysis of the fluorescence decay of **P1-N** in MeOH yielded two components (τ_1 = 0.38 ns and τ_2 = 0.65 ns). The first component had a dominant contribution (>78%) over all the detection wavelengths. As the detection wavelength increased, the contribution of the second component increased, resulting in

a slightly longer lifetime at longer wavelength. In aqueous solution, the global analysis of the fluorescence decay of **P1-N** gave a similar result with two decay components. The average lifetime of **P1-N** in aqueous solution was the same as that in methanol, indicating that **P1-N** was molecularly dissolved in aqueous solution.

The fluorescence decay of **P2-N** in both MeOH and H_2O were processed by global fitting algorithm. Two decay components were obtained for the fluorescence of **P2-N** in both MeOH and H_2O. It was found that the fluorescence of **P2-N** in MeOH was not dependent on the detection wavelength with the first component (τ_1 = 0.17 ns) contributing ~ 25% and the second component contributing ~ 75%. Similar results were observed for the fluorescence decay of **P2-N** in aqueous solution. Compared with **P1-N**, the longer lifetime component had a dominant role in the overall amplitude. The mean fluorescence lifetime of both **P1-N** and **P2-N** were similar ~ 0.42 ns in both MeOH and H_2O.

Table 5-3. Fluorescence lifetime of **P1-N** and **P2-N**.

		RA (%)[a]								
		MeOH				H_2O[b]				
	τ (ns)	420 nm	450 nm	470 nm	500 nm	τ (ns)	420 nm	450 nm	470 nm	500 nm
P1-N	τ_1 = 0.38	94	89	86	78	τ_1 = 0.42	99	98	96	88
	τ_2 = 0.65	6	11	14	22	τ_2 = 1.17	1	2	4	12
	χ^2	0.96	1.02	1.00	1.02	χ^2	1.05	1.03	0.970	1.01
	τ (ns)	450 nm	470 nm	500 nm	520 nm	τ (ns)	450 nm	470 nm	500 nm	520 nm
P2-N	τ_1 = 0.17	29	19	22	25	τ_1 = 0.18	20	21	25	25
	τ_2 = 0.50	71	81	78	74	τ_2 = 0.47	80	79	75	75
	χ^2	1.00	1.01	1.03	0.99	χ^2	0.99	1.06	1.00	1.02

[a] Data were processed by global fitting algorithm. Typical limits of error on τ_i are less than 3%. [b] H_2O at pH = 6.5.

Steady State Fluorescence Quenching Experiments

As mentioned in previous chapters, PPEs are attractive targets for study of the amplified quenching effects. In order to investigate the amplified quenching effects, steady sate fluorescence quenching experiments of **P1-N** and **P2-N** were performed by AQS (9.10-anthraquinone- 2,6-disulfonic acid disodium salt) and $K_4Fe(CN)_6$ in aqueous solution.

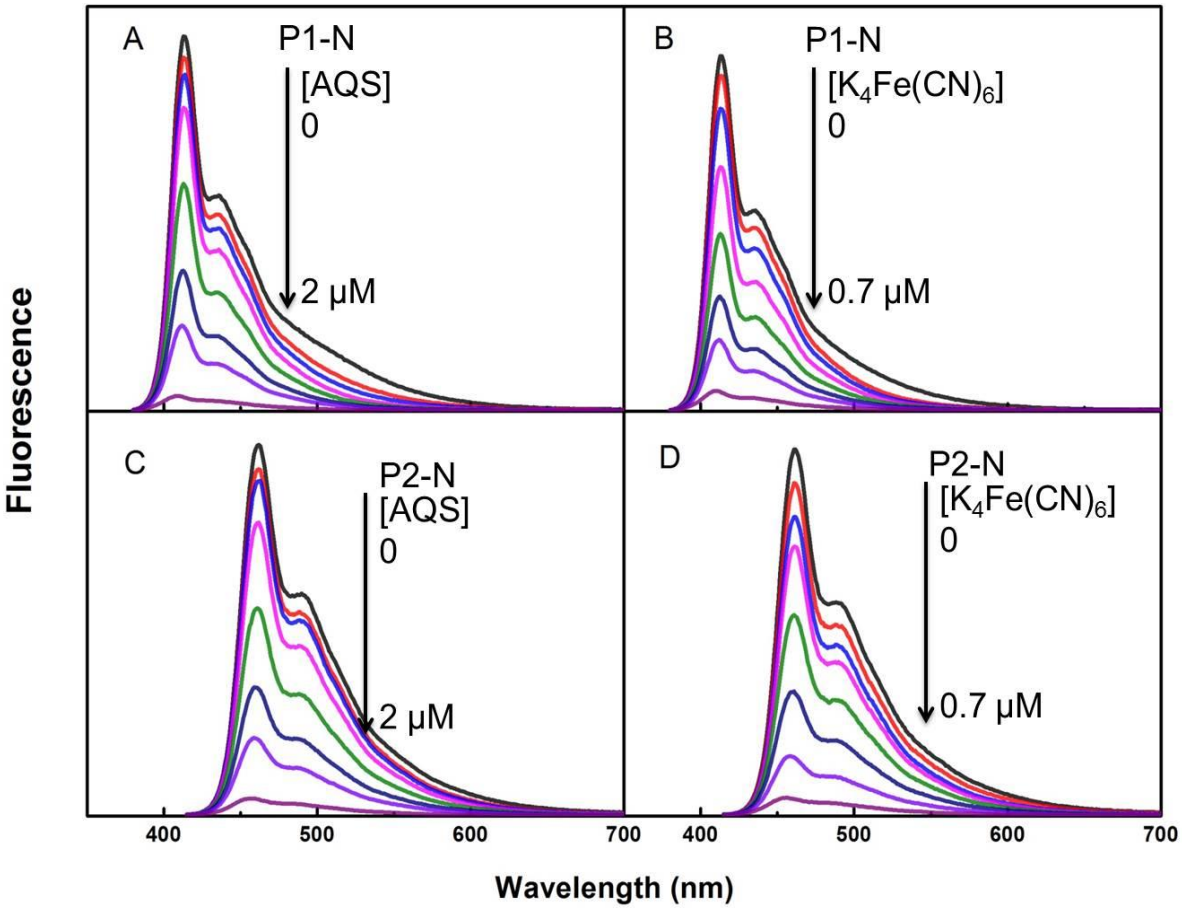

Figure 5-7. Fluorescence spectra of PPEs in H_2O upon addition of quenchers. (A) **P1-N** by AQS; (B) **P1-N** by $K_4Fe(CN)_6$; (C) **P2-N** by AQS; (D) **P2-N** by $K_4Fe(CN)_6$. [Polymer] = 2 μM. H_2O at pH = 6.5.

Figure 5-7 shows the fluorescence spectra of the polymers upon additions of different quenchers. Addition of AQS (2 μM) in the aqueous solution of **P1-N** resulted in significant quenching (>95%) with a loss of the vibronic structure in the fluorescence

spectra. Compared with AQS, $K_4Fe(CN)_6$ exhibited a stronger quenching ability that addition of $K_4Fe(CN)_6$ (0.7 μM) quenched most of the fluorescence of **P1-N**. Similar results were obtained for polymer **P2-N**.

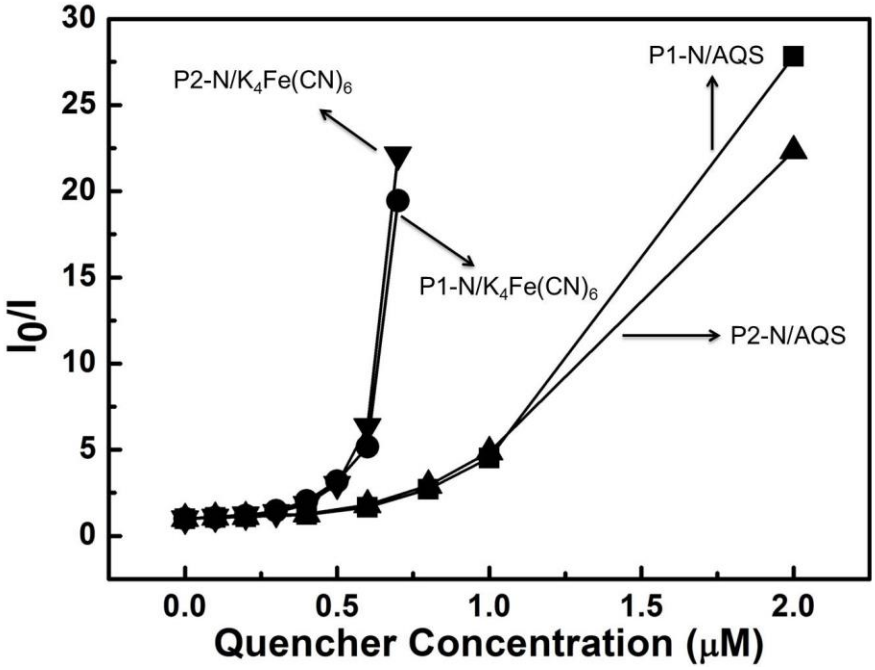

Figure 5-8. Stern-Volmer plots of **P1-N** and **P2-N** with various concentrations of the quenchers in H_2O. **P1-N** by AQS (■); **P1-N** by $K_4Fe(CN)_6$ (●); **P2-N** by AQS (▲); **P2-N** by $K_4Fe(CN)_6$ (▼). [Polymer] = 2 μM; H_2O at pH = 6.5.

Table 5-4. Stern-Volmer constant and $[Q_{90}]$ for 2 μM polymer in H_2O with AQS and $K_4Fe(CN)_6$.

Polymer	Quencher	K_{sv} (M^{-1})	$[Q_{90}]$ (μM)
P1-N	AQS	5.9×10^5	1.2
	$K_4Fe(CN)_6$	8.2×10^5	0.6
P2-N	AQS	6.4×10^5	1.3
	$K_4Fe(CN)_6$	1.1×10^6	0.6

Figure 5-8 shows the Stern-Volmer plots of PPEs (**P1-N** and **P2-N**) with various concentrations of the quenchers. In general, the Stern-Volmer plot of each case curved

upward and quencher $K_4Fe(CN)_6$ had a better efficiency to quench the fluorescence of both **P1-N** and **P2-N**. Stern-Volmer constants were calculated at the linear range when the quencher concentration was low. For **P1-N**, quencher AQS had a smaller K_{sv} value ~ 5.9 x 10^5 M^{-1}, while $K_4Fe(CN)_6$ exhibited a bigger K_{sv} value ~ 8.2 x 10^5 M^{-1} and a bigger [Q_{90}] value ~ 0.6 μM. The K_{sv} values for **P2-N** were slightly larger compared with those for **P1-N** (6.4 x 10^5 M^{-1} for AQS and 1.1 x 10^6 M^{-1} for $K_4Fe(CN)_6$, respectively). This can be explained by the different conformations of **P1-N** and **P2-N** in aqueous solution: **P1-N** is more like rigid-rod while **P2-N** was able to form helix structure because of the thiophene unit. Table 5-4 summarizes the Stern-Volmer constants and the [Q_{90}] values, which is defined as the quencher concentration when 90% of the fluorescence is quenched. The [Q_{90}] values of AQS were 1.2 μM for **P1-N** and 1.3 μM for **P2-N**, respectively. The [Q_{90}] values of $K_4Fe(CN)_6$ were smaller compared with AQS (0.6 μM for both **P1-N** and **P2-N**).

Application to Adenosine Triphosphate Sensing

Adenosine triphosphate (ATP) is a multifunctional nucleoside available in cells. It is often referred to as molecular unit of currency, because ATP transports chemical energy within cells for metabolism. One ATP molecule contains three phosphate groups (Figure 5-9). Under the catalysis of the alkaline phosphatase (ALP), ATP can lose one 5'-phosphate group to form ADP (adenosine diphosphate) or two 5'-phosphate groups to form AMP (adenosine monophosphate).[130] Herein, we report that the conjugated polymer **P1-N** can be utilized as probes for sensitive and selective fluorescence sensor for ATP due to formation of conjugated polymer/phosphate substrates complex by electrostatic interaction.

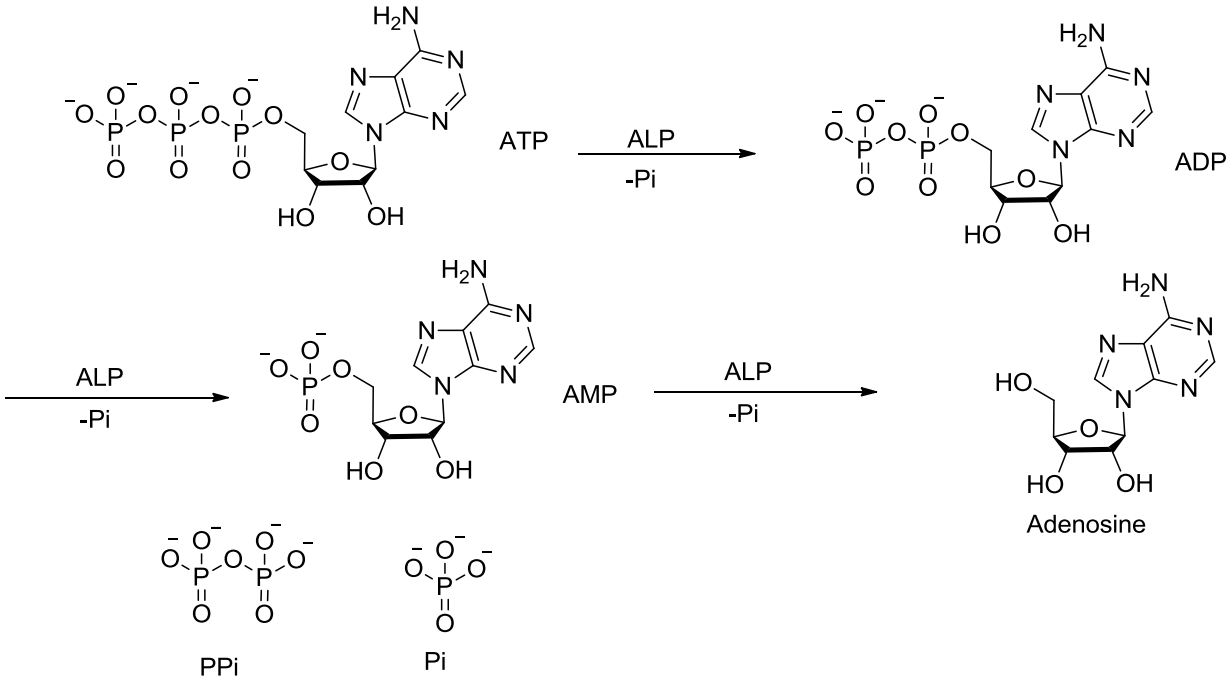

Figure 5-9. Dephosphorylation of adenosine triphosphate (ATP) by alkaline phosphatase (ALP).

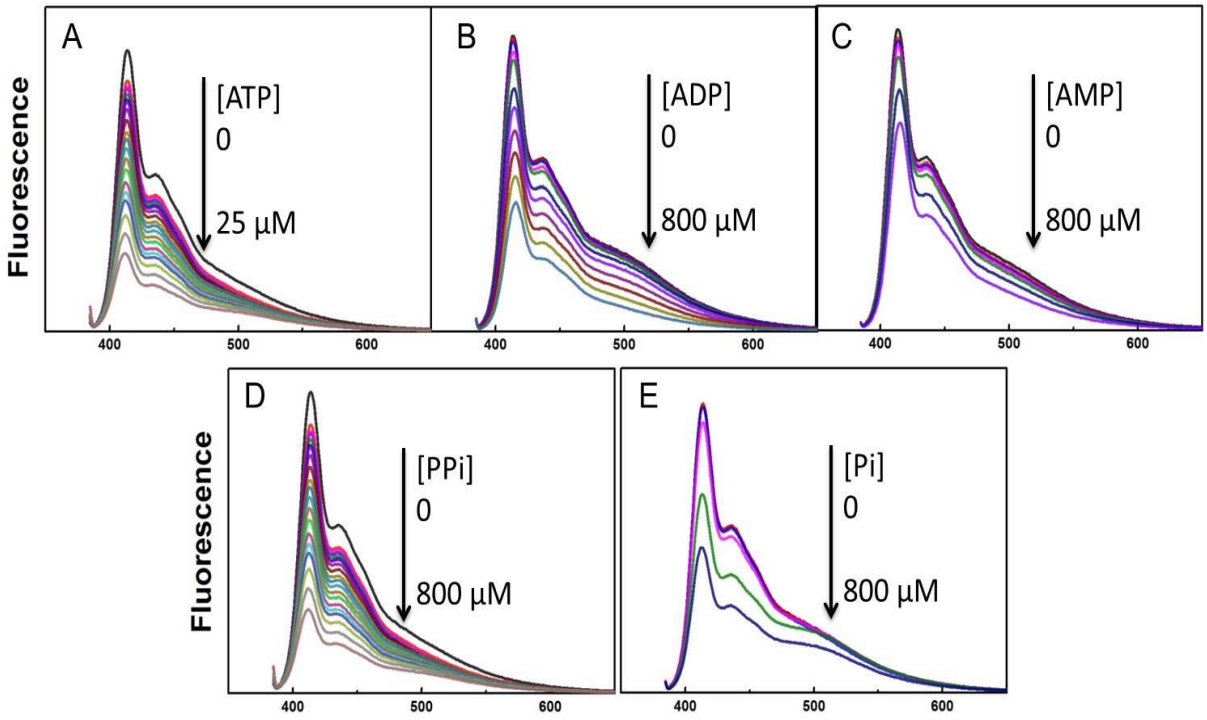

Figure 5-10. Fluorescence spectra of **P1-N** (2 μM) in MES buffer (10 mM, pH = 6.5) upon addition of ATP (A), ADP (B), AMP (C) ,PPi (D) and Pi (E).

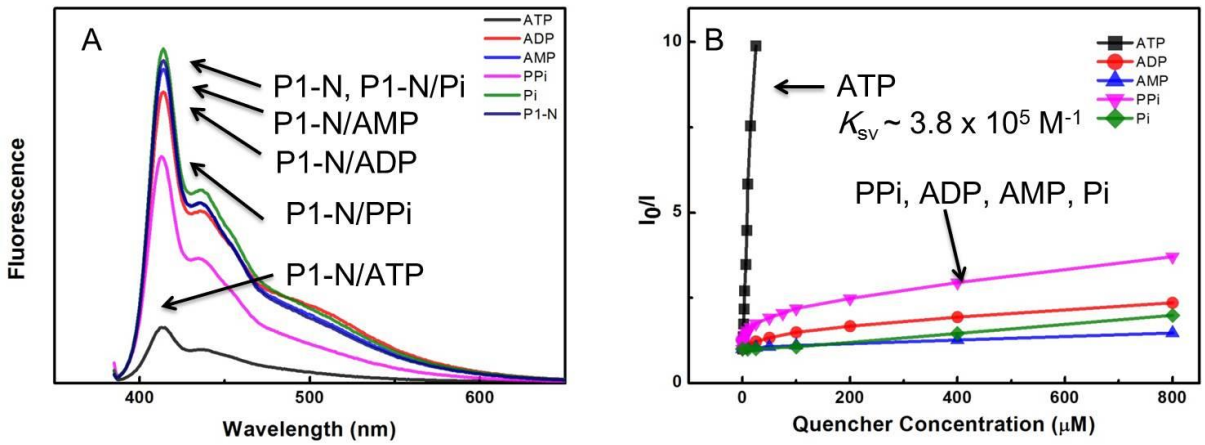

Figure 5-11. (A) Fluorescence spectra of **P1-N** (2 μM) in MES buffer (10 mM, pH = 6.5) upon addition of 10 μM of different quenchers. (B) Stern-Volmer plots of **P1-N** (2 μM) in MES buffer (10 mM, pH = 6.5) upon addition of different quenchers.

Figure 5-10 shows the fluorescence spectra of **P1-N** in MES (2-(N-mopholine) ethane sulfonic acid) buffer (10 mM, pH 6.5) upon addition of different phosphate substrates including ATP, ADP, AMP, PPi and Pi. The addition of 25 μM of ATP can induce about 90% quenching of the fluorescence intensity of **P1-N**. In contrast, the addition of 800 μM of other quenchers (ADP, AMP, PPi and Pi) reduced the fluorescence intensity by less than 40%. A more distinct comparison of the fluorescence spectra of **P1-N** with 10 μM of different quenchers is shown in Figure 5-11A. In the MES buffer solution, 10 μM of Pi and AMP barely induced any change to the fluorescence spectra compared to the pure polymer solution. After the introduction of 10 μM of ADP, the fluorescence was quenched by ~ 10%. In contrast, more than 80% of the fluorescence of **P1-N** was quenched by 10 μM of ATP, indicating that **P1-N** was highly selective for ATP over the other phosphate substrates. As a comparison, 10 μM of PPi quenched ~ 40% fluorescence of **P1-N**. Figure 5-11B shows the Stern-Volmer plots of **P1-N** in MES buffer solution upon addition of different quenchers. While ADP, AMP, PPi and Pi failed to induce substantial quenching, ATP quenched the fluorescence very

efficiently with a K_{sv} value ~ 3.8 x 10^5 M^{-1}. There are several advantages of this sensor compared with the ATP sensor in literatures.[131,132] First, the polymer itself was highly fluorescent with a quantum yield ~0.30 in aqueous solution. The sensitivity of the fluorescent sensor based on **P1-N** is higher than zinc complex-based chemo-sensors. Second, this sensor had a better selectivity for ATP over PPi compared to the poor ability to differentiate them by sensors in literatures.[24,129] Addition of 10 μM ATP quenched more than 90% of the fluorescence intensity at 415 nm, while the same amount of PPi quenched less than 30%. In addition, the direct detection of ATP using this sensor is fast and rapid, since the polymer **P1-N** is well solvated in aqueous solution.

In conclusion, a sensitive and selective fluorescence sensor for ATP has been successfully developed based on a highly fluorescent cationic PPE (**P1-N**). The fluorescence of **P1-N** in MES buffer solution was efficiently quenched by ATP. This sensor can be applied to build a fluorescence assay for alkaline phosphatase (ALP) in the future study.

Summary

In this chapter, a new series of conjugated polyelectrolytes based on the poly(phenylene ethynylene) backbone featuring methylene ammonium side groups have been synthesized and characterized. These polymers were prepared using a "direct" route, in which polymerization directly led to cationic water soluble PPEs (**P1-N** and **P2-N**). Investigations of the photophysical properties of the PPEs proved that both **P1-N** and **P2-N** existed as single chains in water, with high fluorescence quantum yields, comparable fluorescence spectra and fluorescence lifetime to those in methanol.

Steady state fluorescence quenching of **P1-N** and **P2-N** with AQS and $K_4Fe(CN)_6$ revealed the amplified quenching effects.

A fluorescence “turn-off” sensor for ATP is developed by taking advantage of the interaction between water soluble **P1-N** and the phosphate substrates driven by the electrostatic interaction. In MES buffer solution, the fluorescence of the polymer **P1-N** was sensitive to the concentration of ATP with high selectivity over ADP, AMP, PPi and Pi. We are currently developing biological assays for enzymes such as ALP using this system and we believe the design principles can be applied to other anion species of interest.

Experimental

Materials

$Pd(PPh_3)_4$ was purchased from Strem Chemical Company and used as received. Sodium phosphate (Pi), 2-(N-mopholine)ethane sulfonic acid (MES), trimethylamine, 9.10-anthraquinone- 2,6-disulfonic acid disodium salt (AQS), sodium adenosine triphosphate (ATP), sodium adenosine diphosphate (ADP), sodium adenosine monophosphate (AMP), and sodium pyrophosphate (PPi) were purchased from Sigma-Aldrich and used without further purification. Potassium acetate, sulfuric acid, acetic acid, acetic anhydride and potassium ferrous cyanide ($K_4Fe(CN)_6$) were purchased from Fisher Scientific Company and used as received. THF and DMF were purified by solvent dispensing system. All other chemicals were purchased from commercial sources unless specially mentioned. Stock solutions (0.5 mM) of all PPEs were prepared in H_2O and have been stored at 4 ^{o} C. For all photophysical experiments, the PPEs solutions were prepared in deionized H_2O with pH adjusted to 6.5. MES buffer (10

mM, pH = 6.5) was prepared by dissolving MES into deionized water and the pH was adjusted by adding dilute HCl according to the pH meter.

Instruments and General Methods

NMR spectra were recorded using a Gemini-300 NMR operating at 300 MHz for ^{1}H NMR and at 75 MHz for ^{13}C NMR for small organic compounds. ^{1}H NMR spectra of the polymers were measured in Inova2-500 NMR operating at 500 MHz at 50 ^{o}C after water signal suppression. The polymer NMR spectra were measured by Dr. Ion. UV absorption spectra were measured on a Shimadzu UV-1800 spectrophotometer. Luminescence spectra were measured on a PTI (Photon Technology International) fluorescence spectrometer. Fluorescence lifetimes were determined by time-correlated single photon counting on a FluoTime 100 spectrometer (Pico Quant) equipped with 370 nm diode laser as excitation source. Fluorescence quantum yields are reported relative to known standards. The optical density of solutions at the excitation wavelength was <0.1 and corrections were applied for differences in the refractive index of standard and sample solutions. FCS measurements were taken on a homemade setup using a 405 nm diode laser (Coherent, CUBE) as the excitation light. Fluorescein (30 nM in 10 mM phosphate buffer, pH = 8) was used as the calibration for the system.

Synthetic Procedures

1,4-Phenylenebis(methylene) diacetate (1). To a solution of dichloro-p-xylene (3.9 g, 22 mmol) in 100 mL DMF, potassium acetate (21.2 g, 0.22 mol) was added. The reaction was stirred at 60 ^{o}C for overnight. After cooling to room temperature, the mixture was poured into cold water. The white precipitate was collected by filtration and washed several times with water (yield: 3.5 g, 73%). ^{1}H NMR (300 MHz, $CDCl_3$): δ 7.30

(s, 4H), 5.0 (s, 4H), 2.05 (s, 6H). ^{13}C NMR (75 MHz, $CDCl_3$): δ 170.85, 136.09, 120.53, 65.97, 21.08.

(2,5-Diiodo-1,4-phenylene)bis(methylene) diacetate (2). Sodium periodate (1.68 g) and diiodine (6.2 g, 40% excess) were stirred into a mixture of glacial acetic acid (15 mL) and acetic anhydride (8 mL) at 5 ^{o} C for 30 mins. Then concentrated sulfuric acid (2 mL) was then added slowly to the stirring suspension. Compound **1** (2 g, 9 mmol) was added to this solution and stirred continuously for 24 h at 60 ^{o} C. The reaction was then poured into an ice water mixture, saturated with Na_2SO_3. All precipitate was collected by filtration and washed with cold ethanol. Recrystallization of the product from ethanol resulted in pure white solid (yield: 3.3 g, 77%). ^{1}H NMR (300 MHz, $CDCl_3$): δ 7.80 (s, 2H), 5.05 (s, 4H), 2.17 (s, 6H). ^{13}C NMR (75 MHz, $CDCl_3$): δ 170.56, 140.21, 139.59, 97.78, 68.99, 21.13.

(2,5-Diiodo-1,4-phenylene)dimethanol (3). To a solution of compound **2** (1 g, 2.1 mmol) in a mixture of $CHCl_3$ (100 mL) and MeOH (100 mL), potassium carbonate (10 g) was added. The reaction was stirred at room temperature for 24 h. The solvents were then removed under vacuum and 300 mL water was added to the residue. The resulting mixture was stirred for 2 h. The insoluble white solid was collected and dried under vacuum (yield: 0.75 g, 80%). ^{1}H NMR (300 MHz, DMSO-d_6): δ 7.00 (s, 2H), 5.55 (t, 2H), 4.36 (d, 4H). ^{13}C NMR (75 MHz, DMSO-d_6): 144.10, 136.97, 96.53, 66.39.

1,4-Bis(bromomethyl)-2,5-diiodobenzene (4). To a solution of compound **3** (0.88 g, 2.5 mmol) in THF (50 mL), PBr_3 (0.24 mL) was added slowly at 0 ^{o} C. The reaction was stirred at room temperature for 24 h. The organic solvent was removed under vacuum and the residue was dissolved in $CHCl_3$ (100 mL) and washed with water

for 3 times. After drying over anhydrous Na_2SO_4, the organic solvent was removed to yield compound **4** as a white solid (yield: 0.72 g, 60%). ^{1}H NMR (300 MHz, $CDCl_3$): δ 7.86 (s, 2H), 4.45 (s, 4H). ^{13}C NMR (75 MHz, $CDCl_3$): δ 141.90, 140.80, 99.70, 36.80.

Monomer N1. To a solution of compound **4** (0.47 g, 0.96 mmol) in a mixture of ethanol (30 mL) and acetone (30 mL), trimethylamine in water solution (25%, 30 mL) was added. The reaction was refluxed for 24 h. Then the solvents were removed under vacuum and the residue was dried (yield: 0.55 g, 93%). ^{1}H NMR (500 MHz, D_2O): δ 8.20 (s, 2H), 4.75 (s, 4H), 3.20 (s, 18H). ^{13}C NMR (125 MHz, D_2O): δ 145.59, 135.14, 103.56, 70.78, 53.50.

General procedure for polymerization. Monomer **N1** (63.4 mg, 0.1 mmol) and 0.1 mmol of the corresponding co-monomers (1,4-diethynyl)benzene for **P1-N**, 2,5-diethynyl)thiophene for **P2-N**) were dissolved in a mixture of DMF (15 mL), H_2O (5 mL) and diisopropylamine (5 mL). The solution was degassed for 1 hour, followed by the addition of $Pd(PPh_3)_4$ (15 mg) and CuI (10 mg) under argon atmosphere. The reaction was stirred at 70^{o}C for 48 hours. Then the resulting mixture was concentrated to 2 mL and poured into acetone (50 mL). The yellow fiber precipitate was collected by centrifugation and dissolved into H_2O (2 mL). The polymer was further purified by multiple precipitation in acetone, followed by the dialysis against Millipore water using Fisher Brand dialysis membrane (12 kD molecular weight cut off) for 3 days. Brown yellow solids were obtained after lypholization.

P1-N: ^{1}H NMR (500 MHz, D_2O): δ 7.50 ~ 8.25 (br, 6H), 5.00 (s, 4H), 3.32 (br, 18H). Integration of the peak ~ 5.00 pm was slightly less than 4, due to the suppression of the water signal nearby.

P2-N: ^{1}H NMR (500 MHz, D_2O): δ 8.20 (br, 2H), 7.65 (br, 2H), 5.00 (br, 4H), 3.33 (br, 18H). Integration of the peak ~ 5.00 pm was slightly less than 4, due to the suppression of the water signal nearby.

CHAPTER 6
CONCLUSION

In conclusion, the design and synthesis of functional poly(phenylene ethynylene)s (PPEs) have been presented and discussed. Their photophysical properties and aggregation behaviors in different solvents have been investigated as a guide to sensor application. Especially, the discovery of the methylene carboxylate or methylene ammonium side groups to suppress aggregation of PPEs provides the polymer chemists with new approaches to develop and synthesize novel non-aggregated conjugated polyelectrolytes. By taking advantage the analyte-induced aggregation mechanism, several fluorescent sensors have been built.

Traditional PPE-types CPEs

As discussed in chapter 1, PPEs with linear side groups always aggregated in aqueous solution, driven by the hydrophobic interaction and π-π stacking. In order to improve the photophysical properties for sensor application, usually surfactant was needed. For example, surfactant (Triton X-100) drastically improved the fluorescence property of **GU-P1**, which made the PPi sensor possible. Many efforts have been made to avoid the aggregation. Swager and coworkers incorporated Iptycenes as building blocks into the PPE backbone. Lptycenes can provide steric blocking, which can inhibit strong interactions between polymer chains which have a strong tendency to form non-emissive excimer complexes.[52,128,133] Hecht and coworkers discovered that the introduction of the oligo(ethylene glycol) as side groups can significantly induce the steric hindrance between polymers, resulted in non-aggregated PPEs.[62] However, the bulky oligo(ethylene glycol) side groups wrap the polymer backbone and block other molecule from getting close.[39,63,64] Our group (Schanze group) also has devoted a lot of

efforts to get non-aggregated PPEs by changing different solubilizing groups and attaching bulky polyionic side groups.[24,48]

There is one problem that has not been answered or even asked: What caused the PPEs to aggregate in aqueous solution? Before this dissertation, almost all of the PPEs in literatures share a common feature. They have an oxygen atom on the solubilizing group directly attached to the polymer backbone. The reason for this is simple: the monomers of PPEs were synthesized from 1,4-diiodo-2,5-dihydroxylbenzen. It is easy to put different solubilizing groups to the PPE-type CPEs by a substitution reaction. In 2013, Feng and Schanze discovered that a set of OPEs without that oxygen linkage exhibited remarkable fluorescence quantum yield in aqueous solution (>0.80).[134] Following his discovery, this dissertation will explore the methylene carboxylate and methylene ammonium side groups to achieve non-aggregated PPEs.

Non-oxygen PPE-type CPEs

In this dissertation, two sets of PPE-type CPEs were synthesized and characterized in chapter 4 and 5. Their photophysical properties and aggregation behavior in aqueous solution were carefully investigated. It was found that the introduction of both methylene carboxylate (-CH_2-CO_2Na) and methylene ammonium (-CH_2-NMe_3Br) significantly suppressed the aggregation of PPEs in aqueous solution. Most of the PPEs had a comparable fluorescence properties in H_2O compared with those in MeOH. The fluorescence quantum yields of most PPEs were ~ 0.16, much bigger than the traditional PPEs. These differences between the traditional PPEs and non-oxygen PPEs were attributed to the aggregation behavior in aqueous solution. In a collaboration work with Dr. Feng, the TEM images of PPEs with oxygen linker showed large aggregates while non-oxygen PPEs stayed unaggregated as small particles. Until

now, we could not answer what causes the differences with complete confidence but we have some hypothesis that may provide a way to explain. In an unpublished simulation experiment by Winkel in our group, it was found that OPE (20 repeat units) with oxygen had higher HOMO energy (~ 0.3 eV higher) than the non-oxygen OPE. In the traditional PPEs, the benzene with oxygen linker may behave like a donor, and the other benzene without oxygen is lower in energy. This donor-acceptor-like effect may promote inter-chain aggregation and stable the aggregates. However, in chapter 4, we designed two donor-acceptor polymers (**P3** and **P4**) and both polymers did not form large aggregates.

Another possibility is that the oxygen in traditional PPEs interacts with water molecule in aqueous solution, resulting in a very fast energy relaxation pathway. This idea can also explain the low quantum yield of **P3** in aqueous solution, because **P3** had an oxygen linker directly attached to the backbone. In addition, the photo-induced electron transfer between the polymer backbone and the oxygen lone pairs may also exist.

Non-aggregated PPEs

Taken together, the basic principle to achieve non-aggregated PPE-type CPEs is to prevent the inter-chain interaction and suppress π-π stacking. Based on our discovery, it is a good idea to change the oxygen linker to methylene linker, which results in non-aggregated PPEs in aqueous solution. If you want to get even better photophysical properties, you can combine the advantages of polyionic side groups and methylene linker. The non-aggregated PPEs can be favorably used in sensor application based on analyte-induced aggregation mechanism. High performance devices including DSSCs can be obtained using non-aggregated PPEs.

APPENDIX A
NMR SPECTRA

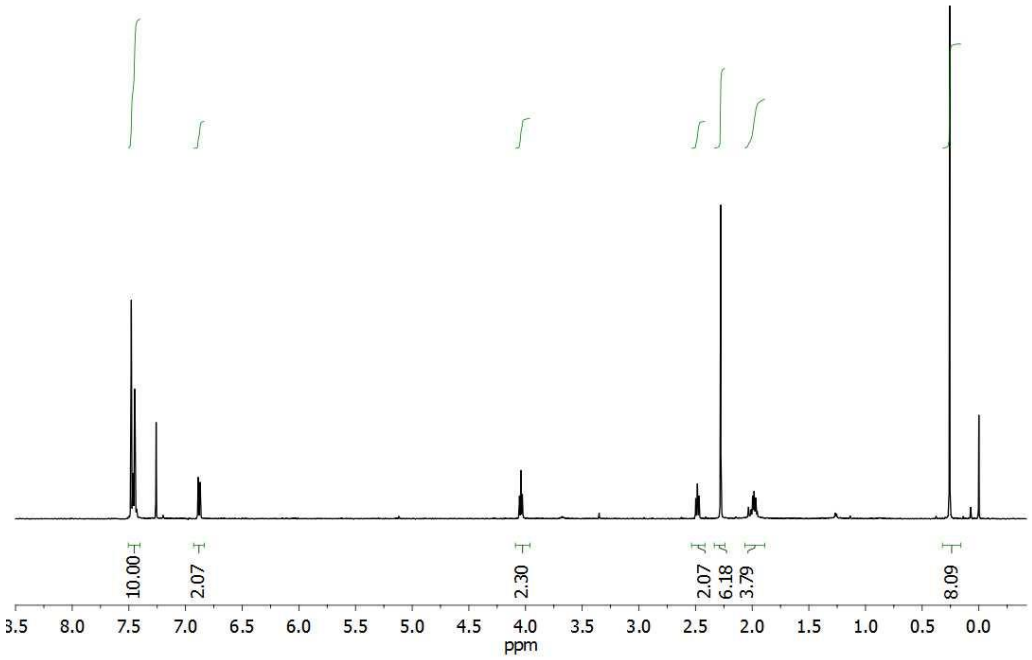

Figure A-1. ^{1}H NMR spectrum (500 MHz, $CDCl_3$) of compound **5** (chapter 2).

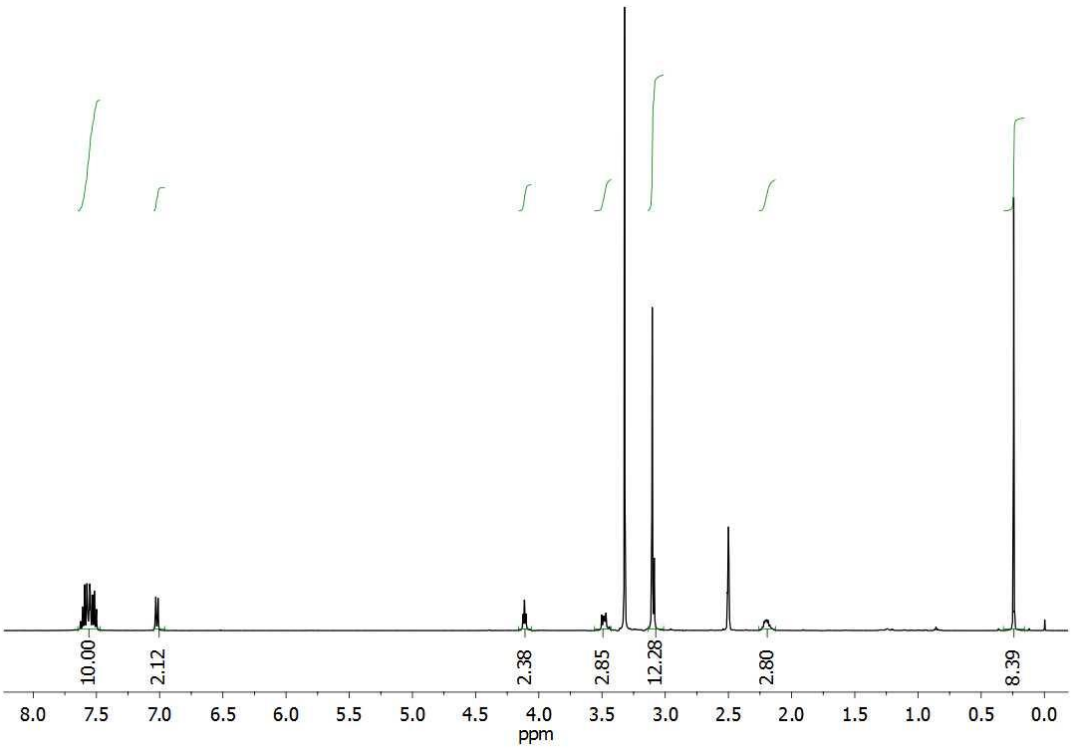

Figure A-2. ^{1}H NMR spectrum (500 MHz, DMSO-d_6) of **OPEC1** (chapter 2).

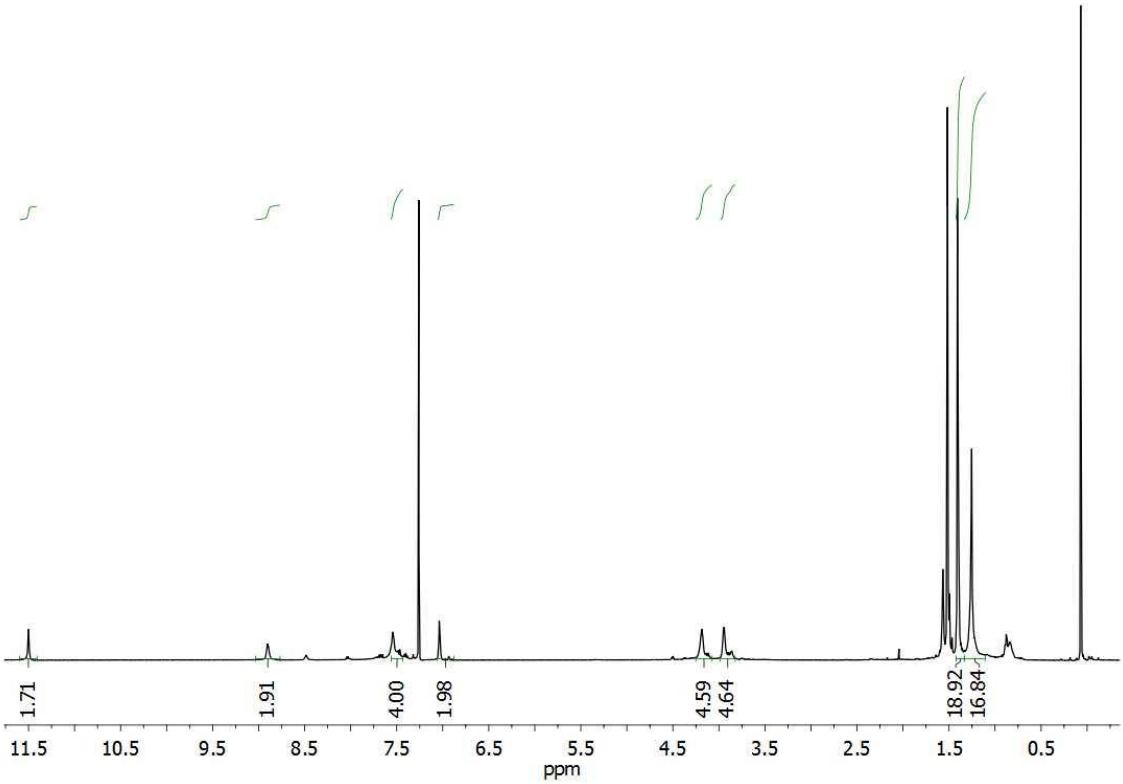

Figure A-3. ^{1}H NMR spectrum (500 MHz, $CDCl_3$) of **GU-P1-Boc** (chapter 3).

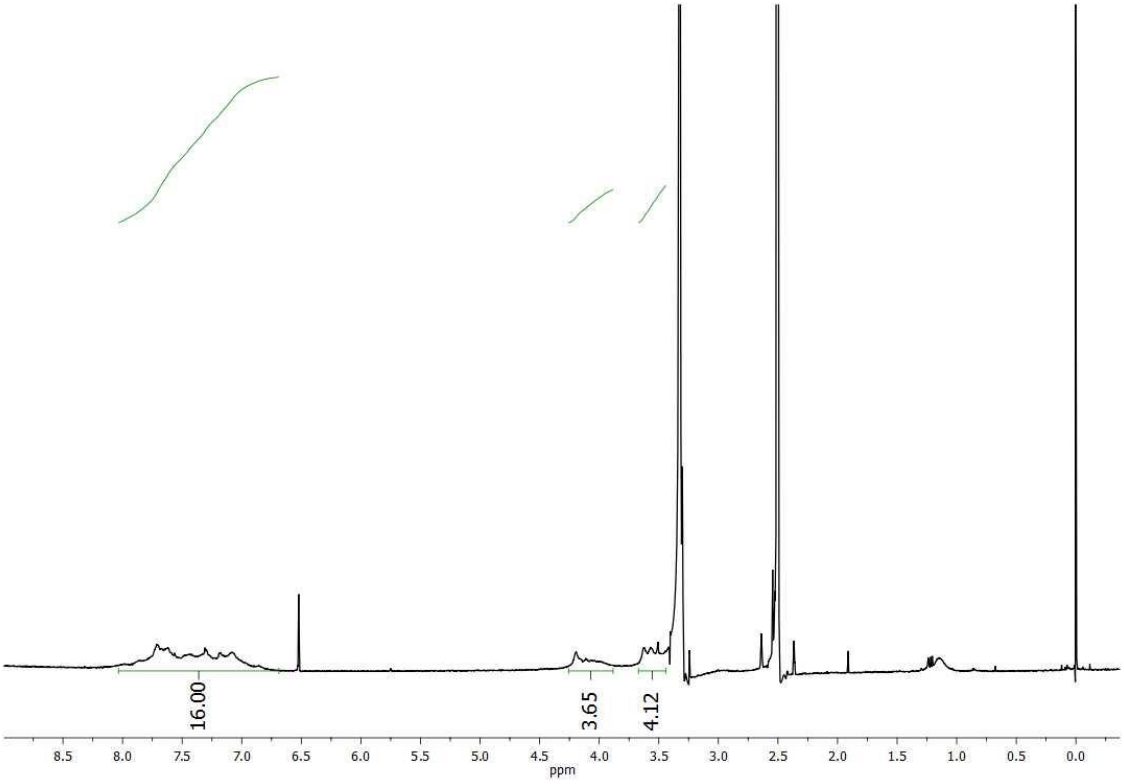

Figure A-4. ^{1}H NMR spectrum (500 MHz, DMSO-d_6) of **GU-P1** (chapter 3).

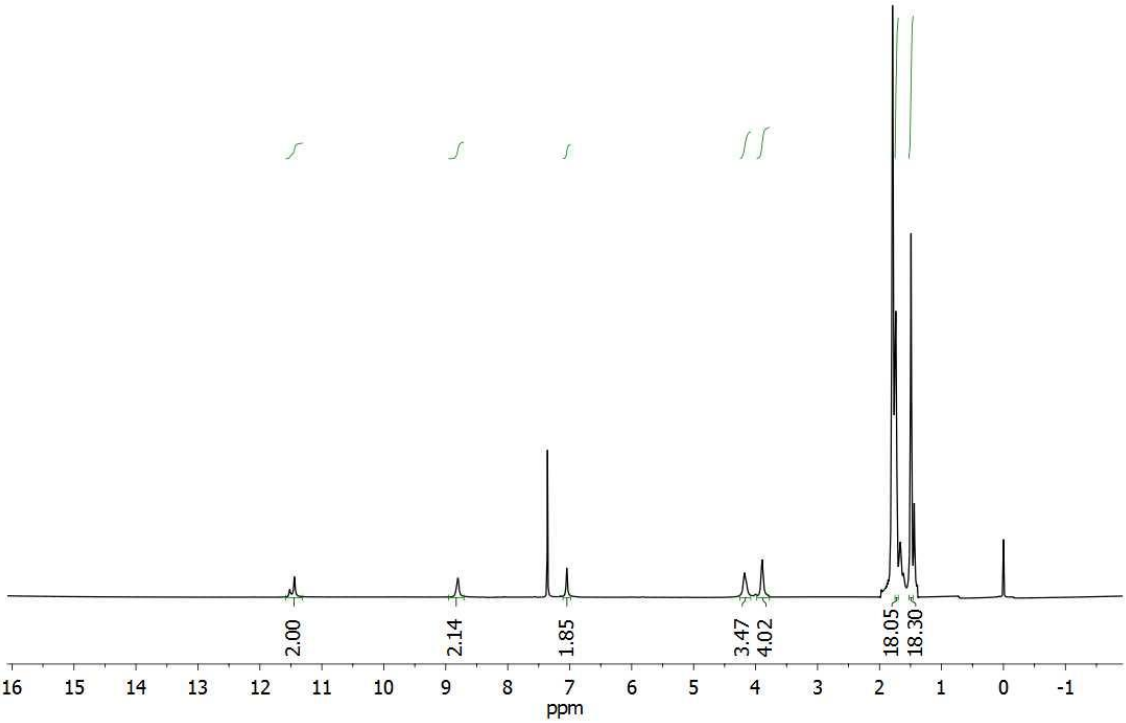

Figure A-5. ^{1}H NMR spectrum (500 MHz, $CDCl_3$) of **GU-P2-Boc** (chapter 3).

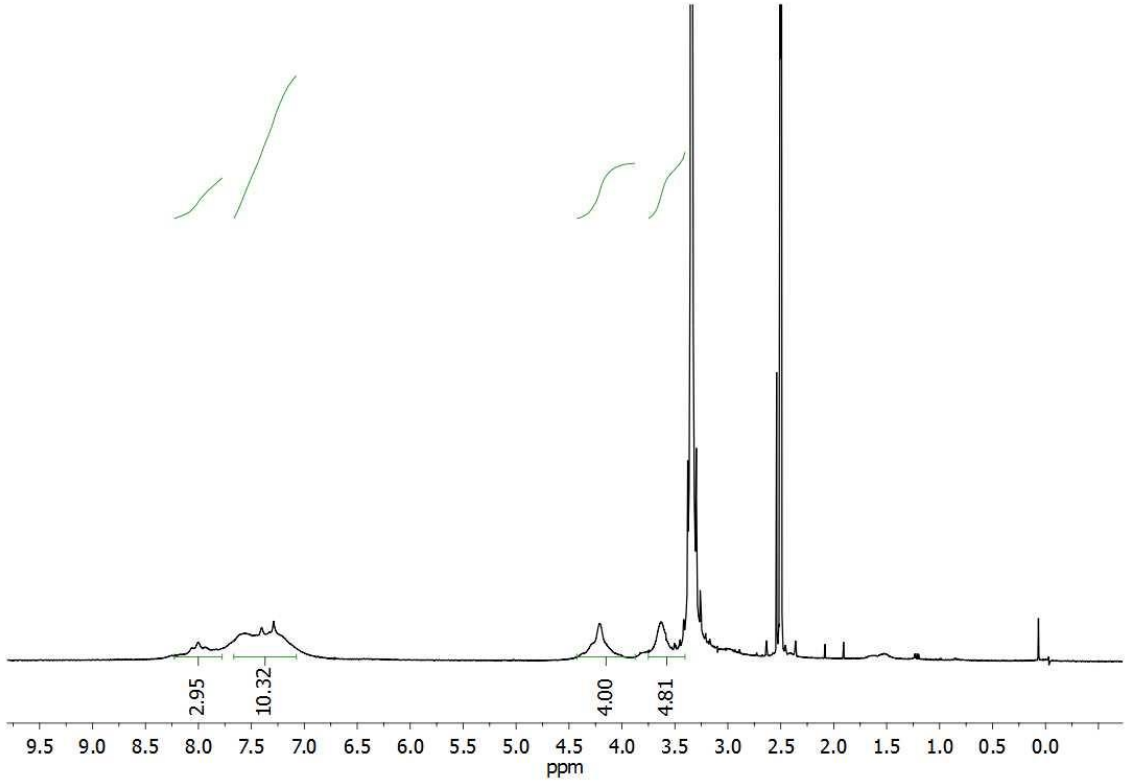

Figure A-6. ^{1}H NMR spectrum (500 MHz, DMSO-d_6) of **GU-P2** (chapter 3).

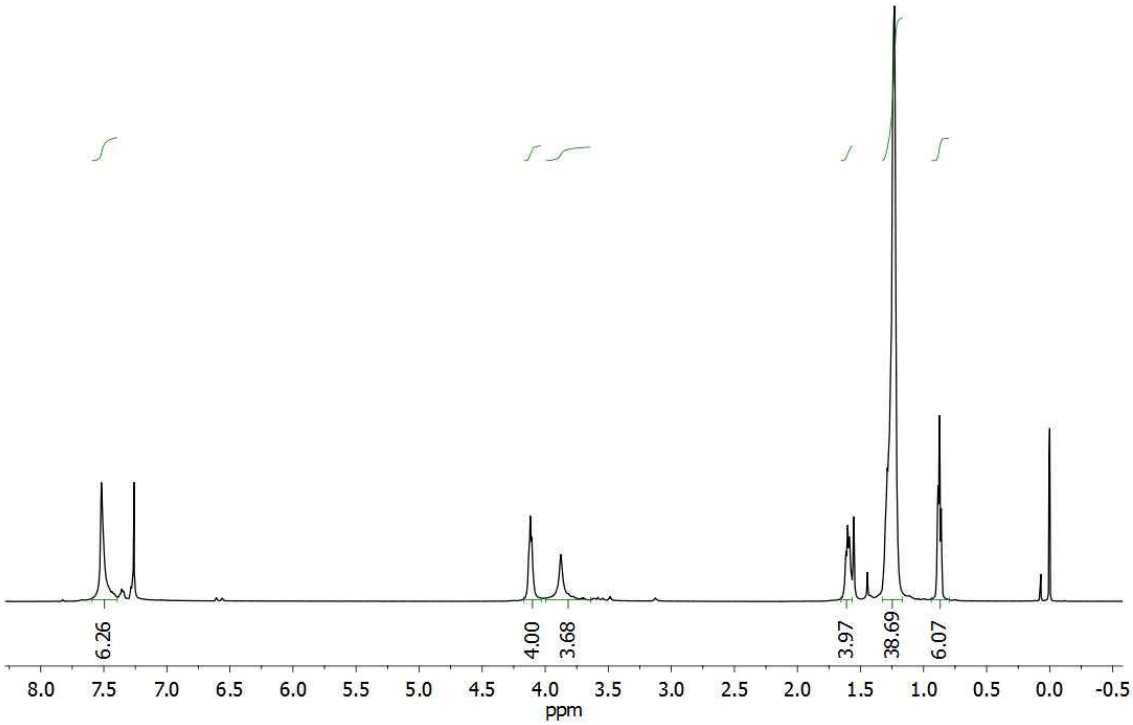

Figure A-7. ^{1}H NMR spectrum (500 MHz, $CDCl_3$) of **P1-E** (chapter 4).

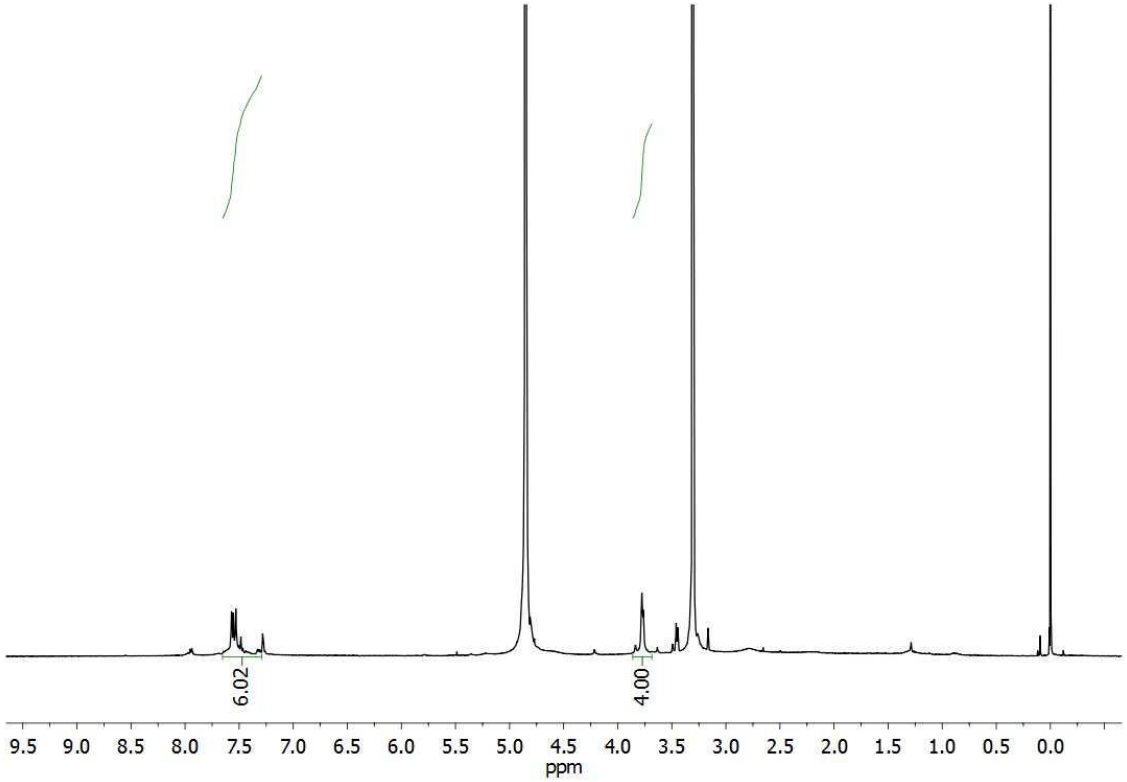

Figure A-8. ^{1}H NMR spectrum (500 MHz, CD_3OD) of **P1** (chapter 4).

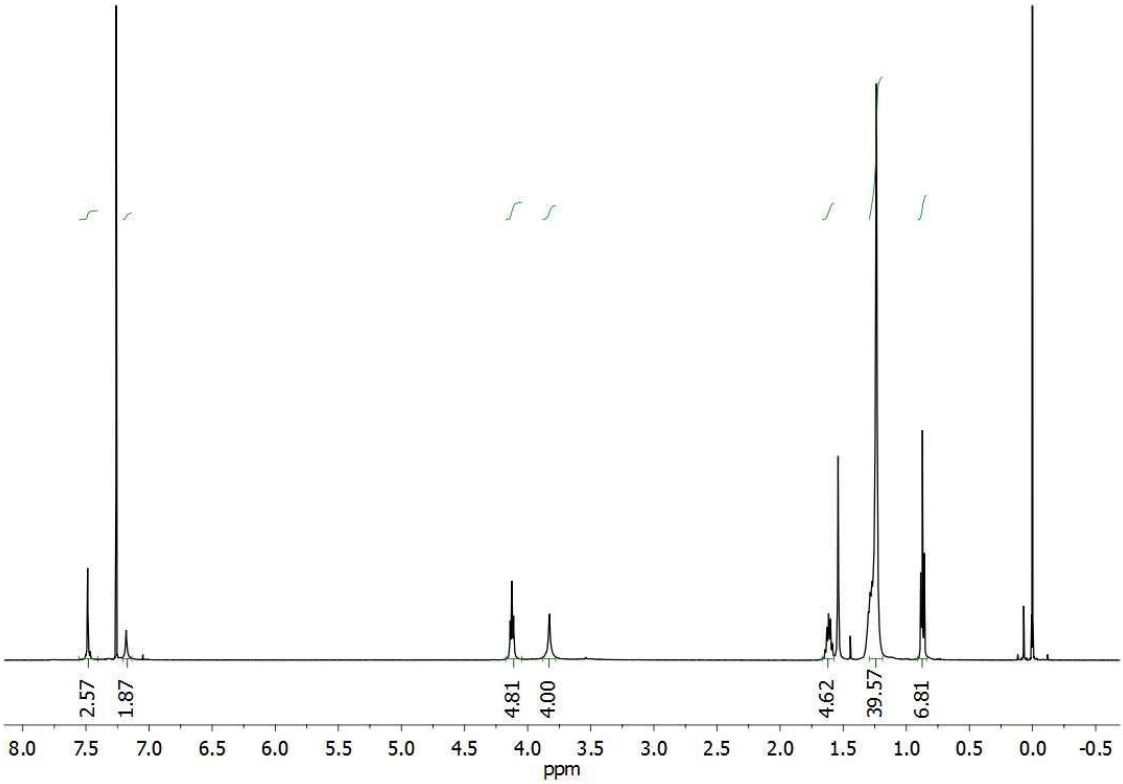

Figure A-9. ^{1}H NMR spectrum (500 MHz, $CDCl_3$) of **P2-E** (chapter 4).

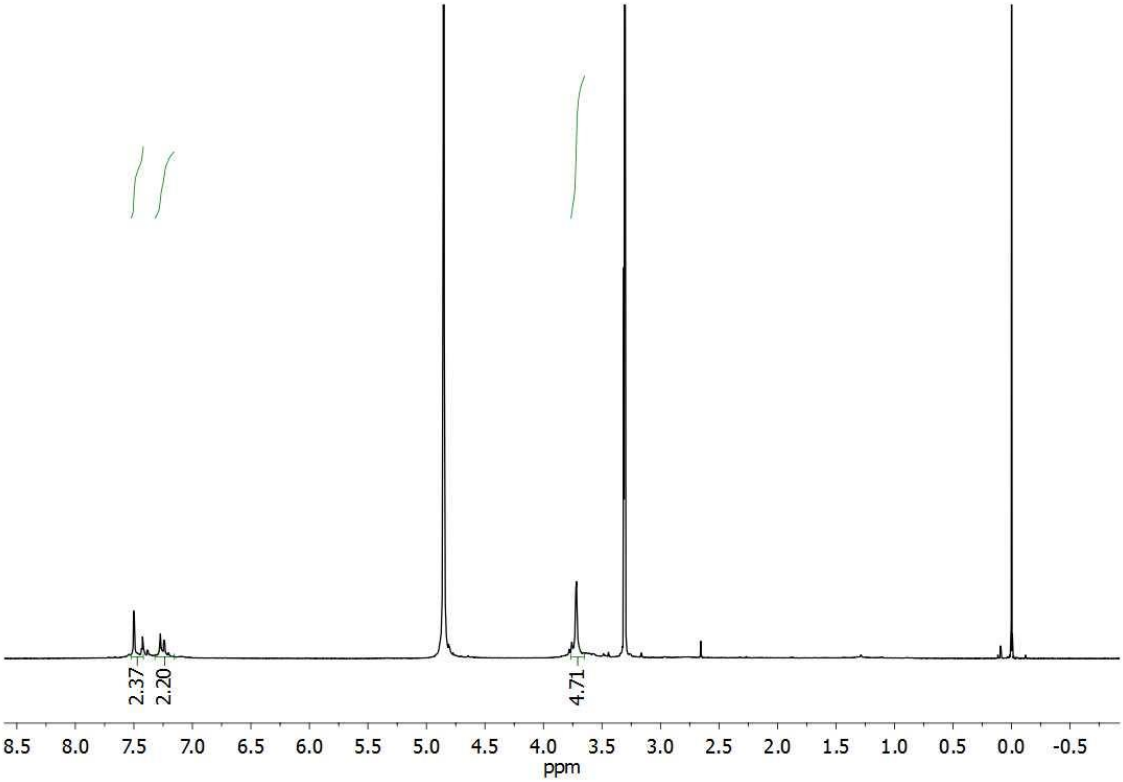

Figure A-10. ^{1}H NMR spectrum (500 MHz, CD_3OD) of **P2** (chapter 4).

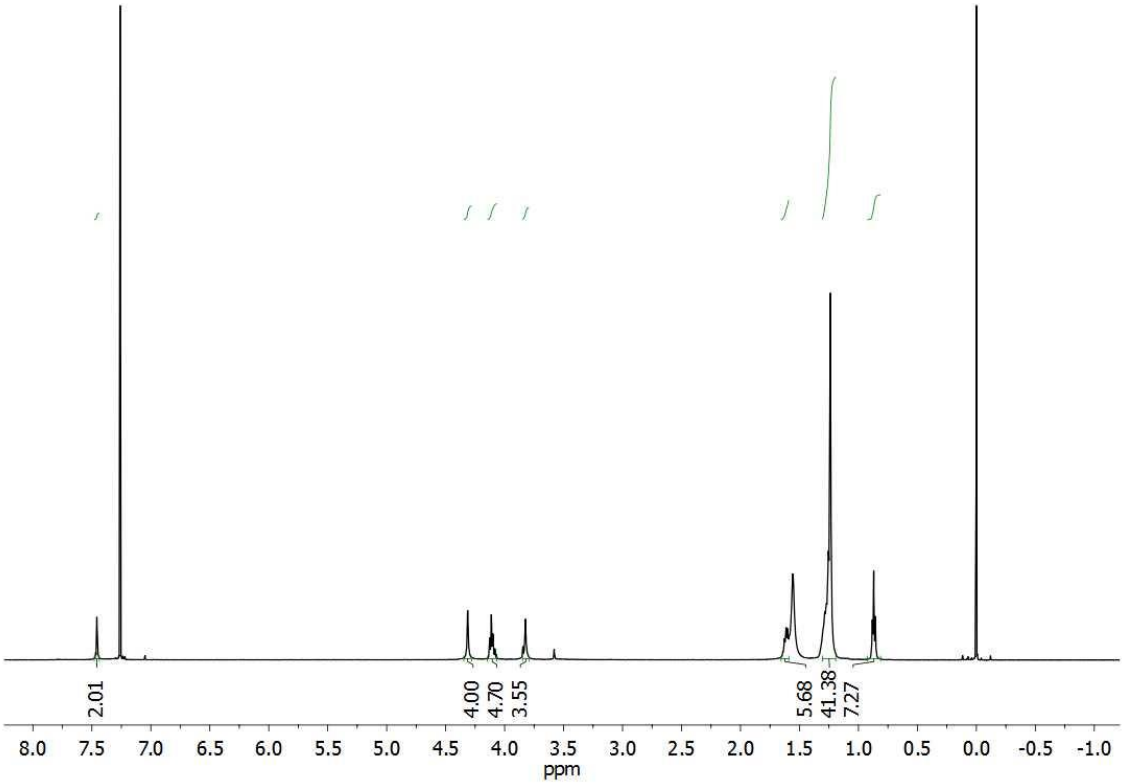

Figure A-11. ^{1}H NMR spectrum (500 MHz, $CDCl_3$) of **P3-E** (chapter 4).

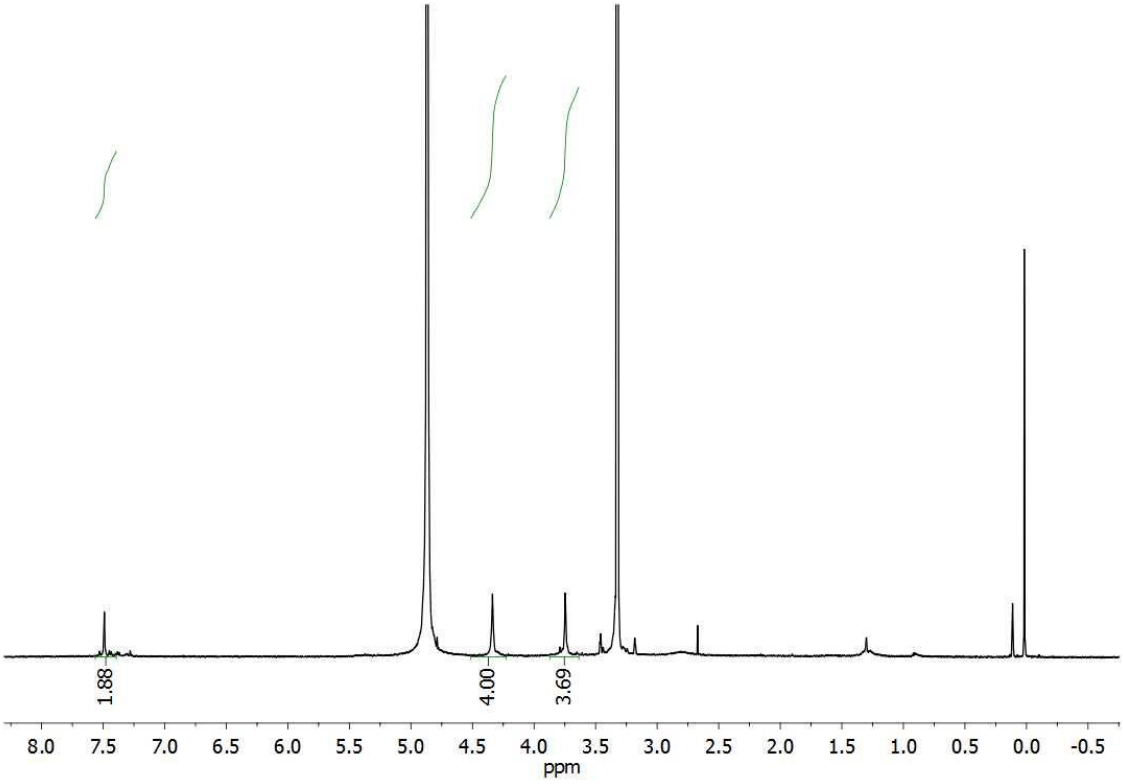

Figure A-12. ^{1}H NMR spectrum (500 MHz, CD_3OD) of **P3** (chapter 4).

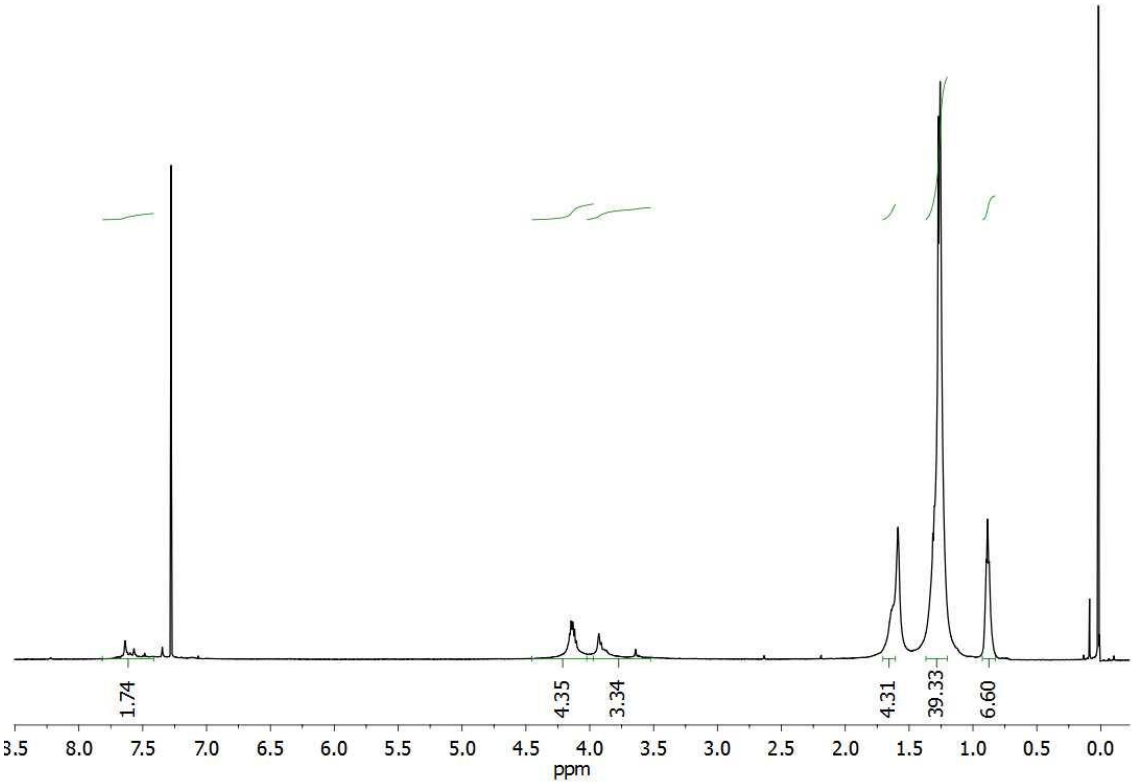

Figure A-13. ^{1}H NMR spectrum (500 MHz, $CDCl_3$) of **P4-E** (chapter 4).

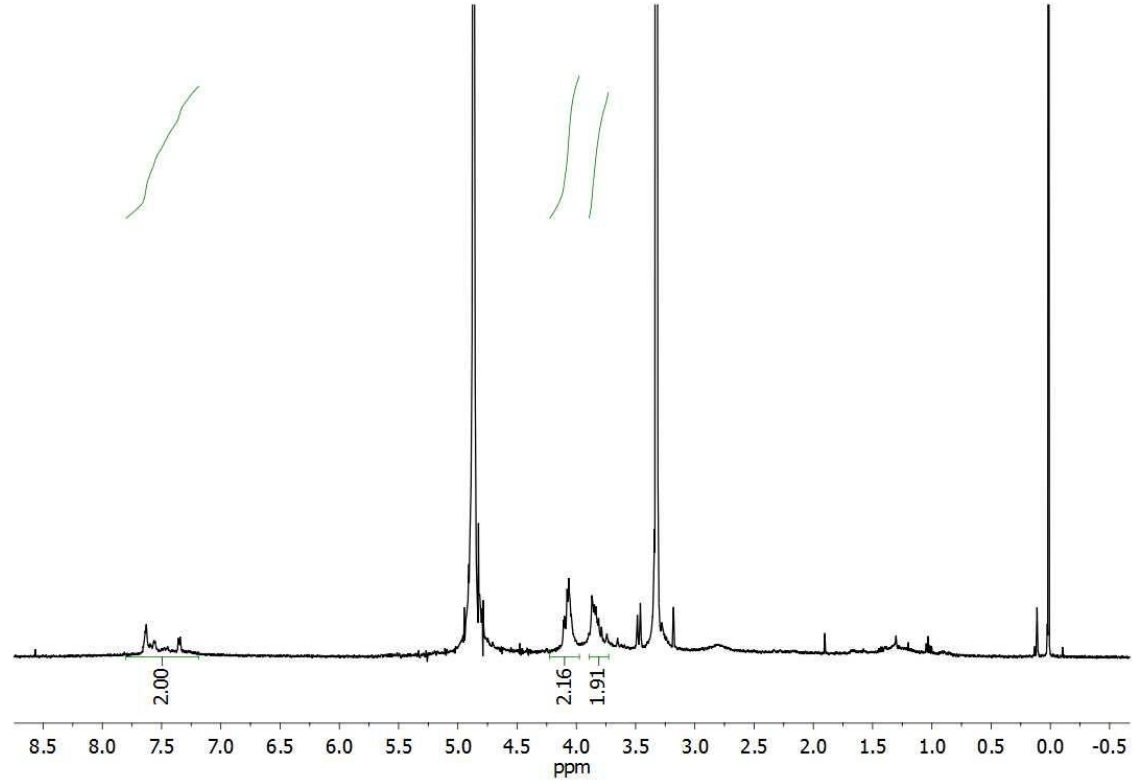

Figure A-14. ^{1}H NMR spectrum (500 MHz, CD_3OD) of **P4** (chapter 4).

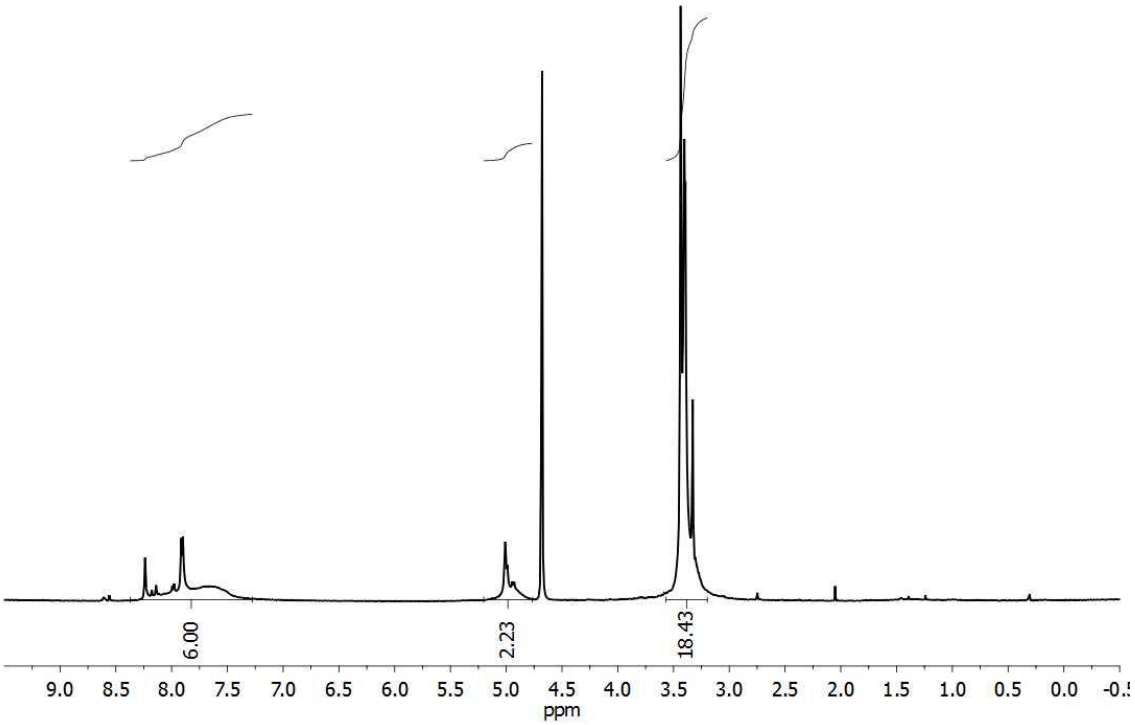

Figure A-15. ^{1}H NMR spectrum (500 MHz, D_2O, 50 ^{o} C) of **P1-N** (chapter 5).

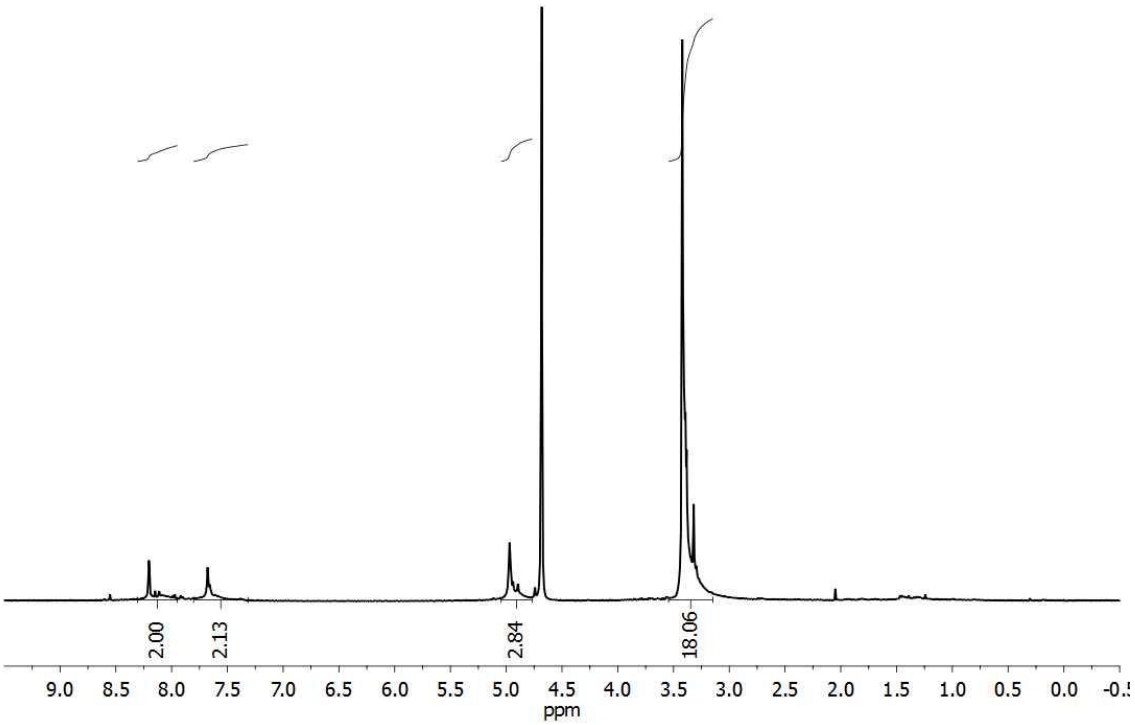

Figure A-16. ^{1}H NMR spectrum (500 MHz, D_2O, 50 ^{o} C) of **P2-N** (chapter 5).

APPENDIX B
MASS SPECTRA

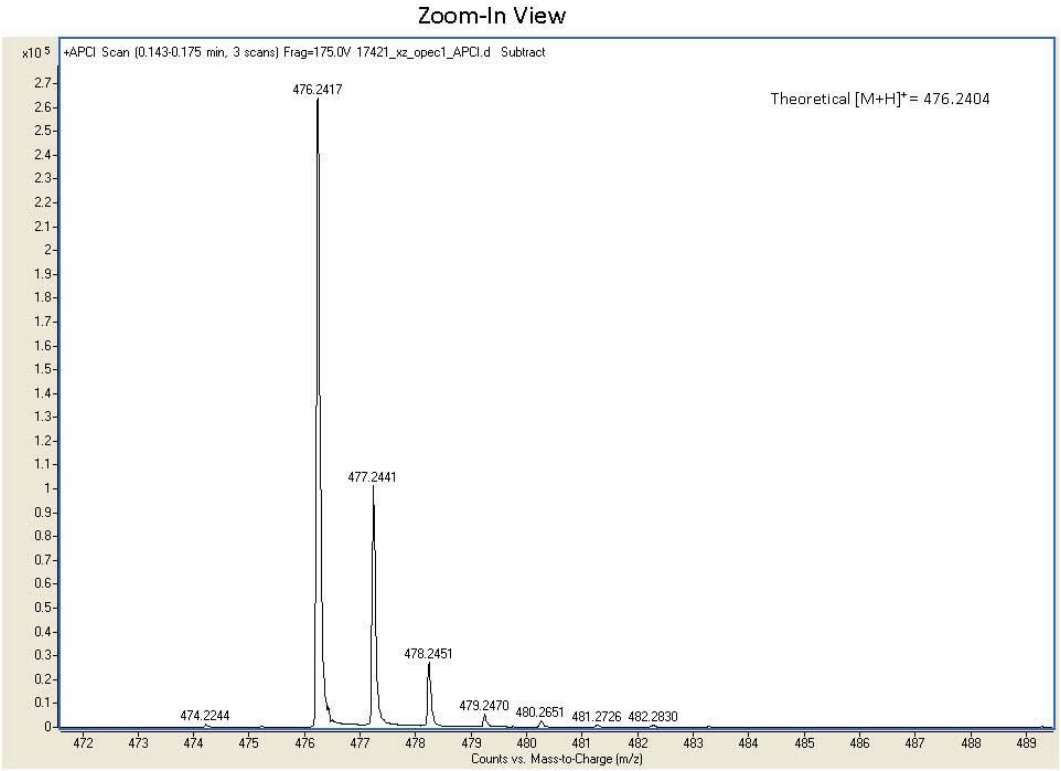

Figure B-1. Mass spectrum of Compound **5** (chapter 2).

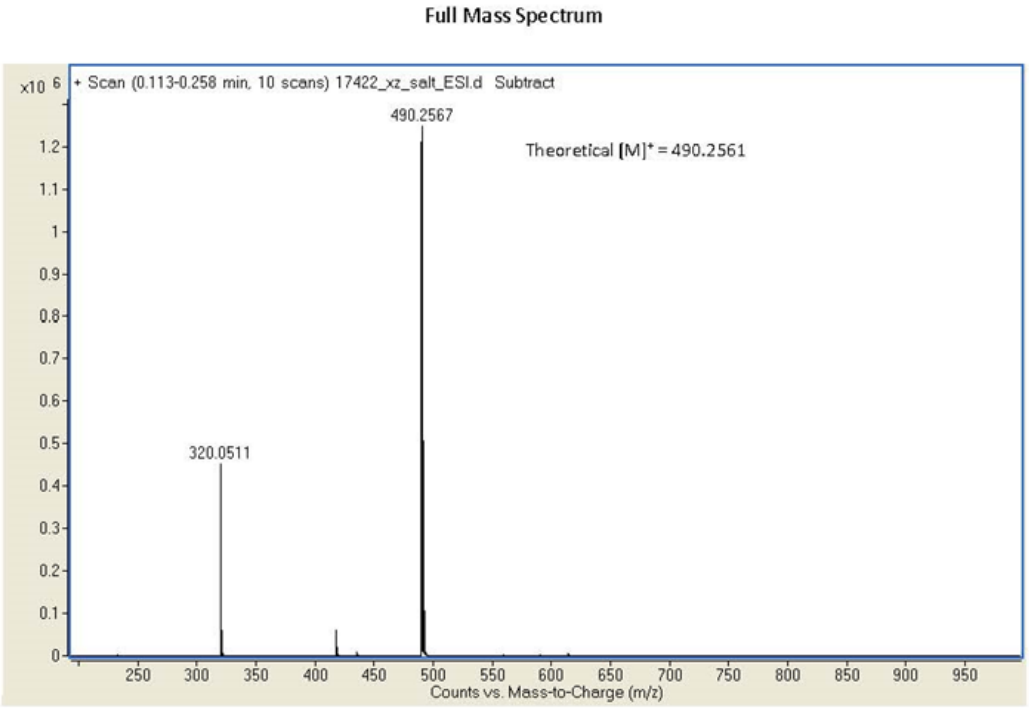

Figure B-2. Mass spectrum of **OPEC1** (chapter 2).

APPENDIX C
FCS CALCULATION

In principle, fluctuations in the fluorescence signal are quantified by temporal autocorrelation of the recorded emission signals collected within the confocal volume. The normalized autocorrelation function, $G(\tau)$, defined as[72]

$$G(\tau) = \frac{\langle F(t)\cdot F(t+\tau)\rangle - \langle F(t)\rangle^2}{\langle F(t)\rangle^2} = \frac{\langle \delta F(t)\cdot \delta F(t+\tau)\rangle}{\langle F(t)\rangle^2} \quad \text{(C-1)}$$

is used to characterize the temporal fluctuations. In Equation C-1, $\delta F(t) = F(t) - < F >$ describes the fluctuation of the fluorescence signal $F(t)$, as deviations from the temporal average of the signal $< F >$ at time *t.* A three dimensional fitting model, representing a single-component system is written as:

$$G_{3D}(\tau) = \frac{1}{N} \times \frac{1}{1+\frac{\tau}{\tau_D}} \times \frac{1}{\sqrt{1+\frac{\tau}{\omega^2 \times \tau_D}}} \quad \text{(C-2)}$$

where ω_z is the longitudinal radius and ω_r is the transversal or waist radius of the confocal volume; and ω, the structure parameter, equates to $\frac{\omega_z}{\omega_r}$**.** *N* is the average number of fluorescent molecules in the confocal volume; τ_D is the average time of fluorescent molecules diffusing in the detection volume, which is characteristic for a specific molecule.

The relationship of τ_D to the molecular diffusion coefficient *D* (m^2s^{-1}) is given by:

$$\tau_D = \frac{{\omega_r}^2}{4D} \quad \text{(C-3)}$$

The waist radius is obtained from its conversion equation:

$$\omega_r = \sqrt{4D_{free\ dye} \cdot \tau_D} \quad \text{(C-4)}$$

where $D_{free\ dye}$ is the diffusion coefficient of the standard calibration dye.

The translational diffusion coefficient, *D,* of a molecule is related to its size by the Stokes-Einstein equation:

$$D = \frac{kT}{6\pi\eta R} \tag{C-5}$$

where *k* is Boltzmann's constant; *T* is the temperature; η is the viscosity of the solvent; and *R* is the hydrodynamic radius. Equation C-5 can be used to estimate the size of diffusing particles by assuming the particles has a spherical shape with radius *R*, which is related to the molecular weight *MW* of the molecule with a specific gravity $\bar{\nu}$ by

$$V = MW\bar{\nu} = \frac{4}{3}\pi R^3 \tag{C-6}$$

where *V* is the volume of molecule. Thus we have

$$R = \left(\frac{3MW\bar{\nu}}{4\pi}\right)^{1/3} \tag{C-7}$$

These equations show that the radius *R* and diffusion coefficient *D* are weakly dependent on the molecular weight. By combining Equation C-5 and C-7, we have:

$$D = \left[\frac{kT}{6\pi\eta}\left(\frac{4\pi}{3\bar{\nu}}\right)^{1/3}\right] MW^{-1/3} \tag{C-8}$$

This relationship is useful for estimation of the molecular weight of a spherical particle from its diffusion coefficient.

For most of our polymers discussed in this presentation, they are not spherical but more like rigid rod. Therefore, the hydrodynamic radius calculated using the spherical model usually gave us a smaller number than the actual size. We can use some simple consideration to calculate the frictional confident for rod-like particles.[135]

Suppose a rod-like particle has a length 2a and radius b. The volume is given by the formula:

$$V_{rod} = 2\pi ab^2 \tag{C-9}$$

Where V_{rod} is the volue of the rod-like particle. The axial ratio P is defined as:

$$P = a/b \tag{C-10}$$

For a rod-like particle, the frictional confident can be found to be[136,137]

$$f = f_0 \frac{\sqrt[2]{2P^2/3}}{\ln 2P - 0.30} \tag{C-11}$$

Where f is the frictional confident for the rod-like particle, f_0 is the frictional confident for a spherical particle and defined as:

$$f_0 = 6\pi\eta R_0 \tag{C-12}$$

Where η is the viscosity of the solvent, R_0 is the radius that has a volume equal to the volume of rod with axial ratio P. Therefore, the relationship between a and R_0 is:

$$V = \frac{4}{3}\pi {R_0}^3 = 2\pi a b^2 \tag{C-13}$$

Combined with Equation C-10, one can find that:

$$a = R_0 \sqrt[3]{\frac{2}{3}P^2} \tag{C-14}$$

If we combine Equations C-5, C-11, C-12 and C-14, we can find that:

$$a = (\ln 2P - 0.3)\frac{kT}{6\pi\eta D} \tag{C-15}$$

If we define a factor $C = \ln 2P - 0.3$, the value of C will be $4 < C < 5$, when $40 < P < 100$. In the PPEs system, the radius b does not change as molecular weight increases. Therefore, the relationship between the molecular weight of the particles and the length will be linear, if we assume the radius b does not change. We can find:

$$\frac{M_{n2}}{M_{n1}} = \frac{a_2}{a_1} \tag{C-16}$$

LIST OF REFERENCES

(1) McQuade, D. T.; Pullen, A. E.; Swager, T. M. *Chem Rev* **2000**, *100*, 2537.

(2) Gunes, S.; Neugebauer, H.; Sariciftci, N. S. *Chem Rev* **2007**, *107*, 1324.

(3) Kraft, A.; Grimsdale, A. C.; Holmes, A. B. *Angew Chem Int Edit* **1998**, *37*, 402.

(4) Torsi, L.; Dodabalapur, A.; Rothberg, L. J.; Fung, A. W. P.; Katz, H. E. *Science* **1996**, *272*, 1462.

(5) Montali, A.; Smith, P.; Weder, C. *Synthetic Met* **1998**, *97*, 123.

(6) Tan, C. Y.; Pinto, M. R.; Schanze, K. S. *Chem Commun* **2002**, 446.

(7) Jiang, H.; Taranekar, P.; Reynolds, J. R.; Schanze, K. S. *Angew Chem Int Edit* **2009**, *48*, 4300.

(8) Shi, S. Q.; Wudl, F. *Macromolecules* **1990**, *23*, 2119.

(9) Chen, L. H.; McBranch, D. W.; Wang, H. L.; Helgeson, R.; Wudl, F.; Whitten, D. G. *P Natl Acad Sci USA* **1999**, *96*, 12287.

(10) Bolink, H. J.; Brine, H.; Coronado, E.; Sessolo, M. *Acs Appl Mater Inter* **2010**, *2*, 2694.

(11) Seo, J. H.; Gutacker, A.; Walker, B.; Cho, S. N.; Garcia, A.; Yang, R. Q.; Nguyen, T. Q.; Heeger, A. J.; Bazan, G. C. *J Am Chem Soc* **2009**, *131*, 18220.

(12) Seo, J. H.; Namdas, E. B.; Gutacker, A.; Heeger, A. J.; Bazan, G. C. *Adv Funct Mater* **2011**, *21*, 3667.

(13) Sirringhaus, H. *Adv Mater* **2005**, *17*, 2411.

(14) Jiang, H.; Zhao, X. Y.; Shelton, A. H.; Lee, S. H.; Reynolds, J. R.; Schanze, K. S. *Acs Appl Mater Inter* **2009**, *1*, 381.

(15) Fang, Z.; Schanze, K. S. *Abstr Pap Am Chem S* **2011**, *241*.

(16) Sambur, J. B.; Averill, C. M.; Bradley, C.; Schuttlefield, J.; Lee, S. H.; Reynods, J. R.; Schanze, K. S.; Parkinson, B. A. *Langmuir* **2011**, *27*, 11906.

(17) Ogawa, K.; Chemburu, S.; Lopez, G. P.; Whitten, D. G.; Schanze, K. S. *Langmuir* **2007**, *23*, 4541.

(18) Chemburu, S.; Ji, E.; Casana, Y.; Wu, Y.; Buranda, T.; Schanze, K. S.; Lopez, G. P.; Whitten, D. G. *J Phys Chem B* **2008**, *112*, 14492.

(19) Corbitt, T. S.; Ding, L.; Ji, E.; Ista, L. K.; Ogawa, K.; Lopez, G. P.; Schanze, K. S.; Whitten, D. G. *Photoch Photobio Sci* **2009**, *8*, 998.

(20) Tang, Y. L.; Zhou, Z. J.; Ogawa, K.; Lopez, G. P.; Schanze, K. S.; Whitten, D. G. *Langmuir* **2009**, *25*, 21.

(21) Zhou, Z. J.; Corbitt, T. S.; Parthasarathy, A.; Tang, Y. L.; Ista, L. F.; Schanze, K. S.; Whitten, D. G. *J Phys Chem Lett* **2010**, *1*, 3207.

(22) Wang, Y.; Tang, Y. L.; Zhou, Z. J.; Ji, E.; Lopez, G. P.; Chi, E. Y.; Schanze, K. S.; Whitten, D. G. *Langmuir* **2010**, *26*, 12509.

(23) Parthasarathy, A.; Ji, E.; Zhou, Z. J.; Corbitt, T.; Ista, L.; Whitten, D. G.; Schanze, K. S. *Abstr Pap Am Chem S* **2011**, *242*.

(24) Zhao, X.; Schanze, K. S. *Chem Commun* **2010**, *46*, 6075.

(25) Zhao, X. Y.; Liu, Y.; Schanze, K. S. *Chem Commun* **2007**, 2914.

(26) Bunz, U. H. F. *Chem Rev* **2000**, *100*, 1605.

(27) Sonogashira, K.; Tohda, Y.; Hagihara, N. *Tetrahedron Lett* **1975**, 4467.

(28) Sonogashira, K. *J Organomet Chem* **2002**, *653*, 46.

(29) Chemburu, S.; Corbitt, T. S.; Ista, L. K.; Ji, E.; Fulghum, J.; Lopez, G. P.; Ogawa, K.; Schanze, K. S.; Whitten, D. G. *Langmuir* **2008**, *24*, 11053.

(30) Wilson, J. S.; Frampton, M. J.; Michels, J. J.; Sardone, L.; Marletta, G.; Friend, R. H.; Samori, P.; Anderson, H. L.; Cacialli, F. *Adv Mater* **2005**, *17*, 2659.

(31) Yang, J. S.; Swager, T. M. *J Am Chem Soc* **1998**, *120*, 11864.

(32) Williams, V.; Yang, J. S.; Swager, T. M. *Abstr Pap Am Chem S* **1998**, *216*, U354.

(33) Yang, J. S.; Swager, T. M. *J Am Chem Soc* **1998**, *120*, 5321.

(34) Miao, Y. J.; Kim, J. S.; Swager, T. M. *Abstr Pap Am Chem S* **1999**, *218*, U455.

(35) Liu, S. J.; Fang, C.; Zhao, Q.; Fan, Q. L.; Huang, W. *Macromol Rapid Comm* **2008**, *29*, 1212.

(36) Li, J.; Meng, J.; Huang, X. B.; Cheng, Y. X.; Zhu, C. J. *Polymer* **2010**, *51*, 3425.

(37) Gaylord, B. S.; Heeger, A. J.; Bazan, G. C. *J Am Chem Soc* **2003**, *125*, 896.

(38) Lee, K.; Povlich, L. K.; Kim, J. *Adv Funct Mater* **2007**, *17*, 2580.

(39) Lee, K.; Rouillard, J. M.; Pham, T.; Gulari, E.; Kim, J. *Angew Chem Int Edit* **2007**, *46*, 4667.

(40) Heinzerling, P.; Schrader, F.; Schanze, S. *J Chem Educ* **2012**, *89*, 1582.

(41) Liu, Y.; Schanze, K. S. *Anal Chem* **2009**, *81*, 231.

(42) Wu, D. L.; Feng, F. D.; Xie, D. P.; Chen, Y.; Tan, W. H.; Schanze, K. S. *J Phys Chem Lett* **2012**, *3*, 1711.

(43) Zhao, X. Y.; Schanze, K. S. *Langmuir* **2006**, *22*, 4856.

(44) Samori, P.; Francke, V.; Mullen, K.; Rabe, J. P. *Chem-Eur J* **1999**, *5*, 2312.

(45) Schnablegger, H.; Antonietti, M.; Goltner, C.; Hartmann, J.; Colfen, H.; Samori, P.; Rabe, J. P.; Hager, H.; Heitz, W. *J Colloid Interf Sci* **1999**, *212*, 24.

(46) Chinchilla, R.; Najera, C. *Chem Rev* **2007**, *107*, 874.

(47) Zhao, X. Y.; Pinto, M. R.; Hardison, L. M.; Mwaura, J.; Muller, J.; Jiang, H.; Witker, D.; Kleiman, V. D.; Reynolds, J. R.; Schanze, K. S. *Macromolecules* **2006**, *39*, 6355.

(48) Lee, S. H.; Komurlu, S.; Zhao, X. Y.; Jiang, H.; Moriena, G.; Kleiman, V. D.; Schanze, K. S. *Macromolecules* **2011**, *44*, 4742.

(49) Fang, Z.; Eshbaugh, A. A.; Schanze, K. S. *J Am Chem Soc* **2011**, *133*, 3063.

(50) Zhao, X. Y.; Jiang, H.; Schanze, K. S. *Macromolecules* **2008**, *41*, 3422.

(51) Zhou, Q.; Swager, T. M. *J Am Chem Soc* **1995**, *117*, 12593.

(52) Thomas, S. W.; Joly, G. D.; Swager, T. M. *Chem Rev* **2007**, *107*, 1339.

(53) J. R. Lakowicz, Principles of Fluorescence Spectroscopy, 2nd ed., Kluwer Academic/Plenum Publishers, New York, 1999.

(54) Tan, C. Y.; Alas, E.; Muller, J. G.; Pinto, M. R.; Kleiman, V. D.; Schanze, K. S. *J Am Chem Soc* **2004**, *126*, 13685.

(55) Halkyard, C. E.; Rampey, M. E.; Kloppenburg, L.; Studer-Martinez, S. L.; Bunz, U. H. F. *Macromolecules* **1998**, *31*, 8655.

(56) Kim, J.; Swager, M. *Nature* **2001**, *413*, 548.

(57) Levitus, M.; Zepeda, G.; Dang, H.; Godinez, C.; Khuong, T. A. V.; Schmieder, K.; Garcia-Garibay, M. A. *J Org Chem* **2001**, *66*, 3188.

(58) Walters, K. A.; Ley, K. D.; Schanze, K. S. *Langmuir* **1999**, *15*, 5676.

(59) Kim, I. B.; Dunkhorst, A.; Gilbert, J.; Bunz, U. H. F. *Macromolecules* **2005**, *38*, 4560.

(60) Pinto, M. R.; Schanze, K. S. *P Natl Acad Sci USA* **2004**, *101*, 7505.

(61) Haskins-Glusac, K.; Pinto, M. R.; Tan, C. Y.; Schanze, K. S. *J Am Chem Soc* **2004**, *126*, 14964.

(62) Khan, A.; Muller, S.; Hecht, S. *Chem Commun* **2005**, 584.

(63) Pun, C. C.; Lee, K.; Kim, H. J.; Kim, J. *Macromolecules* **2006**, *39*, 7461.

(64) Lee, K.; Kim, H. J.; Kim, J. *Adv Funct Mater* **2012**, *22*, 1076.

(65) Magde, D.; Webb, W. W.; Elson, E. *Phys Rev Lett* **1972**, *29*, 705.

(66) Krichevsky, O.; Bonnet, G. *Reports on Progress in Physics* **2002**, *65*, 251.

(67) Yin, Y. D.; Yuan, R. F.; Zhao, X. S. *J Phys Chem Lett* **2013**, *4*, 304.

(68) Shin, H. S.; Okamoto, A.; Sako, Y.; Kim, S. W.; Kim, S. Y.; Pack, C. G. *J Phys Chem A* **2013**, *117*, 27.

(69) Zettl, U.; Hoffmann, S. T.; Koberling, F.; Krausch, G.; Enderlein, J.; Harnau, L.; Ballauff, M. *Macromolecules* **2009**, *42*, 9537.

(70) Fogarty, K.; Van Orden, A. *Methods* **2009**, *47*, 151.

(71) Waldeck, D. H.; Kaur, P.; Yue, H. J.; Wu, M. Y.; Liu, M.; Treece, J.; Xue, C. H.; Liu, H. Y. *J Phys Chem B* **2007**, *111*, 8589.

(72) Haustein, E.; Schwille, P. *Annu Rev Bioph Biom* **2007**, *36*, 151.

(73) Liu, Y.; Ogawa, K.; Schanze, K. S. *Anal Chem* **2008**, *80*, 150.

(74) Gaylord, B. S.; Heeger, A. J.; Bazan, G. C. *P Natl Acad Sci USA* **2002**, *99*, 10954.

(75) Tang, Y.; Corbitt, T. S.; Parthasarathy, A.; Zhou, Z.; Schanze, K. S.; Whitten, D. G. *Langmuir* **2011**, *27*, 4956.

(76) Ji, E.; Parthasarathy, A.; Corbitt, T. S.; Schanze, K. S.; Whitten, D. G. *Langmuir* **2011**, *27*, 10763.

(77) Wang, Y.; Zhou, Z. J.; Zhu, J. S.; Tang, Y. L.; Canady, T. D.; Chi, E. Y.; Schanze, K. S.; Whitten, D. G. *Polymers-Basel* **2011**, *3*, 1199.

(78) Tang, Y. L.; Corbitt, T. S.; Parthasarathy, A.; Zhou, Z. J.; Schanze, K. S.; Whitten, D. G. *Langmuir* **2011**, *27*, 4956.

(79) Pearson, D. L.; Tour, J. M. *J Org Chem* **1997**, *62*, 1376.

(80) McQuade, D. T.; Hegedus, A. H.; Swager, T. M. *J Am Chem Soc* **2000**, *122*, 12389.

(81) Feng, F. D.; Lee, S. H.; Schanze, K. S. *J Phys Chem Lett* **2012**, *3*, 1707.

(82) Kim, S. K.; Lee, D. H.; Hong, J. I.; Yoon, J. *Accounts Chem Res* **2009**, *42*, 23.

(83) Ronaghi, M.; Karamohamed, S.; Pettersson, B.; Uhlen, M.; Nyren, P. *Anal Biochem* **1996**, *242*, 84.

(84) Metzger, A.; Anslyn, E. V. *Angew Chem Int Edit* **1998**, *37*, 649.

(85) Best, M. D.; Tobey, S. L.; Anslyn, E. V. *Coordin Chem Rev* **2003**, *240*, 3.

(86) Tobey, S. L.; Anslyn, E. V. *J Am Chem Soc* **2003**, *125*, 14807.

(87) Blondeau, P.; Segura, M.; Perez-Fernandez, R.; de Mendoza, J. *Chem Soc Rev* **2007**, *36*, 198.

(88) George, W. N.; Giles, M.; McCulloch, I.; Steinke, J. H. G.; deMello, J. C. *Chemphyschem* **2011**, *12*, 765.

(89) Nishizawa, S.; Kato, Y.; Teramae, N. *J Am Chem Soc* **1999**, *121*, 9463.

(90) Pinto, M. R.; Kristal, B. M.; Schanze, K. S. *Langmuir* **2003**, *19*, 6523.

(91) Jiang, H.; Zhao, X. Y.; Schanze, K. S. *Langmuir* **2007**, *23*, 9481.

(92) Porcheddu, A.; Giacomelli, G.; Chighine, A.; Masala, S. *Org Lett* **2004**, *6*, 4925.

(93) Baumann, J.; Fayer, M. D. *J Chem Phys* **1986**, *85*, 4087.

(94) Levitsky, I. A.; Kim, J. S.; Swager, T. M. *J Am Chem Soc* **1999**, *121*, 1466.

(95) Beljonne, D.; Pourtois, G.; Silva, C.; Hennebicq, E.; Herz, L. M.; Friend, R. H.; Scholes, G. D.; Setayesh, S.; Mullen, K.; Bredas, J. L. *P Natl Acad Sci USA* **2002**, *99*, 10982.

(96) Liu, Y.; Schanze, K. S. *Anal Chem* **2008**, *80*, 8605.

(97) Chen, L. H.; Xu, S.; McBranch, D.; Whitten, D. *J Am Chem Soc* **2000**, *122*, 9302.

(98) Kaur, P.; Yue, H. J.; Wu, M. Y.; Liu, M.; Treece, J.; Waldeck, D. H.; Xue, C. H.; Liu, H. Y. *J Phys Chem B* **2007**, *111*, 8589.

(99) Liu, B.; Bazan, G. C. *Chem Mater* **2004**, *16*, 4467.

(100) Feng, F. D.; Tang, Y. L.; He, F.; Yu, M. H.; Duan, X. R.; Wang, S.; Li, Y. L.; Zhu, D. B. *Adv Mater* **2007**, *19*, 3490.

(101) Jiang, H.; Zhao, X. Y.; Schanze, K. S. *Langmuir* **2006**, *22*, 5541.

(102) Feng, F.; Yang, J.; Xie, D. P.; McCarley, T. D.; Schanze, K. S. J. Phys. Chem. Lett. 2013, 9, 1410

(103) Mahler, C.; Muller, U.; Muller, W. M.; Enkelmann, V.; Moon, C.; Brunklaus, G.; Zimmermann, H.; Hoger, S. *Chem Commun* **2008**, 4816.

(104) Waybright, S. M.; Singleton, C. P.; Wachter, K.; Murphy, C. J.; Bunz, U. H. F. *J Am Chem Soc* **2001**, *123*, 1828.

(105) Faucher, A. M.; White, P. W.; Brochu, C.; Grand-Maitre, C.; Rancourt, J.; Fazal, G. *J Med Chem* **2004**, *47*, 18.

(106) Dippy, J. F. J.; Hughes, S. R. C.; Rozanski, A. *J Chem Soc* **1959**, 2492.

(107) Mwaura, J. K.; Zhao, X. Y.; Jiang, H.; Schanze, K. S.; Reynolds, J. R. *Chem Mater* **2006**, *18*, 6109.

(108) Schanze, K. S.; Shelton, A. H. *Langmuir* **2009**, *25*, 13698.

(109) Takeda, N.; Parkinson, B. A. *J Am Chem Soc* **2003**, *125*, 5559.

(110) Ushiroda, S.; Ruzycki, N.; Lu, Y.; Spitler, M. T.; Parkinson, B. A. *J Am Chem Soc* **2005**, *127*, 5158.

(111) Wenger, B.; Gratzel, M.; Moser, J. E. *J Am Chem Soc* **2005**, *127*, 12150.

(112) Hamann, T. W.; Martinson, A. B. F.; Elam, J. W.; Pellin, M. J.; Hupp, J. T. *J Phys Chem C* **2008**, *112*, 10303.

(113) Groves, C.; Reid, O. G.; Ginger, D. S. *Accounts Chem Res* **2010**, *43*, 612.

(114) Giridharagopal, R.; Shao, G. Z.; Groves, C.; Ginger, D. S. *Mater Today* **2010**, *13*, 50.

(115) Tiwana, P.; Docampo, P.; Johnston, M. B.; Snaith, H. J.; Herz, L. M. *Acs Nano* **2011**, *5*, 5158.

(116) Anta, J. A.; Guillen, E.; Tena-Zaera, R. *J Phys Chem C* **2012**, *116*, 11413.

(117) Bernardi, M.; Giulianini, M.; Grossman, J. C. *Acs Nano* **2010**, *4*, 6599.

(118) Lu, Y. F.; Choi, D. J.; Nelson, J.; Yang, O. B.; Parkinson, B. A. *J Electrochem Soc* **2006**, *153*, E131.

(119) Liu, D. B.; Wang, S. J.; Swierczewska, M.; Huang, X. L.; Bhirde, A. A.; Sun, J. S.; Wang, Z.; Yang, M.; Jiang, X. Y.; Chen, X. Y. *Acs Nano* **2012**, *6*, 10999.

(120) Boening, D. W. *Chemosphere* **2000**, *40*, 1335.

(121) Zheng, W.; Aschner, M.; Ghersi-Egea, J. F. *Toxicol Appl Pharm* **2003**, *192*, 1.

(122) Huang, W. J.; Wu, W. H. *J Appl Polym Sci* **2012**, *124*, 2055.

(123) Shi, W.; Ma, H. M. *Chem Commun* **2008**, 1856.

(124) Luxami, V.; Verma, M.; Rani, R.; Paul, K.; Kumar, S. *Org Biomol Chem* **2012**, *10*, 8076.

(125) Rode, A. B.; Kim, J.; Kim, S. H.; Gupta, G.; Hong, I. S. *Tetrahedron Lett* **2012**, *53*, 2571.

(126) Neenan, T. X.; Whitesides, G. M. *J Org Chem* **1988**, *53*, 2489.

(127) Jiang, D. L.; Choi, C. K.; Honda, K.; Li, W. S.; Yuzawa, T.; Aida, T. *J Am Chem Soc* **2004**, *126*, 12084.

(128) Swager, T. M. *Accounts Chem Res* **2008**, *41*, 1181.

(129) An, L. L.; Tang, Y. L.; Feng, F. D.; He, F.; Wang, S. *J Mater Chem* **2007**, *17*, 4147.

(130) Nutiu, R.; Yu, J. M. Y.; Li, Y. F. *Chembiochem* **2004**, *5*, 1139.

(131) Li, C.; Numata, M.; Takeuchi, M.; Shinkai, S. *Angew Chem Int Edit* **2005**, *44*, 6371.

(132) Ojida, A.; Miyahara, Y.; Wongkongkatep, A.; Tamaru, S.; Sada, K.; Hamachi, I. *Chem-Asian J* **2006**, *1*, 555.

(133) Narayanan, A.; Varnavski, O. P.; Swager, T. M.; Goodson, T. *J Phys Chem C* **2008**, *112*, 881.

(134) Feng, F.; Yang, J.; Xie, D. P.; McCarley, T. D.; Schanze, K. S. J. Phys. Chem. Lett. 2013, 9, 1410

(135) Atkins, P.; De Paula, J. Physical Chemistry for the Life Science W H Freeman & Co 2011

(136) Tirado, M. M.; Martinez, C. L.; Delatorre, J. G. *J Chem Phys* **1984**, *81*, 2047.

(137) Broersma, S. *J Chem Phys* **1981**, *74*, 6989.

BIOGRAPHICAL SKETCH

Xuzhi Zhu was born in Wuhu, Anhui Province, China in 1988. Xuzhi Zhu started his undergraduate studies at Fudan University (Shanghai, China) in 2005. Four years later, he received his bachelor's degree of science in Macromolecular Science and Engineering. During the same year, Xuzhi went to United States to continue his graduate studies in Department of Chemistry at University of Florida, where he joined Dr. Schanze's group. In the past four years, he focused his research on the topic of Conjugated Polyelectrolytes under the supervision of Dr. Kirk S. Schanze. Xuzhi received his Ph. D. from University of Florida in the summer of 2013. In 2013, Xuzhi will go back to China to work in chemistry industry and in education industry.